PERFORMANCE EVALUATION OF NEW CORRUGATED-TYPE EMBOSSMENTS FOR COMPOSITE DECK

By:

Grace Shen

Thesis submitted to the faculty of the
Virginia Polytechnic Institute and State University
In partial fulfillment of the requirements for the degree of

MASTER OF SCIENCE
IN
CIVIL ENGINEERING

Approved:

_____

Dr. W. Samuel Easterling, Chairperson

_____ _____

Dr. Thomas Cousins **Dr. Carin Roberts-Wollmann**

August 8, 2001
Blacksburg, VA

Keywords: Composite Deck, Embossments, Longitudinal Shear, Shear Bond

PERFORMANCE EVALUATION OF NEW CORRUGATED-TYPE EMBOSSMENTS FOR COMPOSITE DECK

By:
Grace Shen

(ABSTRACT)

The purpose of this research is to evaluate the performance of new corrugated-type embossments developed by Vulcraft Research and Development for their 2VLI and 3VLI composite deck. Performance of deck with the proposed embossment types is compared with that of deck with the existing embossment type, resulting in the recommendation of which type to further investigate for production. The evaluation consists of uniformly loaded full-scale slab tests whose flexural strengths are compared with those given by different strength prediction methods that are alternatives to full-scale testing. The methods used in this study are the First Yield Method (Heagler 1992), the ASCE Appendix D Alternate Method (*Standard* 1992), and Widjaja's (1997) Iterative Method. Shear bond tests are also performed for deck with each embossment type to evaluate shear resistance specifically, and to provide shear bond data needed to perform the Iterative Method.

ACKNOWLEDGEMENTS

I want to express my appreciation to the members of my committee for the integral parts they played in this research: Dr. W. Samuel Easterling, for initiating this research and providing valuable direction and support throughout the process to complete it; to Dr. Thomas Cousins for his support inside and outside of the academic realm, and to Dr. Carin Roberts-Wollman for her guidance and enthusiasm.

I am also appreciative of NUCOR Research and Development for sponsoring this research to be done at Virginia Tech.

My numerous hours at the Structures and Materials Laboratory were made much more enjoyable by the indispensable aid of many. I want to thank Brett Farmer, Dennis Huffman, and Ricky Woods for their willing technical advice and labor, cheerful greetings, occasional serenades, and kind words. I am also indebted to my fellow classmates Marcela Guirola, Thad Chapman, and Ben Mason for their significant and generous help with my experimental testing and for their companionship at the lab. I also want to thank J. R. Mujagic and Jason Piotter for their tutorial help with the instrumentation. Special thanks also goes to Redzuan Abdullah for contributing his computer programming expertise.

I am thankful for the many friendships that have developed here at Virginia Tech and am especially grateful for Yan Ping Wong (and parents), Marcela Guirola, Sally White, Thad Chapman, Steve Alvis, Chris Waldron, and Trevor and Donna Kirkpatrick who provided encouraging emotional support through the most difficult times.

Most importantly, I want to acknowledge my parents, Stewart and Shawmei Shen, and my sister, Alice Liu, who have been a constant source of love and support for me. I am greatly indebted to my parents for always striving to provide the best for their daughters. For this I will always be grateful.

TABLE OF CONTENTS

LIST OF FIGURES

LIST OF TABLES

LIST OF NOTATIONS

a = depth of compressive stress block

A_s = deck area per unit width

b = unit width of slab

b_d = test slab width

B_b = width of the bottom flange of the deck (Figure 5.1)

Bt = width of the top flange of the deck (Figure 5.1)

CGS = centroid of the deck

C_s = spacing of the deck cells (Figure 5.2)

d = effective slab depth

D = nominal total slab depth

D_w = diagonal dimension of the deck web (Figure 5.1)

d_d = depth of deck

e_1 = lever arm from centriod of concrete compressive block to the top flange of the deck (Figure 5.1)

e_2 = lever arm from centriod of concrete compressive block to the centroid of the web of the deck (Figure 5.1)

e_3 = lever arm from centriod of concrete compressive block to the bottom flange of the deck (Figure 5.1)

f_c = stress in deck due to casting

f'_c = concrete compressive strength

f_s = stress in deck due to shear transfer

f_w = stress in deck due to the force in the welds

f_y^* = remaining yield strength, accounting for casting, welds, and shear transfer

f_{yc} = yield stress of deck, corrected to account for casting stresses

F_s = shear force transferred between the deck and concrete (Figure 5.3.1)

F_y = minimum yield stress of deck (not to exceed 60 ksi)

H = total height of the slab

k = experimentally determined relaxation factor for shear bond equations, which is equal to the coordinate intercept of reduced experimental shear-bond line

k_1 = coefficient that measures the influence of the steel deck depth on the development of the shear bond along the shear span

k_2 = coefficient that indicates the mechanical bond performance along the shear span

k_3 = coefficient that accounts for the increase in efficiency of the embossment with increasing slab width

k_4 = relaxation factor that accounts for the influence of the shear span and depth of deck.

l_e = average embossment length (Figure 5.2)

L = span length

L' = length of shear span

m = experimentally determined slope of reduced experimental shear-bond line

M_n = nominal moment capacity

$M_{noncomposite}$ = remaining additional noncomposite strength of deck (beyond the partial composite strength used)

$M_{composite}$ = partially composite slab strength

M_s = shoring removal moment

M_{et} = First Yield Moment per unit width

$M_{p.Rd}$ = Design resistance (Eurocode)

M_{pr} = bending capacity of noncomposite deck (Eurocode)

n = modular ratio, $\frac{E_s}{E_c}$

N_b = embossment length at the bottom (Figure 3.2.2)

N_c = tensile force in the deck

N_h = length of horizontal embossments (Figure 5.2)

N_v = length of vertical embossments (Figure 5.2)

N_t = embossment length at the top (Figure 3.2.2)

N.A. = neutral axis

p_h = embossment height

s = spacing of shear transferring devices

S = section modulus of noncomposite steel deck

t = thickness of the deck

T_1 = tensile force component from the top flange of the deck

T_2 = tensile force component from the web of the deck

T_3 = tensile force component from the bottom flange of the deck

V_u = ultimate transverse shear-bond resistance (per unit width)

V_n = nominal shear-bond strength (per unit width)

w = average width of embossments (Figure 5.2)

w_{et} = theoretical applied distributed load that results in M_{et} (First Yield Moment)

w_n = theoretical applied distributed load that results in M_n using the calculated material properties

w_t = theoretical applied distributed load that results in M_t (Flexural capacity using ASCE App. D Method)

W = wind load perpendicular to slab

W_b = embossment width at the bottom (Figure 3.2.2)

W_t = embossment width at the top (Figure 3.2.2)

y_{cc} = distance of the centroid from the top of the slab (Figure 5.1)

z = lever arm between compressive and tensile forces

ρ = reinforcement ratio, $\frac{A_s}{b\,d}$

ε_u = compressive strain in concrete at ultimate strength (0.003)

γ = coefficient for the proportion of dead load added upon removal of shore

$$\lambda = \frac{E_s \varepsilon_u}{0.85 \beta_1 f'_c} \qquad \text{(Equation 2-12)}$$

ϕ = Flexural capacity reduction factor

τ_u = the shear bond capacity

$\tau_{u.Rk}$ = characteristic shear strength

CHAPTER 1: INTRODUCTION

1.1 General

The use of steel deck in the construction of floors began in the 1920's (Dallaine 1971). The deck commonly was the main structural component for the floors of steel framed buildings. The addition of concrete cover provided no structural strength, but rather served the purposes of fire protection, a means to level the top surface of the floor, and a means to distribute the load. A contrasting philosophy for the use of steel deck was to have it serve only as formwork for the traditionally reinforced concrete slab, which provided the full structural capacity.

The concept of using steel deck to act compositely with the concrete slab began in the 1950's. Composite deck is more efficient than noncomposite deck because it makes use of the strength of both the steel and the concrete components, resulting in lighter, more cost-effective floors. Another benefit is that the cellular shape of some decks provides room for the flush fitting of ceiling fixtures. Composite floors are also advantageous during the construction stage. They are easier and faster to construct than traditional reinforced concrete slabs because it is easier to install the deck, which acts as the reinforcing, than to lay out a series of reinforcing bars. The elimination of formwork also simplifies construction, and the steel deck provides a working platform while the floor is built. Also, the deck provides lateral restraint for the steel beams during erection. (Stark 1978)

As use of composite slabs gained popularity, research has focused on two areas: 1.) improving the composite interaction between the deck and concrete and 2.) the development of composite design methods. To improve composite interaction, deck manufacturers have been investigating the use of several different shear transfer devices

such as: deck embossments, shear studs, interlocking deck profile geometry, and end restraint such as pour stop. Several different design methods exist worldwide. However, the accepted practice by manufactures is still to perform multiple full-scale slab tests of the deck to determine its performance. The development and confirmation of design procedures are still continuing worldwide.

1.2 Objective and Scope of Research

The objective of this research is to evaluate the shear resistance effectiveness of proposed embossment patterns of varying depths for Vulcraft's 2VLI and 3VLI deck by performing full-scale slab tests and to compare the test results with different design and strength prediction procedures. The study will result in a recommendation of which type of embossment to pursue for further development.

A series of twenty full-scale slabs consisting of a set of tests for the 2 in. deep deck (2VLI) and another set for the 3 in. deep deck (3VLI) was tested to failure. Each full-scale test set consisted of two specimens for each of the four proposed embossment types and for the existing embossments type.

The design and strength prediction methods evaluated were: 1.) the First Yield method (Heagler 1992) 2.) the ASCE Appendix D alternate procedure (*Standard* 1992) and 3.) Widjaja's (1997) Iterative Method using shear resistance test data. A series of twenty-three shear bond tests was performed (a minumum of two specimens for each type of deck) to obtain the shear resistance data used in Widjaja's Iterative Method.

1.3 Overview

This thesis is organized as follows. Chapter two contains a summary of previous and current research on the design, testing, and behavior of composite slabs. The summary is limited to slabs with only steel deck and concrete (excludes factors such as additional reinforcing, end restraint, shear studs, etc.) and focuses on the shear bond failure mode. Chapters three and four describe the shear bond test and full-scale slab test procedure and results, respectively. Chapter five contains a brief summary of the following design and

strength prediction methods: 1.) the First Yield method 2.) the ASCE Appendix D alternate procedure and 3.) Widjaja's Iterative Method using shear resistance test data. The composite slab strengths given by these different methods are then compared with the full-scale slab test results and evaluated for suitability. Chapter six contains a summary and conclusions with some recommendations for further research.

CHAPTER 2: LITERATURE REVIEW

The development of composite steel deck began in the 1950's. Composite floors are systems in which the steel deck acts as the primary tensile reinforcement because there is some form of mechanical interlocking between the steel and concrete. Granco Steel Products introduced the first composite deck: "COFAR," which used steel wires welded to the web of the deck to transfer shear. The practice of welding decking greatly raised construction costs, causing manufactures to look to other mechanical shear transfer devices. In the 1960's companies began developing easily installable and completely shop manufactured deck profiles with mechanical interlocking capabilities. The two basic deck profile types are trapezoidal and re-entrant, as illustrated in Figure 2.1. Some manufacturers pressed indentations or embossments of various shapes into the deck to provide shear resistance. The addition of shear studs also aids composite action. (Heagler et al 1992)

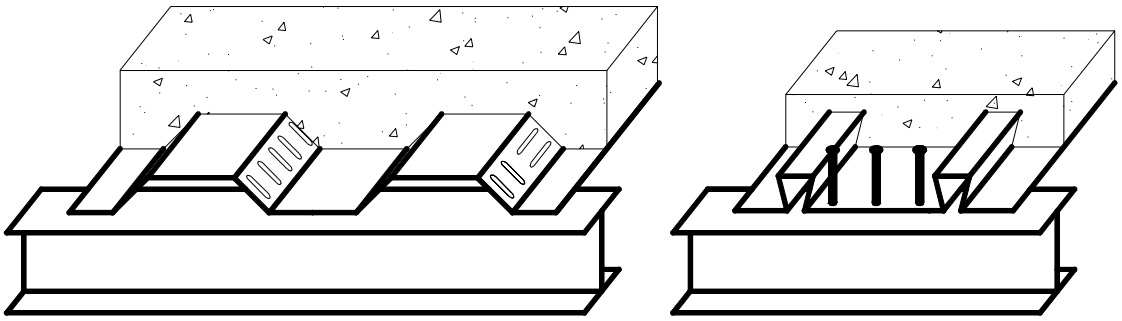

Figure 2. 1 Typical Types of Composite Deck and Shear Transfer Devices

Since the inception of composite deck, many institutions have investigated its behavior. In the early stages, as manufacturers created new deck designs, they had to determine the strength of their product experimentally by performing numerous full-scale tests. These tests were costly and tedious because they had to be very specific to the

configurations under consideration (concrete strength, gage of deck, profile shape, etc). (Seleim 1979)

In 1967 the American Iron and Steel Institute (AISI) sponsored research at Iowa State University to develop a standard design procedure for composite slab floors. Ekberg directed the testing of 353 full-scale composite floor specimens with various configurations. From the performance of the tested slabs, Porter and Ekberg (1975; 1976) made numerous observations on the behavior of composite slabs. They determined that failure occurs in three modes:

1. longitudinal shear bond failure
2. flexure of an under-reinforced section
3. flexure of an over-reinforced section

Other researchers later added vertical shear as a possible mode of failure, but it is rarely attained before the other modes (Daniels and Crisinel 1988). Longitudinal shear failure is "characterized by the formation of a diagonal tension crack in the concrete at or near one of the load points followed by end-slip at one end." (Porter and Ekberg 1975) The distance from this crack to the support is called the "shear span," L', as shown in Figure 2.2. Because there is only partial shear connection between the steel deck and the concrete slab, the system cannot reach its full bending strength. Flexural failure at full bending strength occurs only when there is complete interaction between the concrete and steel components. As in traditional reinforced concrete theory, flexural failure can occur due to concrete crushing (over-reinforced) or steel yielding (under-reinforced). (Porter and Ekberg 1976)

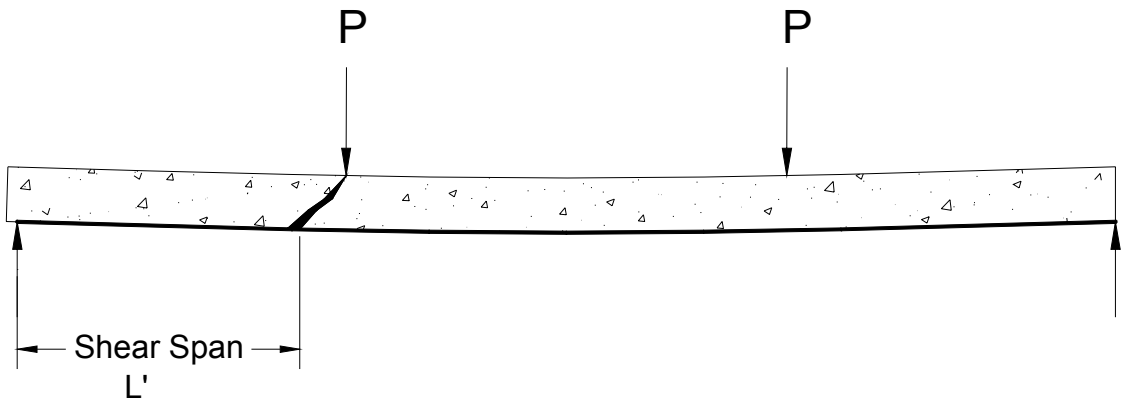

Figure 2. 2 Shear Span

Numerous tests have shown that longitudinal shear failure is most often the governing mode (Porter and Ekberg 1975; 1976; Ong and Mansu 1986). Therefore, shear bond strength is the focus of much of the research. The sequence of shear bond failure with increasing loads occurs as follows (Seleim and Schuster 1985):

1. Shear transfer devices are completely effective
2. Cracking initiates at the critical section, increasing the difference in stress of the concrete and the deck, which increases the bond stress, further increasing cracking. The deck and slab begin to separate, lessening the effectiveness of the embossments.
3. Shear transfer devices fail completely, resulting in end slip.
4. The degree of cracking is unacceptable and the shear span is completely separated from the deck at ultimate load.

The result of the research at Iowa State and later research at the University of Waterloo was the development of three proposed shear bond design equations.

Schuster:

$$\frac{V_u s}{b d} = m\frac{d\sqrt{f'_c}}{L'} + k\rho \qquad \text{(Schuster 1970)} \qquad (2\text{-}1)$$

Porter and Ekberg:

$$\frac{V_u s}{b d} = m\frac{\rho d}{L'} + k\sqrt{f'_c} \qquad \text{(Porter and Ekberg 1975; 1976)} \qquad (2\text{-}2)$$

Seleim:

$$\frac{V_u}{b d} = k_1\frac{t}{L'} + k_2\frac{1}{L'} + k_3\ t + k_4 \qquad \text{(Seleim 1979)} \qquad (2\text{-}3)$$

where:

V_u = ultimate transverse shear-bond resistance (per unit width)

b = unit width of slab

d = effective slab depth

s = spacing of shear transferring devices

m, k = determined experimentally

ρ = reinforcement ratio, $\frac{A_s}{b\,d}$

L’ = length of shear span

f’$_c$ = concrete compressive strength

The shear span, L', is the critical slab length over which longitudinal shear failure occurs. L' for a slab that has a uniformly distributed load is determined by equating the area of the shear diagram for a concentrated load case to that of a uniform load case, with the support reactions being equal. L' is commonly taken to be one-fourth the total span length for a uniformly loaded slab, but some researchers argue that it should be one-third the total span length (Tenhovuori et al 1996; Veljkovic 2000). For a two-point concentrated load case, the shear span is the length from the support to the point load. (Porter and Ekberg 1975; 1976)

Equations 2-1 and 2-2 above are in the familiar form of an equation for a straight line: "y = mx + k" where "m" represents the slope and "k" represents the y-axis intercept. These methods require the plotting of the behavior of a series of full-scale slab tests for one particular type of deck (characterized by factors such as geometry, embossment pattern, surface conditions, yield strength of steel, unit weight of concrete, deck thickness, and deck width), while varying the shear span and/or reinforcement ratio, on a set of axes that includes the contributing parameters of the specimen. The third method is similar but also considers the effect of varying the deck thickness. Test data should cover a range of x-axis and y-axis values for a better representation of the deck's behavior. Porter and Ekberg (1976) recommended using data points from at least eight tests of each deck thickness and product type. A linear regression of the data gives values for "m" and "k" and a multi-linear regression analysis gives values for $k_{1,\,2,\,3,\,4}$. Substitution of these values into the above equations gives predictions of the strength of slabs whose parameters correspond to intermediate points on the graph, which may not have actually been tested.

Seleim and Schuster (1985) evaluated the above equations with test data from 196 experiments conducted at Iowa State University and the University of Waterloo. They compared three sets of data: 1.) specimens with the same deck thickness but varying

product type whose characteristics such as embossment patterns varied 2.) specimens of the same product but with varying deck thicknesses, and 3.) specimens of the same product and thickness, but a varying shear span length. All three shear bond equations gave slab strengths that correlated well with the experimental results in the first comparison set. In the second comparison set, Seleim's equation gave the best correlation, which explains the constraint for the first two equations that the deck thickness should remain constant while creating the linear regression plot for a particular type of deck. The third comparison set evaluated only results from Seleim's equation, which gave correlation to test results within a 15% band. Seleim and Schuster concluded that neither the reinforcement ratio nor the compressive strength of concrete has a significant influence on the shear bond resistance, but deck thickness was a governing parameter. (Seleim and Schuster 1985)

Although the above methods proved effective in predicting experimental strengths, there was debate that the simple span laboratory tests did not accurately represent continuous slabs in buildings. Composite slabs in the field would have additional shear resistance because continuity of the spans would resist slip. In the early 1970's the Steel Deck Institute sponsored research at West Virginia University to better predict composite slab strengths in the field. This research involved testing 25 slabs (both single span and two-span continuous) of varying width in which embossed deck acted as the only reinforcing. The embossments were generally horizontal or vertical. The analysis was based on the limitation of stresses at the extreme fibers and on the consideration of shear bond failure. (Luttrell and Davison 1973)

Luttrell performed an exhaustive analysis on the results of these and other experimental tests from eighteen years of testing at West Virginia University. Failure of the embossed decks occurred more gradually than plain deck: the slab continued to sustain load even after slip initiated. He postulated that the embossments not only increased strength by providing mechanical shear resistance, but also increased the stiffness of the webs. Greater web stiffness increased the resistance to over-ride, which occurs when the concrete moves vertically to go over the deck as it slips horizontally. Deeper embossments and thicker decks also improved this resistance. He remarked that deeper decks tended to have greater vertical separation when slipping horizontally.

Deeper slabs also seemed to provide better shear resistance allowing it to more closely approach full bending capacity. (Luttrell 1987)

Luttrell also made some observations regarding the end conditions of the slab specimens. He determined that continuous specimens did have capacities about 10%-15% greater than simple span specimens. The use of shear studs did significantly increase strength. (Luttrell 1987) The investigation of end anchorage conditions later continued at Virginia Tech with multi-span tests consisting of different end conditions such as pour-stop, shear studs, and a welded angle. These end anchorage devices did improve performance. If the system had a sufficient number of shear studs, the slab did attain its maximum plastic bending capacity. (Easterling and Young 1992; Terry 1994)

Luttrell observed that the three phases of shear resistance are sequential, not additive and occur in the following order: 1.) Chemical bond 2.) mechanical resistance from embossments and friction and 3.) shear studs (if applicable). He echoed Seleim's observation that shear resistance had little dependence, if any, on f'_c. (Luttrell 1987) Later, Daniels (1988) and Bode and Sauerborn (1992) also made this conclusion. Luttrell contributed this lack of dependence on the fact that the failure rarely occurs because of concrete crushing, but instead occurs when the deck flexes away from the concrete (Luttrell 1987).

When comparing decks with embossments of mostly vertical shape versus mostly horizontal, Luttrell concluded that the vertical embossments are almost 50% more effective in shear resistance than the horizontal ones. The decks with only horizontal embossments did not sustain much load after the chemical bond was destroyed. However, the horizontal embossments helped resist vertical separation, thereby also contributing to composite interaction. (Luttrell and Davison 1973; Luttrell 1987)

Stark (1978) also experimentally investigated the behavior of composite slabs. He classified slabs to be either ductile or brittle. Brittle behavior occurs when the maximum flexural strength is reached soon after shear failure or slip initiates. The sustained load drops suddenly. A ductile slab, however, continues to sustain load even after slip initiates. The curvature of the slab increases and the steel and concrete components no longer have a common neutral axis. The European code later specifically defined ductile behavior as occurring when the failure load is greater than 110% of the

load at first slip (Eurocode 4). First slip was defined by Veljkovic (1994a) to be 0.5 mm ≈ 0.02 in.

Stark also determined that decks with re-entrant geometries are beneficial because they prevent vertical separation of the deck and concrete. Another means of improving shear resistance is to use shear studs to connect the deck to the supporting members. Lack of lateral support in the test specimens seemed to cause instability of the deck webs at the edges of the slab, resulting in earlier failure. Slabs in the field would have lateral support from neighboring sections. (Stark 1978)

Three components comprise the shear bond resistance: friction, chemical adhesion, and mechanical interlocking. Friction effects are greatest at the supports where the normal force is the greatest, but friction also acts along the span for decks with re-entrant geometries. (Veljkovic 1994a, Schuurman and Stark 1996) When unknown, the coefficient of friction can be taken as 0.5- 0.6 (Kitoh and Sonoda 1996; Bode and Dauwel 1999). Chemical adhesion is brittle and difficult to predict since it depends on the curing process of the concrete and the surface conditions of the deck. Mechanical interlocking is resistance to slip due to obstacles such as embossments in the deck, transverse wires welded to the deck (a practice no longer used due to cost), fabricated holes in the deck webs, or shear studs.

Luttrell and Prasannan (1984) reconsidered the assumption that in the flexure mode, the slab behaves like a reinforced concrete section with the deck's tensile force acting at its centroid. They argued that the steel deck behaves differently than embedded reinforcing bars because the deck is only bonded on one surface and is free to deflect on the other surface. Therefore the geometry of the deck has a great effect on the shear resistance. They developed Equation 2-4 below for the ultimate moment capacity based on a transformed area and by dividing the tensile force of the deck to each of the flanges (T_1, T_3) and the web (T_2) separately. This procedure gives three tensile forces with their respective moment arms (y_1, y_3, y_2), as shown in Figure 2.3. This development is particularly advantageous for predicting the performance of a newly created deck without having to perform numerous costly full-scale tests.

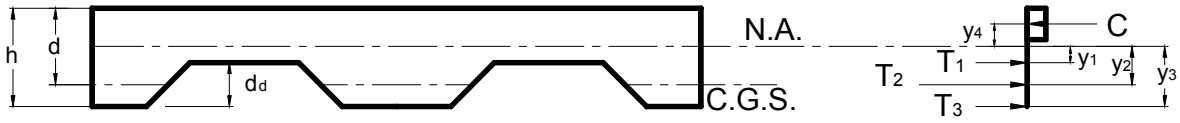

Figure 2. 3 Slab Section and Force Distribution (Luttrell and Prasannan 1984)

$$M_f = T_1 y_1 + T_2 y_2 + T_3 y_3 + C y_4 \tag{2-4}$$

To include effects from shoring removal:

$$M'_f = M_f - M_s \tag{2-5}$$

M_s = shoring removal moment

The resulting moment capacity available for applied load is:

$$M_t = K\, M'_f - k_4 S' \tag{2-6}$$

S' = shear span reduction, L/2 - L'

$$K = \frac{k_3}{k_1 + k_2} \tag{2-7}$$

k_1 and k_2 correspond to the embossment quality and other deck parameters. k_3 describes the number of embossed shear planes available for shear transfer. k_4 accounts for the influence of the shear span and depth of deck.

Other researchers continued to study the behavior of the full-scale specimens, making the following additional observations:

- Flexural failure occurred in specimens with very long shear spans, corresponding to low shear stress values and plastification of the deck. Behavior was ductile. (Daniels 1988; Daniels and Crisinel 1988)
- Specimens that failed in horizontal shear were ductile when the shear span was longer (Daniels and Crisinel 1988).
- Webs deformed elastically at ultimate moment. Some concrete crushing may occur for very deep embossments. (Daniels and Crisinel 1988)
- Plain, unembossed Australian decks Condeck and Bondeck failed significantly before full plastic capacity, demonstrating the need for embossments or end anchorage (Patrick and Bridge 1988)

- Location of the concentrated loads had a greater effect on behavior than the number of loads (Daniels and Crisinel 1993)
- Of the component material properties, deck yield strength had the greatest influence on strength. (Daniels and Crisinel 1993)
- Greater slab depths had greater longitudinal shear resistance (Tenhovuori and Laeskela 1998)

Full-scale specimens are very costly and time-consuming to test, so attention turned to the development of small-scale tests. The intent of these smaller specimens was to test the shear bond specifically, which consistently was the governing mode of failure. The development of shear bond tests stemmed from existing push-off tests that measure the shear connection between a slab and a girder in composite systems. Different researchers developed their own configuration for the test as shown in Figure 2.4. The test set-ups all consisted of concrete cast onto the steel deck and the application of a load to shear the concrete off the deck. The shear resistance of the specimens was displayed in graphs of the end slip versus shear load.

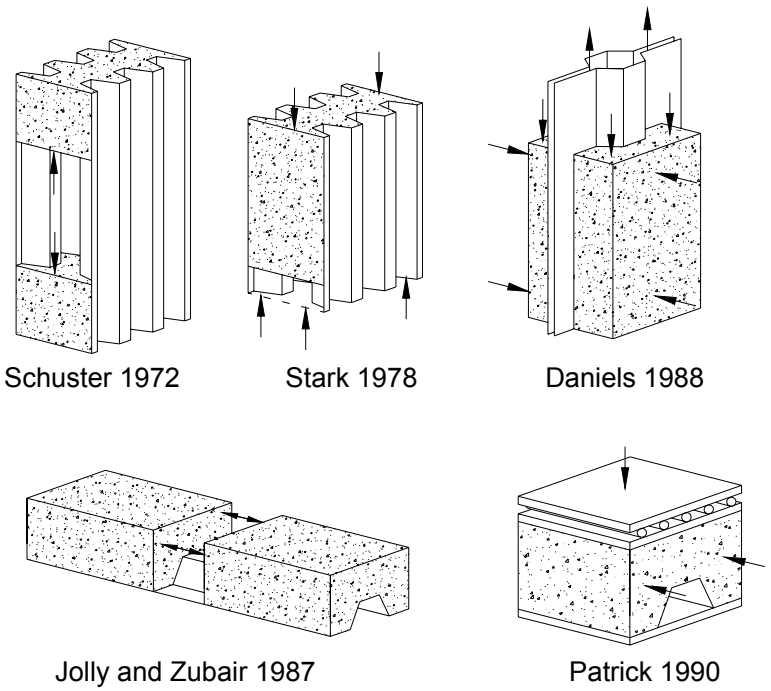

Figure 2. 4 Various Shear Bond Tests

Shear bond tests are particularly useful for comparing different mechanical interlocking devices in the development of a new deck product. Daniels (Daniels 1988; Daniels and Crisinel 1988) investigated the shear strength of several manufacturers' product using his pull-out test. The tested specimens included embossed deck with re-entrant geometries and open-rib geometries. The applied lateral force could be either deflection controlled or force controlled. Daniels recommended future tests to be force-controlled and that the magnitude of the lateral force should correspond to the weight of at least 10 cm of concrete cover to simulate the full-scale conditions. Application of greater lateral forces gave higher shear strengths since it increased the frictional resistance.

Daniels (1988) made several conclusions from his tests results. The behavior of the shear stress-slip graph was consistent for each specimen of the same product type and embossment. The shape of the graph indicates that the chemical bond acts first and then the mechanical bond due to the embossments. He developed equations for determining shear stress at the deck-concrete interface of full-scale specimens by assuming linearly varying shear before the initiation of end slip, and a uniform shear after the initiation of end slip. These values can be compared to the shear strength given by shear bond tests. The measured strength of the chemical bond was inconsistent but was reasonably similar to that determined from full-scale tests. Crisinel and Schumacher (1999; 2000) also later noted this inconsistency. Daniels (1988) described the mechanical bond given by the pull-out tests to be reasonable and conservative although the differences were significant. He also observed ductile and brittle behavior in the test specimens. Ductile specimens had significant post-slip capacity while the brittle specimens had a large initial slip, but then could not sustain additional load. This behavior corresponds to that of full-scale slab test specimens.

Several other researchers have considered the effect of deck and embossment parameters using shear bond tests. A summary of their findings is as follows:

- Embossments with the greatest vertical face against the concrete were the most effective in shear resistance, even if that face did not have the greatest overall vertical height. Faces that are perpendicular to slip are more effective than

inclined faces. (Jolly and Zubair 1987) V-shaped and straight embossments behave similarly (Makelainen and Sun 1998).

- Discontinuities of embossment shape (such as a cross) caused more flexibility of the deck, promoting concrete over-ride (Jolly and Zubair 1987).
- Increasing embossment frequency, which required decreasing size did not improve shear resistance (Jolly and Zubair 1987).
- Increased embossment depths were most effective, but caution should be taken against tear during production. Depth was the most influential shape factor. (Jolly and Zubair 1987; Makelainen and Sun 1998, and Crisinel and Schumaker 2000)
- The optimal embossment location was at the middle of the web. Embossments at the corner of the web and flange were very difficult to construct and did not display much improvement in shear resistance. Embossments in the tension flange flattened upon loading, decreasing their effectiveness. Those in the compression flange acted as initial deformations, which promote buckling. (Jolly and Zubair 1987, Makelainen and Sun 1998)
- Increasing embossment length increased performance, but there seemed to be a length limit when improvement ceased (Makelainen and Sun 1998).
- Penetrant embossments greatly improved shear resistance by the concrete that entered the holes (Makelainen and Sun 1998).
- Increased deck thickness also improved shear resistance (Jolly and Zubair 1987, Makelainen and Sun 1998).
- Re-entrant profiles improved performance by 63%-88%, with a linear dependence of performance verses the area of concrete under the re-entrant portion. However, unembossed deck of this type still provided only 50% the shear strength of embossed deck. (Wright and Essawy 1996).
- A study of flat plates with embossments showed failure occurred by bearing due to the local crushing of concrete when the embossment height to spacing ratio was less than 0.10. When this ratio was greater than 0.19, the specimen failed in concrete shearing at a plane that extends from the top of one embossment to the next. (Kitoh and Sonoda 1996)

SDI compiled the results from numerous research projects and developed a composite slab design procedure based largely on recommendations made by Porter and Ekberg (1976). SDI's design procedure was verified by research at Lehigh University, Virginia Tech, and Iowa State University, each finding M_{test}/M_n ratios between 1.01 and 1.31 (Heagler et. al 1992).

A summary of the ASCE design standards for composite slabs follows. The Steel Deck Institute has also adopted the under-reinforced capacity and longitudinal shear failure equations in their design standards. Loads due to casting act on the noncomposite deck. The capacity available for live loads is the full capacity minus casting stresses.

Flexural failure

Flexural failure occurs when the slab has full composite interaction. This mode of failure is divided into under-reinforced slabs or over-reinforced slabs. The balanced steel ratio for determining under or over-reinforced conditions is:

$$\rho_b = \frac{0.85\,\beta_1 f'_c}{F_y}\left[\frac{\varepsilon_s E_s (D - d_d)}{(\varepsilon_s E_s + F_y) d}\right] \qquad (2\text{-}8)$$

β_1 = 0.85 for concrete with f'_c < 4,000 psi

(reduced at a rate of 0.05 for each 1,000 psi of strength over 4,000 psi to a minimum of β_1 = 0.65)

f'_c = concrete compressive strength

F_y = minimum yield stress of deck (not to exceed 60,000 psi)

ε_c= maximum concretecompressive strain (0.003)

D = nominal total slab depth

E_s = modulus of elasticity of steel deck

d_d = depth of deck

d = distance from top of slab to centroid of steel deck

Under-reinforced capacity ($\rho<\rho_b$):

$$\phi M_n = \phi A_s F_y \left(d - \frac{a}{2}\right) \qquad (2\text{-}9)$$

ϕ = 0.85 (0.65 when f_u/f_y < 1.08)

M_n = nominal moment capacity

A_s = deck area per unit width

a = depth of compressive stress block

However, caution should be used when applying Equation 2-9 to decks deeper than 3 in. This equation assumes the full section of the deck yields, but a deep deck may not have adequate ductility to reach full yield of the entire section before the concrete crushes. (Sabnis 1979)

Over-reinforced capacity ($\rho > \rho_b$) as recommended by Porter and Ekberg (1976):

$$\phi M_n = \phi \frac{0.85 \beta_1 f'_c b d^2 k_u}{12} \left(1 - \beta_2 k_u\right) \tag{2-10}$$

ϕ = Flexural capacity reduction factor, = 0.70

β_2 = 0.425 for $f'_c < 4{,}000$ psi

(reduced at a rate of 0.025 for each 1,000 psi of strength over 4,000 psi)

b = unit width

$$k_u = \sqrt{\rho \lambda + \left(\frac{\rho \lambda}{2}\right)^2} - \frac{\rho \lambda}{2} \tag{2-11}$$

$$\lambda = \frac{E_s \varepsilon_u}{0.85 \beta_1 f'_c} \tag{2-12}$$

ρ = reinforcement ratio, $\frac{A_s}{b\,d}$

ε_u = compressive strain in concrete at ultimate strength (0.003)

Longitudinal Shear Failure

This method is based on the Porter and Ekberg (1975) m-k method described earlier that uses graphs of data from full-scale simple span slab tests. A typical graph is shown in Figure 2.5. The design reduces the regression line by 15% to account for scatter of the test results.

no shoring :

$$\phi V_n = \phi \frac{b\,d}{s} \left(\frac{m \rho d}{L'} + k \sqrt{f'_c}\right) \tag{2-13}$$

shoring:

$$\phi V_n = \phi \frac{d}{s}\left[\left(\frac{m \rho d}{L'} + 12 k \sqrt{f'_c}\right) + \frac{\gamma W_1 L}{2}\right] \quad (2\text{-}14)$$

ϕ = strength reduction factor , = 0.75

V_n = nominal shear-bond strength (per unit width)

b = unit width of slab

d = effective slab depth

m = slope of reduced experimental shear-bond line

ρ = reinforcement ratio, $\frac{A_s}{b\,d}$

L' = length of shear span (¼ L for uniformly loaded slabs)

k = coordinate intercept of reduced experimental shear-bond line

f'_c = concrete compressive strength

γ = coefficient for the proportion of dead load added upon removal of shore

W = wind load perpendicular to slab

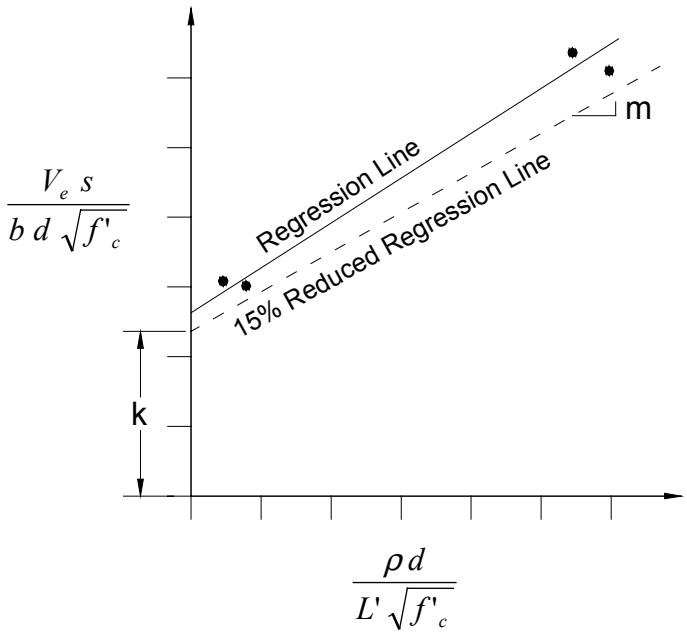

Figure 2. 5 Typical m-k Graph (Porter and Ekberg 1975)

ASCE also includes an alternative method of design in Appendix D of the Standard, which was based on Luttrell's design recommendations that the tensile forces should be divided into components at each of the deck flanges and at the web. Design capacity is determined to be when the bottom flange of the deck first reaches yield stress. Application of a modification factor, K, adjusts the tension force to be equal to the shear bond strength, which is determined by the properties of the deck and its embossments. This "first yield" strength may be increased by 10% if the slab contains welded wire fabric reinforcement. (Luttrell and Prassanan 1984).

The Eurocode 4 delineates Europe's design procedures. These procedures are very similar to the U.S. standards, but include an additional method for determining capacity limited by longitudinal shear strength, called the "Partial Shear Connection Method" (PSC) or the "τ- Method" (Stark 1991). This method stems from the partial connection method used for composite beams and is applicable only for ductile specimens. Patrick developed the basis for this method in 1990, using constitutive laws to determine the stress distribution along the cross-section (Patrick and Bridge 1990). PSC is preferred over the m-k method because it is mechanically based and more intuitive for the designer. It is also advantageous because it gives behavior that is specific to the loading conditions. Because it is mechanically based, it is possible to include end anchorage effects such as continuity, frictional forces, and shear studs, as described by numerous researchers (Bode and Dauwel 1999; Bode and Sauerborn 1992; Schuurman and Stark 2000). This method also allows the incorporation of increased strength due to additional reinforcing bars. (Stark 1991, Bode and Sauerborn 1992)

The Partial Shear Connection method uses the development of a graph showing moment capacity versus degree of shear connection, as shown in Figure 2.6. The design capacity is determined as follows:

$$M_{p.Rd} = N_c \; z + M_{pr} \qquad (2\text{-}15)$$

$M_{p.Rd}$ = Design resistance

N_c = tensile force in the deck

z = lever arm between compressive and tensile forces

M_{pr} = bending capacity of noncomposite deck

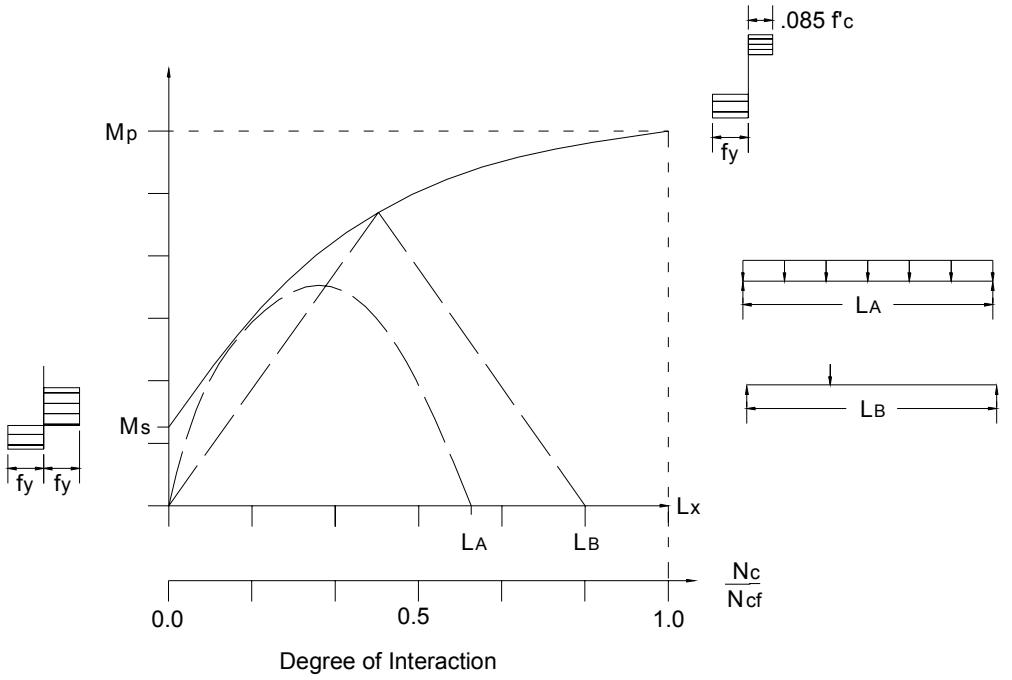

Figure 2. 6 Partial Interaction Diagram (Bode and Sauerborn 1992)

It is necessary to perform a series of full-scale slab tests of the type of deck under consideration to determine the shear bond capacity, τ_u given by:

$$\tau_u = \frac{\eta N_{cf}}{b(L_s + L_o)} \tag{2-16}$$

The characteristic shear strength $\tau_{u.Rk}$ is the minimum experimental value reduced by 10% and divided by a partial safety factor for bonding resistance of γv =1.25. The construction of design graphs is based on equilibrating the compressive and tensile forces and requires the use of a computer analysis. Slabs with end anchorage would have design plots that are shifted horizontally by an amount that represents the percent of total shear resistance that the end anchorage device contributes. The partial shear connection method gives slab designs that are more economical than those given by the m-k method. (Bode and Sauerborn 1992, Bode and Dauwel 1999, Stark 1991)

More recent research has determined some deficiencies in the prescribed PSC method. Its applicability is limited to ductile slabs only, a constraint that especially must be checked for short span slabs which tend to be brittle. Testing of full-scale slab

specimens, which is an expensive and time-consuming process, is still necessary for determining the shear bond strength. The experimental shear strength depends on the degree to which the shear resistance is developed, which is dependent on the loading conditions of the test. Therefore, selection of the loading configuration must be made carefully. (Veljkovic 2000)

Widjaja (1997) at Virginia Tech used the Partial Shear Connection theory to develop two strength methods that preclude the use of full-scale slab tests by using only shear stress versus slip data from shear bond tests similar to Daniels'. These Methods are the Iterative Method and the Direct Method. Widjaja converted the test data into a shear resistance distribution along the span length of a full slab specimen. Effects from clamping forces at the support were ignored. The Iterative Method involved determining the strength of the slab by considering the location of the critical section at which cracking initiates. Because this method determined the strength of the slab throughout its loading history, an elasto-plastic model described the stress distribution at the face of a cross-section instead of a plastic model. The concrete strain is determined from its relationship with the slip between the deck and the concrete. This method is different from Patrick's PSC method because it considers the remaining noncomposite strength of the deck beyond the shear bond transfer strength. The Direct Method determines the strength of the slab only at failure by summing the moments due to the forces transferred in shear between the steel and concrete and then adding the remaining noncomposite deck strength. The shear force transferred is determined from the shear bond tests.

Calixto and his colleagues (1998) developed a new design equation for the PSC method that separates the contribution of friction from mechanical interlocking. Although the equation is slightly more complex, it better describes the behavior of the specimen. The resulting design strengths were more accurate and more closely corresponded to those given by the m-k method.

Schuurman and Stark (2000) are currently developing a new model for the longitudinal shear distribution that includes the increased friction at the supports instead of considering shear to be uniform along the span length. This model uses three parameters: shear at the support, shear away from the support, and the distance over

which the increased support shear acts. Because these parameters are difficult to determine, it is still too early to use this model in a design method.

Veljkovic (1994a; 1994b; 1996; 2000) developed a modified version of the Partial Shear Connection method that is applicable to ductile or brittle slabs and accounts for different loading conditions by using a "transfer length" instead of shear span. Confirmation of this method is still underway. Results from three different shear bond tests describe the shear resistance parameters of the specimen. A "push test" gives the mechanical interlocking behavior, a "tension-push test" determines the reduction of shear strength due to flattening of the embossments under tension, and the "friction test" determines the coefficient of friction. A distribution function used with the results from these tests describes the varying shear bond behavior along the span length. A finite element model uses this distribution to simulate the full-scale slab and determine the average longitudinal shear stress at failure. The model considers how cracking of the concrete affects the shear distribution. Veljkovic uses two correction coefficients to transform the complex behavior given by the finite element model into a simple model easily computed by hand. Use of his design equations gives three points that make up a flexural resistance envelope along the span length, which is applicable to simple span slabs.

Several other researchers have utilized finite element analysis to model slab behavior. Veljkovic used shell elements in his finite element model, but others used the method of layered beams (Tenhovuori and Leskela 1998), or other layer approaches (Sebastian and McConnel 2000). These methods are still under development, but are useful for illustrating behavior.

Daniels and Crisinel (1988; 1993a) developed a numerical analysis method that experimentally requires only shear bond tests and is applicable to continuous and single span slabs. The advantage is that this method does not require full-scale slab tests. A "pull-out test" gives the embossment resistance and a "push-off test" gives the end anchorage resistance. The model makes simplifications and assumptions to the material properties, but accounts for nonlinear material behavior and slip between the concrete and deck. Two parameters define the behavior of each cross section: axial force and curvature. The axial force is the sum of the shear forces in the concrete or deck

components. A nonlinear partial interaction finite element analysis then estimates the behavior of the slab under load. The user increases applied load until numerical instability occurs, which indicates failure. Results from this numerical analysis compared very closely with the existing PSC method and the m-k method.

Crisinel and Schumacher (1999; 2000) are currently developing a "New Simplified Method" which is not dependent on full-scale tests or numerical simulations. The basis of this method is to create a tri-linear moment-curvature plot at the critical section of the slab. The three lines represent three phases: 1.) Linear elastic behavior: full interaction of the concrete and deck, and no concrete cracking or slip 2.) Elastic or elasto-plastic behavior: concrete cracking and slippage begins, but the specimen still has full interaction and 3.) Nonlinear elasto-plastic behavior: concrete has cracked, there is slip, and there is only partial interaction between the concrete and deck. Brittle specimens should fail at the end of region 2, which corresponds to failure of the chemical bond. Ductile specimens should fail at the end of region 3, which corresponds to the failure of the mechanical bond. This method proved less accurate for brittle specimens since chemical bond is very inconsistent, but proved to correspond well to experimental results for ductile specimens.

CHAPTER 3: SHEAR BOND TESTS

3.1 General

To evaluate the effectiveness of Vulcraft's embossment configuration options, it was necessary to study their effectiveness in mechanical shear resistance. An economical way to do this was to perform elemental shear bond tests, which determined the relationship between applied shear force and slip of the concrete with respect to the steel deck. A comparison of the shear resistances of the deck specimens with varying shear transfer devices showed which deck was predicted to be optimal for overall strength. Furthermore, some analytical methods convert the shear bond resistance into a prediction of the strength of a full-scale slab as described in Chapter 5. This is a much more cost-effective strength prediction method than performing numerous full-scale slab tests.

3.2 Test Parameters

Two sets of specimens were tested: 2VLI deck (2 in. deep) and 3VLI deck (3 in. deep). The dimensions of the deck profiles are shown in Figure 3.2.1. The only parameter that changed between the specimens in each set was the embossment pattern. All specimens consisted of 0.035 in thick (20 gage) steel deck. The 2 in. deck specimens had a steel yield stress of 52.5 ksi and concrete compressive strength of 3.5 ksi. The 3 in. deck specimens had a steel yield stress of 52.7 ksi and a concrete compressive strength of 3.4 ksi. Concrete compressive strengths were determined from compressive tests of 4 in. x 8 in. cylinders according to ASTM C39-96 procedure. Steel deck yield was given by the manufacturer and verified by tensile coupon tests performed according to ASTM E8-00b procedure.

Both sets of test specimens had five types of embossments:

1. Existing embossments, depth = 0.100 in. (in only)
2. Proposed Diagonal, depth = 0.100 in. (in only)
3. Proposed Diagonal, depth = 0.125 in. (in only)
4. Proposed Diagonal, depth = 0.125 in. (in and out)
5. Proposed Diagonal, depth = 0.140 in. (in and out)

The embossments of the first three types were rolled in towards the face of the concrete. The embossments of the last two types were rolled both in towards the face of the concrete and out away from the concrete face, for the overall depth given. Figure 3.2.2 shows the typical embossment types and Table 3.2.1 shows their respective dimensions.

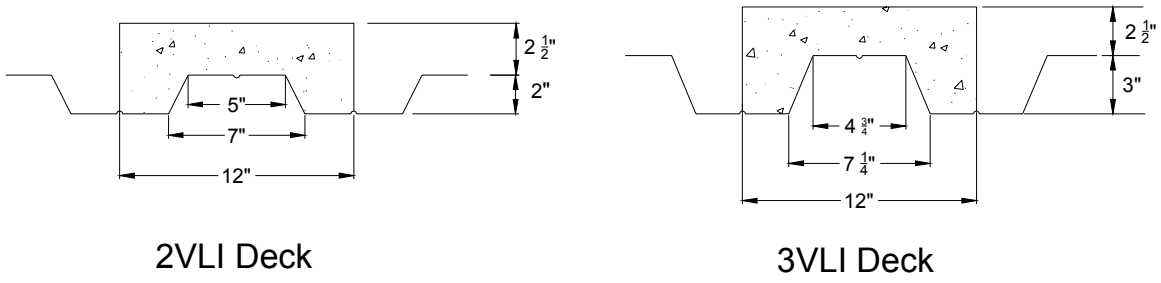

Figure 3.2.1 Deck Profile Dimensions

Table 3.2.1 Embossment Dimensions

	2" Existing		2"	3" Existing		3"
	Vertical	**Horizontal**	**Diagonal**	**Vertical**	**Horizontal**	**Diagonal**
Nb (in.)	0.67	1.85	1.443	2.31	1.77	2.598
Nt (in.)	1.59	1.57	1.550	2.01	1.47	2.309
Wb (in.)	0.68		.506	0.56		0.506
Wt (in.)	0.25		.360	0.35		0.360
Spacing (in.)	3.40		1.00	3.40		1.00

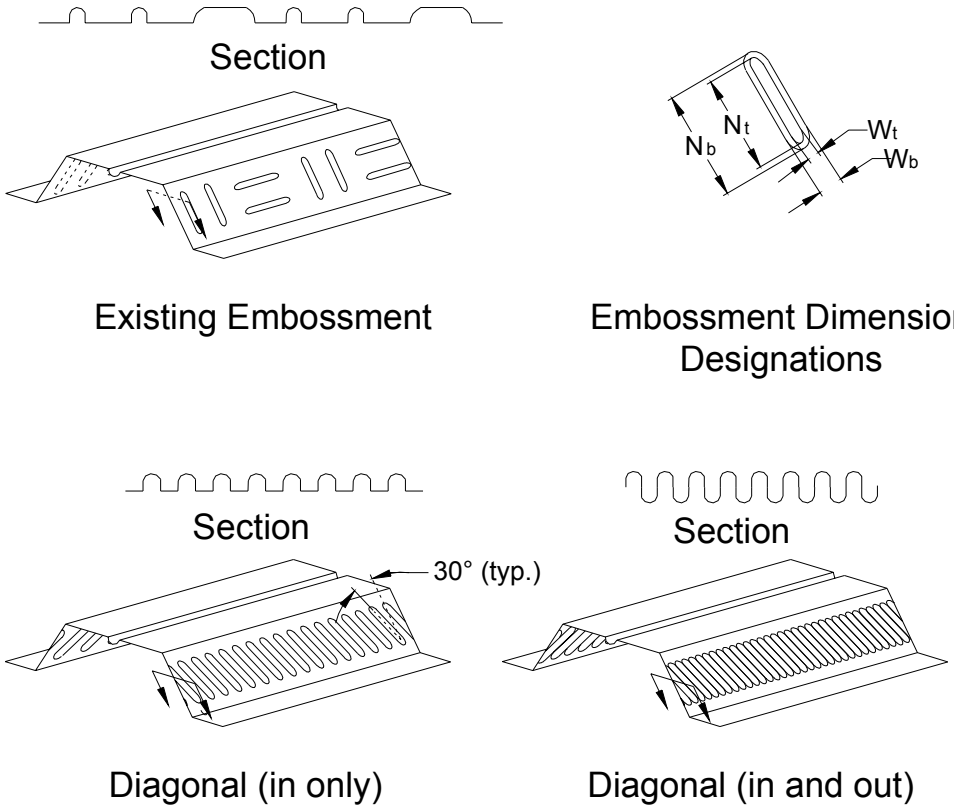

Figure 3.2. 2 Embossment Types

3.3 Test Set up and Instrumentation

The test specimens were prepared in halves consisting of normal weight concrete cast on steel deck, which were bolted to a ¼ in. thick steel plate. The steel plate acted to stiffen the deck and prevent bending of the specimen during handling. The concrete portion was 2 ft long by 1 ft wide to include a representative portion of the deck profile. The concrete depth was 2.5 in. greater than the depth of the deck. To simulate the construction procedure of full-scale slabs, the specimens were cast horizontally. After 7 days, the formwork was stripped and the specimens were raised into a vertical position. The two halves of each test specimen were then bolted together at the edges of the steel plates. Banding strips were placed around the specimens to preserve their chemical bond during the remaining 21 days of curing. The specimens were cast in two sets: all 2 in. deck specimens and then all 3 in. deck specimens.

When a specimen was ready to be tested, a potentiomer was attached to the underside of the deck of each specimen half. An angle was screwed into the bottom surface of concrete and attached to the end of the potentiometer so that slip between the deck and the concrete could be measured.

A photograph of the test set up is shown in Figure 3.3.1 (a). The specimen was hung by a rod such that the top concrete surface was flush against steel plates in the frame that had been cut to fit around the profile of the deck shown in Figure 3.3.1(b). A manually pumped hydraulic jack raised the rod and deck, while the frame resisted vertical movement of the concrete portion, thereby imposing shear between the deck and concrete. The rod had been instrumented with strain gages and was calibrated as a load cell, therefore allowing the shear load to be measured and recorded during the tests.

Two small frames were clamped onto the test specimen as shown in Figure 3.3.2, providing a lateral pressure that induces frictional resistance present in full-scale specimens. Each lateral frame had a load cell that measured the applied lateral load as shown in Figure 3.3.3. The magnitude of this load could be adjusted by tightening or loosening nuts at the ends of the rods. Another set of threaded rods extended from the lateral frames to the test frame to brace the specimen from rotating.

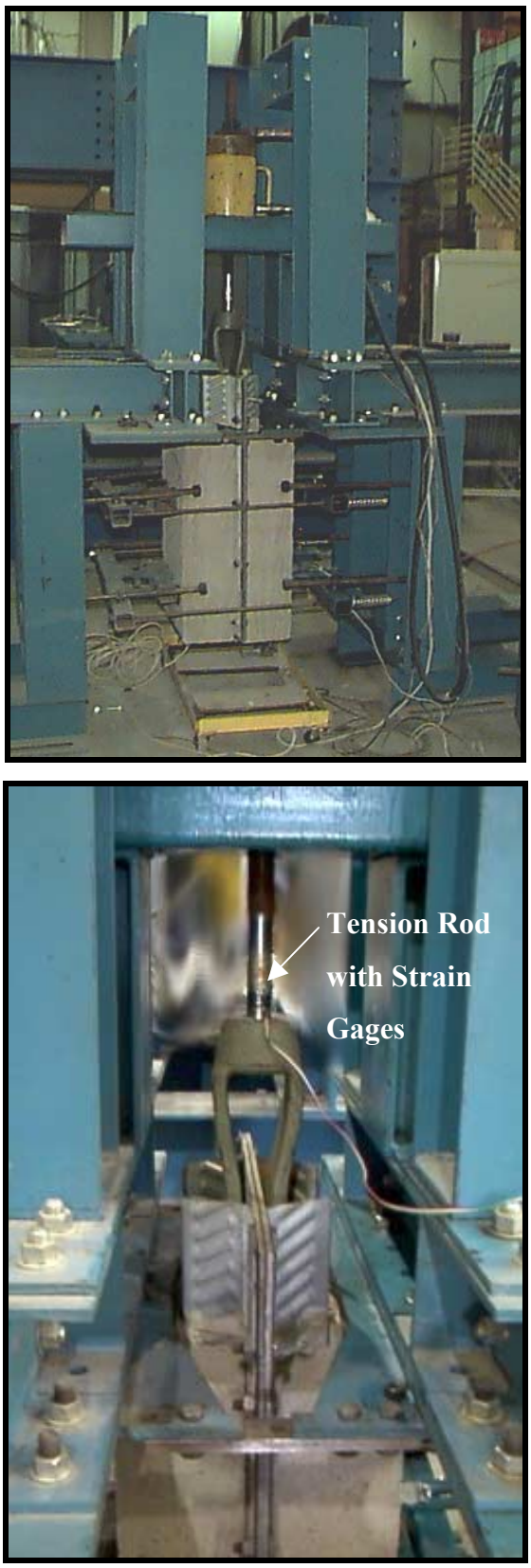

Figure 3.3. 1 Shear Bond Test Set-Up: (a) Test Frame (b) Close Up

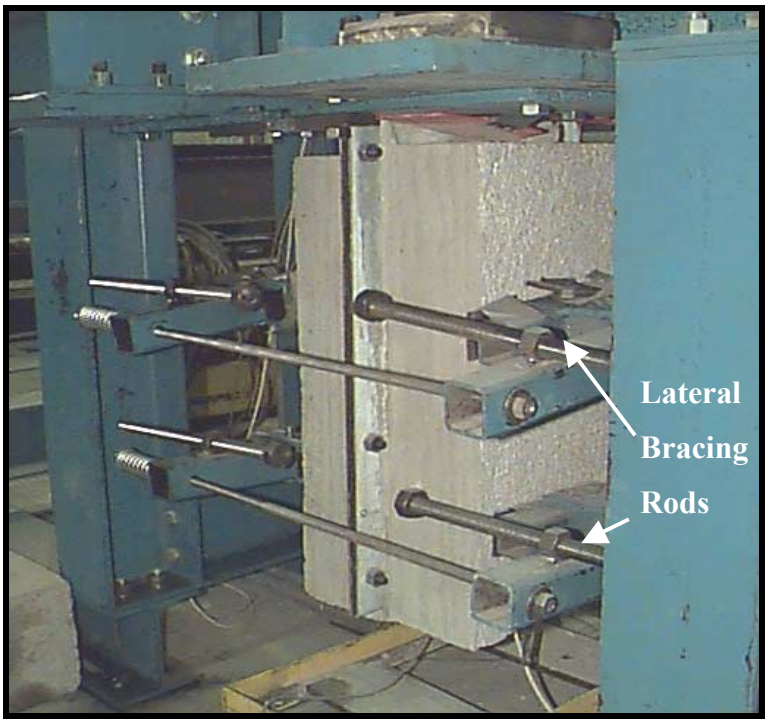

Figure 3.3. 2 Lateral Pressure Frames with Lateral Bracing

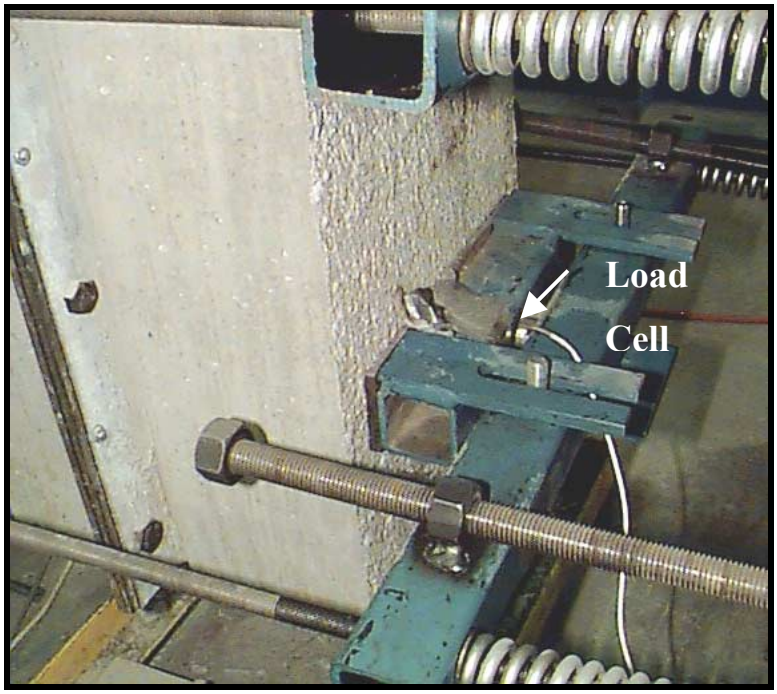

Figure 3.3. 3 Lateral Pressure Load Cell

3.4 Test Procedure

The specimens were loaded at 1 kip increments until a peak shear load was reached. Thereafter, additional load was applied at increments that caused 0.02 in. of slip until the measured shear resistance was minimal. The load was held constant for 2-3 minutes at each step to allow the load to settle. The applied lateral load was adjusted during the test to remain constant at about 300 psf. During loading, it was also necessary to adjust the lateral bracing rods as the specimen rotated. This rotation increased the measured lateral load. Shear, slip, and lateral pressure values were recorded during the tests. At least two specimens of each embossment type were tested. If results were inconsistent, a third test was performed.

After the shear bond tests were performed, the specimens were taken apart and observed for failure modes. The embossment depths were measured to determine if plastic deformation occurred in the steel deck. The specimens were also observed for concrete crushing at the embossments.

3.5 Test Results

Observation of the tested specimens showed that failure occurred mostly by elastic deformation of the deck and concrete over-ride. Because of the inconsistency of the embossment depths when fabricated, it was difficult to determine if any plastic deformation of the embossments occurred. However, the measured post-test depths were in the same range as pre-test depths, indicating that any deformation of the deck was elastic. Concrete crushing at the embossments was minimal, but shear marks were most prevalent in the portion of the embossments closest to the bottom of the deck. Shear marks were greater in the specimens with the proposed embossments than those with the existing embossments. This is an indication that the proposed embossments provided more mechanical shear resistance, which was confirmed by the test data.

Plots of shear stress versus slip behavior as shown in Figures 3.5.2-4 were created for each test. A complete set of graphs for all the specimens is in Appendix A. The slips of the two halves of each specimen were averaged and the shear load was considered to

be divided evenly between both halves over the surface area of the deck, although the exact load distribution between halves was unknown. The specimens were named in the form of Sb*i-jk-l*. "*i*" gives the depth of the deck, "*j*" indicates either diagonal embossment depth or existing embossment type, "*k*" indicates whether the embossments were inward or both inward and outward, and "*l*" designates the order of testing.

The behavior of the first specimen tested is shown in Figure 3.5.2. This test was conducted before the lateral bracing was added. During this test, slip initiated on one side first, causing the specimen to rotate downward toward that side. Most of the load was then transferred to that side. Upon bracing the specimen laterally, the load then was transferred back to the other half, which still had remaining shear resistance capacity. This behavior is shown by the second peak in the graph at 0.6 in. of slip. This imbalance was prevented in future tests by the addition of lateral bracing rods, which caused the load to re-equilibrate when differential slip occurred. Plots from the 3 in. deck series better represents the shear bond behavior since the test procedure was still under refinement during the testing of the 2 in. specimens.

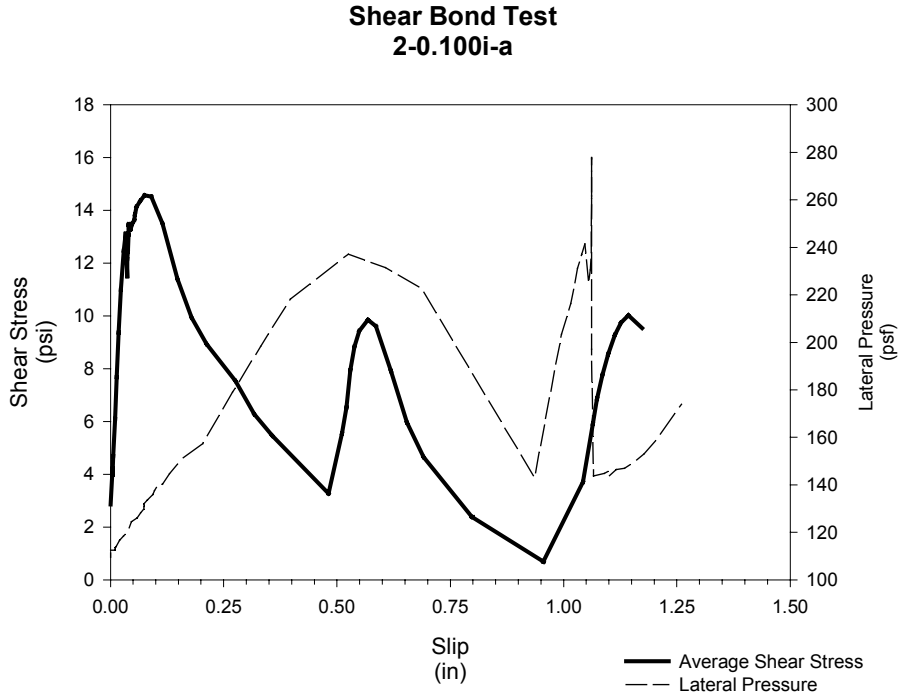

Figure 3.5. 1 Shear Resistance of Specimen SB2-0.10i-a

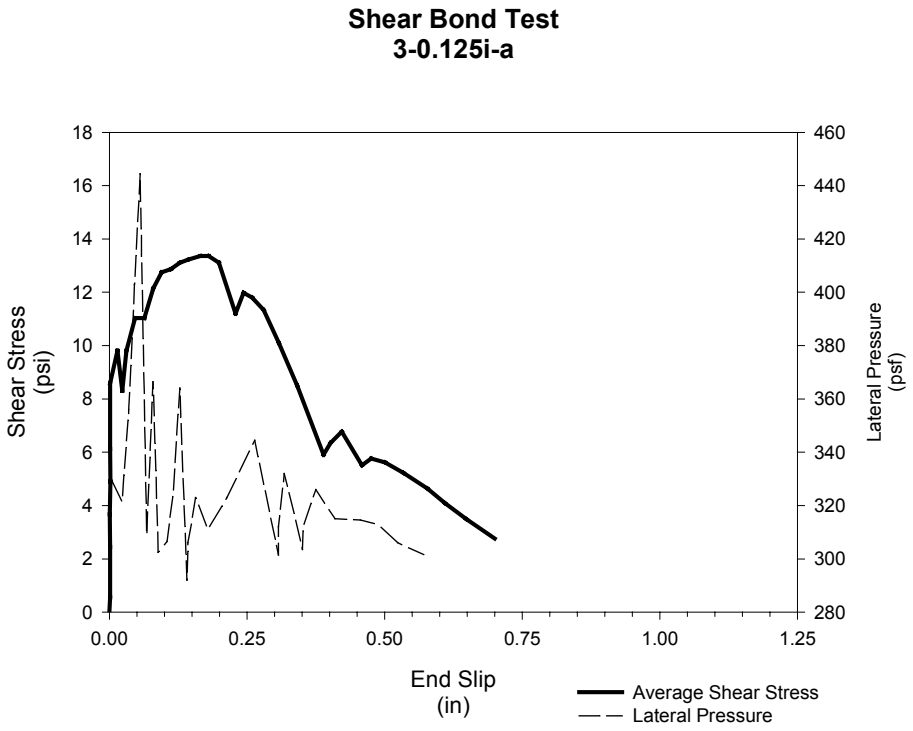

Figure 3.5. 2 Shear Resistance of Specimen SB3-0.125i-a

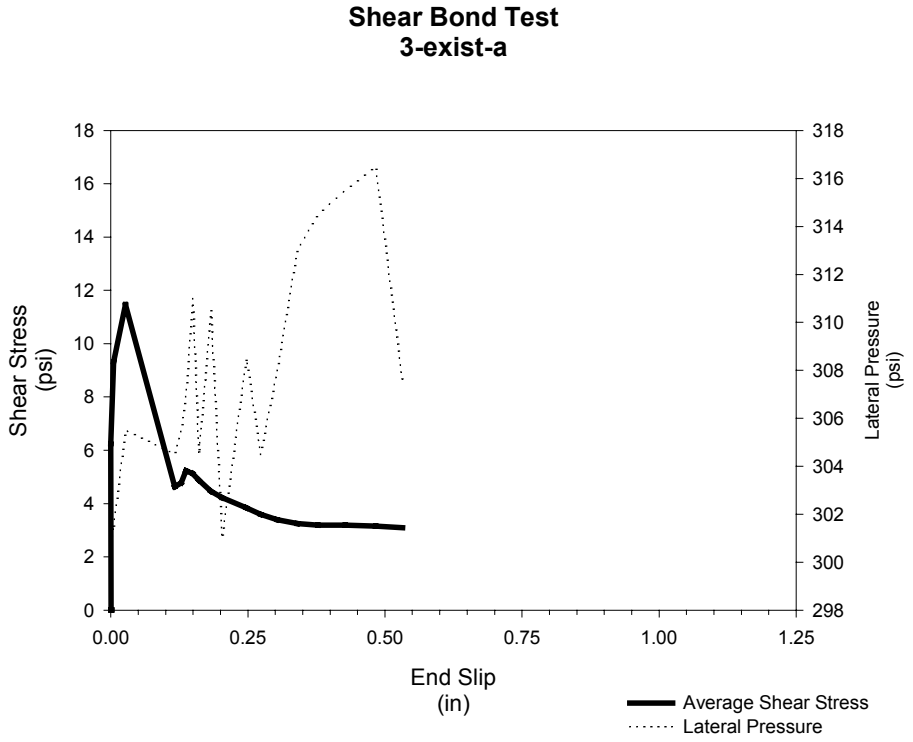

Figure 3.5. 3 Shear Resistance of Specimen SB3-exist-a

The shear versus slip plots display the different components of shear resistance. Shear resistance before any slip occurred was due to the strength of the chemical bond. This value shown in Figure 3.5.3 is approximately 9 psi. It was evident that most of the 2 in. deck specimens lost their chemical bond before testing, since slip occurred at the onset of loading. The strength of the chemical bond that was measured in other specimens was inconsistent. This variance was expected due to factors such as differences in surface conditions of the deck (some had more oxidation than others) and losses during handling.

The additional shear strength beyond the chemical bond shown in the plot by the following peak is due to the mechanical resistance of the embossments. When the mechanical resistance was overcome, the load dropped. Table 3.5.1 shows a summary of the results from the shear bond tests.

Daniels (1988) defined ductile behavior in shear bond tests to be when there is "significant post-slip load carrying capacity," while brittle behavior is "characterized by large initial end slips and the loss of post-slip load carrying capacity." A comparison of the plots in Figures 3.5.3 and Figure 3.5.4 shows that the drop in shear resistance was more sudden for the existing embossment type than for the proposed diagonal embossments, which continued to sustain load a little longer. Therefore, the specimens with existing embossments displayed brittle behavior while the specimens with the proposed embossments displayed ductile behavior. These behaviors were confirmed by the results of the full-scale slab tests described in Chapter 4.

Table 3.5.1 Summary of Shear Bond Test Results

Specimen	Max. Shear (psi)	Average Max Shear (psi)	Slip at Max. Shear (in)	
			Left	Right
Sb2-exist-a	4.91	5.40	0.21	0.12
Sb2-exist-b	5.27		0.10	0.19
Sb2-exist-c	6.02		0.11	0.08
Sb2-0.10i-a	14.57	13.48	0.13	0.02
Sb2-0.10i-b	12.65		0.07	0.27
Sb2-0.10i-c	13.21		0.14	0.08
Sb2-0.125i-a	17.45	17.02	0.12	0.15
Sb2-0.125i-b	16.59		0.12	0.09
Sb2-0.125io-a	10.24	13.77	0.13	0.04
Sb2-0.125io-b	17.30		0.22	0.10
Sb2-0.14io-a	19.43	18.69	0.10	0.10
Sb2-0.14io-b	19.69		0.13	0.00
Sb2-0.14io-c	16.95		0.07	0.17
Sb3-exist-a	11.46	10.85	0.00	0.05
Sb3-exist-b	10.23		0.00	0.00
Sb3-0.10i-a	15.56	13.59	0.11	0.06
Sb3-0.10i-b	11.63		0.13	0.07
Sb3-0.125i-a	13.36	13.20	0.12	0.25
Sb3-0.125i-b	13.05		0.18	0.17
Sb3-0.125io-a	11.27	11.87	0.22	0.11
Sb3-0.125io-b	12.47		0.06	0.13
Sb3-0.14io-a	17.40	15.25	0.10	0.09
Sb3-0.14io-b	13.10		0.17	0.01

3.6 Conclusions and Recommendations

Some observations about the shear bond test procedure were made, resulting in some recommendations for the test procedure. One component of shear resistance is friction, which depends on the magnitude of lateral pressure applied. Further study should be made regarding what magnitude of lateral pressure is appropriate to obtain accurate shear resistance results. Also, the shear load in each half of the specimens should be directly measured instead of following the assumption that the load is evenly distributed to both halves. This is a questionable assumption since slip occurs unevenly between the two halves. Chemical bond is highly variable, but if its behavior is to be studied, extra care must be taken to ensure this bond is not destroyed during handling.

Observations on the shear bond behavior of the different specimens were made. Failure occurred due to concrete over-ride. Only minor concrete crushing or plastic deformation of the deck was observed. Use of the proposed embossments led to ductile behavior while use of the existing embossments resulted in brittle behavior, which corresponded to the behavior shown in full-scale specimens. Therefore, use of shear bond tests is an effective means to study the performance of shear transferring devices such as embossments.

The specimens with the proposed embossments had significantly greater shear resistance than those with the existing embossments. Because the proposed embossments of equal depth (0.100 in.) to the existing embossments displayed improved shear resistance, it was concluded that the proposed embossment pattern is more effective for shear resistance. As expected, specimens with the deepest embossments (0.140 in.) showed the greatest improvement in shear resistance. There was no marked improvement in shear resistance of the "in and out" embossments over the "in only" embossments of equal depth, therefore the selection between the two types should be made based on ease of fabrication.

CHAPTER 4: FULL-SCALE COMPOSITE SLAB TESTS

4.1 General

Because analytical methods are still under development, it remains current practice for deck manufacturers to perform multiple full-scale slab tests to determine the capacity and behavior of decks they produce. The manufacturers use strengths given by these tests to produce catalogs with recommended allowable loads for given span lengths and deck configurations. Engineers generally rely on these catalog recommendations for their selections in design. Following this practice, Vulcraft sponsored the testing of full-scale slab specimens of deck with new embossment types under development. The performances of the deck with the proposed embossments were to be compared with the deck that had the existing embossment type.

4.2 Test Parameters

Twenty full scale-slab tests were performed: two tests for each type of deck under consideration. The simple span slabs consisted of two panels, making them each 6 ft. wide, and all deck was approximately 0.035 in. thick (20 gage steel). Details of the deck profile and embossment geometries are given in Chapter 3. All parameters within each set (2VLI deck and 3VLI deck) were intended to remain constant except for the embossment type. The concrete compressive strengths did vary, however, since the specimens were cast and tested at different times. Concrete compressive strengths were determined from compressive tests of 4 in. x 8 in. cylinders according to ASTM C39-96 procedure. Steel deck yield was given by the manufacturer and verified by tensile coupon tests performed according to ASTM E8-00b procedure.

Tables 4.2.1-2 list the parameters of each test. The specimens were named in the form of "*i-jk-l*." "*i*" gives the depth of the deck, "*j*" indicates either proposed diagonal

embossment depth or existing embossment type, "*k*" indicates whether the embossments were inward or both inward and outward, and "*l*" designates the order of testing.

Table 4.2.1 Test Parameters for 2VLI, 2 in. Deck Slabs

Specimen Designation	Embossment Depth (in.)	Total Slab Depth (in.)	Span Length (in.)	f'_c (ksi)	f_y (ksi)
2-exist-a	0.100	4.5	112	4.3	52.5
2-exist-b	0.100	4.5	112	4.3	52.5
2-0.10i-a	0.100	4.5	112	3.3	52.5
2-0.10i-b	0.100	4.5	112	3.3	52.5
2-0.125i-a	0.125	4.5	112	4.1	52.5
2-0.125i-b	0.125	4.5	112	4.2	52.5
2-0.125io-a	0.125	4.5	112	3.3	52.5
2-0.125io-b	0.125	4.5	112	3.4	52.5
2-0.14io-a	0.140	4.5	112	4.2	52.5
2-0.14io-b	0.140	4.5	112	4.2	52.5

Table 4.2.2 Test Parameters for 3VLI, 3 in. Deck Slabs

Specimen Designation	Embossment Depth (in.)	Total Slab Depth (in)	Span Length (in.)	f'_c (ksi)	f_y (ksi)
3-exist-a	0.100	5.5	136	3.5	52.7
3-exist-b	0.100	5.5	136	3.5	52.7
3-0.10i-a	0.100	5.5	136	4.5	52.7
3-0.10i-b	0.100	5.5	136	4.5	52.7
3-0.125i-a	0.125	5.5	136	3.4	52.7
3-0.125i-b	0.125	5.5	136	3.4	52.7
3-0.125io-a	0.125	5.5	136	3.6	52.7
3-0.125io-b	0.125	5.5	136	3.6	52.7
3-0.14io-a	0.140	5.5	136	3.4	52.7
3-0.14io-b	0.140	5.5	136	3.4	52.7

4.3 Test Set Up and Instrumentation

Each slab specimen was prepared in a similar manner. The bare deck was cut to the appropriate length. Eight strain gages were put on the underside of the deck at midspan: four on the top flange and four on the bottom flange. Two deck panels were button punched together at 12 in. intervals along the span length and arc puddle welded (¾ in. visible diameter) at the ends to the support beams at the locations of the bottom flanges of the deck (approximately 12 in.). Pour stop was temporarily screwed to the deck along each of the four sides for the cast. The deck surface was brushed clean and a layer of standard welded wire fabric (WWF 6x6-W1.4xW1.4) was placed on the deck. In order to maintain a constant slab width and height by preventing outward bowing of the pour stop, thin threaded rods connected the pour stop of opposite faces at two locations along the span. Wire pot displacement transducers were placed at midspan and the quarter points to measure deflections during the casting and testing. Strain gage and wire pot locations are shown in Figure 4.3.1.

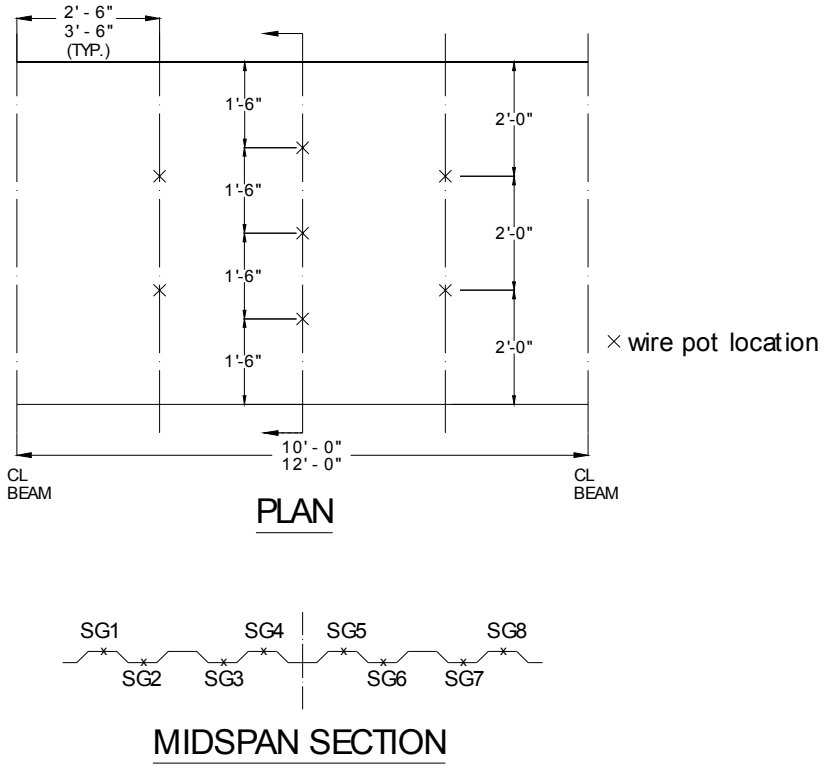

Figure 4.3. 1 Strain Gage and Wire Pot Locations

The slabs were cast with normal weight, 3,000 psi concrete. The concrete was vibrated and screeded during placement. Deck strains and deflections due to the weight of the concrete were measured and recorded. The specimens were covered with plastic and moist cured for seven days. After seven days, the plastic was removed and the pour stop was stripped. Curing continued for at least 21 more days.

When the specimens were ready to be tested, three potentiometers were fixed to the slab at each end of the slab. A small angle was glued to the bottom of the deck at the location of each potentiometer and tied to the tip of the potentiometer so that end slip of the concrete with respect to the deck could be measured, as illustrated in Figure 4.3.2.

Figure 4.3. 2 Potentiometers

The slab was loaded uniformly with a 6 ft x 10 ft rubber airbag. The top of the airbag had two valves: one connected to the airhose to input the pressure, and the other connected to a calibrated pressure transducer, which measured the pressure in the airbag. A steel test frame that was bolted to the reaction floor resisted the pressure from the airbag as it inflated, thereby applying the uniform load to the slab. Sheets of ¾ in. plywood with holes for the airbag valves were placed between the airbag and the test frame to distribute the pressure. Figure 4.3.3 illustrates the test set up.

Figure 4.3. 3 Full-Scale Slab Test Set Up

4.4 Test Procedure

The slabs were first loaded to about one tenth the load expected to cause first yield (35 psf for the 2 in. deck, 25 psf for the 3 in. deck). The specimen was then unloaded and re-zeroed. It was then slowly reloaded at this load increment until it reached first yield. Additional load increments were 10 psf until the vertical deflection increased while the applied load did not. Further load increments were then set at those that caused 0.1 in. of vertical deflection until the slab completely failed. Pauses were taken between loadings and midspan deflection, quarter-point deflection, end slips, deck strains and applied pressure were recorded. The load increments at which sounds of debonding and cracking were heard were recorded and the slab was observed for cracks. Any visible cracks were traced with a marker and labeled.

After the test, the locations of the cracks along the span were measured and recorded and the slabs were disassembled and observed. The concrete at its interface with the deck was observed for adequate vibration during casting and for crushing at the location of the embossments during loading. The steel deck was also observed for deformations of the embossments.

4.5 Test Results

Observations were made about the failure mode of the slabs. When the bottom flange of the deck began to yield, cracks began to form in the concrete due to the differential strain. The shear span was then loaded to its shear resistance capacity, causing unacceptable slip and noncomposite interaction. The slabs then failed in flexure of the noncomposite deck and concrete components. Figure 4.5.1 shows the end slip failure, which occurred in specimens with proposed and existing embossments.

The test data were plotted into graphs of applied load verses midspan deflection, end slip, deck top flange strain, and deck bottom flange strain. The complete set of graphs is in Appendix B. When the first set of specimens (2-0.14io-a/b and 2-0.125i-a/b) were taken apart after being tested, honeycombing of the bottom surface of the concrete was observed as shown in Figure 4.5.2. This honeycombing occurred because vibration was done with only the vibratory screed. The remaining specimens were cast with the use of a wand-type vibrator. No significant concrete crushing at the embossments or deformation of the deck embossments due to testing was noticed. Therefore slip must have been due to concrete over-riding the deck while the deck web flexed away from the concrete, as also described by Luttrell (1987). This behavior was confirmed by the observation of the progression of vertical separation of the concrete and deck as the applied load increased.

Figure 4.5. 1 End Slip of Failed Specimens

Figure 4.5. 2 Honeycombing of the 2-0.125i-a Specimen

4.5.1 Behavior Comparison

To illustrate existing embossment versus proposed embossment behavior, a representative comparison is made here between the 2-exist-b and 2-0.125i-a specimens. Figures 4.5.1.1-2 show that prior to failure, specimens with proposed embossments experienced more cracking than the existing. Cracks were mostly vertical for all specimens, indicating a flexural failure of the slab after the shear bond failed. Figures 4.5.1.3-4 show the failure of the deck.

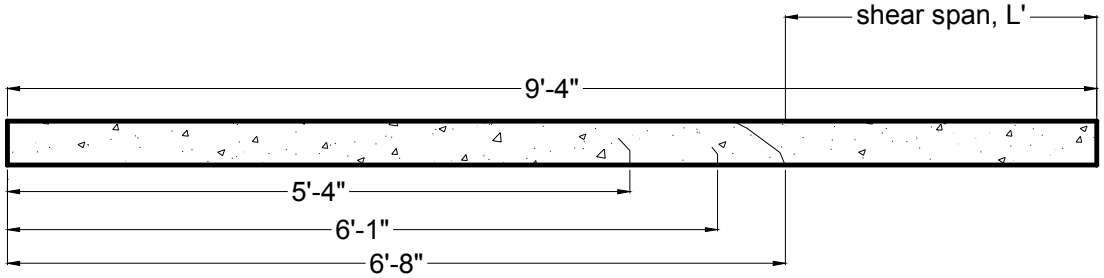

2-exist-b (Front)

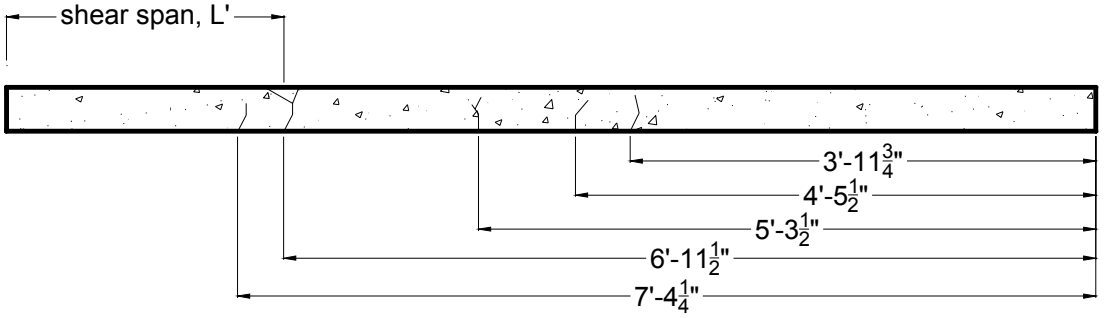

2-exist-b (Back)

Figure 4.5.1.1 Cracking of Failed Slab 2-exist-b

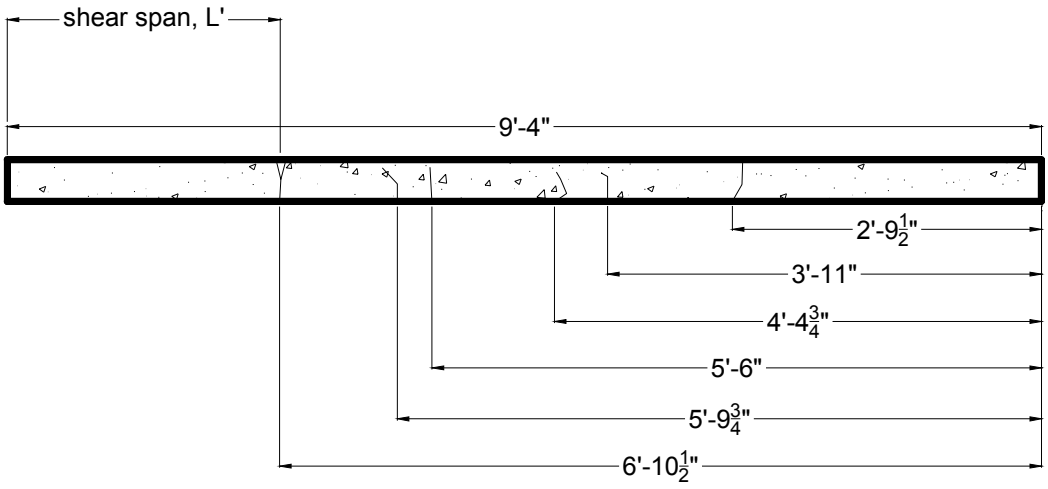

2-0.125i-a (Front)

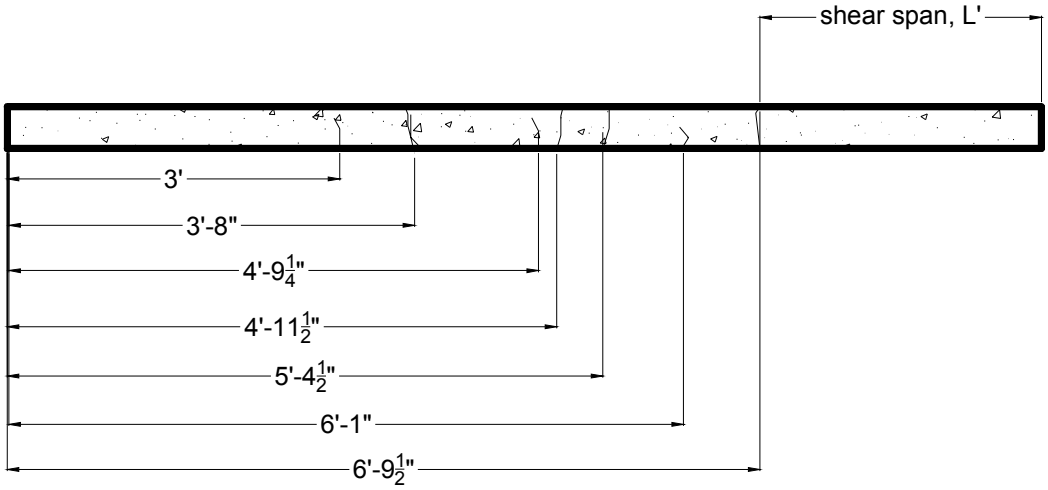

2-0.125i-a (Back)

Figure 4.5.1. 2 Cracking of Failed Slab 2-0.125i-a

Figure 4.5.1. 3 Failed Deck for 2-exist-b Specimen

Figure 4.5.1. 4 Failed Deck for 2-0.125i-a Specimen

Figures 4.5.1.5-6 show their applied load versus midspan deflection graphs. The experimental midspan deflection is shown as well as the theoretical midspan deflection, which assumed full composite action and a stiffness determined from the average cracked and uncracked moments of inertia. A horizontal line shows theoretical design strengths given by the First Yield method and ASCE Appendix D's method. Both methods are described in Chapter 5. The graphs also include plots of the end slips.

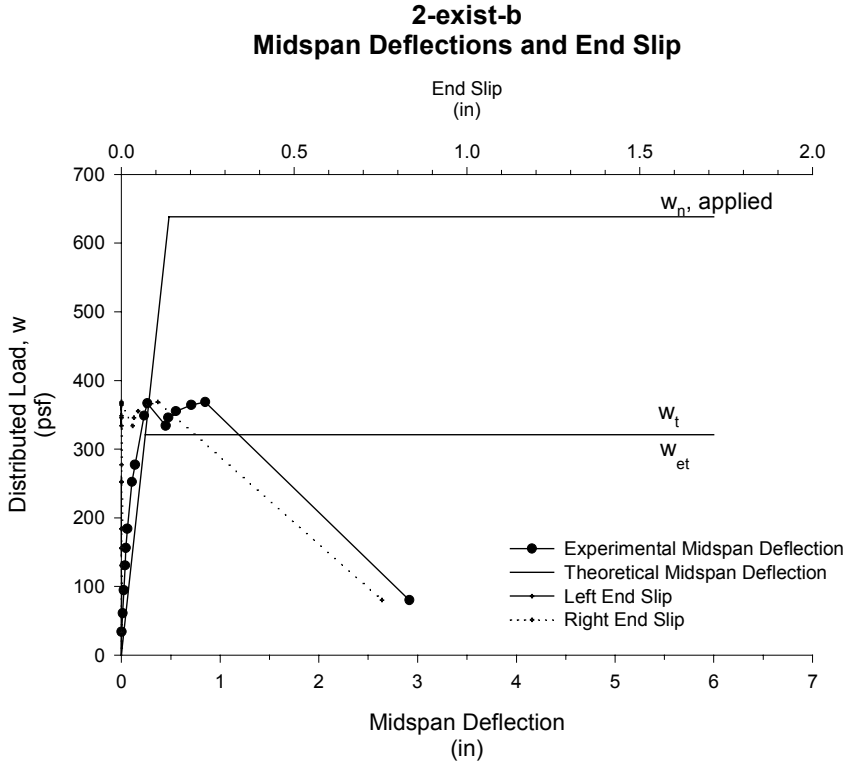

w_n = Theoretical applied distributed load that results in M_n using the calculated material properties

w_t = Theoretical applied distributed load that results in M_t (Flexural Capacity using ASCE App. D Method)

w_{et} = Theoretical applied distributed load that results in M_{et} (First Yield Moment)

Figure 4.5.1. 5 Applied Load vs. Midspan Deflection for 2-exist-b

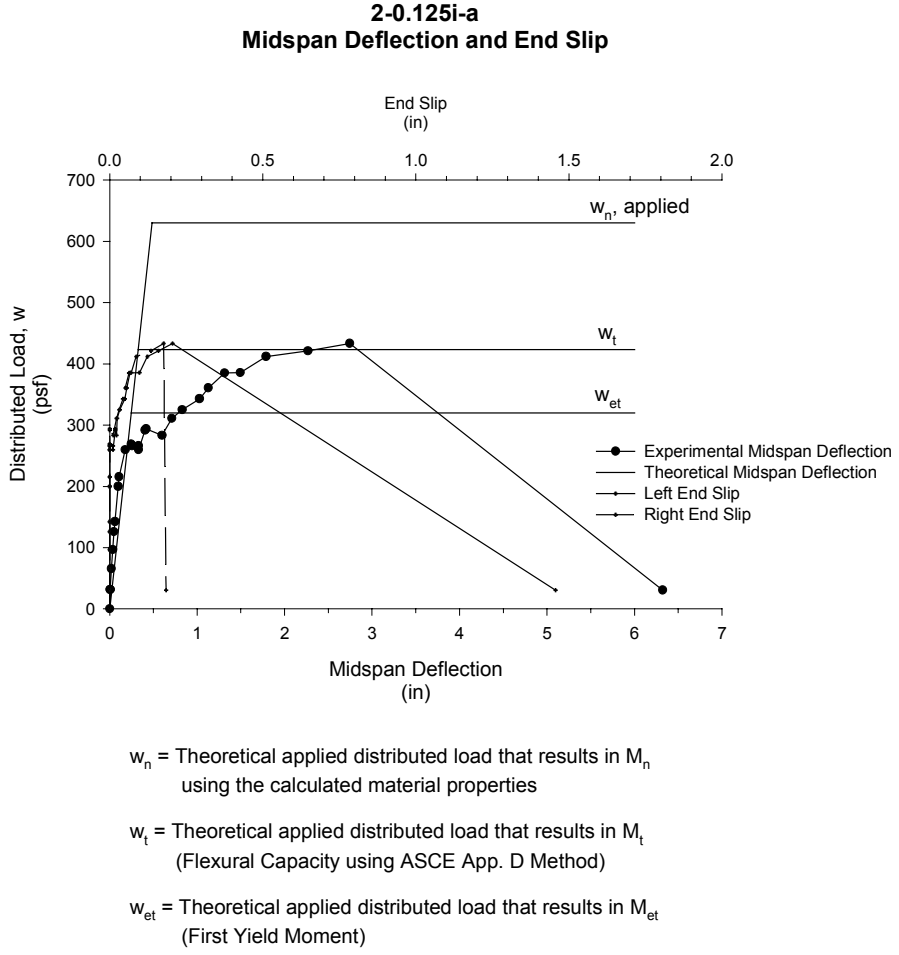

Figure 4.5.1. 6 Applied Load vs. Midspan Deflection for 2-0.125i-a

The different mechanisms of shear strength can be observed from the graphs. The point at which the deflection plot first dropped corresponds to when the chemical bond was broken. Any additional load resistance was due to the friction between the deck and concrete, and the mechanical resistance of the embossments. Figure 4.5.1.5 shows that the existing deck had brittle behavior defined by the Eurocode to be when the failure load was less than 110% the load at which end slip initiated (approximately 0.02 in.). The existing embossments contributed minimally to strength. Figure 4.5.1.6 shows that deck with the proposed embossments behaved in a ductile manner: failure load was significantly higher than 110% of the load at which first slip occurred. The plots also show the correlation between a decrease in stiffness of the slab as end slip initiated. This behavior follows from the fact that slip occurs when cracking begins.

Figures 4.5.1.7-9 show graphs of the bottom flange and top flange strains in the deck. The bottom flange remained in tension throughout the loading cycle for all specimens, as expected. In the early loading stages, the slab acted as a fully composite member, with the entire cross section of steel deck providing tensile reinforcement. This behavior is shown by the fact that both the top and bottom flange strains were in tension in this region and there was no end slip. When the applied load was great enough to initiate concrete cracking and end slip (360 psf for 2-exist-b, 290 psf for 2-0.125i-a), the slab member lost some composite interaction and the deck top flange went into compression. Figure 4.5.1.8 shows that the top flange of the deck with existing embossments stayed in compression after this point. However, for the other specimens, some composite interaction was regained when the proposed embossments were engaged and provided shear resistance. This behavior is illustrated by the fact that the plot of the top flange strains changed direction back toward the tensile strain region, as shown in Figure 4.5.1.9. The top flange did not reach yield strain for any of the specimens.

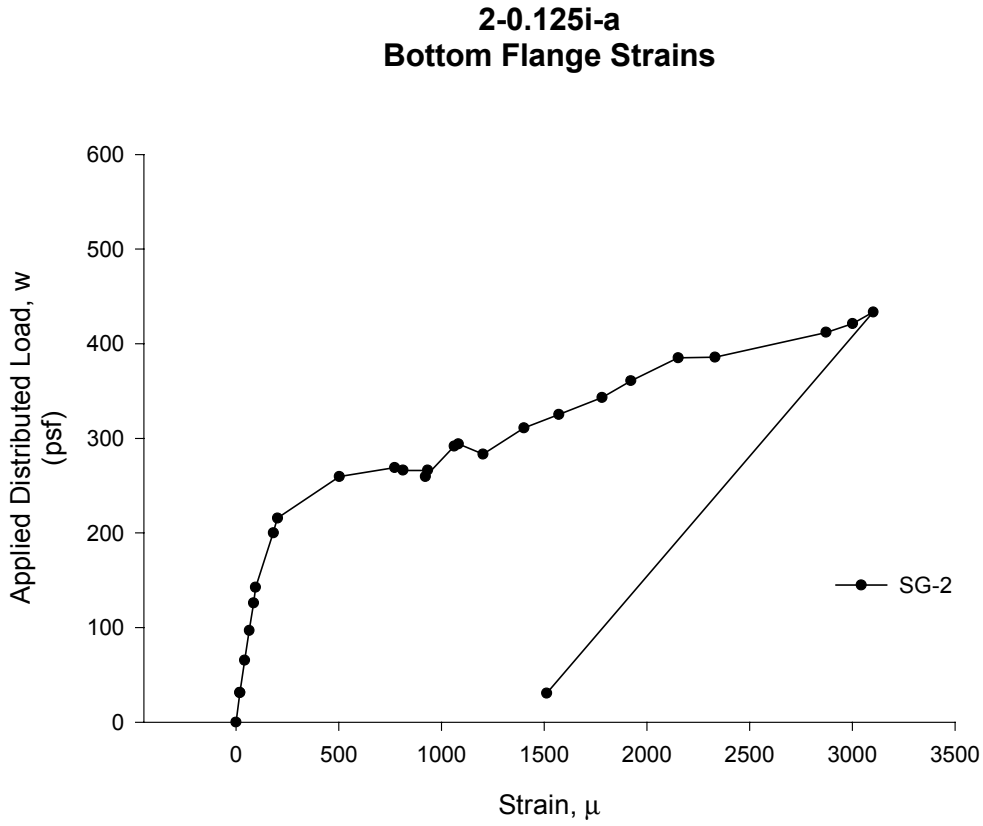

Figure 4.5.1. 7 Applied Load vs. Deck Bottom Flange Strains for 2-0.125i-a

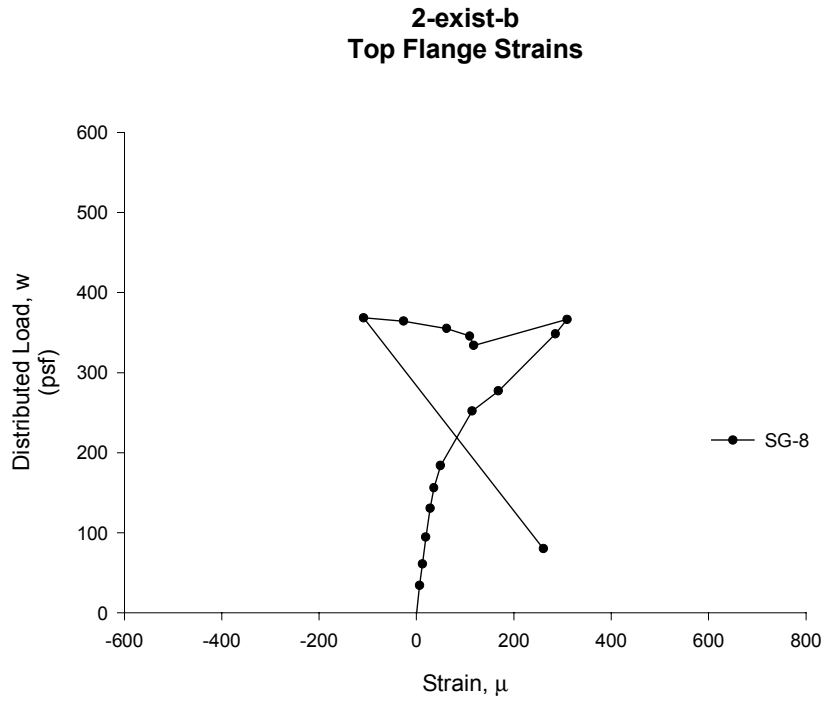

Figure 4.5.1. 8 Applied Load vs. Deck Top Flange Strain for 2-exist-b

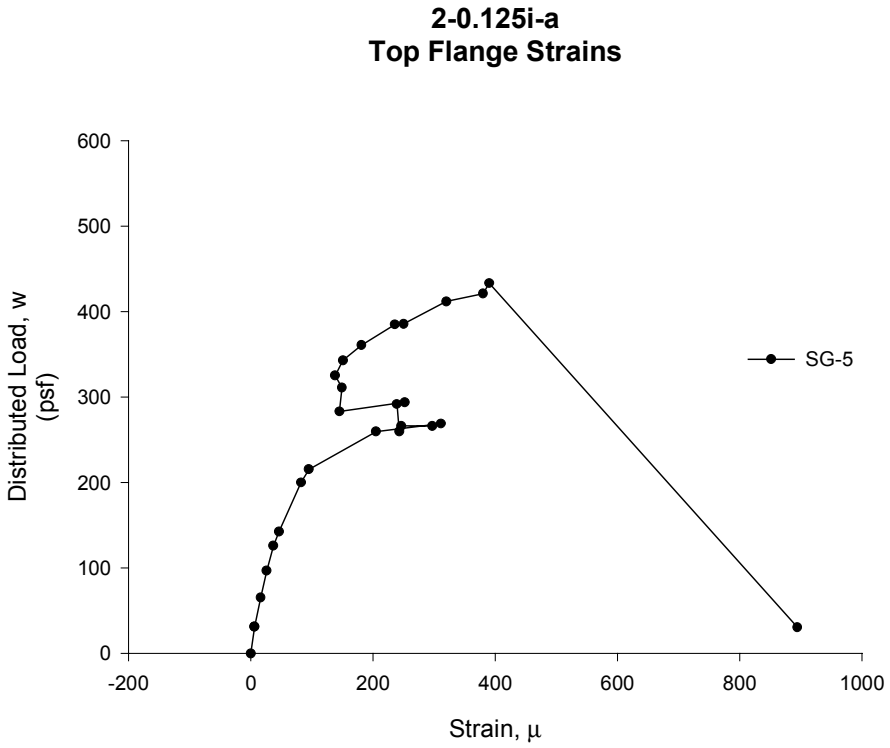

Figure 4.5.1. 9 Applied Load vs. Deck Top Flange Strain for 2-0.125i-a

4.5.2 Strength Comparison

Figures 4.5.2.1 and 4.5.2.2 show comparison plots of the performance of the different types of 2 in. deck and 3 in. deck, respectively. Results from the two tests for each type of embossment were averaged to simplify the graphs. The 2-0.125i and 2-0.14io specimens had lower strengths than the others due to the honeycombing of the concrete, which significantly lessened the shear interaction between the concrete and deck. The graph of the 3 in. deck provides a better comparison. It shows that the proposed embossments gave greater strength (20%-30%) than the existing embossments, with the deepest embossments (0.14io) being most effective. The 0.125i and 0.125io specimens behaved very similarly to each other, giving about the same slab strength.

All the slabs failed at loads significantly higher than the first yield prediction (w_{et}), but none reached full composite moment capacity (w_n). Experimentally measured first yield of the bottom flange of the deck usually occurred at higher loads than were predicted theoretically. However, the 3 in. slabs with proposed embossments did more closely approach the w_n value, which confirms Luttrell's(1987) findings that deeper decks provide better shear resistance.

Tables 4.5.2.1-2 show the slab strengths in tabulated form.

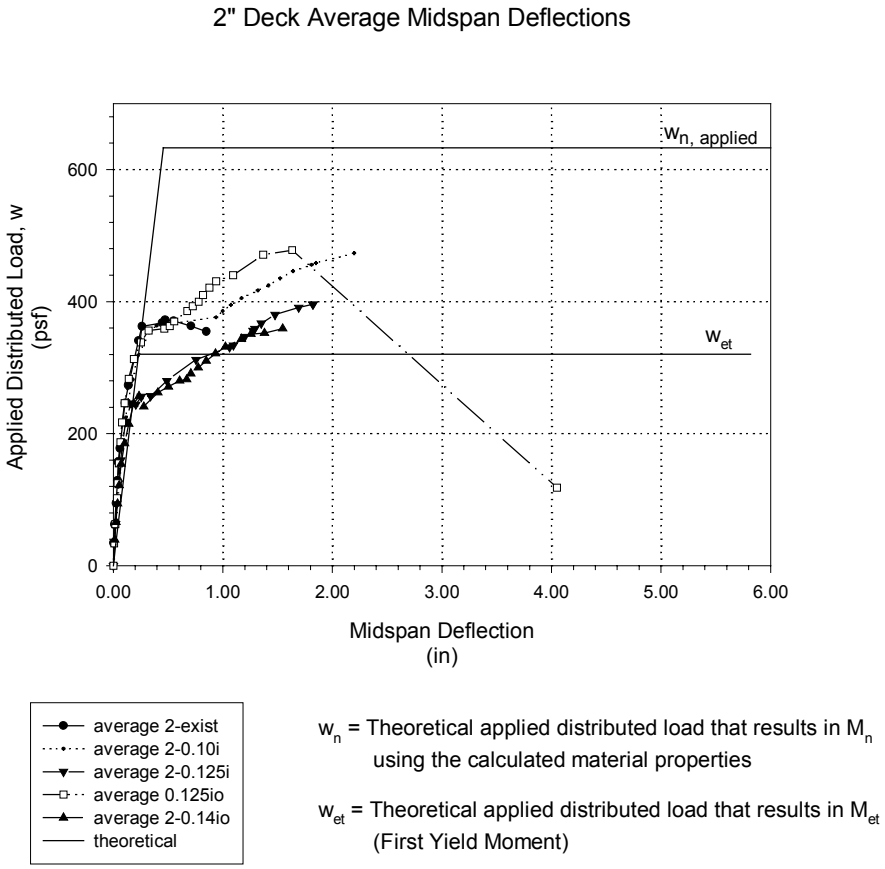

Figure 4.5.2. 1 Comparison of Applied Load vs. Deflection for 2 in. Deck

Table 4.5.2.1 Maximum Applied Load for 2 in. Deck Slabs

Specimen Designation	Maximum Applied Load (psf)	Average Maximum Applied Load (psf)
2-exist-a	417	393
2-exist-b	368	
2-0.10i-a	472	482
2-0.10i-b	492	
2-0.125i-a	433	415
2-0.125i-b	396	
2-0.125io-a	477	439
2-0.125io-b	400	
2-0.14io-a	401	380
2-0.14io-b	359	

Note: Shaded rows indicate specimens whose strengths were lower due to honeycombing

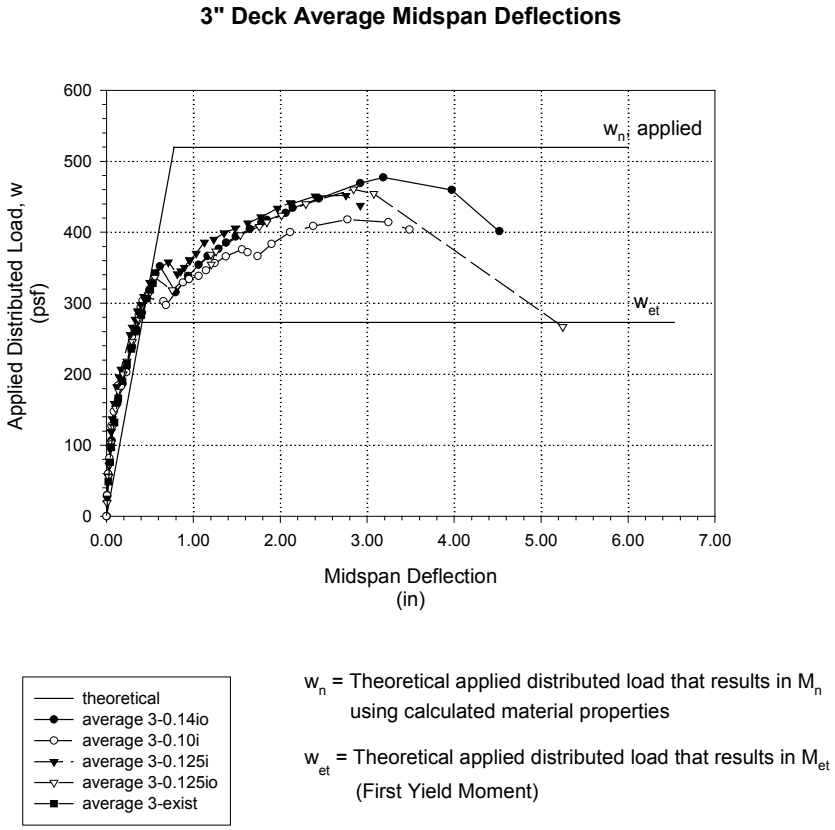

Figure 4.5.2. 2 Comparison of Applied Load vs. Deflection for 3 in. Deck

Table 4.5.2.2 Maximum Applied Load for 3 in. Deck Slabs

Specimen Designation	Maximum Applied Load (psf)	Average Maximum Applied Load (psf)
3-exist-a	327	336
3-exist-b	345	
3-0.10i-a	422	420
3-0.10i-b	418	
3-0.125i-a	469	463
3-0.125i-b	456	
3-0.125io-a	440	425
3-0.125io-b	410	
3-0.14io-a	500	481
3-0.14io-b	462	

4.6 Conclusions and Recommendations

The specimens with existing embossments were observed to have different behavior than the specimens with the proposed embossments. The failure of the slabs with the existing embossments was brittle, as defined by Eurocode 4 (1992) to be when the ultimate load is less than 110% of the load at which first slip occurred. Slabs with the proposed embossments had the more favorable ductile behavior, maintaining significant additional load capacity after the initiation of slip.

The deck with proposed embossments showed 20%-30% improved performance over deck with the existing embossments (not including the honeycombed specimens). Because slabs with the proposed embossment of the same depth as the existing embossments (0.100 in.) gave significantly improved composite interaction, it was concluded that the proposed pattern was more effective. Within the range of embossment depths tested, slabs with the deepest of the proposed embossments (0.140 in.) had the highest strength and is therefore recommended for future research and development. Since there was no notable difference between the performance of the "in" and "in and out" patterns, the selection for production should be made based on cost and ease of fabrication.

CHAPTER 5: ANALYSIS METHODS

Three different composite slab strength prediction methods were used for the deck types under consideration. In each method, the dead load due to casting of the concrete was applied to the deck alone to determine the casting stresses. The additional applied load capacity was then determined by subtracting the casting stresses from the composite strength. The following design equations are simplified for the case of no additional reinforcing, no shear studs, and no additional end restraint.

5.1 First Yield Method (Heagler 1992)

This method limits the predicted strength of the composite slab, which is considered fully composite, to the load that causes first yield of the bottom flange of the deck. The concrete is assumed to have cracked so that only concrete above the neutral axis contributes to compressive strength and the tensile loads are distributed into components in the top flange (T_1), the web (T_2), and the bottom flange (T_3) of the deck as shown in Figure 5.1. The effectiveness of embossments is not considered in this method.

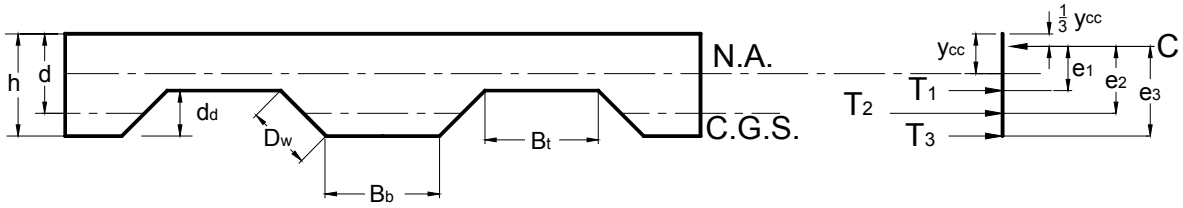

Figure 5. 1 Deck Cross-Section and Force Distribution

The first yield moment per unit width (12 in.) is:

$$M_{et} = \left(T_1\ e_1 + T_2\ e_2 + T_3\ e_3\right) \qquad (5.1\text{-}1)$$

$$e_1 = e_3 - d_d \tag{5.1-2}$$

$$e_2 = e_3 - \frac{d_d}{2} \tag{5.1-3}$$

$$e_3 = h - \frac{y_{cc}}{3} \tag{5.1-4}$$

$$T_1 = f_{yc}\left(B_t\ t\right)\left[\frac{h - y_{cc} - d_d}{h - y_{cc}}\right] \tag{5.1-5}$$

$$T_2 = f_{yc}\left(2D_w\ t\right)\left[\frac{h - y_{cc} - \frac{d_d}{2}}{h - y_{cc}}\right] \tag{5.1-6}$$

$$T_1 = f_{yc}\left(B_b\ t\right) \tag{5.1-7}$$

$$f_{yc} = F_y - f_c \tag{5.1-8}$$

$$y_{cc} = d\left(\sqrt{2\,\rho\,n + (\rho\,n)^2} - \rho\,n\right) \tag{5.1-9}$$

where:

f_{yc} = yield stress of deck, corrected to account for casting stresses

f_c = stress in deck due to casting

ρ = reinforcement ratio, $\frac{A_s}{b\,d}$

n = modular ratio, $\frac{E_s}{E_c}$

5.2 ASCE Appendix D Alternate Method (*Standard* 1994)

This method was developed by Luttrell and Prassanan (1984) at West Virginia University and is based on the shear bond limit state behavior found from numerous full-scale slab tests of deck with various characteristics. A statistical analysis was performed on the test results to determine the effect of the various deck characteristics on strength, resulting in the development of three "relaxation factors." The slab strength is determined by applying these relaxation factors to the first yield strength described in Section 5.1. The dimension designations used in the design equations are illustrated in Figure 5.2.

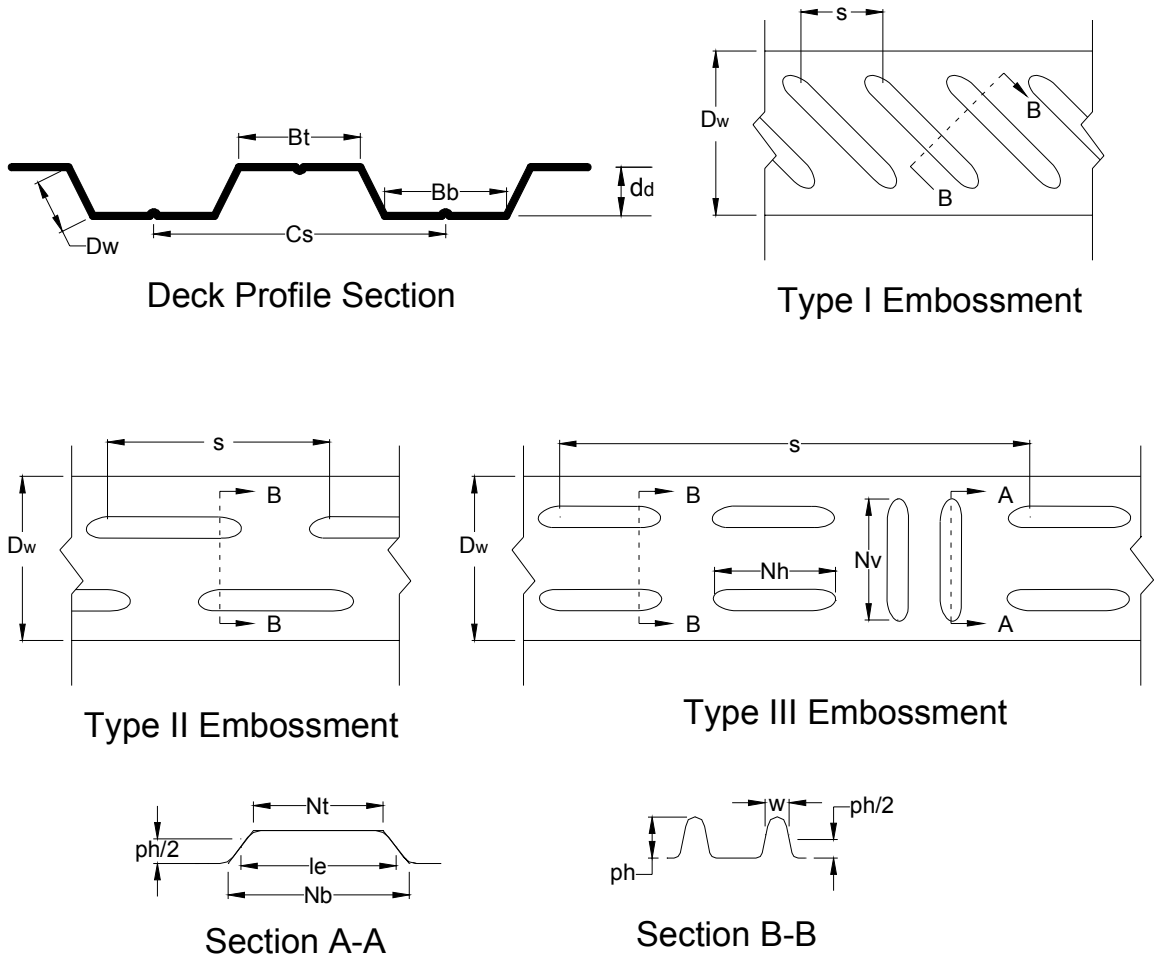

Figure 5. 2 Dimension Designations For ASCE App. D Method (*Standard* 1994)

The flexural strength is:

$$M_t = K\, M_{et}\left(\frac{12}{C_s}\right) \qquad (5.2\text{-}1)$$

M_{et} = First Yield Moment per cell

$$K = \frac{K_3}{K_1 + K_2} \qquad (5.2\text{-}2)$$

K_1 = coefficient that measures the influence of the steel deck depth on the development of the shear bond along the shear span

$$= \sqrt{\frac{d_d}{7.8}} \qquad (5.2\text{-}3)$$

d_d = depth of deck

K_3 = coefficient that accounts for the increase in efficiency of the embossment with increasing slab width

$$= 0.87 + 0.0688\, N - 0.00222\, N^2 \quad \leq \quad 1.4 \qquad (5.2\text{-}4)$$

$$N = \frac{12 b_d}{C_s} \qquad (5.2\text{-}5)$$

b_d = test slab width

C_s = cell spacing

K_2 = coefficient that indicates the mechanical bond performance along the shear span L'

Type I or Type III Deck:

$$K_2 = \frac{D_w{}^{0.8}\left(\frac{K_3}{SS1}\right)}{1.0 + 60\left(p_h{}^2\ \sqrt[3]{p_s}\right)} \qquad (5.2\text{-}6)$$

$$SS1 = \left(\frac{3 l_{nf}}{70}\right)\left(l_{nf} - 14\right) + 3.6 \qquad (5.2\text{-}7)$$

l_{nf} = clear span length

$$p_s = \frac{12 l_e}{s} \qquad \text{(Type I)} \qquad (5.2\text{-}8)$$

$$p_s = \frac{12\left(N_v\, l_e + N_h w\right)}{s} \qquad \text{(Type III)} \qquad (5.2\text{-}9)$$

Type II Deck:

$$K_2 = \frac{627 t^2 \ SS2}{d_d \ e^x} + t\left(\frac{7}{d_d}\right)^2 \qquad (5.2\text{-}10)$$

$$SS2 = \frac{f'_c}{5000} + \frac{\sqrt{\frac{12L}{L'}}}{3.6} \qquad (5.2\text{-}11)$$

L = span length

L' = shear span length

$x = 25\ p_h$

t = thickness of the deck

d_d = depth of deck

The applicability of the above formulas have been previously tested experimentally within the following limitations:

- 0.035 in. ≤ P_h ≤ 0.105 in.
- 55°≤ angle of inclination of the deck web, □ ≤ 90°
- webs have no re-entrant bends in their flat width
- $d_d \leq 3$ in.
- $C_s \leq 12$ in.
- 2500 psi ≤ f'$_c$ □ 6000 psi

5.3 Iterative Method from Shear Bond Tests (Widjaja 1997)

This method involves the use of a computer program written by Widjaja that not only determines the ultimate strength value, but also generates a load-deflection graph for the loading cycle up to failure. The slab system's strength is considered to consist of two components: 1.) partial composite strength and 2.) remaining noncomposite deck strength.

Partial Composite Strength

The partial composite strength is determined using an elasto-plastic rather than plastic model, because the limited shear transfer ability of the deck prevents the steel and concrete stresses from reaching ultimate values. The elasto-plastic strain distribution at the face of a cross section is shown in Figure 5.3.1. Concrete strain and slip values are both unknown and interdependent. An iterative method is used in which the concrete strain determined from a previous iteration is assumed and then used to determine slip. The corresponding concrete strain for this value of slip is then re-determined. Summing the compressive or tensile forces about the neutral axis of the cross section gives the moment at that point.

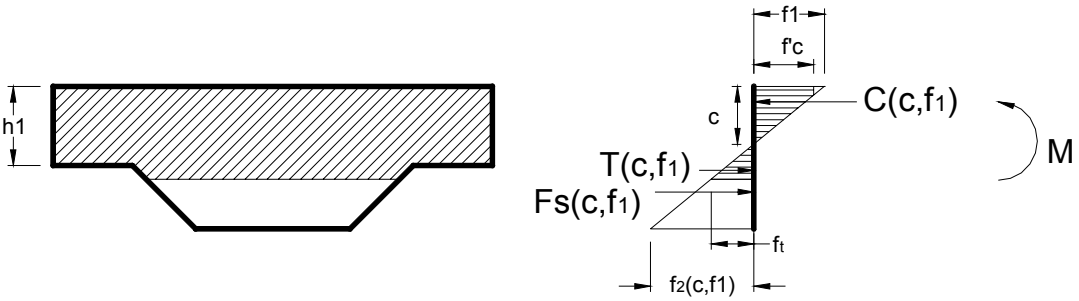

Figure 5.3.1 Elasto-Plastic Force Distribution (Widjaja 1997)

The relationship between slip and concrete strain is determined from the shear resistance given by the shear bond tests described in Chapter 3. A representative graph of the simplified shear resistance behavior is shown in Figure 5.3.2, which is obtained by averaging all the test results for specimens with one type of embossment and then simplifying this average plot into a representative series of several straight line segments. The complete set of simplified shear resistance plots is in Appendix A. Plots of the data from these elemental tests show that shear resistance varies with respect to the amount of slip between the steel and concrete. Slip initiates in a slab at its critical section where cracking begins and then progresses to be greatest at the ends of the slab. Therefore, it is assumed that shear resistance varies along the length of the full-scale slab according to the amount of slip at each location as shown in Figure 5.3.3. A subroutine in the computer program determines this shear resistance distribution by using the simplified

shear resistance versus slip values from elemental tests. The total shear force in the full-scale slab that can be transferred between the steel deck and the concrete slab at any given section is determined by integrating this shear resistance distribution over the shear bond distance to that section. The total shear force is limited to the tensile capacity of the deck, a value which is rarely attained when the embossments are the only shear transfer devices.

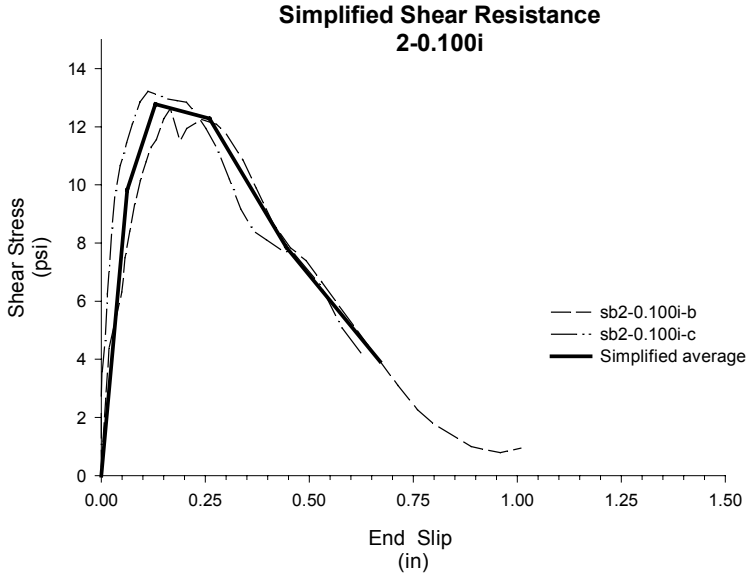

Figure 5.3.2 Simplified Shear Resistance for 2-0.100i

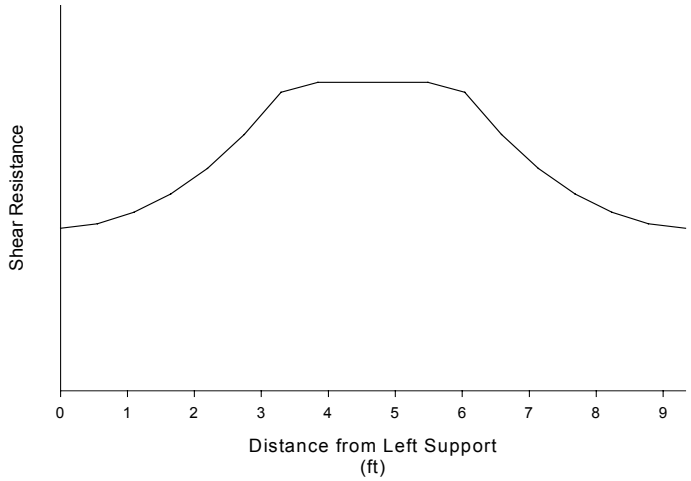

Figure 5.3.3 Typical Shear Resistance Distribution Along the Slab Span

Additional Noncomposite Deck Strength

This additional strength considers the remaining noncomposite strength of the deck unused by the partial composite action. This strength is determined as follows:

$$M_{noncomposite} = f_y^{*}\ S \tag{5.3-1}$$

$$f_y^{*} = f_y - f_{cast} - f_s - f_w \tag{5.3-2}$$

f_y = yield stress of steel deck

f_{cast} = stress in deck due to casting

f_s = stress in deck due to shear transfer

$$= \frac{F_s}{A_s}$$

f_w = stress in deck due to the force in the welds

$$= \frac{F_w}{A_s}$$

S = section modulus of noncomposite steel deck

The total moment capacity for the slab is the sum of the noncomposite and composite strengths:

$$M_{total} = M_{composite} + M_{noncomposite} \tag{5.3-3}$$

Deflection

To plot the Load vs. Midspan Deflection graphs, it is also necessary to determine the deflections during the loading cycle. This is done by using the cracked stiffness of the concrete slab plus the additional stiffness of the unused noncomposite strength of the deck. The noncomposite and composite stiffness contributions are considered to be proportional to the noncomposite and composite strength contributions. Because cracking varies along the slab length, the slab has a nonprismatic effective section, requiring the performance of numerical integration to determine deflection.

5.4 Evaluation of Experimental Results with Analytical Methods

The above analytical methods were applied to the 2VLI and 3VLI deck specimens of each embossment type. The results given by these methods were then compared to the experimental results determined from the full-scale slab tests and plotted for each specimen tested. Figures 5.4.1-2 show representative graphs of these plot comparisons for the 2-exist-b and 2-0.10i-a slab specimens. The full set of graphs for all the specimens tested is in Appendix C. A numerical summary of the results for the 2VLI and 3VLI decks is presented in Tables 5.4.1-2. The specimens whose shear resistance was compromised due to honeycombing of the concrete at the deck interface are designated with shaded values.

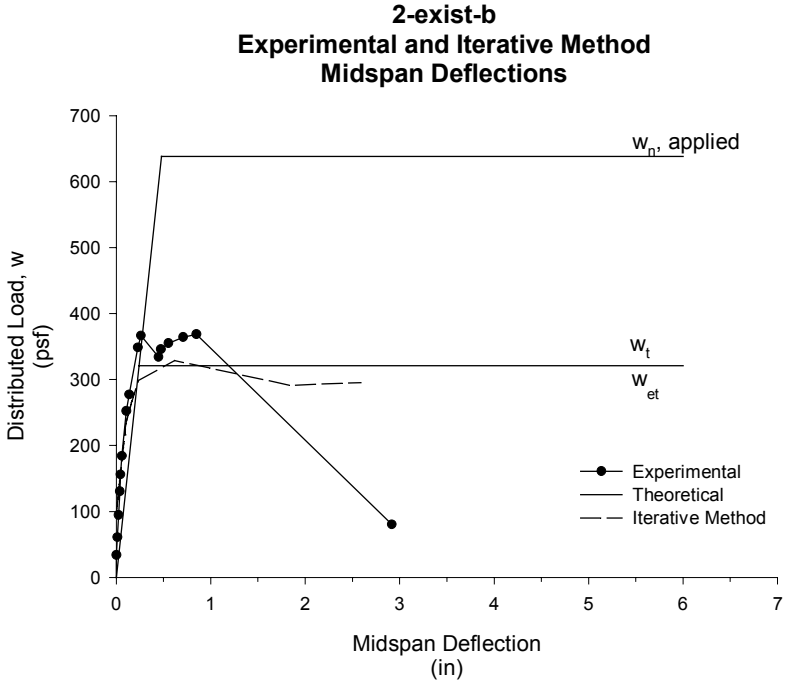

w_n = Theoretical applied distributed load that results in M_n using the calculated material properties

w_t = Theoretical applied distributed load that results in M_t (Flexural Capacity using ASCE App. D Method)

w_{et} = Theoretical applied distributed load that results in M_{et} (First Yield Moment)

Figure 5.4 1 Experimental and Analytical Plots for 2-exist-b

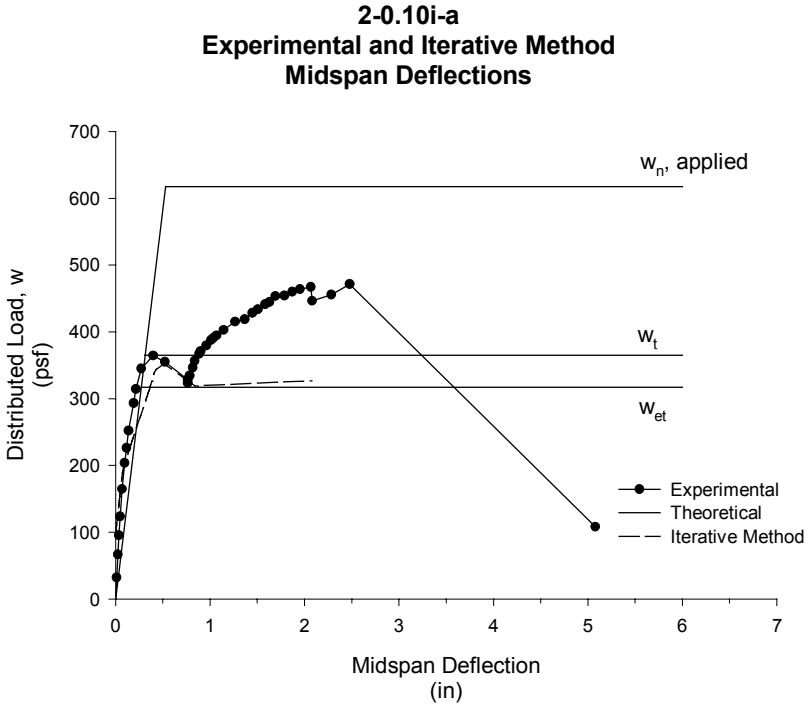

w_n = Theoretical applied distributed load that results in M_n using the calculated material properties

w_t = Theoretical applied distributed load that results in M_t (Flexural Capacity using ASCE App. D Method)

w_{et} = Theoretical applied distributed load that results in M_{et} (First Yield Moment)

Figure 5.4. 2 Experimental and Analytical Plots for 2-0.10i-a

Table 5.4. 1 Comparison of Experimental and Predicted Applied Load Capacities for 2VLI Deck

Test Designation	Max. Experimental Wtest (psf)	First Yield Wet (psf)	ASCE App. D Wt (psf)	Ultimate Wn (psf)	Iterative Method Witer (psf)	Wtest/Wet (psf)	Wtest/Wt (psf)	Wtest/Wn (psf)	Wtest/Witer (psf)
2-0.10i-a	472	317	365	618	351	1.49	1.29	0.76	1.34
2-0.10i-b	492					1.55	1.35	0.80	1.40
2-0.125i-a	433	320	423	635	355	1.35	1.02	0.68	1.22
2-0.125i-b	396					1.24	0.94	0.62	1.12
2-0.125io-a	477	320	424	635	338	1.49	1.13	0.75	1.41
2-0.125io-b	396					1.24	0.93	0.62	1.17
2-0.140io-a	400	320	455	637	342	1.25	0.88	0.63	1.17
2-0.140io-b	359					1.12	0.79	0.56	1.05
2-exist-a	417	321	326	638	328	1.30	1.28	0.65	1.27
2-exist-b	368					1.15	1.13	0.58	1.12
					mean:	1.32	1.07	0.67	1.23
					standard deviation:	0.15	0.19	0.08	0.13
					coefficient of variation:	11.3%	17.8%	12.0%	10.2%

Notes:

1. Shaded values indicate test slab specimens had lower test strengths due to honeycombing of the concrete;
2. First Yield was determined using a calculated (not measured) stress due to casting

Table 5.4. 2 Comparison of Experimental and Predicted Applied Load Capacities for 3VLI Deck

Test Designation	Max. Experimental Wtest (psf)	First Yield Wet (psf)	ASCE App. D Wt (psf)	Ultimate Wh (psf)	Iterative Method Witer (psf)	Wtest/Wet (psf)	Wtest/Wt (psf)	Wtest/Wh (psf)	Wtest/Witer (psf)
3-0.10i-a	422	281	309	538	322	1.50	1.37	0.78	1.31
3-0.10i-b	418					1.49	1.35	0.78	1.30
3-0.125i-a	469	255	318	521	323	1.84	1.47	0.90	1.45
3-0.125i-b	456					1.79	1.43	0.88	1.41
3-0.125io-a	456	256	319	525	303	1.78	1.43	0.87	1.50
3-0.125io-b	461					1.80	1.45	0.88	1.52
3-0.14io-a	500	255	337	520	319	1.96	1.48	0.96	1.57
3-0.14io-b	462					1.81	1.37	0.89	1.45
3-exist-a	327	256	256	518	276	1.28	1.28	0.63	1.18
3-exist-b	345					1.35	1.35	0.67	1.25
					mean:	1.66	1.40	0.82	1.39
					standard deviation:	0.23	0.07	0.11	0.13
					coefficient of variation :	14.1%	4.7%	13.0%	9.1%

Note:

1. First Yield was determined using a calculated (not measured) stress due to casting

The two ASCE design methods provided conservative approximations for the slabs that were tested (excluding the honeycombed specimens). The standard First Yield Method (w_{et}) gave the most conservative strength predictions, with a mean w_{test}/w_{et} value of 1.32 for the 2VLI specimens, and 1.66 for the 3VLI specimens. A comparison of the calculated First Yield versus the experimentally determined load at which the bottom flange of the deck reached yield stress is presented in Tables 5.4.3-4. Calculated First Yield values were determined using calculated stresses due to casting. Experimental first yield values were slightly higher (within 30%) than calculated values, which may be due to the additional strength from the welded wire fabric. Therefore, the theoretical first yield load does appear to correspond well with the actual measured first yield load.

Table 5.4. 3 Calculated and Experimental First Yield Comparison for 2VLI Deck

Test Designation	Calculated First Yield Wet (calc) (psf)	Experimental First Yield Wet (test) (psf)	Wet (test) / Wet (calc)
2-0.10i-a	317	350	1.10
2-0.10i-b		416	1.31
2-0.125i-a	320	283	0.88
2-0.125i-b		256	0.80
2-0.125io-a	320	386	1.21
2-0.125io-b		321	1.00
2-0.140io-a	320	279	0.87
2-0.140io-b		265	0.83
2-exist-a	321	420	1.31
2-exist-b		364	1.13
		mean:	1.05
		standard deviation:	0.20
		coefficient of variation:	18.67%

Note: Shaded values denote test slab specimens had lower test strengths due to honeycombing of the concrete

Table 5.4. 4 Calculated and Experimental First Yield Comparison for 3VLI Deck

Test Designation	Calculated First Yield Wet (calc) (psf)	Experimental First Yield Wet (test) (psf)	Wet (test) / Wet (calc)
3-0.10i-a	281	307	1.09
3-0.10i-b		319	1.14
3-0.125i-a	255	326	1.28
3-0.125i-b		306	1.20
3-0.125io-a	256	300	1.17
3-0.125io-b		308	1.20
3-0.14io-a	255	309	1.21
3-0.14io-b		300	1.18
3-exist-a	256	287	1.12
3-exist-b		327	1.28
		mean:	1.19
		standard deviation:	0.06
		coefficient of variation:	0.05

Use of the ASCE Appendix D Alternate Method had some specified restrictions to limit its use to embossment types that had been previously verified experimentally. For this analysis, all these criteria were met except that the proposed embossments (p_h = 0.125 in. to 0.140 in.) had depths greater than those recommended for the application of this method (0.035 in. □ p_h □0.105 in.). However, use of this method still seemed to still be valid because there was no noticeable decrease in accuracy for the specimens with the deeper embossments. The Appendix D Alternate Method (w_t) more closely predicted the strengths than the First Yield Method and gave mean w_{test}/w_t values of 1.05 and 1.19 for the 2VLI and 3VLI specimens, respectively.

Although not very accurate predictions of experimental strengths, both ASCE design methods provide a good lower bound strength prediction that is easy to calculate and does not require any experimental testing.

Use of the Iterative Method (w_{iter}) produced a plot of Applied Load versus Midspan Deflection that fairly closely followed the experimental plot until reaching the first drop in the experimental plot, which occurred at the initiation of slip and flexural cracking. Results from the Iterative Method seemed to indicate failure at first slip

regardless of the magnitude of shear resistance input into the computer analysis program. Inputting greater shear resistances merely increased the slab's capacity before the initiation of slip. Therefore, this method seemed to be inadequate in accounting for the fact that additional shear resistance from the embossments provided composite interaction even after slip and cracking initiated. The Iterative Method strength predictions were also conservative, giving mean w_{test}/w_{iter} ratios of 1.23 and 1.40 for the 2VLI and 3VLI specimens respectively. This method was most accurate for the specimens with the existing embossment pattern because they had brittle behavior. The w_{test}/w_{iter} ratios for the specimens with the existing embossment patterns were: 1.12-1.27 (2VLI) and 1.19-1.25 (3VLI).

5.5 Conclusions

Each of the analytical methods provided conservative strength predictions when compared to the experimental strengths. The First Yield method and ASCE's Appendix D Alternate method are advantageous because they give reliable lower bound strengths, do not require experimental tests, and are easy to calculate. Although some of the proposed embossment depths were greater than the recommended limits for applicability of the Appendix D Method, this method still seemed applicable. The Appendix D method is slightly more complicated than the straight First Yield method but gives a more accurate prediction because it includes deck and embossment factors that describe the shear transfer ability of the specific deck under consideration. Widjaja's Iterative Method is considerably more complex in theory because it evaluates the slab during the entire loading cycle, and in application because it requires the performance of elemental shear bond tests and a computer analysis program. This method allows the possibility of inconsistent strength predictions because the results are dependant on the data from the shear bond tests, the procedure of which is still not adequately standardized. The strength predictions given by this method are not noticeably better than those given by the first two methods because it does not seem to properly account for additional partial composite strength due to the continued shear resistance of the embossments after slip initiates. However, the Iterative Method is useful for determining the behavior of the slab

during the loading cycle, instead of just at failure. For design purposes, it is recommended that either the First Yield method or the Appendix D method be used because of their simplicity.

CHAPTER 6: SUMMARY, CONCLUSIONS, AND RECOMMENDATIONS

6.1 Summary

Composite floor systems have been gaining popularity in steel-framed structures over the last few decades. The most common governing mode of failure for these floor systems is failure of the shear bond between the steel deck and the concrete slab components. At shear bond failure the composite interaction breaks down, resulting in a lower-capacity system than if it were fully composite. Therefore, some deck manufacturers are making efforts to enhance the shear bond strength through means such as improved embossments in the deck.

This study focused on the effect on strength of four proposed embossment patterns as compared to the existing embossment pattern for Vulcraft's 2VLI (2 in. deep) and 3VLI (3 in. deep) decks. The proposed embossments were patterned such that they had a corrugating effect on the web of the deck. These embossments had varying depths with some rolled into the face of the concrete only, while others were rolled both into the face of the concrete and outward: 0.100 in. (in only), 0.125 in. (in only), 0.125 in. (in and out), and 0.140 in. (in and out). The existing embossments had a depth of 0.100 in (in only) and consisted of a repeating pattern of a pair of horizontal embossments followed by a pair of vertical embossments.

Shear bond tests were performed for at least two specimens of each type of embossment for both depths of deck. The performance of small elemental shear bond tests was a relatively convenient way to examine specifically the shear resistance performance of different embossment patterns. In this test, the concrete portion was sheared over the steel deck while recording the slip and corresponding shear force. These results were then plotted for observation of the shear resistance behavior. The tested

specimens were then taken apart and examined for their failure modes. The shear resistance behavior of the specimens with the proposed embossments was compared to that of the specimens with the existing embossment patterns.

Although there do exist a few standard design methods, current practice still remains for deck manufacturers to perform multiple full-scale slab tests to determine the capacities of the decks they produce. The manufacturers then publish design catalogues with recommendations for allowable loads and span lengths of their product. In accordance with this practice, this study also involved the performance of a series of two full-scale slab tests of each type of deck (2VLI and 3VLI deck with the proposed and existing embossments) to determine their capacities. The slabs were uniformly loaded with an air bag while measuring the applied load, midspan deflection, end slip, deck bottom flange strains, deck top flange strains, and concrete cracking. The behavior and capacities of the slabs with proposed embossments in the deck were compared with slabs having the existing deck embossments.

To preclude the expensive and time consuming use of full-scale slab tests, some researchers have developed methods of predicting composite slab strength based on analytical methods. In this study, three such methods were evaluated for their applicability by comparing capacities determined by using these methods with the experimentally determined capacities. These three methods are: the First Yield Method of design (Heagler 1992), the ASCE Appendix D Alternate Method of Design (*Standard* 1994), and Widjaja's Iterative Method (1997). The First Yield Method predicts the slab capacity to be the load that causes the bottom flange of the deck to reach yield stress. The Alternate Appendix D Method considers the shear transfer ability of different decks by the application of relaxation factors that describe the deck and embossment properties. The design strength is the multiplication product of the first yield strength and the relaxation factor. The Iterative Method not only determines a final strength prediction, but also determines the load-deflection behavior of the slab during its loading history until failure. This method requires the performance of elemental shear bond tests to determine the shear resistance capacity of the deck, which is input into a computer analysis program developed by Widjaja.

6.2 Conclusions

The following conclusions were made as a result of this study:

Shear Bond Test Conclusions

- Standardization of the shear bond test procedure is necessary to obtain consistent results. Some factors to be considered are: specification of the magnitude of the lateral pressure applied to the test specimen, a means to directly measure the shear force in each specimen half rather than assuming an equal distribution to the two halves, use of lateral bracing to prevent rotation of the specimen when slip of one half initiates before the other half, a means to preserve the chemical bond if it is to be studied.
- Failure of the tested specimens occurred due to the concrete riding over the deck rather than concrete crushing or plastic deformation of the embossments. Only minor concrete crushing was observed.
- Specimens consisting of deck with the existing embossments had brittle shear bond behavior, failing suddenly and with the initiation of minor slip.
- Specimens consisting of deck with the proposed embossments had ductile shear bond behavior, maintaining shear resistance even after significant slip occurred.
- The shear resistance of specimens with the proposed embossments was considerably greater than specimens with the existing embossments for the 2VLI and 3VLI deck.
- The "in and out" embossment pattern did not exhibit better shear resistance than the "in" embossment pattern.
- For the range of embossment depths tested in this study (0.100 in. - 0.140 in), increasing the depth of the proposed embossment generally improved the shear resistance of the specimen.
- Because the behavior of the specimens given by the shear bond tests corresponded well to behavior found in the full-scale tests, it can be concluded that shear bond tests are effective small-scale tests when comparing the performance of different decks or embossment patterns.

Full-Scale Slab Test Conclusions:

- The failure mechanisms of the full-scale slabs were observed as follows: 1.) first yield of the bottom flange of the deck, 2.) concrete cracking due to differential strains in the deck and concrete, 3.) the attainment of maximum longitudinal shear resistance of the shear span, 4.) excessive slip of the concrete over the deck resulting in noncomposite interaction, and 5.) flexural failure of the slab because of its decreased noncomposite strength.
- Slabs with the proposed embossments had ductile behavior as defined by the Eurocode to be when slabs have ultimate strengths greater than 110% of the load at which first slip occurred.
- Slabs with the existing embossments had brittle behavior, according to Eurocode's definition.
- Slabs with the proposed embossments had higher ultimate strengths (approximately 25%) than slabs with the existing embossments of the same depth for both the 2VLI and 3VLI decks.
- The "in and out" embossment pattern did not provide greater ultimate strengths than the "in" embossment pattern.
- For the range of embossment depths tested in this study (0.100 in. - 0.140 in), increasing the depth of the proposed embossment generally improved the ultimate capacity of the specimen.

Evaluation of Analysis Methods Conclusions:

- The First Yield Method of Design (Heagler 1992), the ASCE Appendix D Alternate Method of Design (*Standard* 1994), and Widjaja's Iterative Method (1997) all provided satisfactory lower bound strength predictions when compared to the experimentally determined ultimate strength for slabs with the proposed and existing embossments in the 2VLI and 3VLI deck.
- The accuracy of the strength prediction given by the ASCE Appendix D Method was not compromised for slabs with embossments deeper than the recommended limits for use of this method. Therefore, it appears that this method is valid for embossment depths up to 0.140 in.

- The ASCE Appendix D Method is slightly more accurate than the First Yield Method, but requires slightly more complicated calculations.
- Widjaja's Iterative Method is beneficial for determining the behavior of the slab during its loading history. However, this method is significantly more complicated to use because it requires the performance of shear bond tests and the use of a computer analysis program. The Iterative Method is based on theory that is much more complex than that of the other two methods, but does not give noticeably better final strength predictions.

6.3 Recommendations for Future Research

The proposed embossment pattern does indeed provide greater strengths than the existing embossment pattern for Vulcraft's deck. Of the depths tested, the 0.140 in. deep embossments were the most effective. An analysis should be made to determine which of the proposed embossment patterns to pursue by considering the cost and ease of fabrication of the different embossment depths and the "in and out" verses the "in only" patterns. Further tests on the deck itself should also be performed to study its shear resistance mechanisms. One such test would be a web-crippling test of deck with the different embossment types, which would predict the flexibility of the decks during over-ride of the concrete in full-scale slab specimens.

Standardization of the Shear Bond Test procedure should be developed. Further investigation should be made regarding what magnitude of lateral pressure should be applied in order to best represent the shear resistance behavior of a full-scale specimen. Consideration should be given to the fact that the full-scale slab resists lateral pressure mostly only at the supports.

Improvements should be made to Widjaja's Iterative Method. Investigation should be made into how to better represent the behavior of the slab after the initiation of slip and cracking. The computer program should be improved so that it is more user-friendly for universal use.

Several other strength prediction methods are under development that should be further explored and compared with the experimental results given in this study. One

such method is ICOM's Simplified Method, which is based on the moment-curvature relationship (Schumacher et al 2000). This method requires the use of results from elemental shear bond tests as described in this study.

REFERENCES

ASTM E8-00b (2001). Standard Test Methods for Tension Testing of Metallic Materials, West Conshohocken, PA.

ASTM C39-96 (2001). Standard Test Method for Compressive Strength of Cylindrical Concrete Specimens, West Conshohocken, PA.

Bode, H. and Sauerborn, I. (1992). "Modern Design Concept for Composite Slabs with Ductile Behaviour," *Proceedings of an Engineering Foundation Conference on Composite Construction in Steel and Concrete II*, ASCE, June, pp. 125-141.

Bode, H. and Dauwel, T., (1999). "Steel-Concrete Composite Slabs – Design Based on Partial Connection," *Steel and Composite Structures International Conference Proceedings*, Deft, Netherlands, pp. 2.1-2.10.

Calixto, J. M., Lavall, A. C., Melo, C. B., Pimenta, R. J., and Monteiro, R. C. (1998). "Behaviour and Strength of Composite Slabs with Ribbed Decking," *Journal of Constructional Steel Research*, Elsevier Science Ltd, Vol. 46, No. 1-3, Paper No. 110.

Crisinel, M., Daniels, B., and Ren, P. (1992). "Numerical Analysis of Composite Slab Behavior," *Proceedings of an Engineering Foundation Conference on Composite Construction in Steel and Concrete II*, ASCE, June, pp. 798-808.

Crisinel, M., Guignard, P., and Schumacher, A. (1999). "Steel-Concrete Composite Slabs. Progress Report ECCA TWG 7.6,"- *Steel and Composite Structures International Conference Proceedings*, Deft, Netherlands, pp. 1.1-1.10.

Dallaine, E. E. (1971). "Cellular Steel Floors Mature." *Civil Engineering*, ASCE, July, pp. 70-74.

Daniels, B. J. (1988). "Shear Bond Pull-Out Tests for Cold-Formed-Steel Composite Slabs," ICOM Publication No. 194, Ecole Polytechnique Federale De Lausanne.

Daniels, B. and Crisinel, M. (1988). "Composite Slabs with Profiled Sheeting," *Proceedings of an Engineering Foundation Conference on Composite Construction in Steel and Concrete*, ASCE, pp. 656-662.

Daniels, B. and Crisinel, M. (1993a). "Composite Slab Behavior and Strength Analysis. Part I: Calculation Procedure," *Journal of Structural Engineering*, ASCE, Vol. 119, No. 1-4, pp. 16-35.

Daniels, B. and Crisinel, M. (1993b). "Composite Slab Behavior and Strength Analysis. Part II: Comparisons with Test Results and Parametric Analysis," *Journal of Structural Engineering*, ASCE, Vol. 119, No. 1-4, pp. 36-49.

Easterling, W. S., and Young, C. Y. (1992). "Strength of Composite Slabs," *Journal of Structural Engineering*, ASCE, Vol. 118, pp. 2370-2389.

Eurocode 4 (1992). Common Unified Rules for Composite Steel and Concrete Structures. ENV 1994-1-1.

Heagler, R. B., Luttrell, L. D., and Easterling, W. S. (1992). "The Steel Deck Institute Method for Composite Slab Design," *Proceedings of an Engineering Foundation Conference on Composite Construction in Steel and Concrete II*, ASCE, June, pp. 287-303.

Jolly, C. and Zubair, A. (1987). "The Efficiency of Shear-Bond Interlock Between Profiled Steel Sheeting and Concrete," *Composite Steel Structures -- Advances, Design, and Construction*, Elsevier Science Publishing Co., Inc., pp. 127-136.

Kitoh, H. and Sonoda, K. (1996). "Bond Characteristics of Embossed Steel Elements," *Proceedings of and Engineering Foundation Conference on Composite Construction in Steel and Concrete III*, ASCE, pp. 909-918.

Leskela, M. V. (1992). "A Finite Beam Element for Layer Structures and Its Use When Analysing Steel-Concrete Composite Flexural Members," *Constructional Steel Design: World Developments*, Elsevier Applied Science, pp. 354-358.

Luttrell, L. D. and Davison, J. H. (1973). "Composite Slabs with Steel Deck Panels," *Proceedings of the Second International Specialty Conference on Cold-Formed Steel Structures*, University of Missouri-Rolla, pp. 573-603.

Luttrell, L. D. and Prassanan, S. (1984). "Strength Formulations for Composite Slabs," *Proceedings of the Seventh International Specialty Conference on Cold-Formed Steel Structures*, University of Missouri-Rolla, pp. 573-603.

Luttrell, L. D. (1987). "Flexural Strength of Composite Slabs," *Composite Steel Structures --Advances, Design and Construction*, Elsevier Science Publishing Co., Inc., pp. 106-116.

Makelainen, P. and Sun, Y. (1998). "Development of a New Profiled Steel Sheeting for Composite Slabs," *Journal of Constructional Steel Research*, Elsevier Science Ltd, Vol. 46, No. 1-3, Paper No. 240.

Ong, K. C. G and Mansu, M. A. (1986). "Shear-Bond Capacity of Composite Slabs made with Profiled Sheeting," *The International Journal of Cement Composites and Lightweight Concrete*, Vol. 8, No. 4, pp. 231-237.

Patrick, M. (1990) "The Slip Block Test- Experience with Some Overseas Profiles (Part A)," Melbourne, Australia.

Patrick, M., Bridge, R. (1988). "Behavior of Australian Composite Slabs," *Proceedings of and Engineering Foundation Conference on Composite Construction in Steel and Concrete*, ASCE, pp. 663-679.

Patrick, M., Bridge, R. (1990). "Partial Shear Connection Design of Composite Slabs"

Patrick, M. (1994) "Shear Connection Performance of Profiled Steel Sheeting in Composite Slabs," Doctoral Thesis, University of Sydney, School of Civil and Mining Engineering

Porter, M. and Ekberg, C. (1975). " Design Recommendations for Steel Deck Floor Slabs," *Proceedings of the Third International Specialty Conference on Cold-Formed Steel Structures*, University of Missouri-Rolla, pp. 761-791.

Porter, M. and Ekberg, C. (1976). "Design Recommendations for Steel Deck Floor Slabs," *ASCE Journal of the Structural Division*, Vol. 102, pp. 2121-2136.

Sabnis, G. (1979). *Handbook of Composite Construction Engineering*, Littleton Educational Publishing.

Schumacher, A., Laane, A, Crisinel, M (2000). "Development of a New Design Approach for Composite Slabs," *Proceedings of and Engineering Foundation Conference on Composite Construction in Steel and Concrete IV*, ASCE, Vol. 1, pp.1-12.

Schuurman, R. G. and Stark, J. W. B. (1996). "Longitudinal Shear Resistance of Composite Slabs – To a Better Understanding of Physical Behaviour," *Proceedings of and Engineering Foundation Conference on Composite Construction in Steel and Concrete III*, ASCE, pp.89-103.

Schuurman, R. G. and Stark, J. W. B. (2000). "Longitudinal Shear Resistance of Composite Slabs – A New Model," *Proceedings of and Engineering Foundation Conference on Composite Construction in Steel and Concrete IV*, ASCE, Vol. 1, pp.1-10.

Sebastian, W. and McConnelm R. (2000). "NonLinear FE Analysis of Steel-Concrete Composite Structures," *Journal of Structural Engineering*, ASCE, Vol. 126, no. 6, pp. 662-674.

Seleim, S. (1979). *Ultimate Shear-Bond Capacity of Composite Steel Deck Concrete Slabs*, M. A. Sc. Thesis, University of Waterloo, Waterloo, Ont.

Seleim, S. and Schuster, R. (1985). "Shear-Bond Resistance of Composite Deck-Slabs," *Canadian Journal of Civil Engineering*, National Research Council of Canada, Vol. 12, pp. 316-324.

Schuster, R. M. (1970). *Strength and Behavior of Cold-Rolled Steel-Deck Reinforced Concrete Floor Slabs*, Ph. D. Thesis, Iowa State University, Ames, IA.

Schuster, R. M. (1972). "Composite Steel-Deck-Reinforced Concrete Systems Failing in Shear-Bond," *Preliminary Report, Ninth Congress of the International Association for Bridge and Structural Engineering*, Zurich, Switzerland, pp. 185-191.

Standard for the Structural Design of Composite Slabs (1992). Steel Deck with Concrete Standards Committee of Management Group F, Codes and Standards, ASCE, 345 East 47th Street, New York, NY 10017-2398.

Stark, J. W. B, (1978). "Design of Composite Floors with Profiled Steel Sheet," *Fourth Specialty Conference on Cold-Formed Steel Structures*, University of Missouri-Rolla, pp. 893-922.

Stark, J. W. B. (1991). "Design of Composite Steel-Concrete Structures According to Eurocode 4," *Proceedings of the International Conference on Steel and Aluminum Structures*, ICSAS 91, Singapore, pp. 23-39.

Tenhovuori, A., Karkkainen, K., and Kanerva, P (1996). "Parameters and Definitions for Classifying the Behaviour of Composite Slabs," *Proceedings of and Engineering Foundation Conference on Composite Construction in Steel and Concrete III*, ASCE, pp.752-765.

Tenhovuori, A. I. and Leskela, M. V. and (1998). "Longitudinal Shear Resistance of Composite Slabs," *Journal of Constructional Steel Research*, Elsevier Science Ltd, Vol. 46, No. 1-3, Paper No. 319.

Terry, A. (1994). *The Effects of Typical Construction Details on the Strength of Composite Slabs,* M. S. Thesis, Virginia Polytechnic Institute and State University, Blacksburg, Virginia.

Veljkovic, M. (1994a). "Sheeting-Concrete Interaction Performances in the Composite Floor Slab," *Nordic Concrete Research*, pp. 18.

Veljkovic, M. (1994b). "3D Nonlinear Analysis of composite slabs," DIANA Computational Mechanics '94. Eds.: G. M. A. Kusters, M. A, N, Hendriks, pp. 394-404.

Veljkovic, M. (1996). "An Improved Partial Connection Method for Composite Slab Design," *Proceedings of and Engineering Foundation Conference on Composite Construction in Steel and Concrete III*, ASCE, pp.644-659.

Veljkovic, M. (2000). "Behaviour and Design of Shallow Composite Slab," *Proceedings of and Engineering Foundation Conference on Composite Construction in Steel and Concrete IV*, ASCE, Vol. 1, pp.1-12.

Widjaja, B. (1997). *Analysis and Design of Steel Deck-Concrete Composite Slabs*, PhD Thesis, Virginia Polytechnic Institute and State University, Blacksburg, Virginia.

Wright, H. D. and Essawy, M (1996). "Bond In Thin Gauge Steel Concrete Composite Structures," *Proceedings of and Engineering Foundation Conference on Composite Construction in Steel and Concrete III*, ASCE, pp.630-643.

APPENDIX A: SHEAR BOND TEST PLOTS

Graphs of the results from the shear bond test specimens are shown in this Appendix. Following the shear bond test results for each set of an embossment type is a graph containing the simplified average shear resistance for that embossment type. This simplified shear resistance was used as input for the Iterative Method of strength prediction.

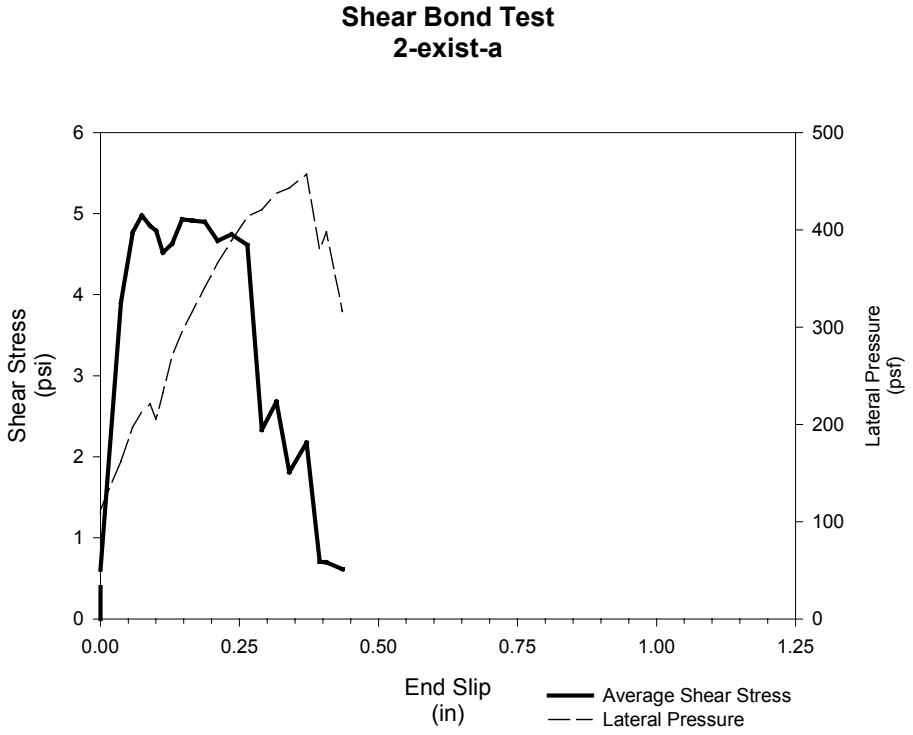

Figure A. 1 Shear Resistance of SB2-exist-a

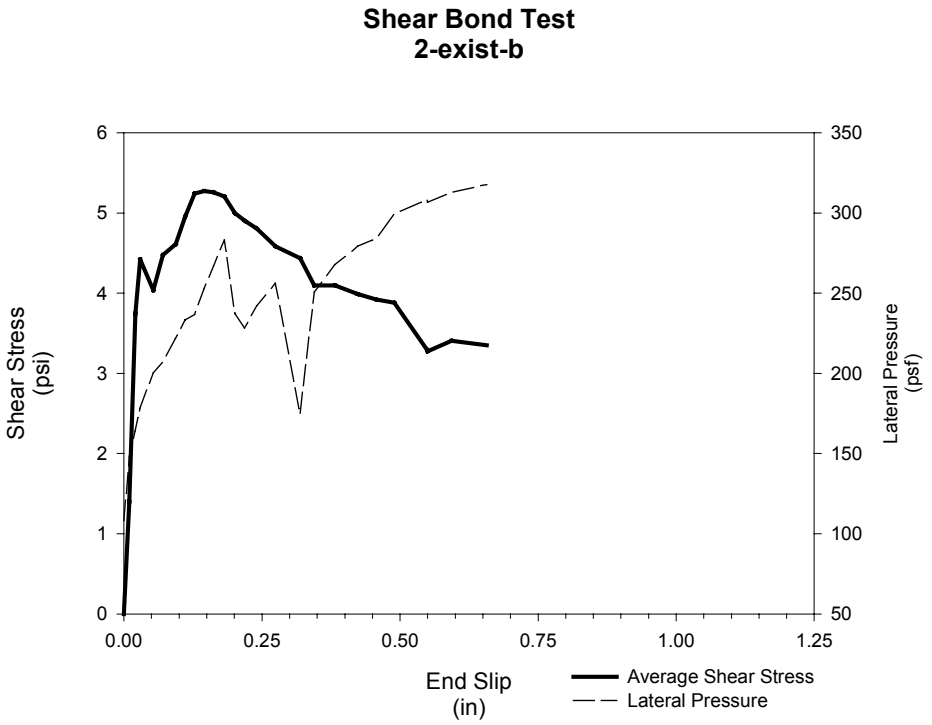

Figure A. 2 Shear Resistance of SB2-exist-b

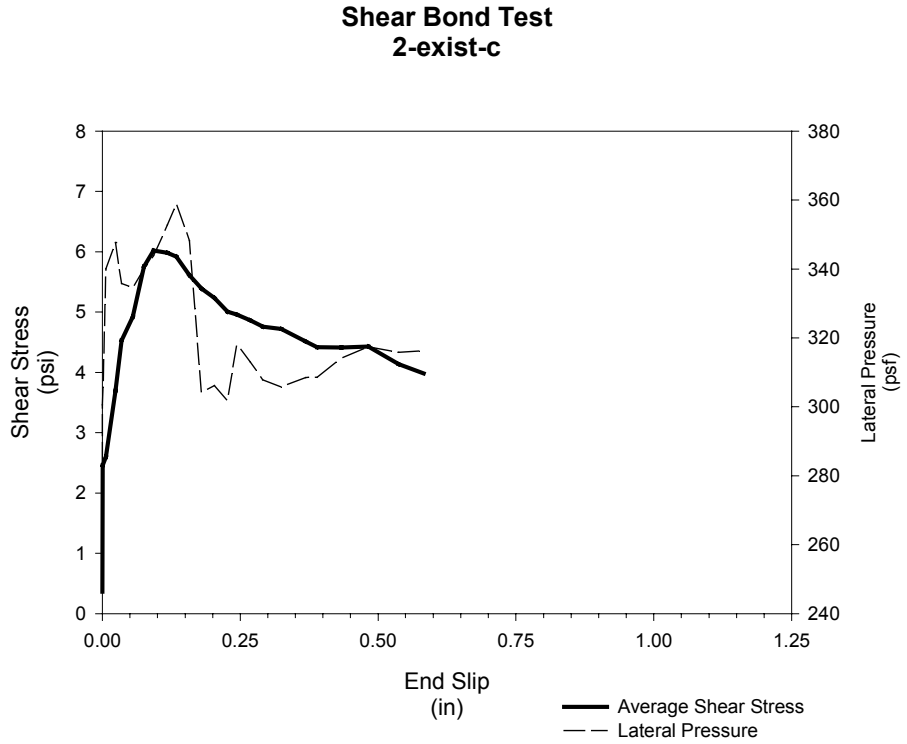

Figure A. 3 Shear Resistance of SB2-exist-c

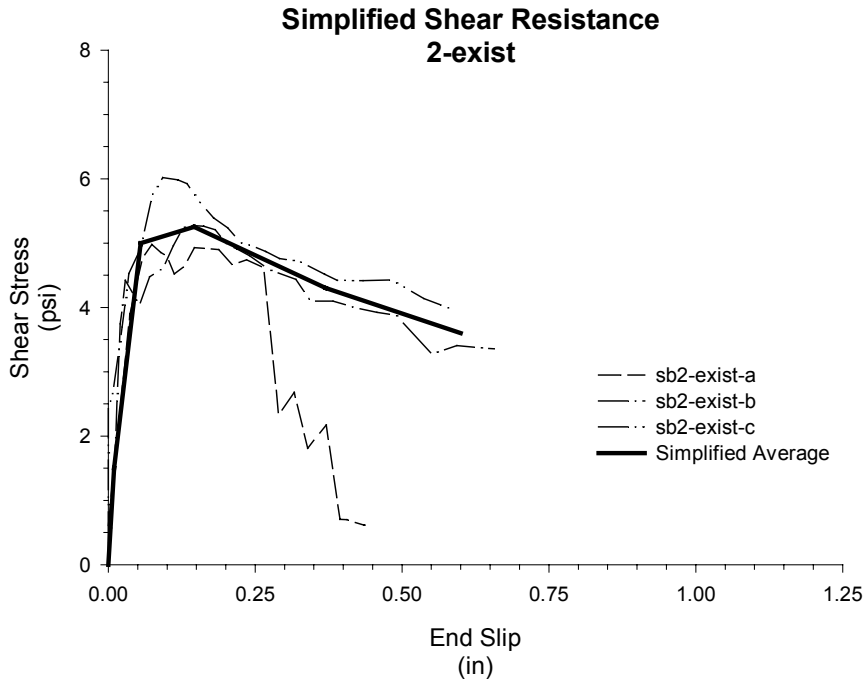

Figure A. 4 Simplified Shear Resistance 2-exist

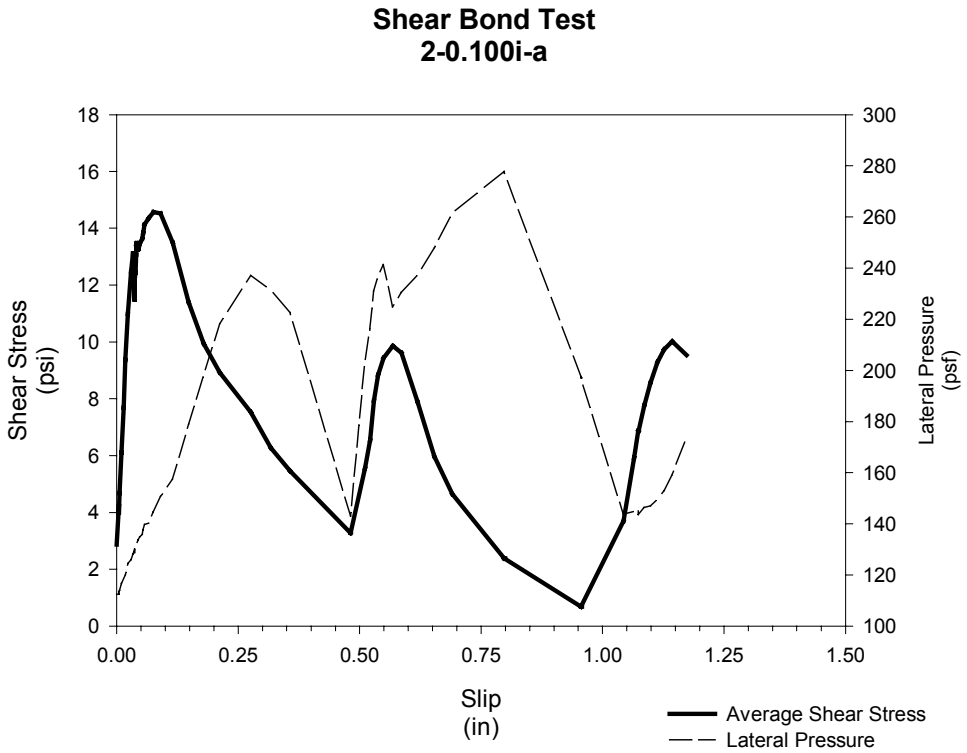

Figure A. 5 Shear Resistance of SB2-0.100i-a

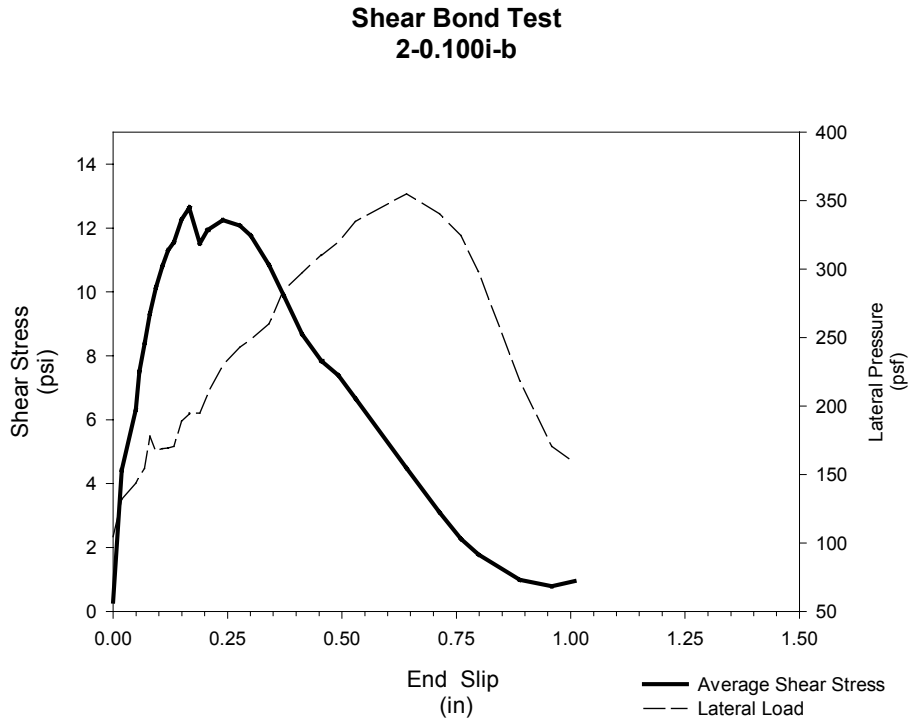

Figure A. 6 Shear Resistance of SB2-0.100i-b

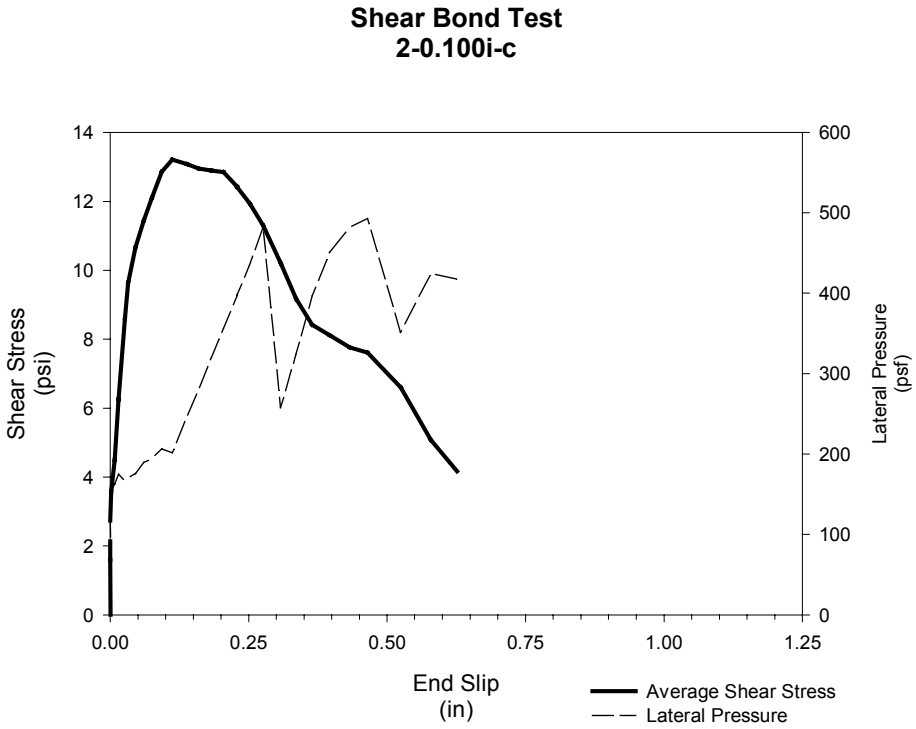

Figure A. 7 Shear Resistance of SB2-0.100i-c

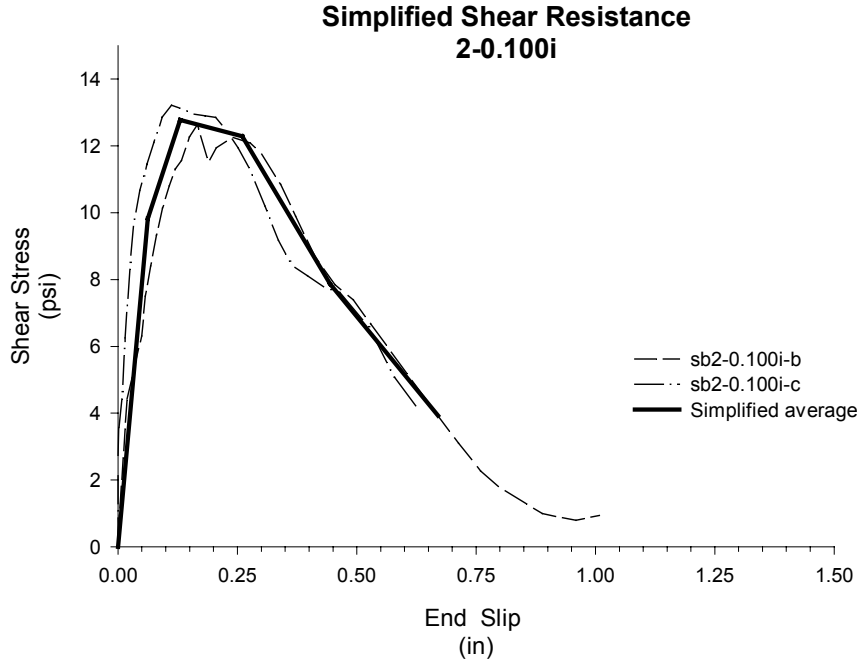

Figure A. 8 Simplified Shear Resistance of 2-0.100i

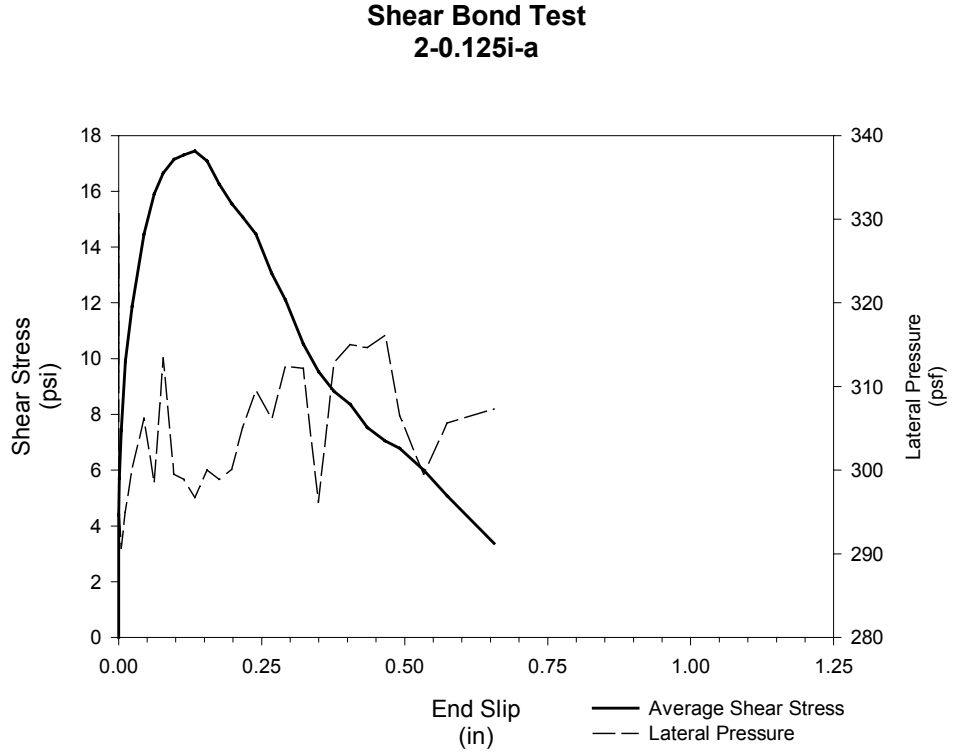

Figure A. 9 Shear Resistance of SB2-0.125i-a

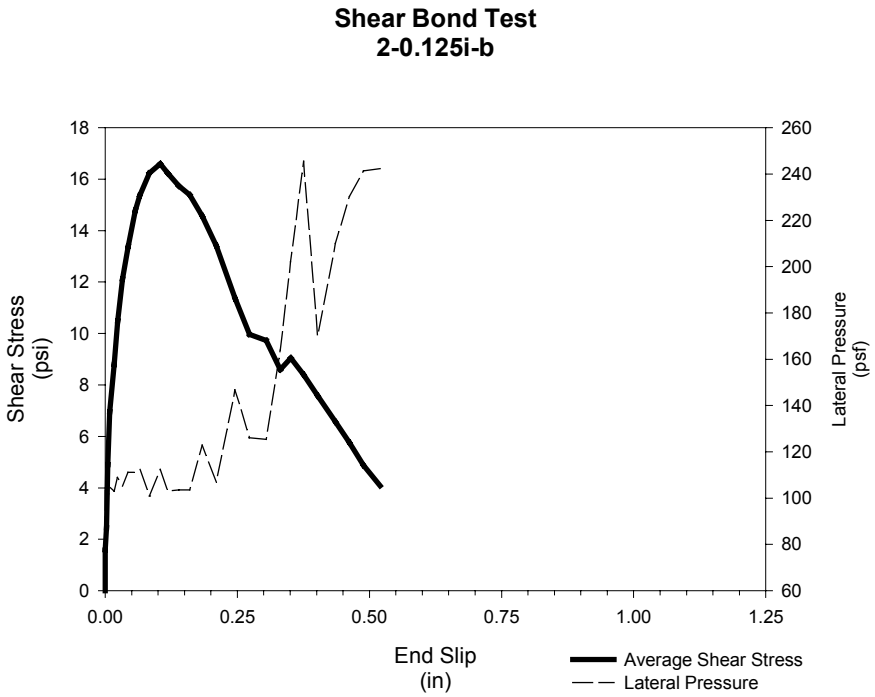

Figure A. 10 Shear Resistance of SB2-0.125i-b

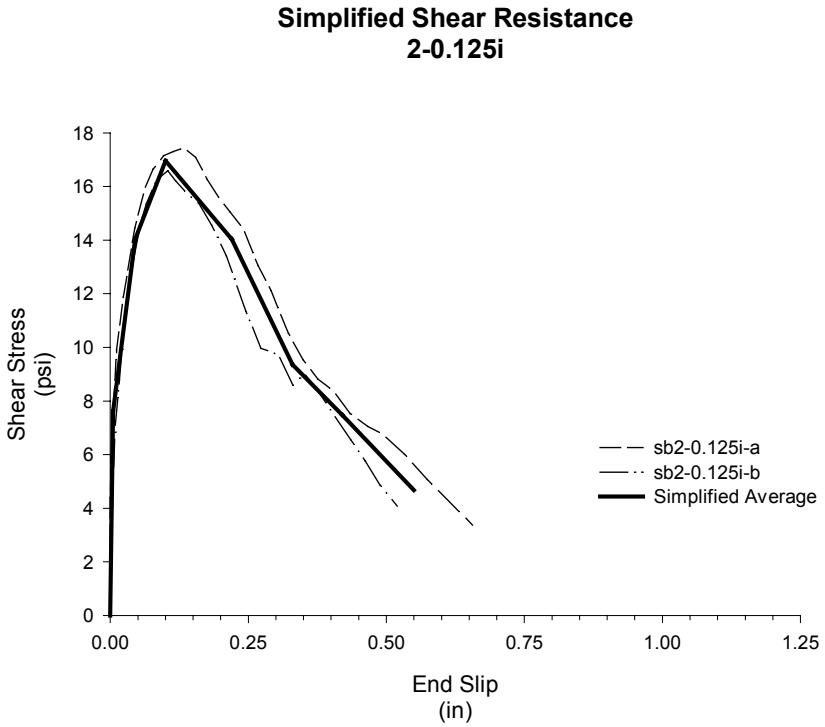

Figure A. 11 Simplified Shear Resistance for 2-0.125i

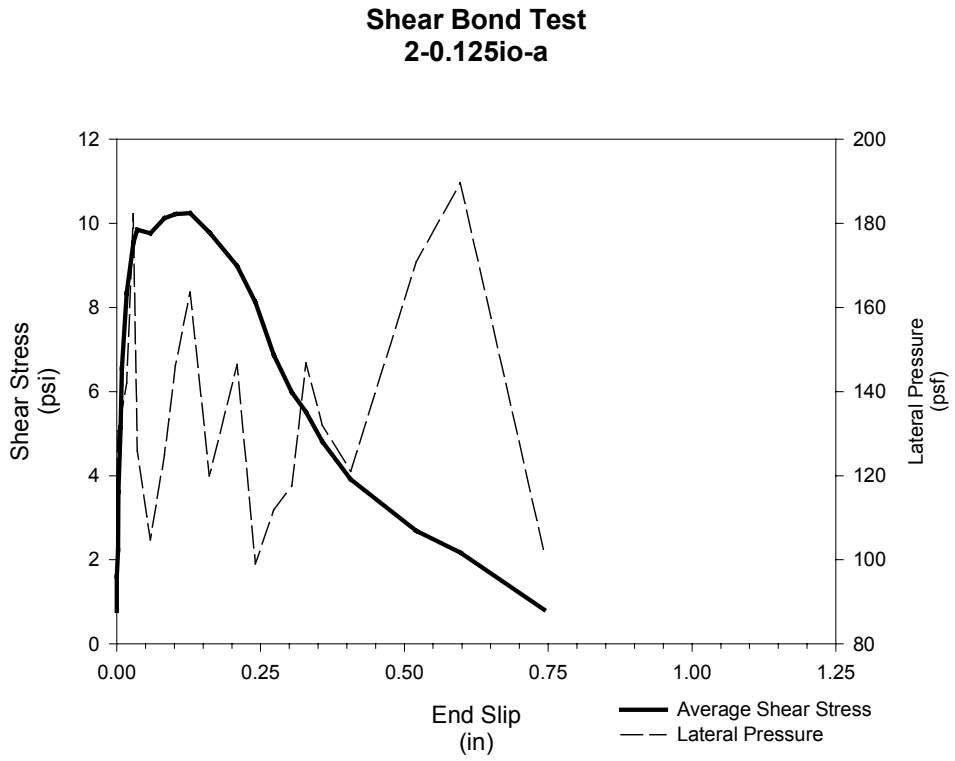

Figure A. 12 Shear Resistance of SB2-0.125io-a

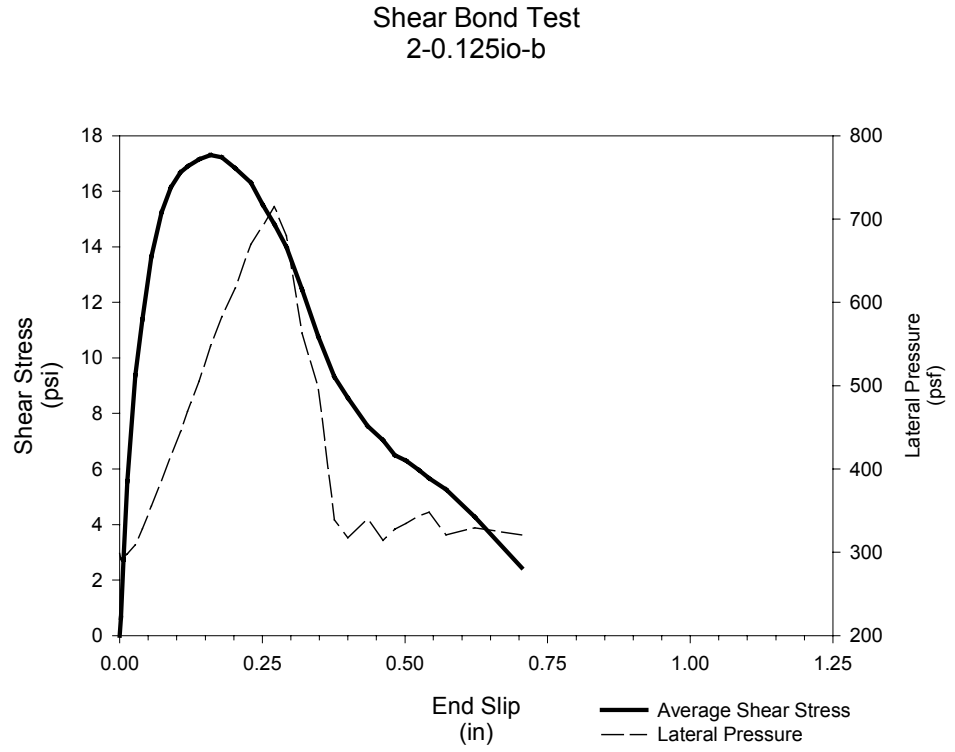

Figure A. 13 Shear Resistance of SB2-0.125io-b

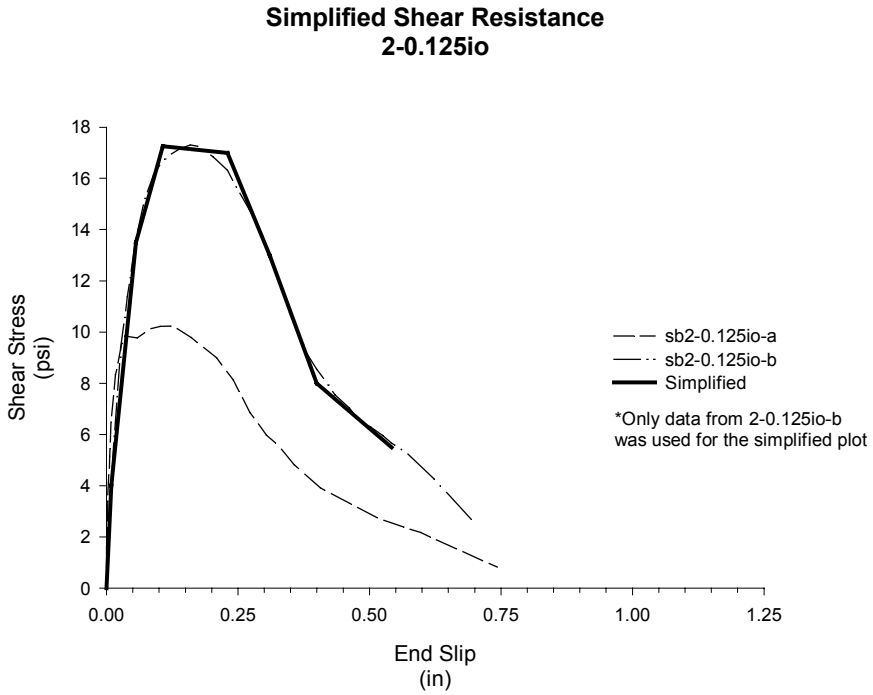

Figure A. 14 Simplified Shear Resistance for 2-0.125io

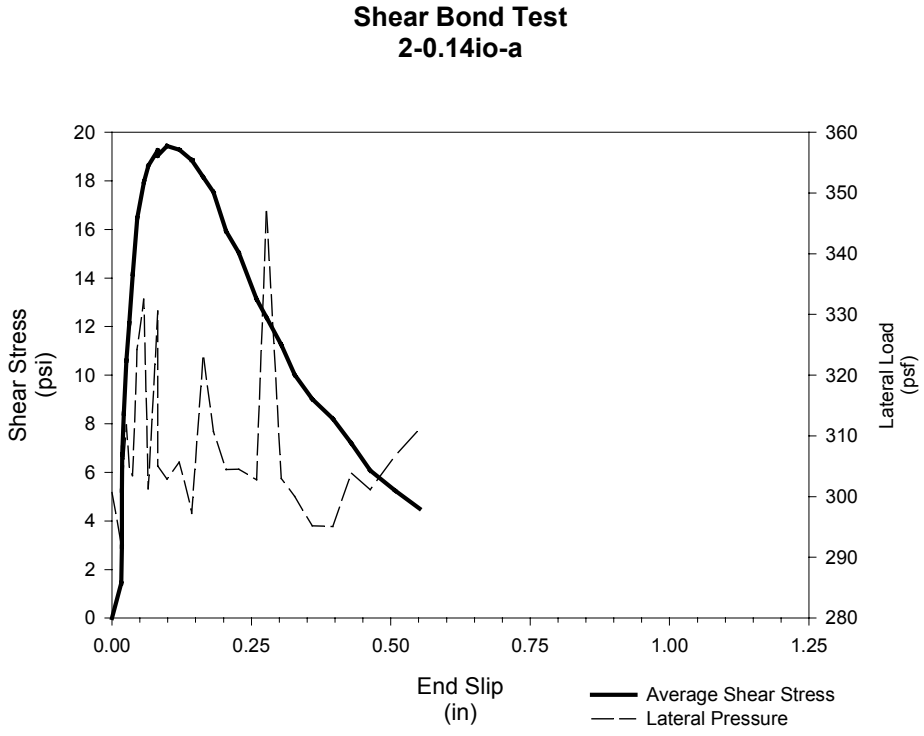

Figure A. 15 Shear Resistance SB2-0.14io-a

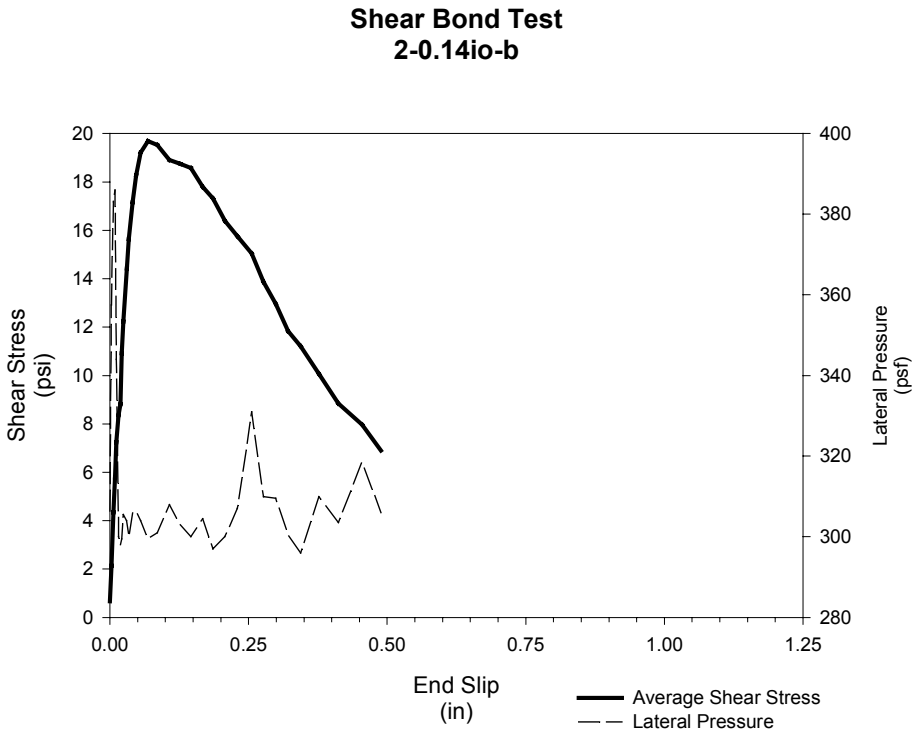

Figure A. 16 Shear Resistance SB2-0.14io-b

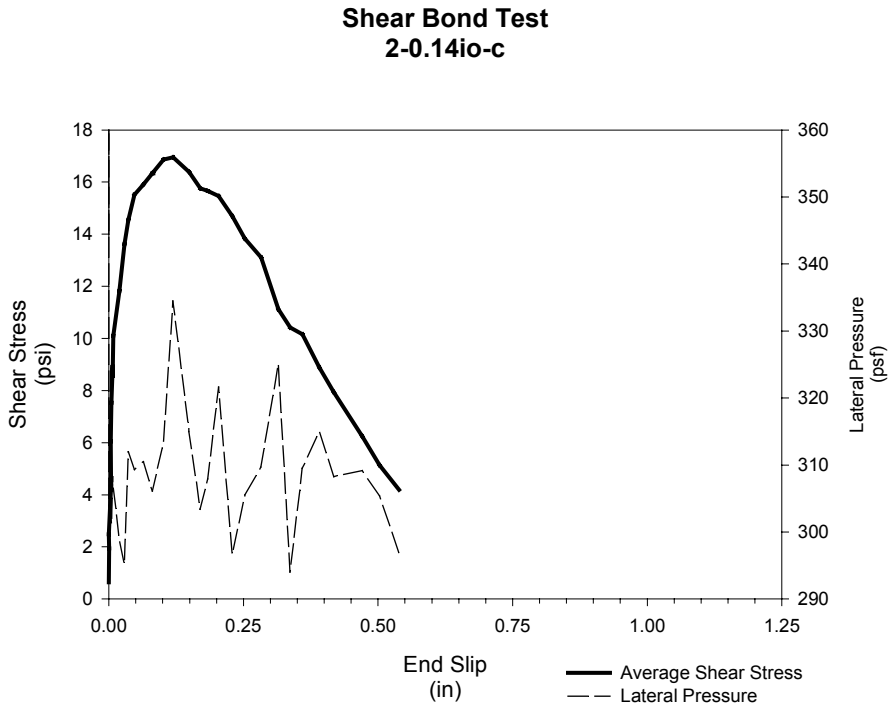

Figure A. 17 Shear Resistance SB2-0.14io-c

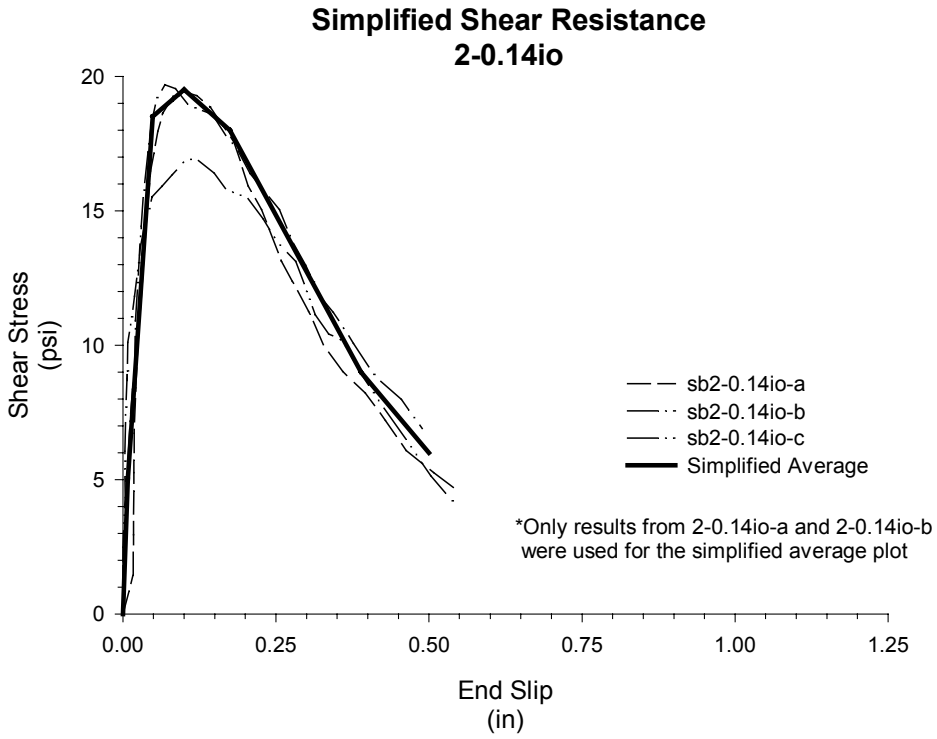

Figure A. 18 Simplified Shear Resistance for 2-0.14io

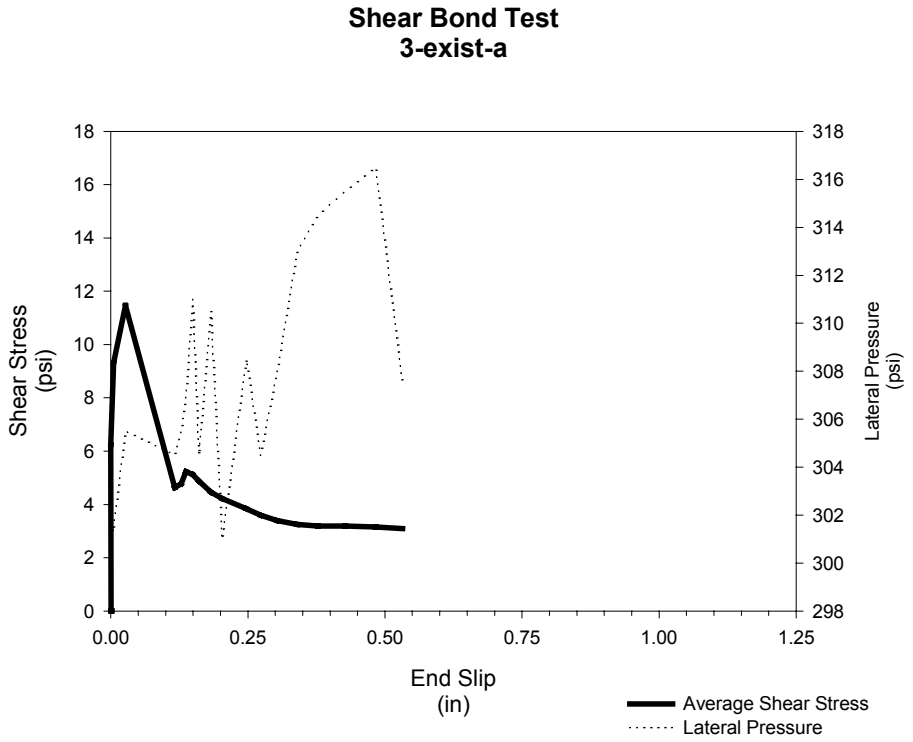

Figure A. 19 Shear Resistance SB3-exist-a

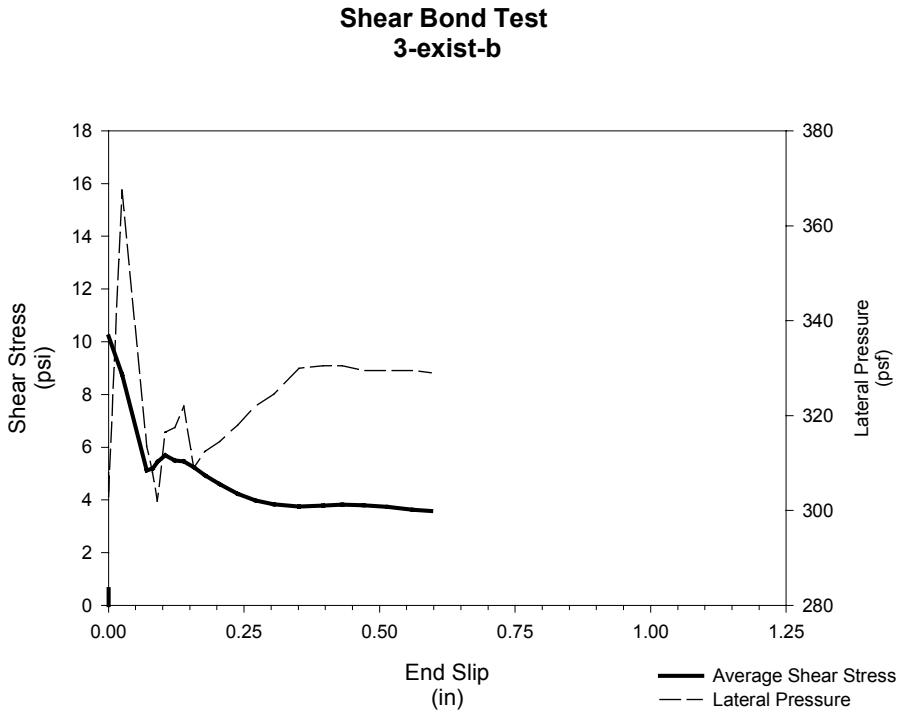

Figure A. 20 Shear Resistance SB3-exist-b

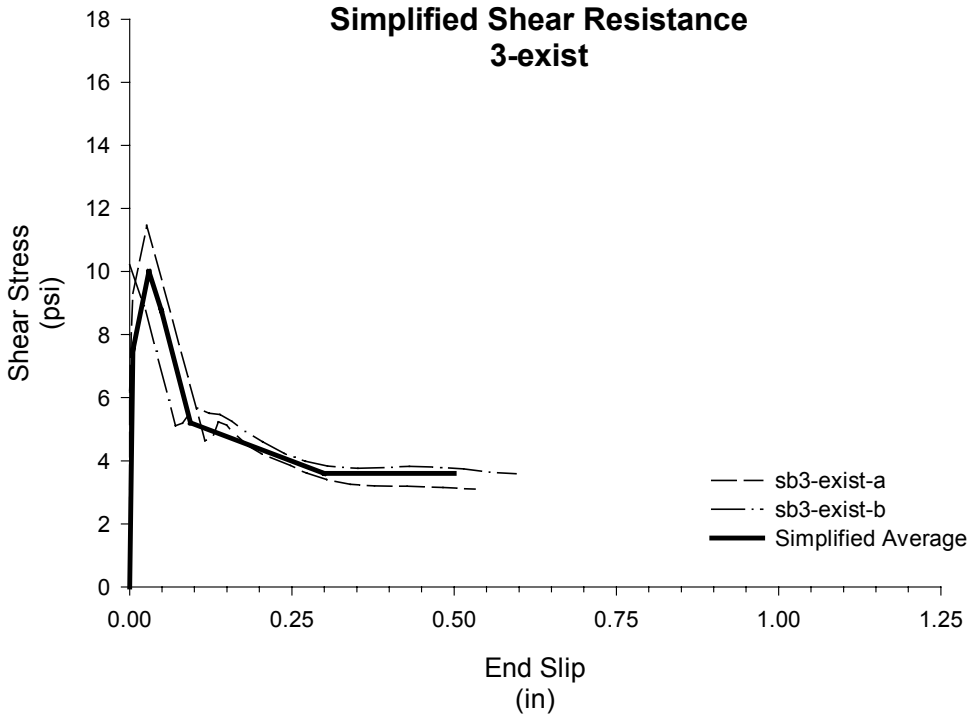

Figure A. 21 Simplified Shear Resistance for 3-exist

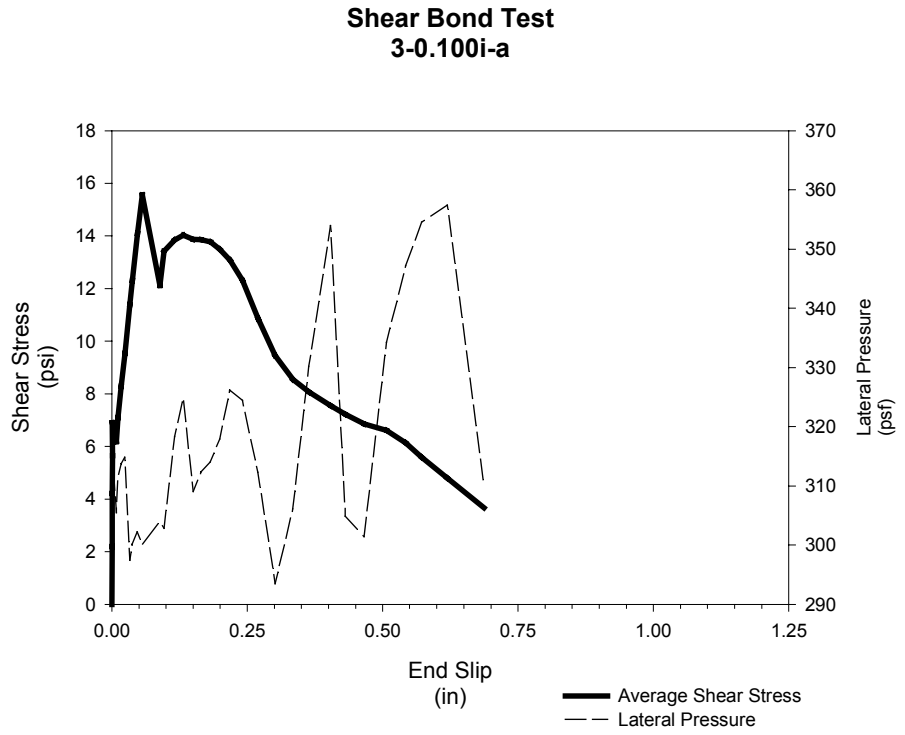

Figure A. 22 Shear Resistance SB3-0.100i-a

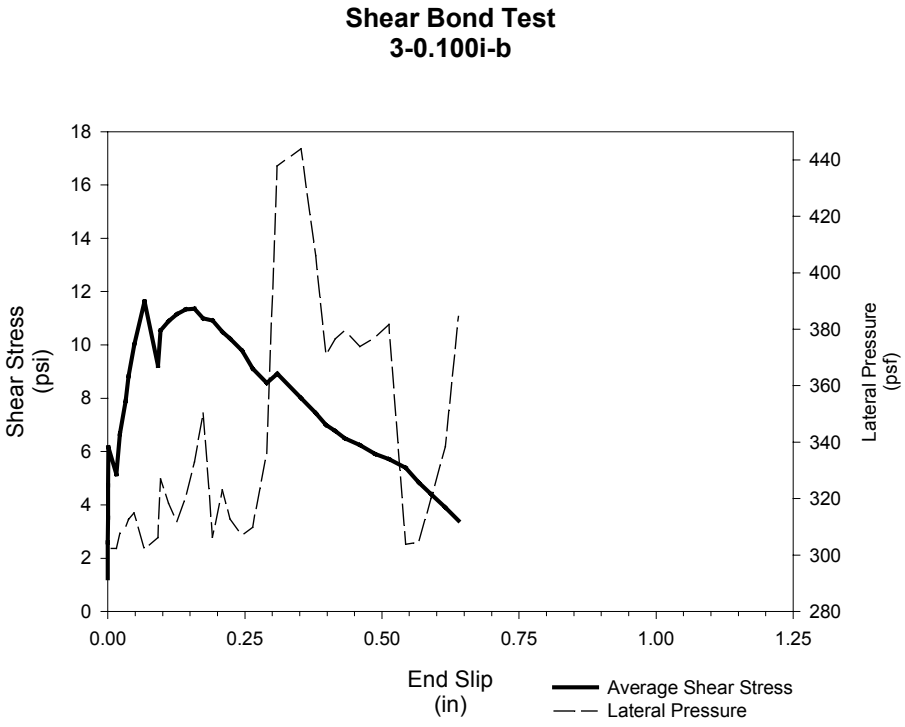

Figure A. 23 Shear Resistance SB3-0.100i-b

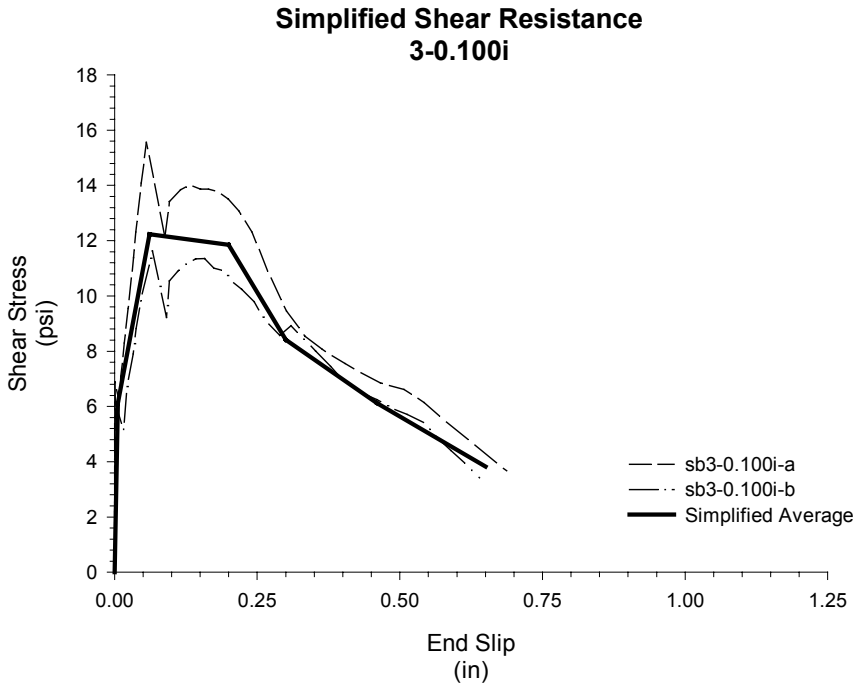

Figure A. 24 Simplified Shear Resistance of 3-0.100i

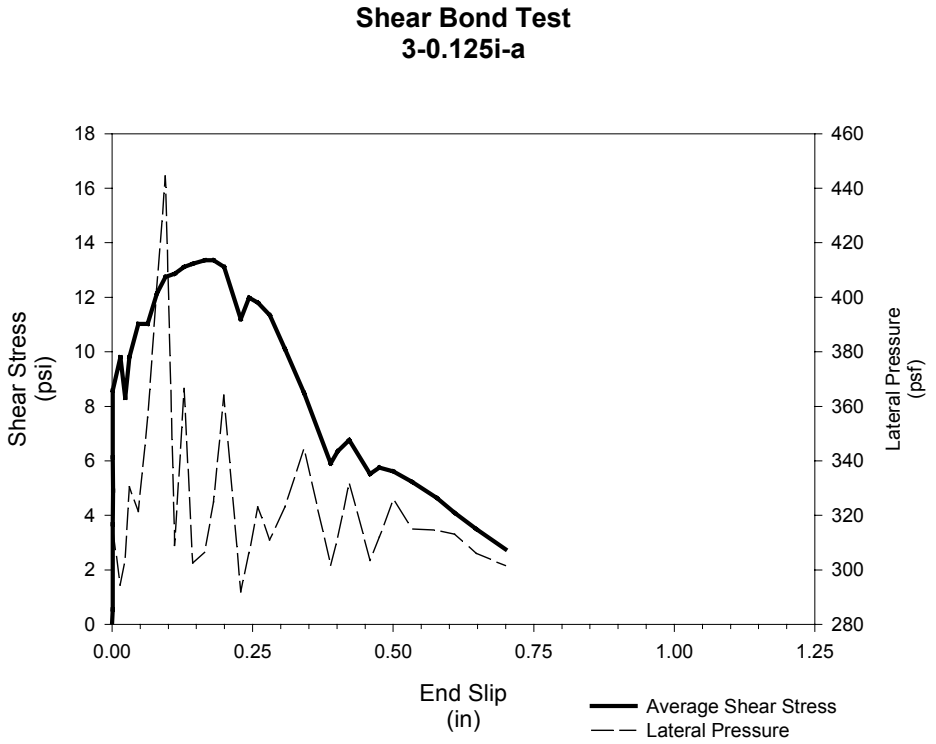

Figure A. 25 Shear Resistance SB3-0.125i-a

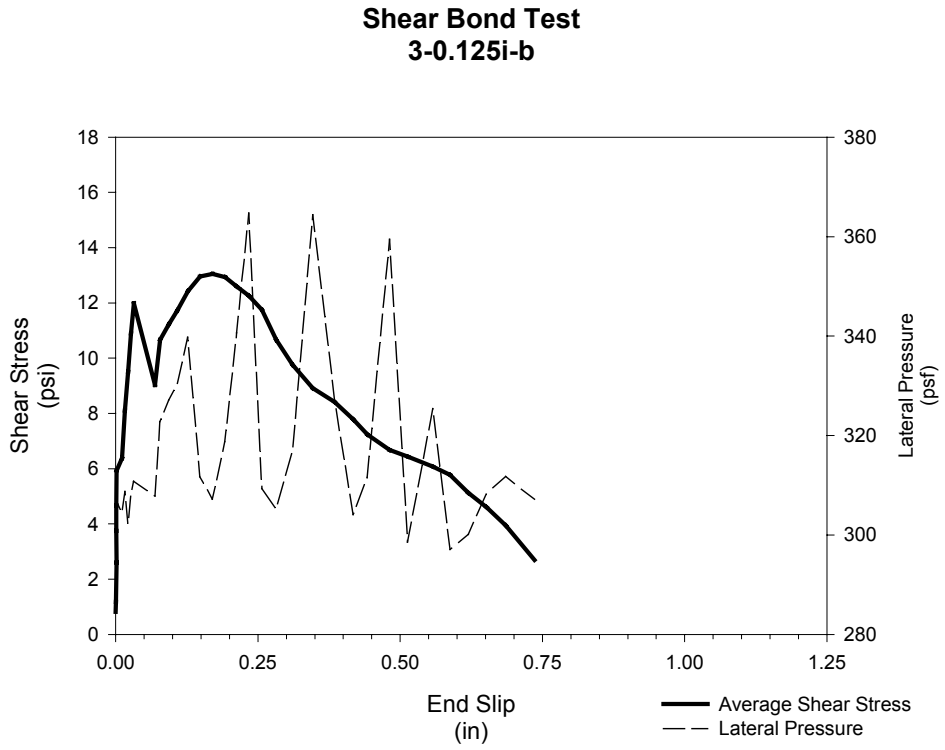

Figure A. 26 Shear Resistance SB3-0.125i-b

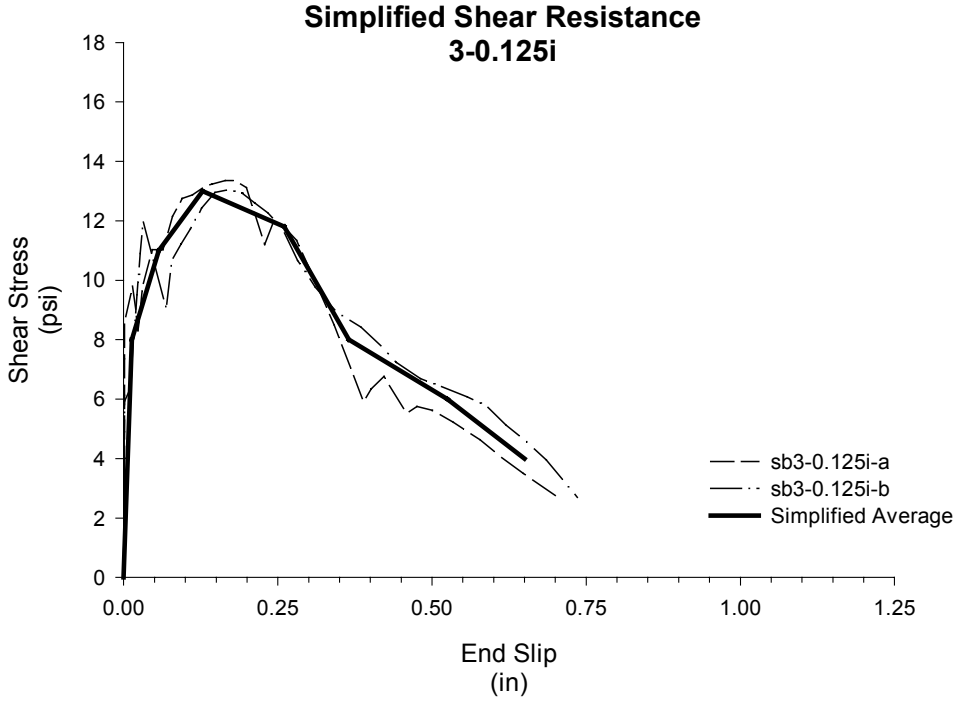

Figure A. 27 Simplified Shear Resistance for 3-0.125i

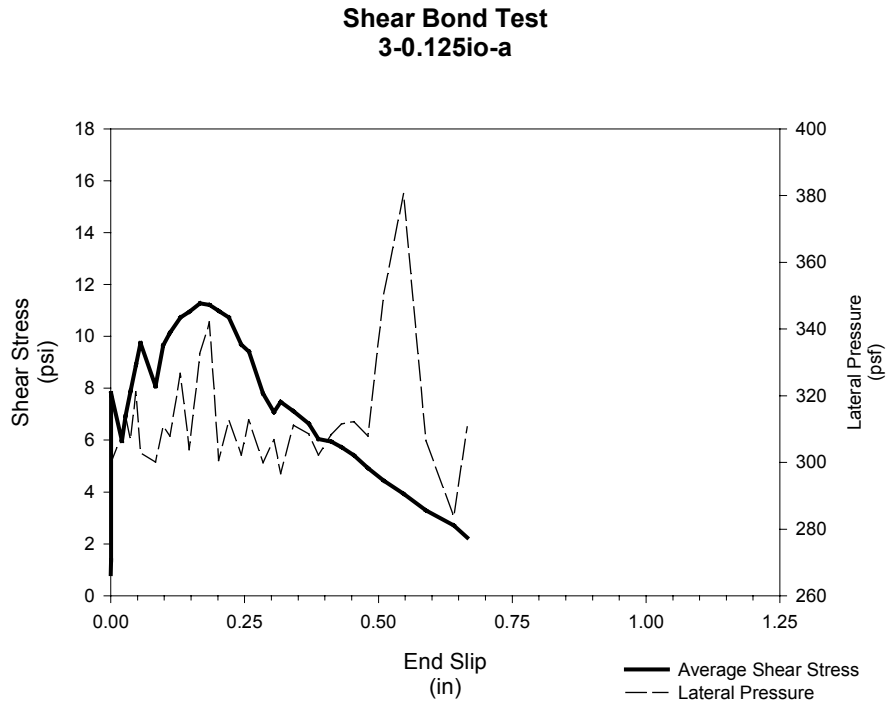

Figure A. 28 Shear Resistance SB3-0.125io-a

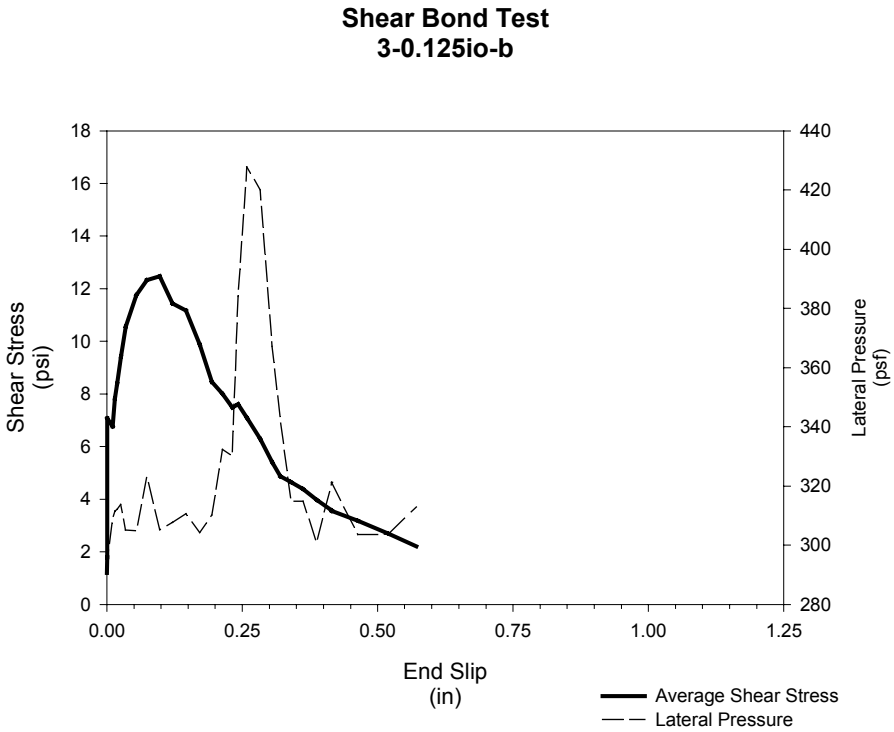

Figure A. 29 Shear Resistance SB3-0.125io-b

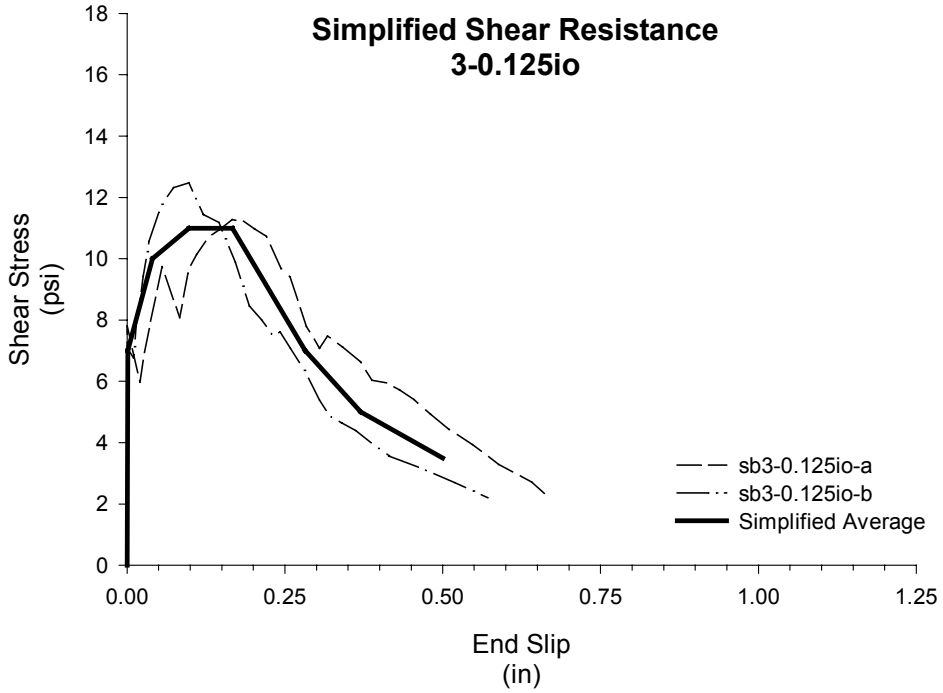

Figure A. 30 Simplified Shear Resistance for 3-0.125io

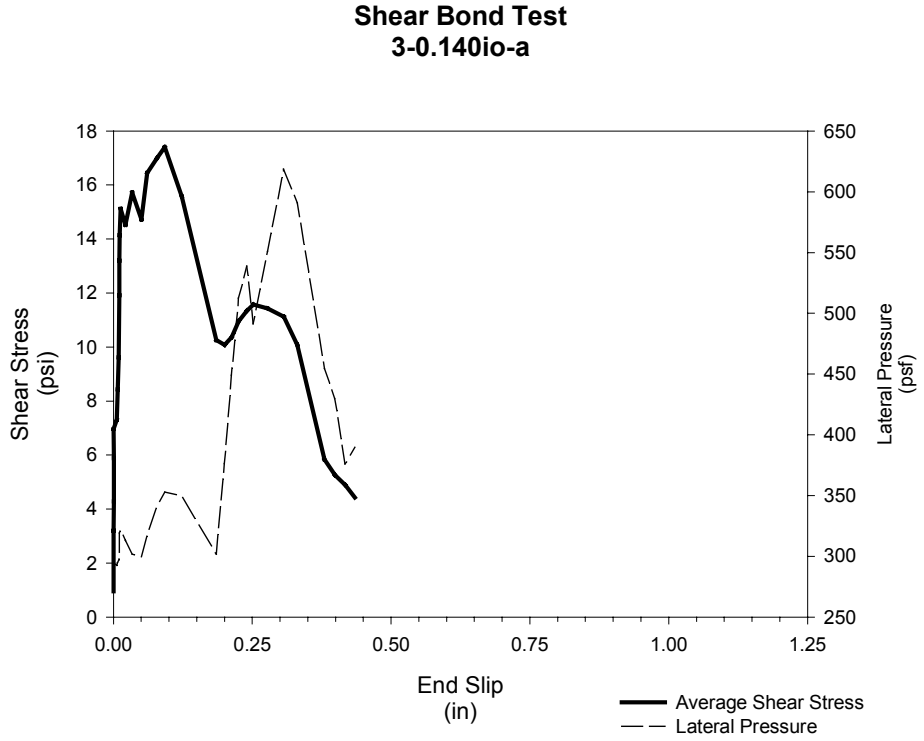

Figure A. 31 Shear Resistance SB3-0.140io-a

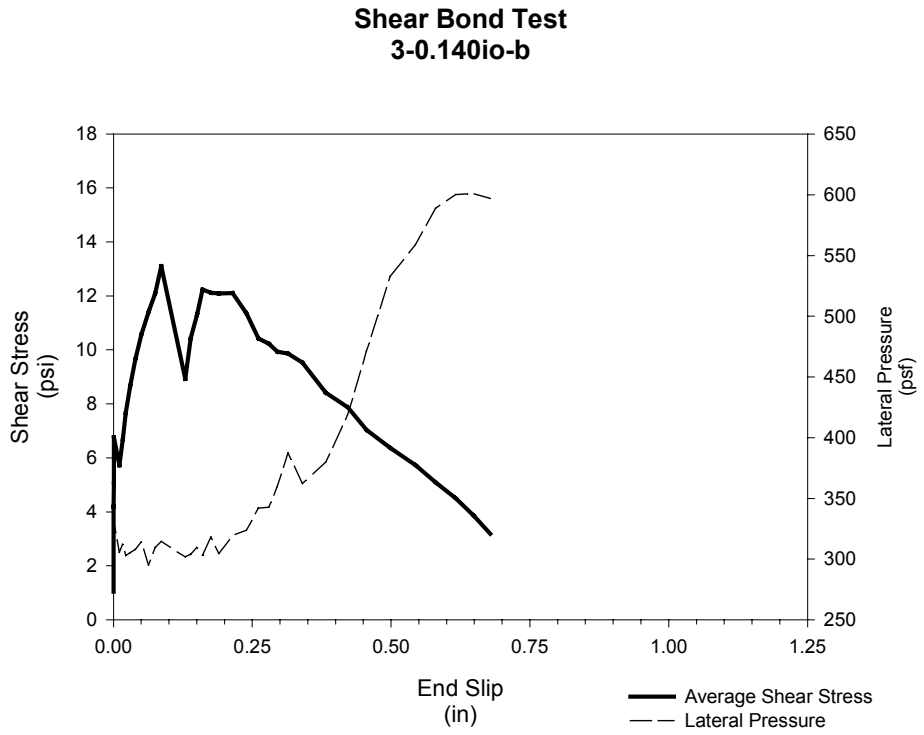

Figure A. 32 Shear Resistance SB3-0.140io-b

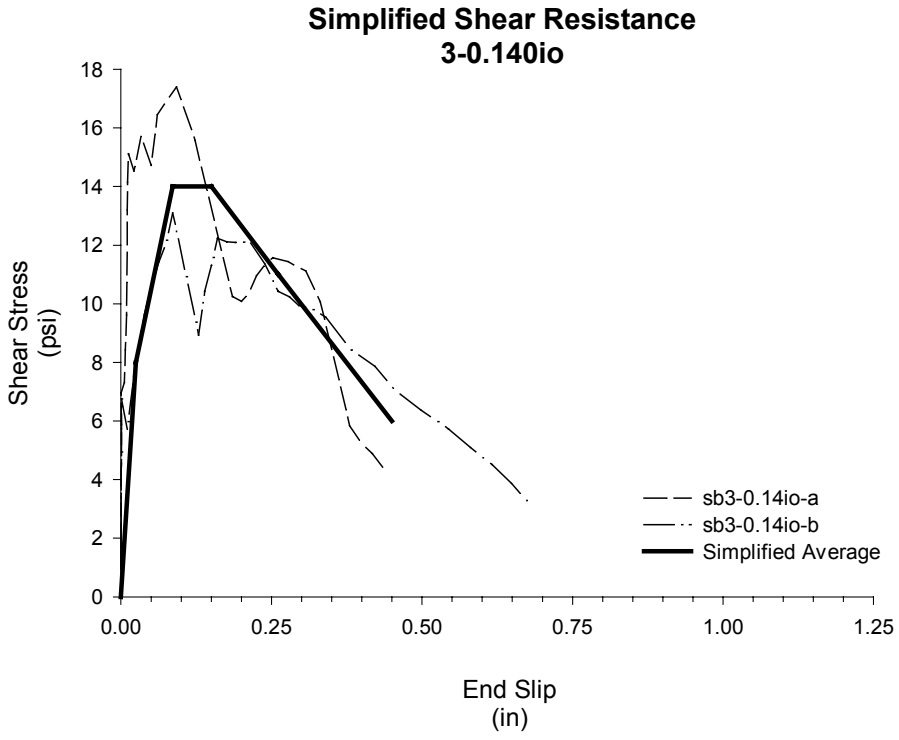

Figure A. 33 Simplified Shear Resistance for 3-0.140io

APPENDIX B: RESULTS FROM FULL-SCALE SLAB TESTS

The results from the full-scale slab tests are shown in this Appendix. Each set of results contains a summary of the test parameters, some quantified results, and graphs of the Applied Load vs. Midspan Deflection, End Slip, Deck Top Flange Strains, and Deck Bottom Flange Strains. The dimensions of the embossments of the deck specimens that were tested are shown in Figure B.1.

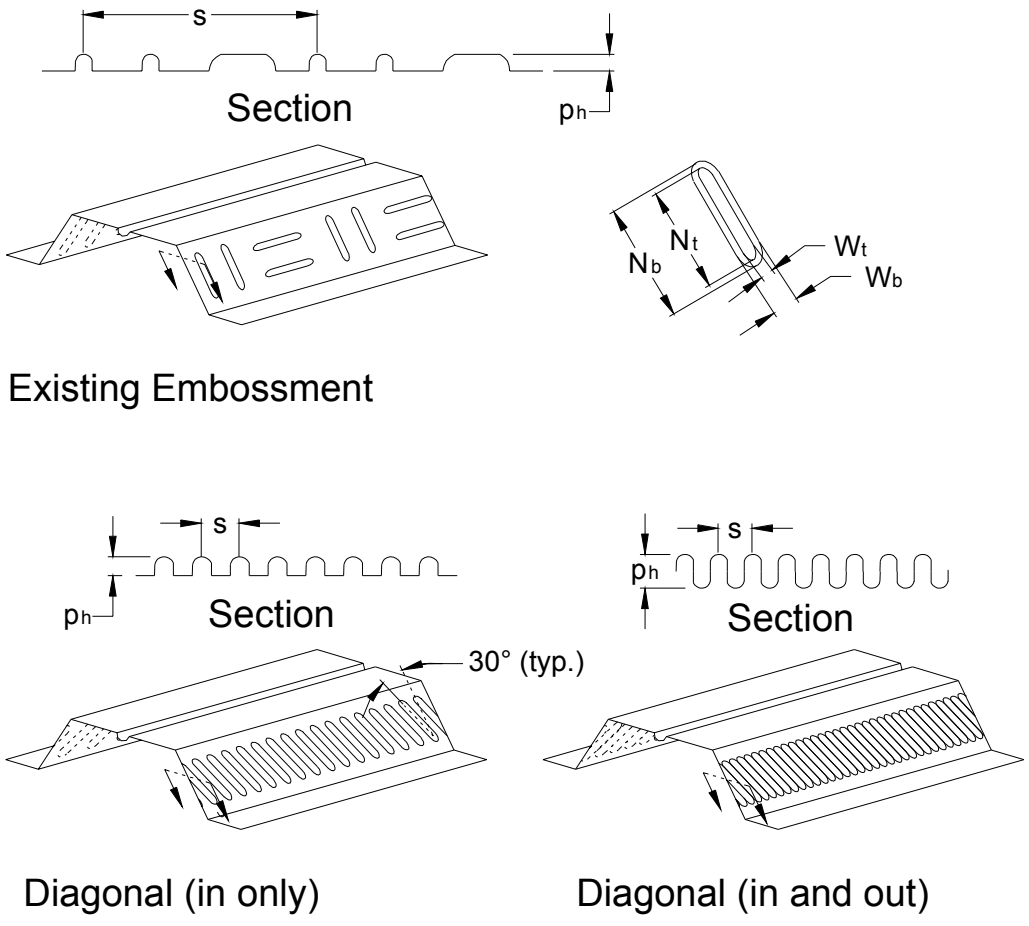

Figure B. 1 Embossment Types and Dimension Designations

Test Designation: 2-exist-a

Test Date: January 18, 2001

Materials and Dimensions

General:

width:	6 feet (2 panels)
span length:	9 ft. 4 in.
deck anchorage type:	arc spot weld, 3/4 in. dia
average anchorage spacing:	1.0 ft.

Deck:

thickness:	0.0350 in. (20 gage)
depth:	2 in.
area:	0.534 in^2
yield stress:	52.5 ksi
ultimate strength:	60.7 ksi

embossment dimensions:

vertical:	horizontal:		
N_b: 0.67 in.	N_b: 1.85 in.	W_b: 0.68 in.	s: 3.36
N_t: 1.59 in.	N_t: 1.57 in.	W_t: 0.25n.	p_h: 0.10in.

Concrete:

type:	normal weight
test strength:	4,300 psi
total depth:	4.5 in.
cover depth:	2.5 in.

RESULTS:

midspan strain due to fresh concrete:	$591x^{-6}$ in./in. (bot. flange)
	$503x10^{-6}$ in./in. (top flange)
maximum load:	417 psf
deflection at maximum load:	0.352 in.
end slip at max load:	0.000 in. (left)
	0.000 in. (right)
end slip at termination of test:	0.000 in. (left)
	0.482 in. (right)

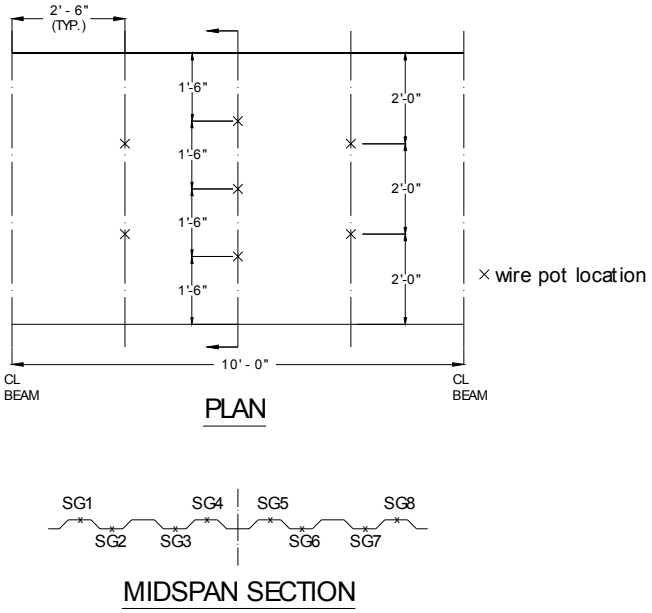

Figure B. 2 Strain Gage and Wire Pot Locations for 2-exist-a

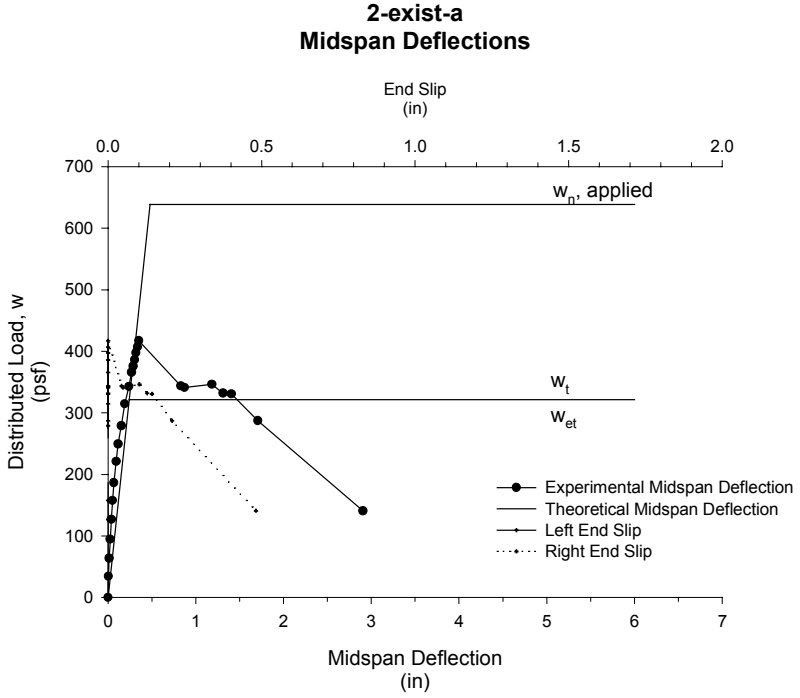

w_n = Theoretical applied distributed load that results in M_n using the calculated material properties

w_t = Theoretical applied distributed load that results in M_t (Flexural Capacity using ASCE App. D Method)

w_{et} = Theoretical applied distributed load that results in M_{et} (First Yield Moment)

Figure B. 3 Applied Load vs. Midspan Deflection and End Slip for 2-exist-a

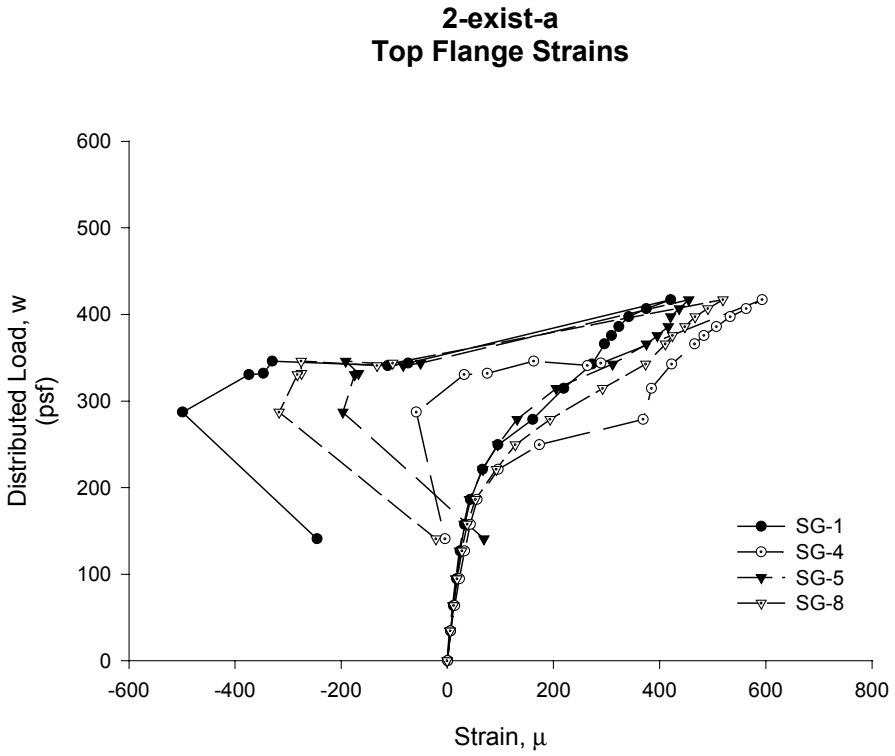

Figure B. 4 Applied Load vs. Deck Top Flange Strain for 2-exist-a

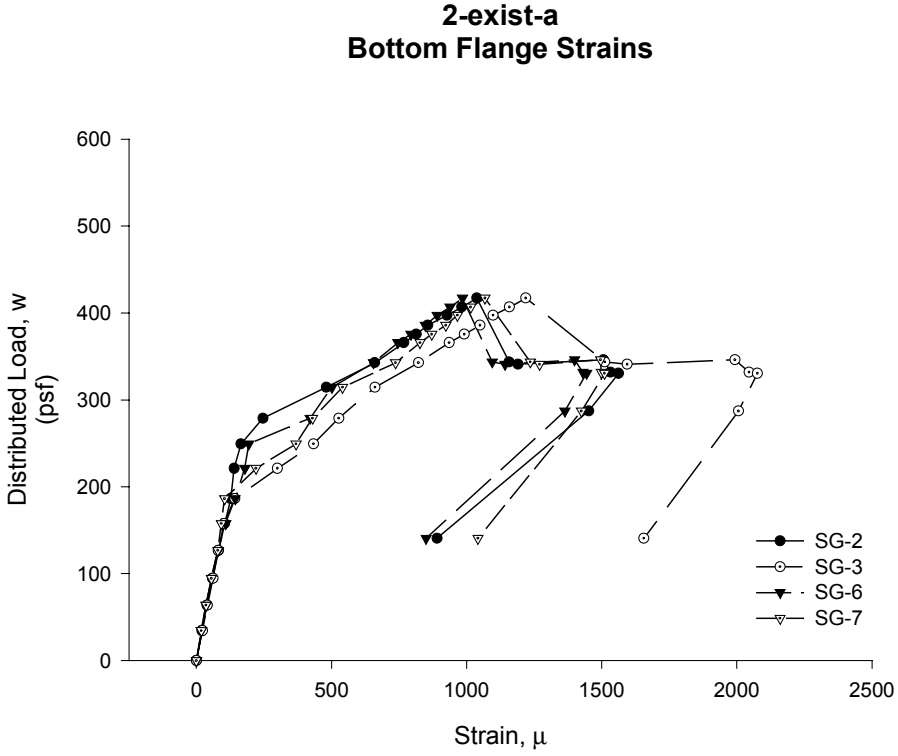

Figure B. 5 Applied Load vs. Deck Bottom Flange Strain for 2-exist-a

Test Designation: 2-exist-b
Test Date: January 18, 2001

Materials and Dimensions

General:

width:	6 feet (2 panels)
span length:	9 ft. 4 in.
deck anchorage type:	arc spot weld, 3/4 in. dia
average anchorage spacing:	1.0 ft.

Deck:

thickness:	0.0350 in. (20 gage)
depth:	2 in.
area:	0.534 in^2
yield stress:	52.5 ksi
ultimate strength:	60.7 ksi

embossment dimensions:

vertical:	horizontal:		
N_b: 0.67 in.	N_b: 1.85 in.	W_b: 0.68 in.	s: 3.36
N_t: 1.59 in.	N_t: 1.57 in.	W_t: 0.25n.	p_h: 0.10in.

Concrete:

type:	normal weight
test strength:	4,300 psi
total depth:	4.5 in.
cover depth:	2.5 in.

RESULTS:

midspan strain due to fresh concrete:	$648x^{-6}$ in./in. (bot. flange)
	$500x10^{-6}$ in./in. (top flange)
maximum load:	369 psf
deflection at maximum load:	0.850 in.
end slip at max load:	0.000 in. (left)
	0.105 in. (right)
end slip at termination of test:	0.000 in. (left)
	0.754 in. (right)

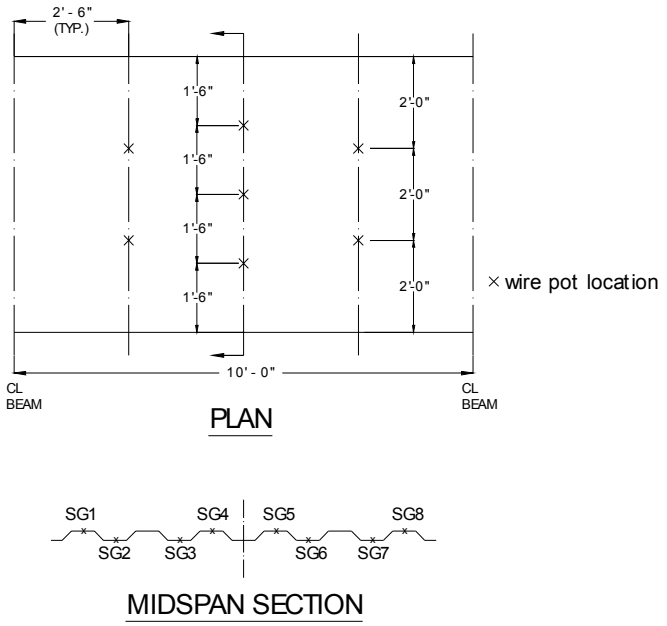

Figure B. 6 Strain Gage and Wire Pot Locations for 2-exist-b

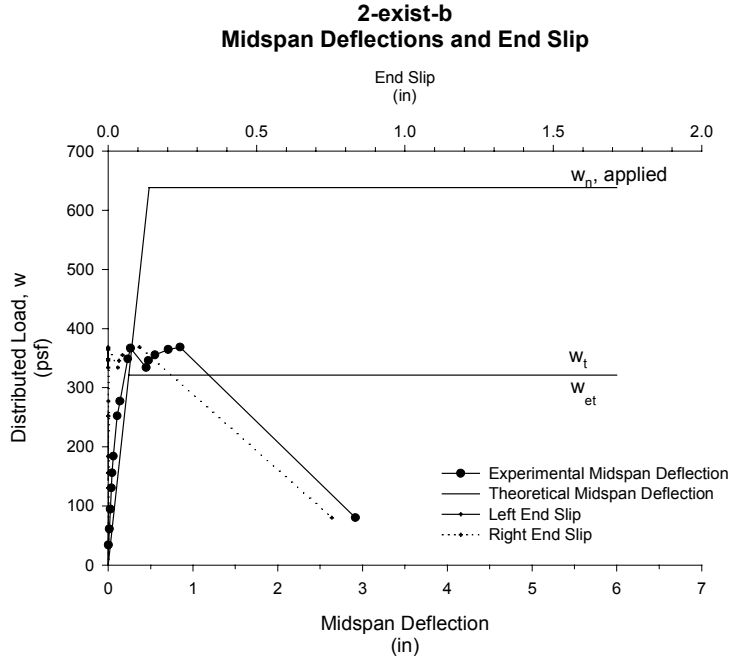

w_n = Theoretical applied distributed load that results in M_n using the calculated material properties

w_t = Theoretical applied distributed load that results in M_t (Flexural Capacity using ASCE App. D Method)

w_{et} = Theoretical applied distributed load that results in M_{et} (First Yield Moment)

Figure B. 7 Applied Load vs. Midspan Deflections and End Slip for 2-exist-b

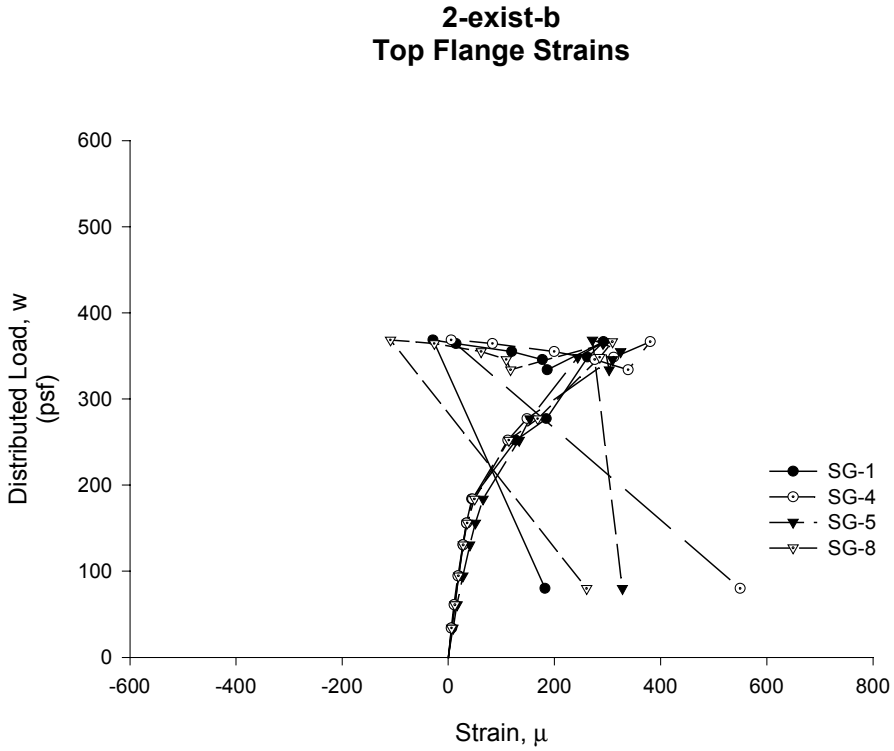

Figure B. 8 Applied Load vs. Deck Top Flange Strains for 2-exist-b

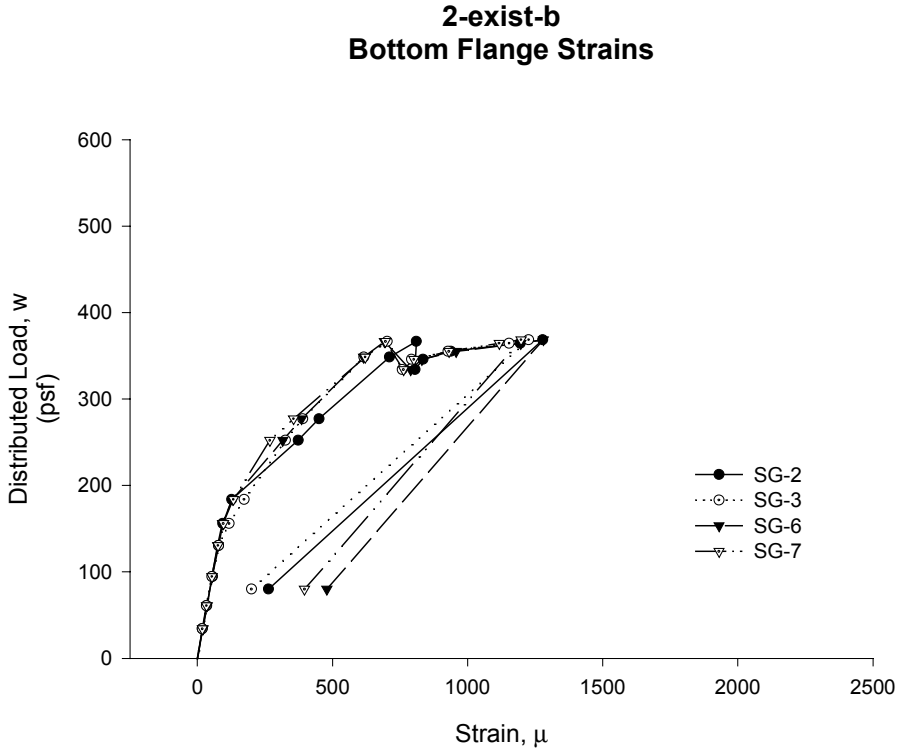

Figure B. 9 Applied Load vs. Deck Bottom Flange Strains for 2-exist-b

Test Designation: 2-0.10i-a
Test Date: December 12, 2000

Materials and Dimensions

General:

width:	6 feet (2 panels)
span length:	9 ft. 4 in.
deck anchorage type:	arc spot weld, 3/4 in. dia
average anchorage spacing:	1.0 ft.

Deck:

thickness:	0.0350 in. (20 gage)	
depth:	2 in.	
area:	0.534 in^2	
yield stress:	52.5 ksi	
ultimate strength:	60.7 ksi	
embossment dimensions:		
N_b: 1.443 in.	W_b: 0.506 in.	s: 1.000 in.
N_t: 1.155 in.	W_t: 0.360 in.	p_h: 0.100 in.

Concrete:

type:	normal weight
test strength:	3,300 psi
total depth:	4.5 in.
cover depth:	2.5 in.

RESULTS:

midspan strain due to fresh concrete:	633×10^{-6} in./in. (bot. flange)
	499×10^{-6} in./in. (top flange)
maximum load:	471 psf
deflection at maximum load:	2.48 in.
end slip at max load:	0.144 in. (left)
	0.101 in. (right)
end slip at termination of test:	0.630 in. (left)
	0.098 in. (right)

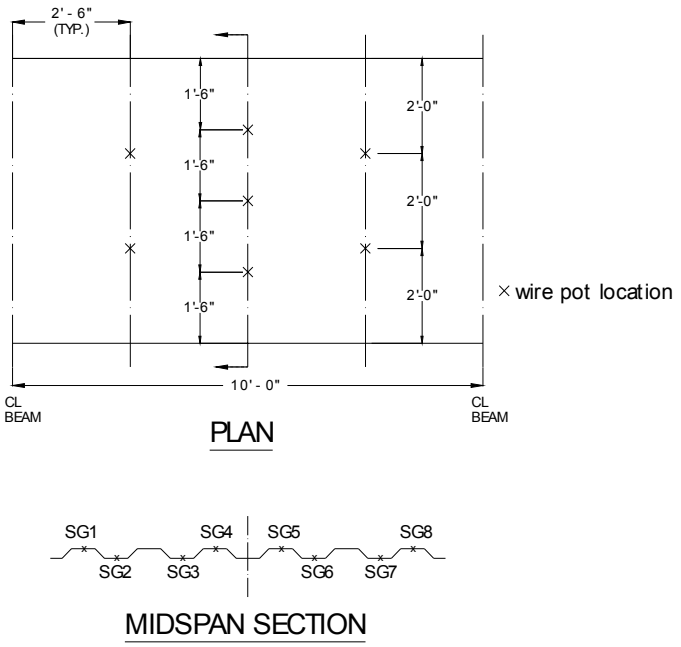

Figure B. 10 Strain Gage and Wire Pot Locations for 2-0.10i-a

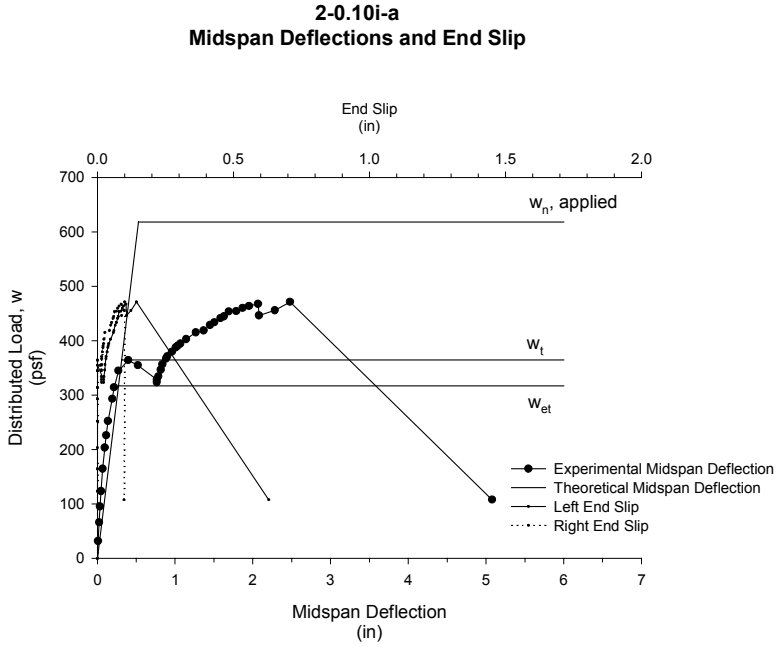

w_n = Theoretical applied distributed load that results in M_n using the calculated material properties

w_t = Theoretical applied distributed load that results in M_t (Flexural Capacity using ASCE App. D Method)

w_{et} = Theoretical applied distributed load that results in M_{et} (First Yield Moment)

Figure B. 11 Applied Load vs. Midspan Deflection and End Slip for 2-0.10i-a

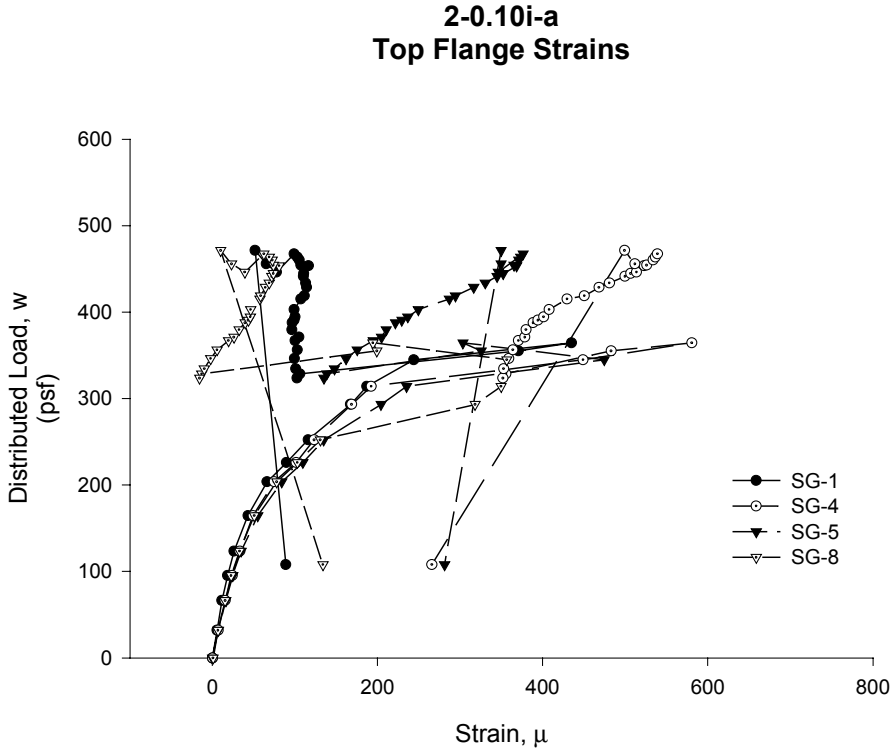

Figure B. 12 Applied Load vs. Deck Top Flange Strain for 2-0.10i-a

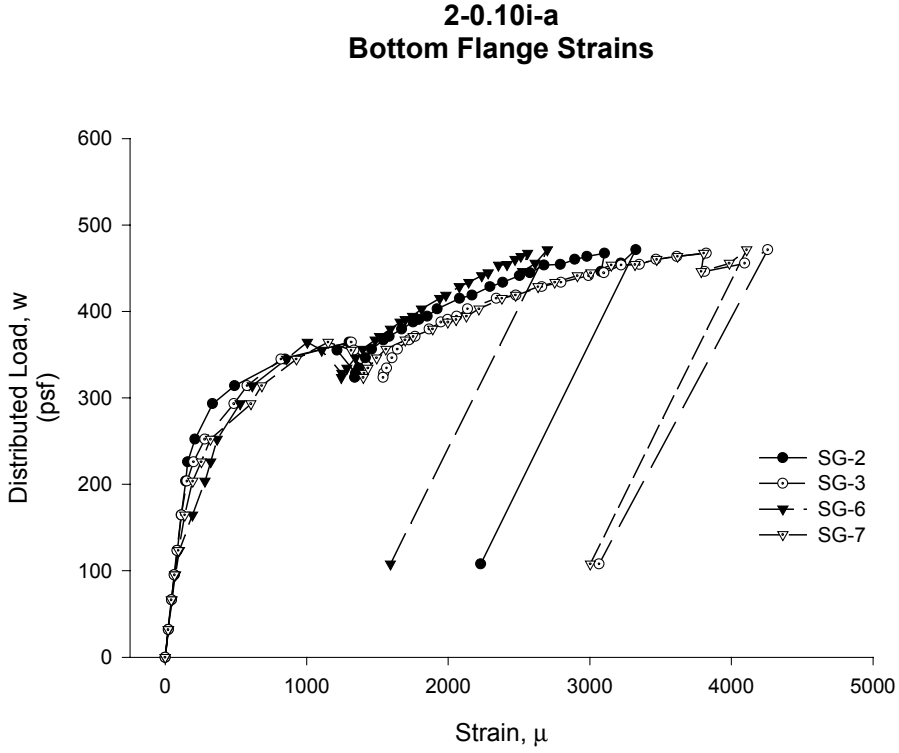

Figure B. 13 Applied Load vs. Deck Bottom Flange Strain for 2-0.10i-a

Test Designation: 2-0.10i-b
Test Date: December 13, 2000

Materials and Dimensions

General:

width:	6 feet (2 panels)
span length:	9 ft. 4 in.
deck anchorage type:	arc spot weld, 3/4 in. dia
average anchorage spacing:	1.0 ft.

Deck:

thickness:	0.0350 in. (20 gage)	
depth:	2 in.	
area:	0.534 in^2	
yield stress:	52.5 ksi	
ultimate strength:	60.7 ksi	
embossment dimensions:		
N_b: 1.443 in.	W_b: 0.506 in.	s: 1.000 in.
N_t: 1.1550 in.	W_t: 0.360 in.	p_h: 0.100 in.

Concrete:

type:	normal weight
test strength:	3,400 psi
total depth:	4.5 in.
cover depth:	2.5 in.

RESULTS:

midspan strain due to fresh concrete:	643×10^{-6} in./in. (bot. flange)
	516×10^{-6} in./in. (top flange)
maximum load:	492 psf
deflection at maximum load:	2.249 in.
end slip at max load:	0.094. (left)
	0.138(right)
end slip at termination of test:	0.097 (left)
	1.318 (right)

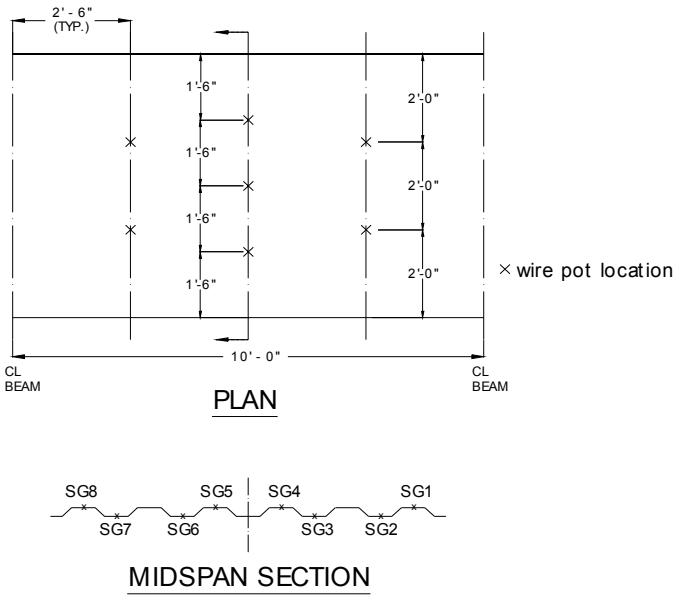

Figure B. 14 Strain Gage and Wire Pot Locations for 2-0.10i-b

2-0.10i-b
Midspan Deflections and End Slip

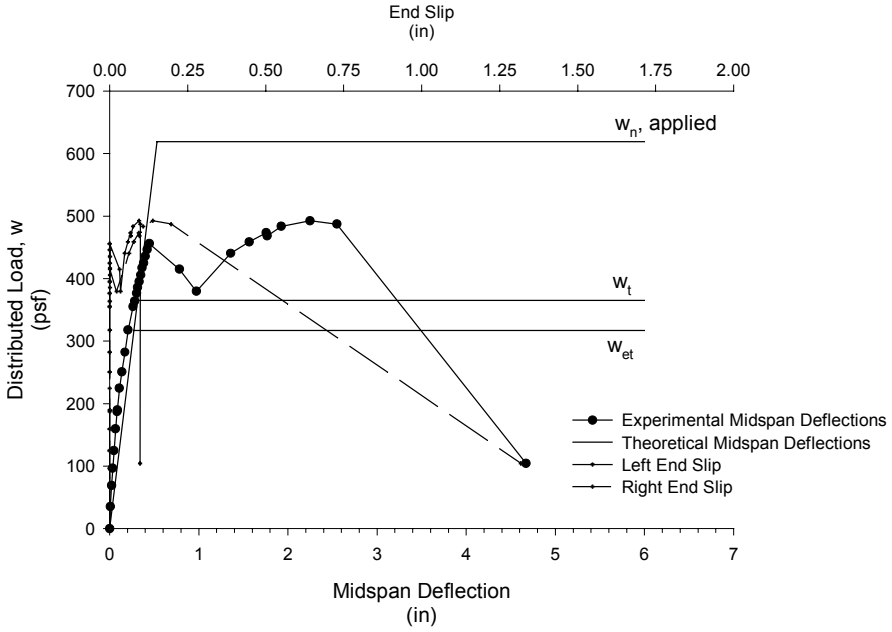

w_n = Theoretical distributed load that results in M_n
using the calculated material properties

w_t = Theoretical applied distributed load that results in M_t
(Flexural Capacity using ASCE App. D Method)

w_{et} = Theoretical applied distributed load that results in M_{et}
(First Yield Moment)

Figure B. 15 Applied Load vs. Midspan Deflection and End Slip for 2-0.10i-b

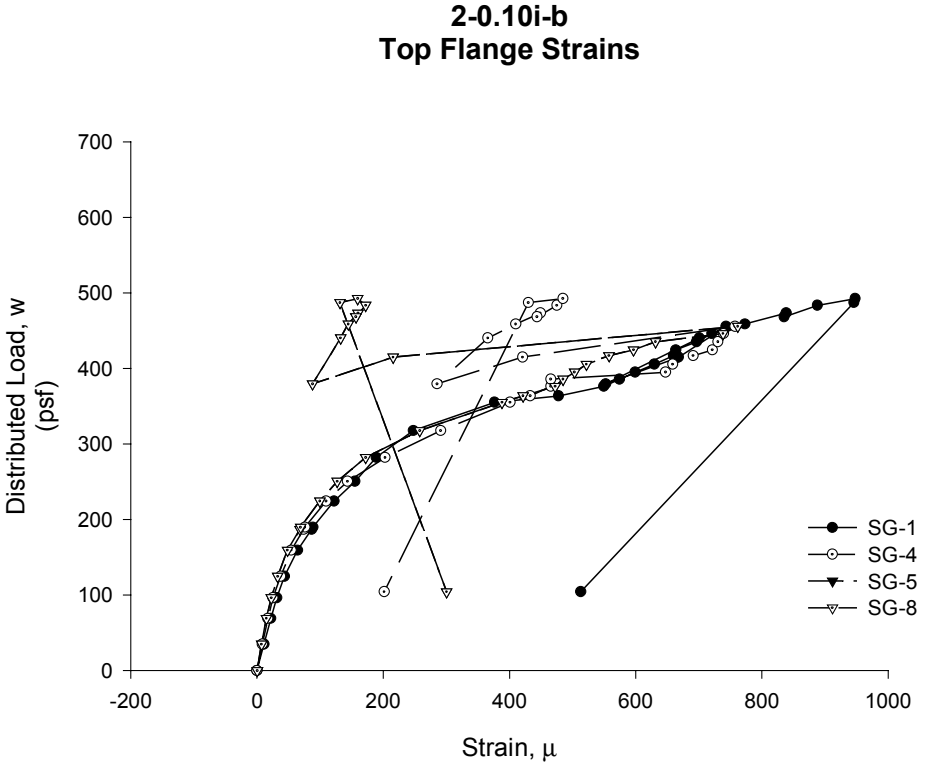

Figure B. 16 Applied Load vs. Deck Top Flange Strain for 2-0.10i-b

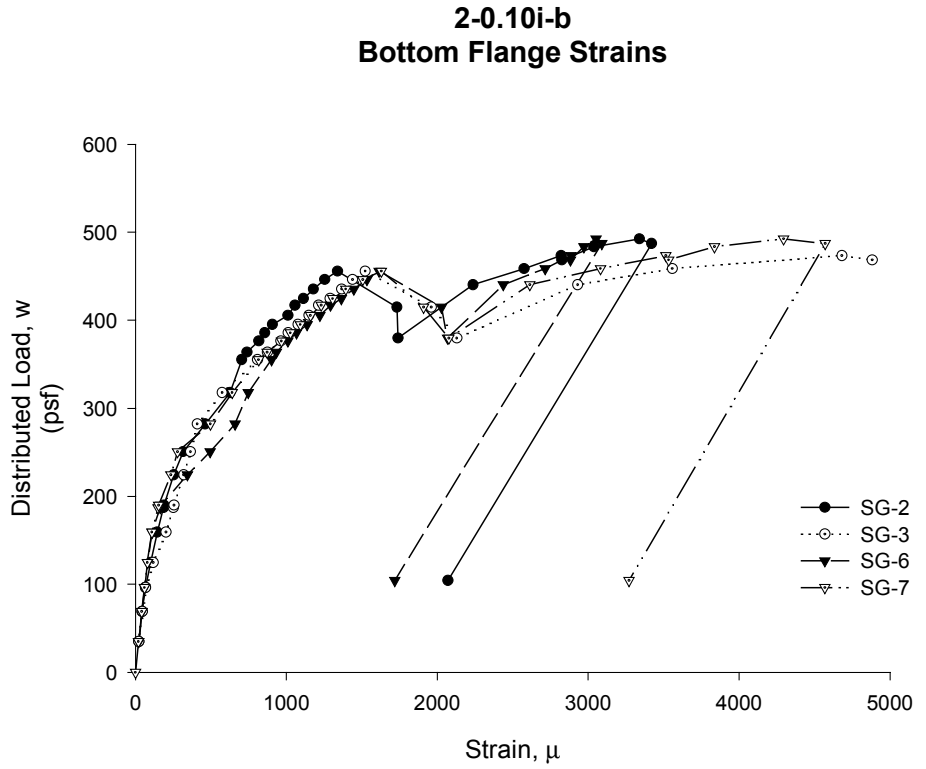

Figure B. 17 Applied Load vs. Deck Bottom Flange Strain for 2-0.10i-b

Test Designation: 2-0.125i-a
Test Date: September 5, 2000

Materials and Dimensions

General:

width:	6 feet (2 panels)
span length:	9 ft. 4 in.
deck anchorage type:	arc spot weld, 3/4 in. dia
average anchorage spacing:	1.0 ft.

Deck:

thickness:	0.0350 in. (20 gage)
depth:	2 in.
area:	0.534 in^2
yield stress:	52.5 ksi
ultimate strength:	60.7 ksi

embossment dimensions:

N_b: 1.443 in.	W_b: 0.506 in.	s: 1.000 in.
N_t: 1.1550 in.	W_t: 0.360 in.	p_h: 0.125 in.

Concrete:

type:	normal weight
test strength:	4,100 psi
total depth:	4.5 in.
cover depth:	2.5 in.

RESULTS:

midspan strain due to fresh concrete:	779×10^{-6} in./in. (bot. flange)
	523×10^{-6} in./in. (top flange)
maximum load:	433 psf
deflection at maximum load:	2.75 in.
end slip at max load:	0.206 in. (left)
	0.177 in. (right)
end slip at termination of test:	1.46 in. (left)
	0.185 in. (right)

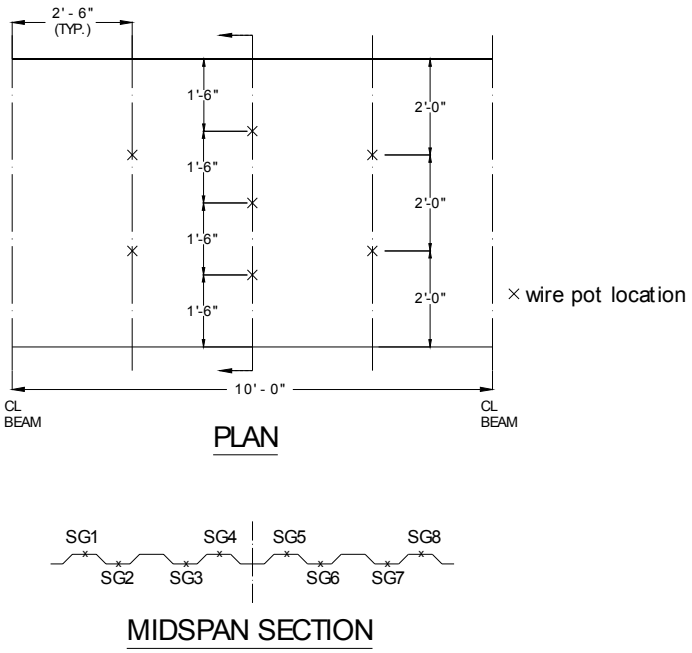

Figure B. 18 Strain Gage and Wire Pot Locations for 2-0.125i-a

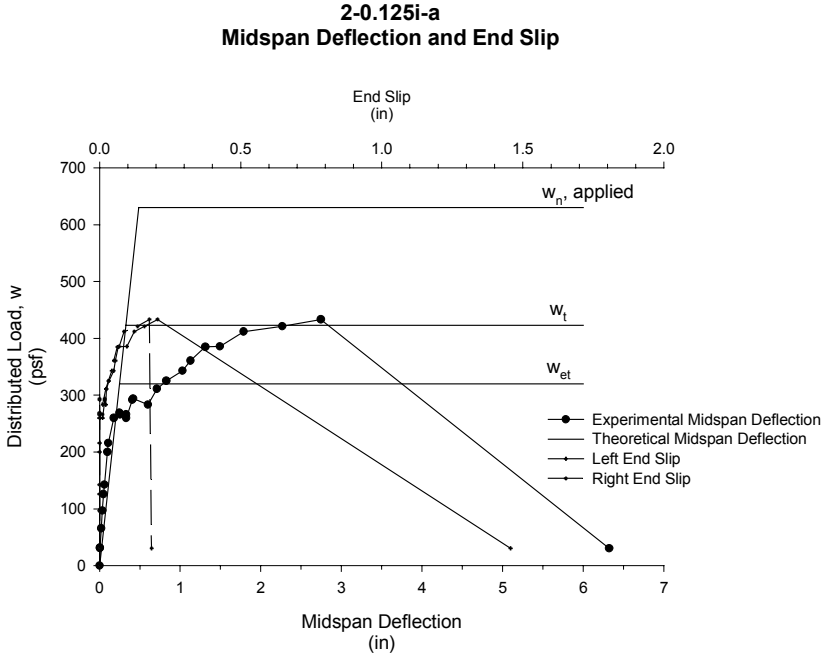

w_n = Theoretical applied distributed load that results in M_n using the calculated material properties

w_t = Theoretical applied distributed load that results in M_t (Flexural Capacity using ASCE App. D Method)

w_{et} = Theoretical applied distributed load that results in M_{et} (First Yield Moment)

Figure B. 19 Applied Load vs. Midspan Deflection and End Slip for 2-0.125i-a

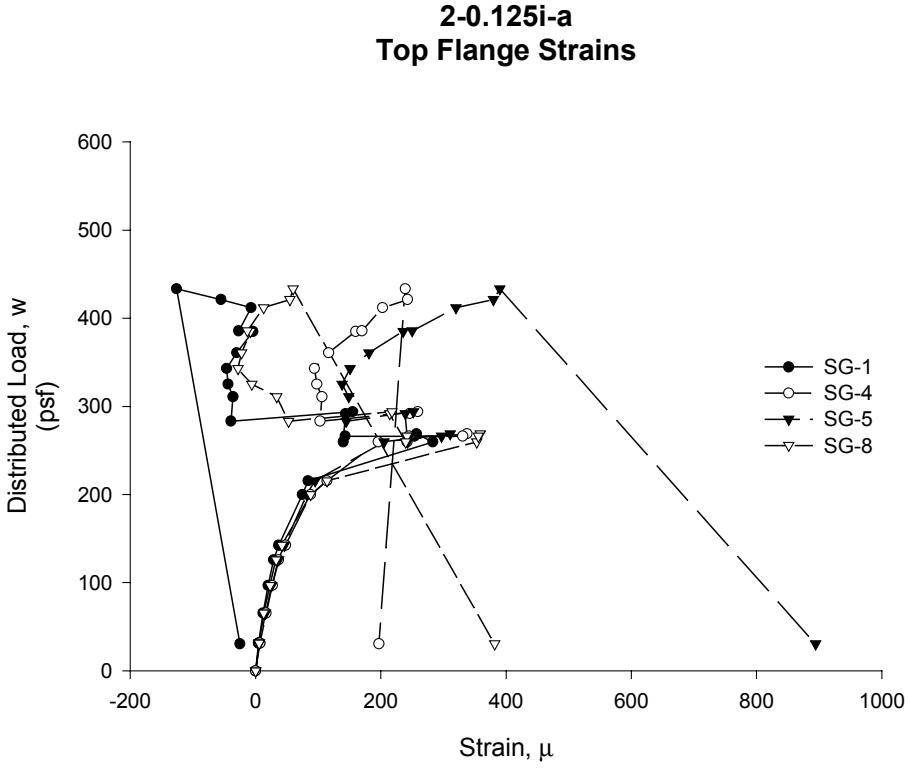

Figure B. 20 Applied Load vs. Deck Top Flange Strain for 2-0.125i-a

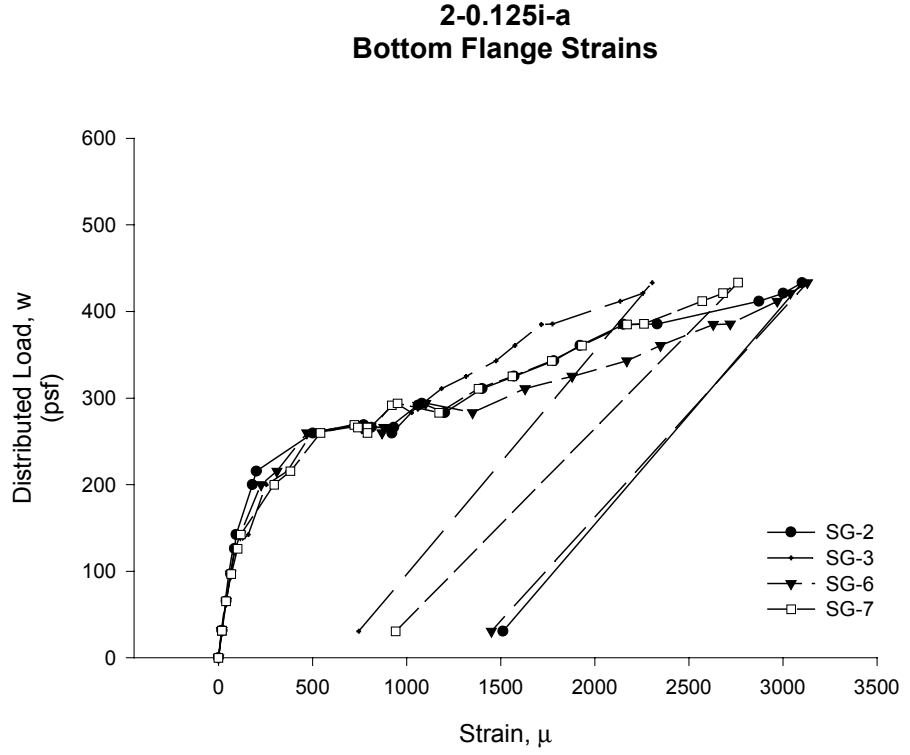

Figure B. 21 Applied Load vs. Deck Bottom Flange Strain for 2-0.125i-a

Test Designation: 2-0.125i-b
Test Date: September 7, 2000

Materials and Dimensions

General:

width:	6 feet (2 panels)
span length:	9 ft. 4 in.
deck anchorage type:	arc spot weld, 3/4 in. dia
average anchorage spacing:	1.0 ft.

Deck:

thickness:	0.0350 in. (20 gage)
depth:	2 in.
area:	0.534 in^2
yield stress:	52.5 ksi
ultimate strength:	60.7 ksi

embossment dimensions:

N_b: 1.443 in.	W_b: 0.506 in.	s: 1.000 in.
N_t: 1.1550 in.	W_t: 0.360 in.	p_h: 0.125 in.

Concrete:

type:	normal weight
test strength:	4,200 psi
total depth:	4.5 in.
cover depth:	2.5 in.

RESULTS:

midspan strain due to fresh concrete:	638×10^{-6} in./in. (bot. flange)
	492×10^{-6} in./in. (top flange)
maximum load:	396 psf
deflection at maximum load:	2.04 in.
end slip at max load:	0.091 in. (left)
	0.105 in. (right)
end slip at termination of test:	0.101 in. (left)
	1.237 in. (right)

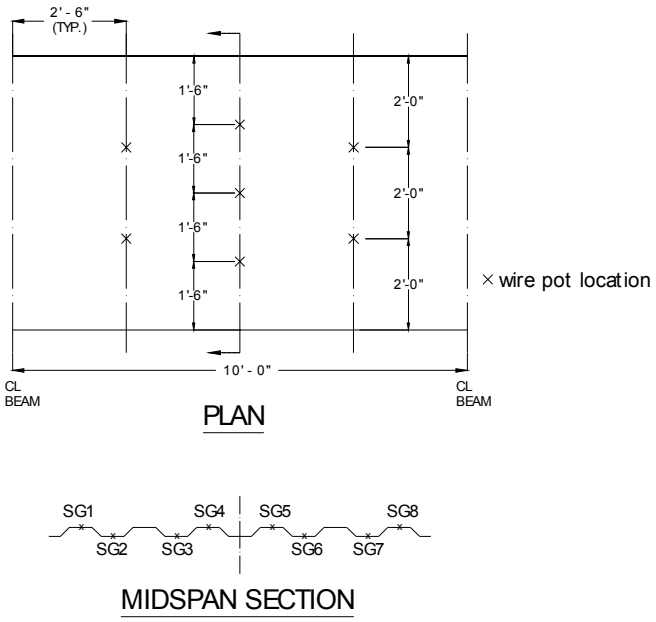

Figure B. 22 Strain Gage and Wire Pot Locations for 2-0.125i-b

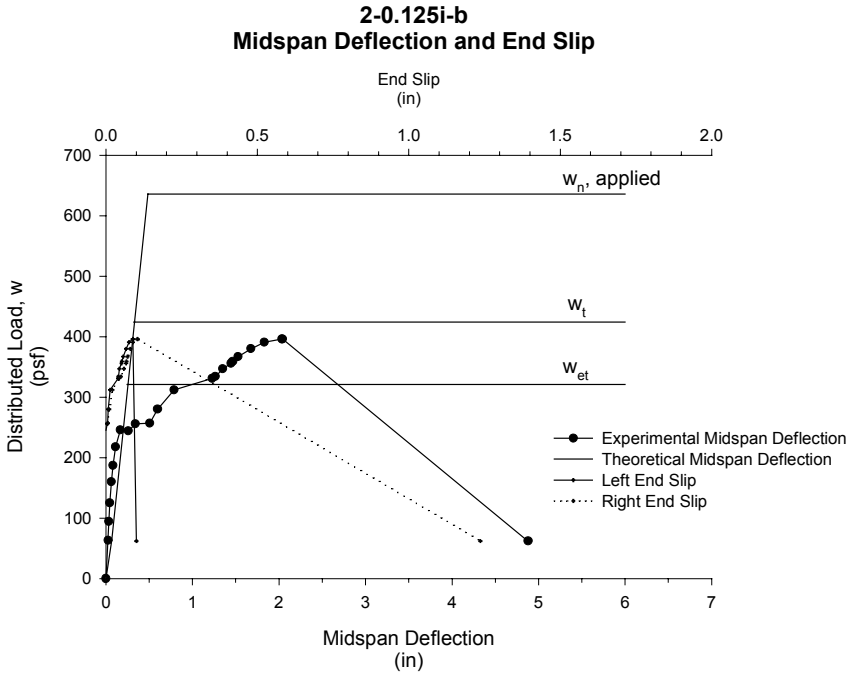

w_n = Theoretical applied distributed load that results in M_n using the calculated material properties

w_t = Theoretical applied distributed load that results in M_t (Flexural Capacity using ASCE App. D Method)

w_{et} = Theoretical applied distributed load that results in M_{et} (First Yield Moment)

Figure B. 23 Applied Load vs. Midspan Deflection and End Slip for 2-0.125i-b

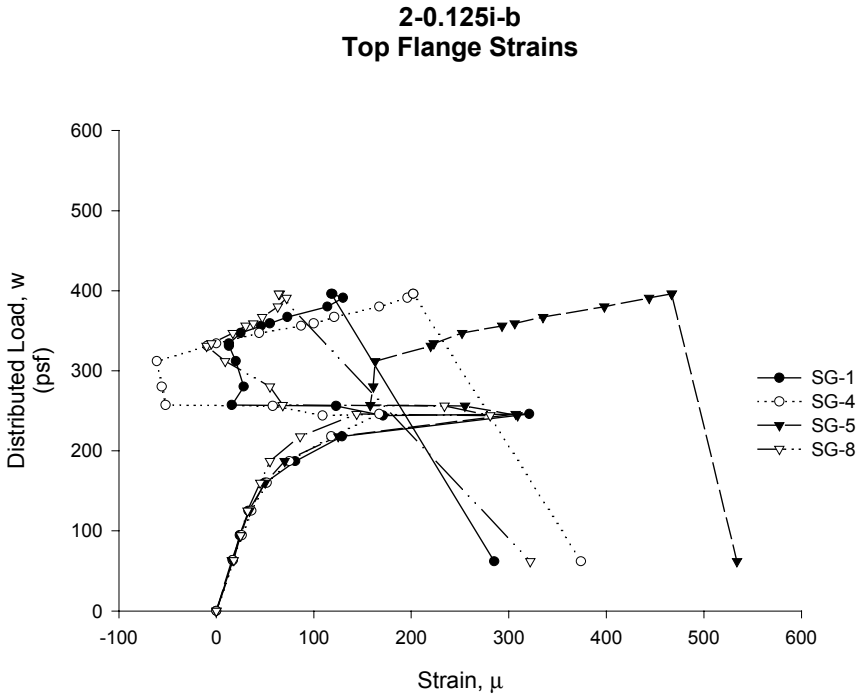

Figure B. 24 Applied Load vs. Deck Top Flange Strain for 2-0.125i-b

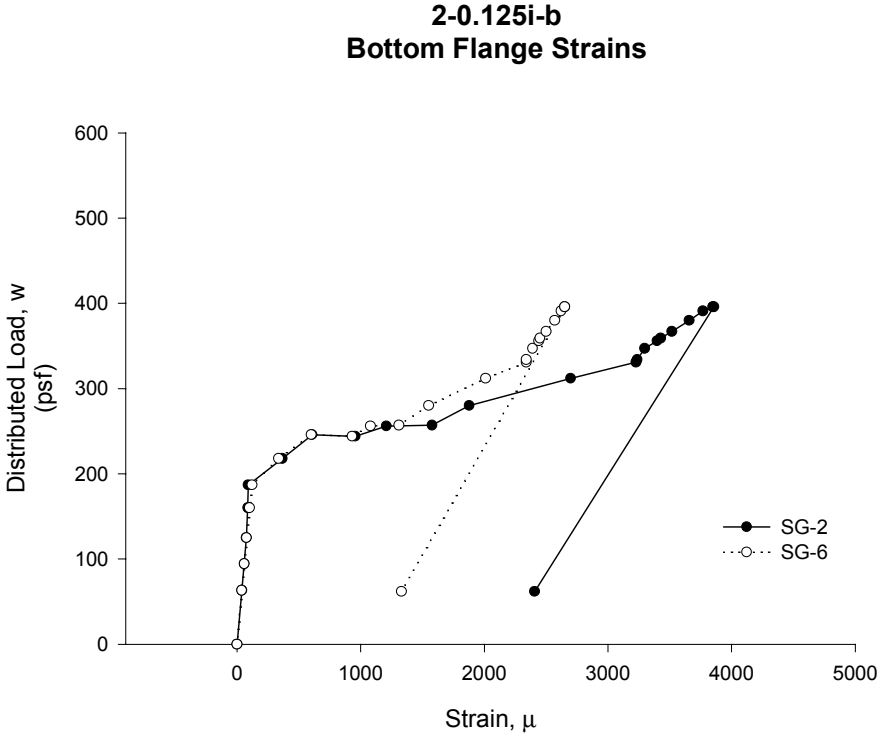

Figure B. 25 Applied Load vs. Deck Bottom Flange Strain for 2-0.125i-b

Test Designation: 2-0.125io-a
Test Date: November 13, 2000

Materials and Dimensions

General:

width:	6 feet (2 panels)
span length:	9 ft. 4 in.
deck anchorage type:	arc spot weld, 3/4 in. dia
average anchorage spacing:	1.0 ft.

Deck:

thickness:	0.0350 in. (20 gage)	
depth:	2 in.	
area:	0.534 in^2	
yield stress:	52.5 ksi	
ultimate strength:	60.7 ksi	
embossment dimensions:		
N_b: 1.443 in.	W_b: 0.506 in.	s: 1.000 in.
N_t: 1.1550 in.	W_t: 0.360 in.	p_h: 0.125 in.

Concrete:

type:	normal weight
test strength:	4,100 psi
total depth:	4.5 in.
cover depth:	2.5 in.

RESULTS:

midspan strain due to fresh concrete:	719×10^{-6} in./in. (bot. flange)
	534×10^{-6} in./in. (top flange)
maximum load:	478 psf
deflection at maximum load:	1.630 in.
end slip at max load:	0.163 in. (left)
	0.058 in. (right)
end slip at termination of test:	1.187 in. (left)
	0.059 in. (right)

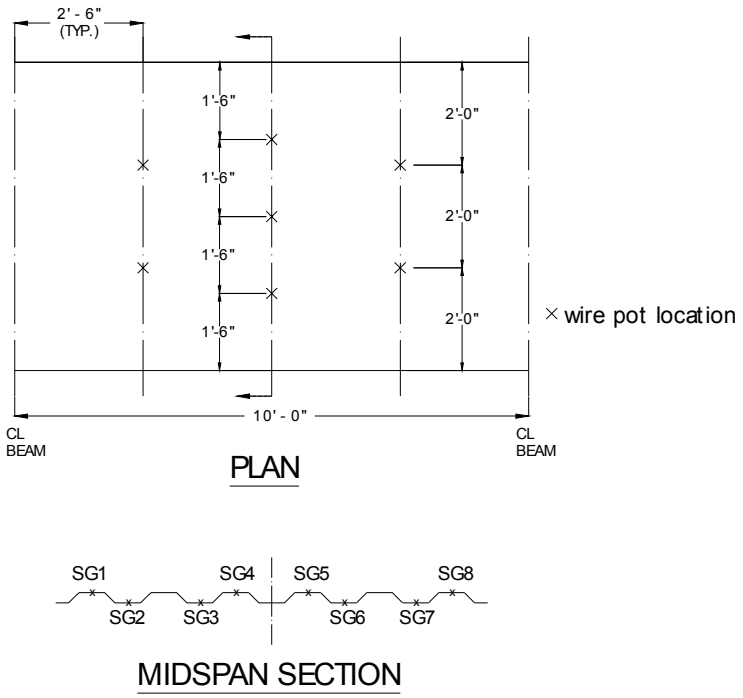

Figure B. 26 Strain Gage and Wire Pot Locations for 2-0.125io-a

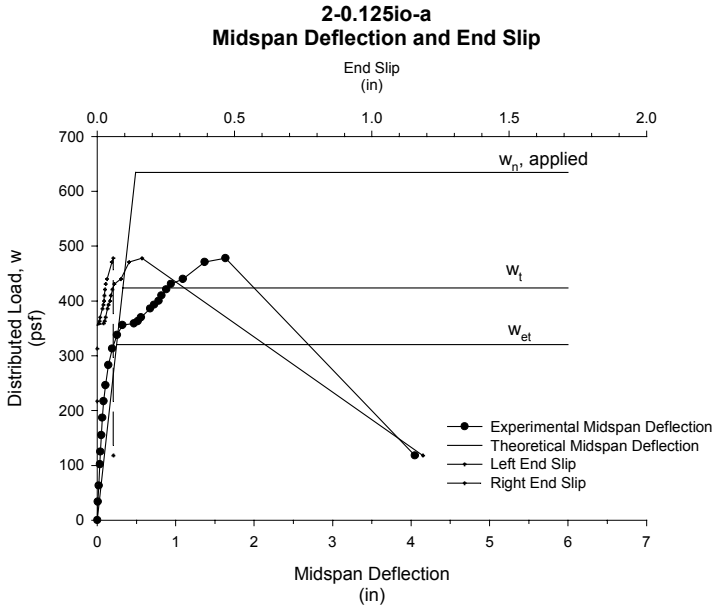

w_n = Theoretical applied distributed load that results in M_n using the calculated material properties

w_t = Theoretical applied distributed load that results in M_t (Flexural Capacity using ASCE App. D Method)

w_{et} = Theoretical applied distributed load that results in M_{et} (First Yield Moment)

Figure B. 27 Applied Load vs. Midspan Deflection and End Slip for 2-0.125io-a

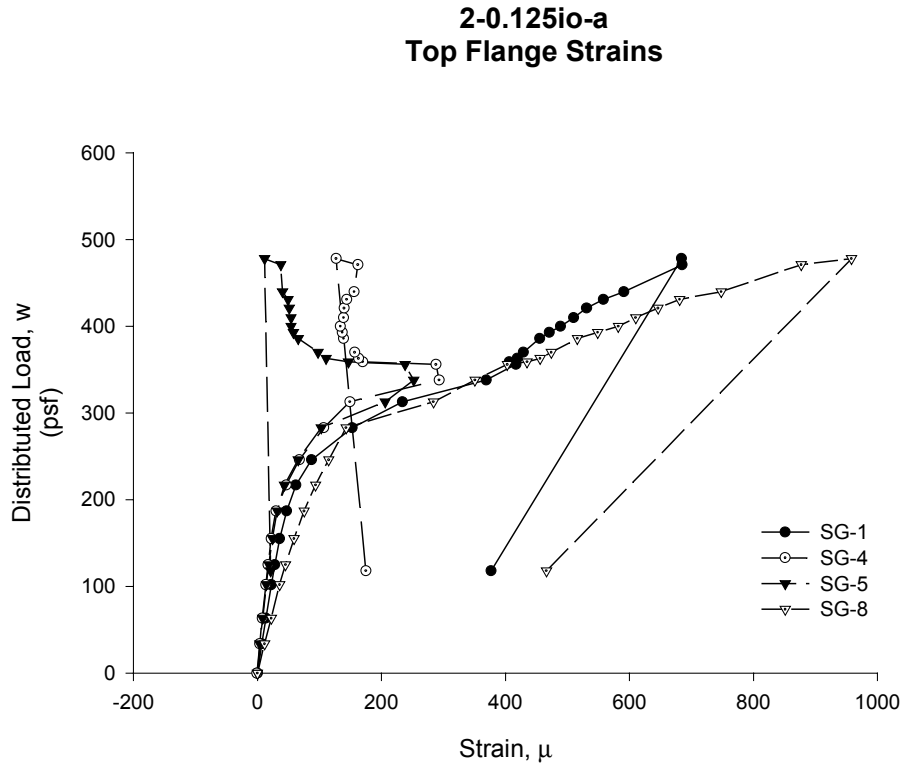

Figure B. 28 Applied Load vs. Deck Top Flange Strain for 2-0.125io-a

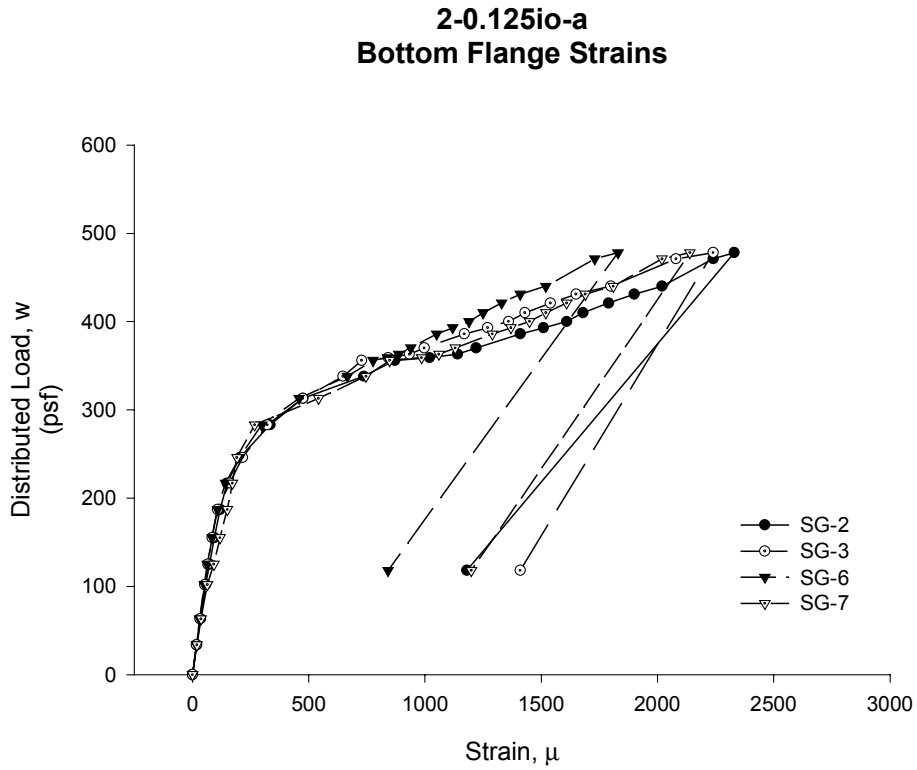

Figure B. 29 Applied Load vs. Deck Bottom Flange Strain for 2-0.125io-a

Test Designation: 2-0.125io-b
Test Date: November 14, 2000

Materials and Dimensions

General:

width:	6 feet (2 panels)
span length:	9 ft. 4 in.
deck anchorage type:	arc spot weld, 3/4 in. dia
average anchorage spacing:	1.0 ft.

Deck:

thickness:	0.0350 in. (20 gage)	
depth:	2 in.	
area:	0.534 in^2	
yield stress:	52.5 ksi	
ultimate strength:	60.7 ksi	
embossment dimensions:		
N_b: 1.443 in.	W_b: 0.506 in.	s: 1.000 in.
N_t: 1.1550 in.	W_t: 0.360 in.	p_h: 0.125 in.

Concrete:

type:	normal weight
test strength:	4,300 psi
total depth:	4.5 in.
cover depth:	2.5 in.

RESULTS:

midspan strain due to fresh concrete:	846×10^{-6} in./in. (bot. flange)
	564×10^{-6} in./in. (top flange)
maximum load:	400 psf
deflection at maximum load:	1.433 in.
end slip at max load:	0.134 in. (left)
	0.029 in. (right)
end slip at termination of test:	0.781 in. (left)
	0.032 in. (right)

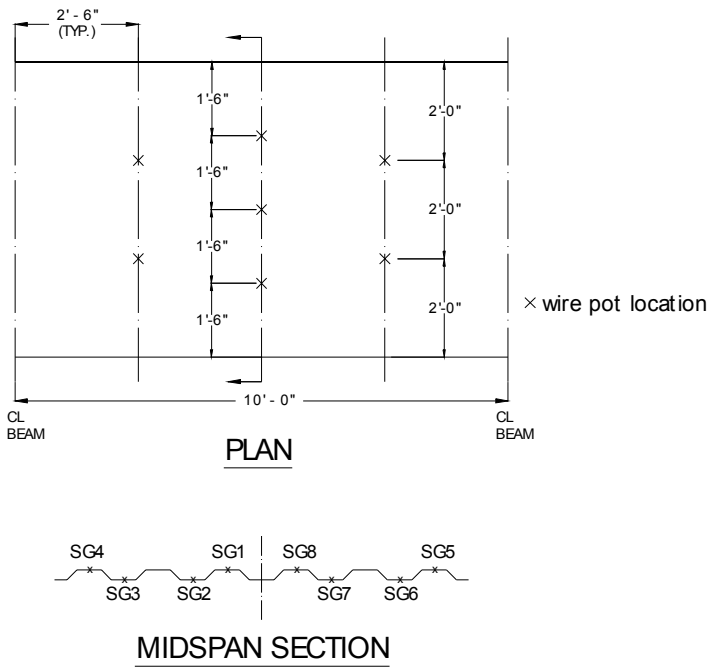

Figure B. 30 Strain Gage and Wire Pot Locations for 2-0.125io-b

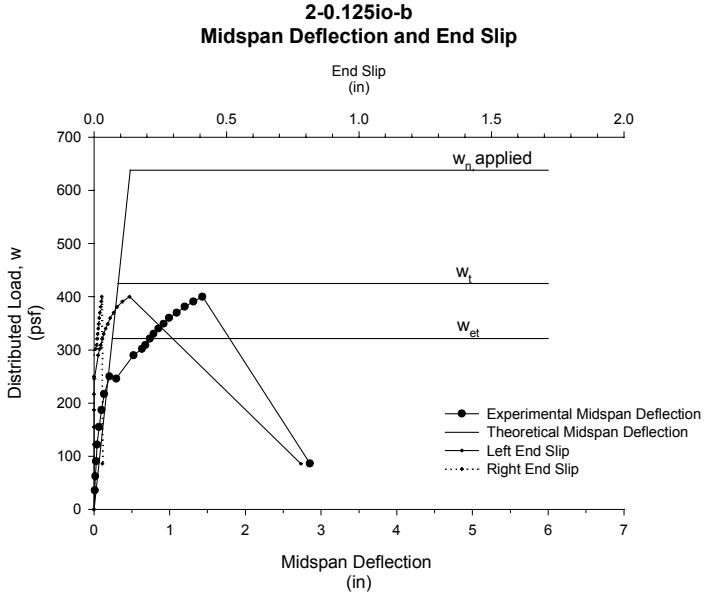

w_n = Theoretical applied distributed load that results in M_n using the calculated material properties

w_t = Theoretical applied distributed load that results in M_t (Flexural Capacity using ASCE App. D Method)

w_{et} = Theoretical applied distributed load that results in M_{et} (First Yield Moment)

Figure B. 31 Applied Load vs. Midspan Deflection and End Slip for 2-0.125io-b

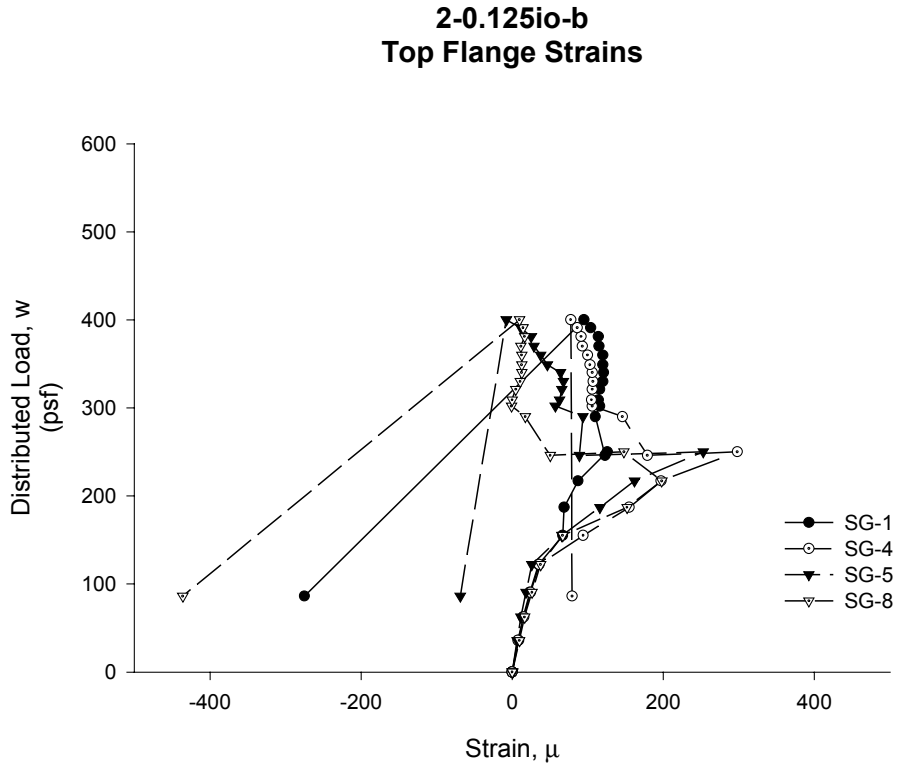

Figure B. 32 Applied Load vs. Deck Top Flange Strain for 2-0.125io-b

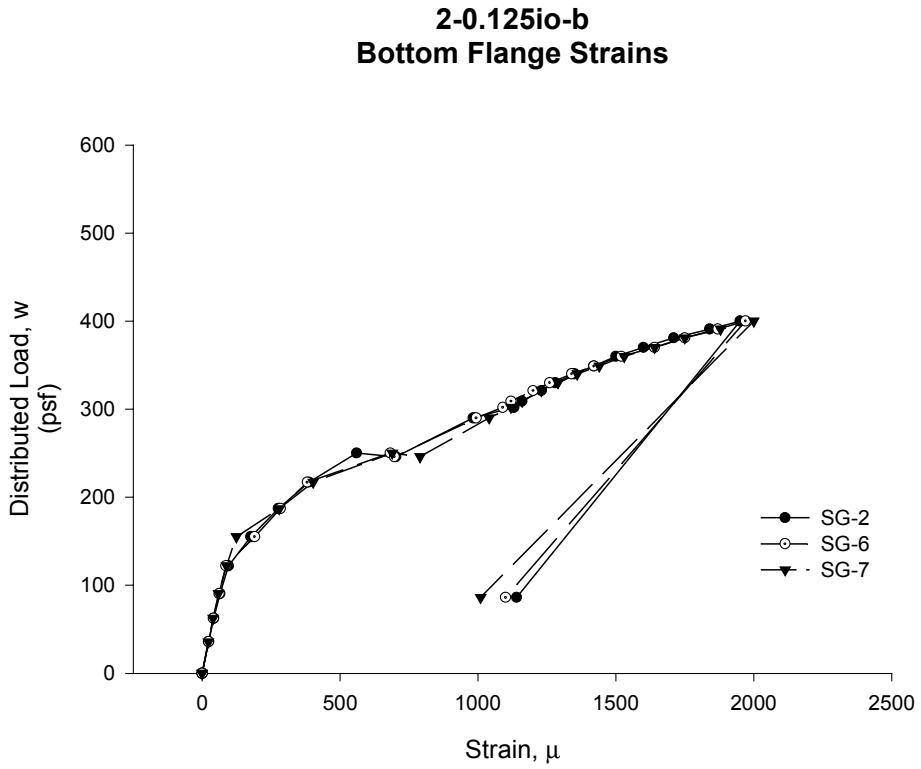

Figure B. 33 Applied Load vs. Deck Bottom Flange Strain for 2-0.125io-b

Test Designation: 2-0.14io-a
Test Date: September 11, 2000

Materials and Dimensions

General:

width:	6 feet (2 panels)
span length:	9 ft. 4 in.
deck anchorage type:	arc spot weld, 3/4 in. dia
average anchorage spacing:	1.0 ft.

Deck:

thickness:	0.0350 in. (20 gage)	
depth:	2 in.	
area:	0.534 in^2	
yield stress:	52.5 ksi	
ultimate strength:	60.7 ksi	
embossment dimensions:		
N_b: 1.443 in.	W_b: 0.506 in.	s: 1.00 in.
N_t: 1.155 in.	W_t: 0.360 in.	p_h: 0.140 in.

Concrete:

type:	normal weight
test strength:	4,000 psi
total depth:	4.5 in.
cover depth:	2.5 in.

RESULTS:

midspan strain due to fresh concrete:	$628x10^{-6}$ in./in. (bot. flange)
	$499x10^{-6}$ in./in. (top flange)
maximum load:	401 psf
deflection at maximum load:	1.88 in.
end slip at max load:	0.07 in. (left)
	0.15 in. (right)
end slip at termination of test:	0.07 in. (left)
	0.99 in. (right)

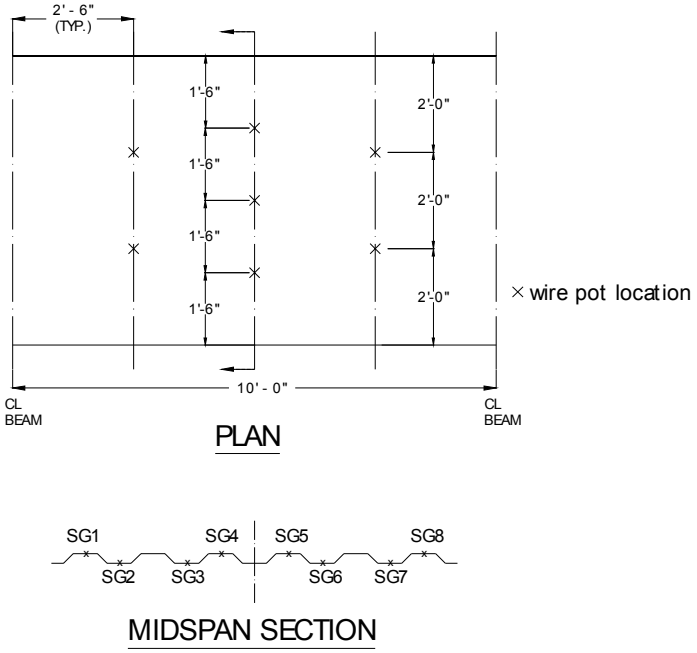

Figure B. 34 Strain Gage and Wire Pot Locations for 2-0.14io-a

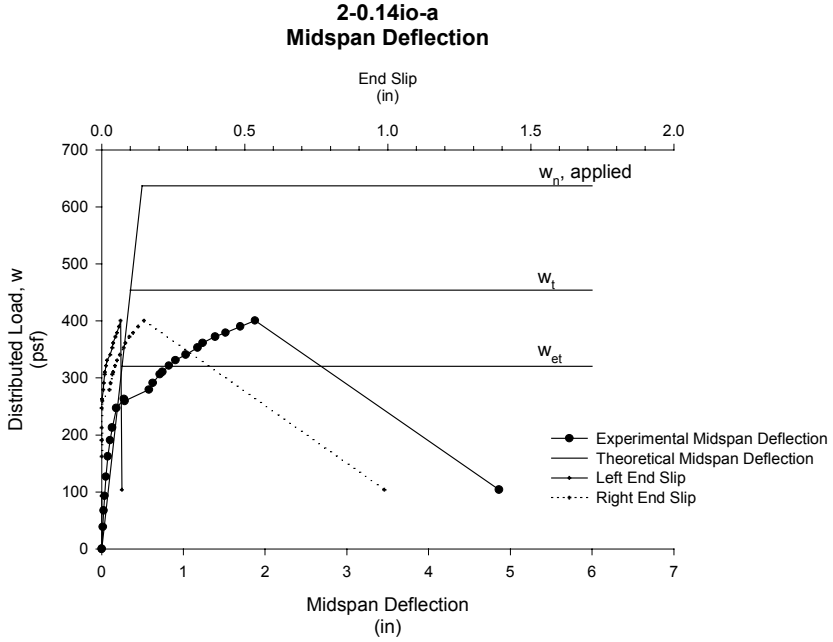

w_n = Theoretical applied distributed load that results in M_n using the calculated material properties

w_t = Theoretical applied distributed load that results in M_t (Flexural Capacity using ASCE App. D Method)

w_{et} = Theoretical applied distributed load that results in M_{et} (First Yield Moment)

Figure B. 35 Applied Load vs. Midspan Deflection and End Slip for 2-0.14io-a

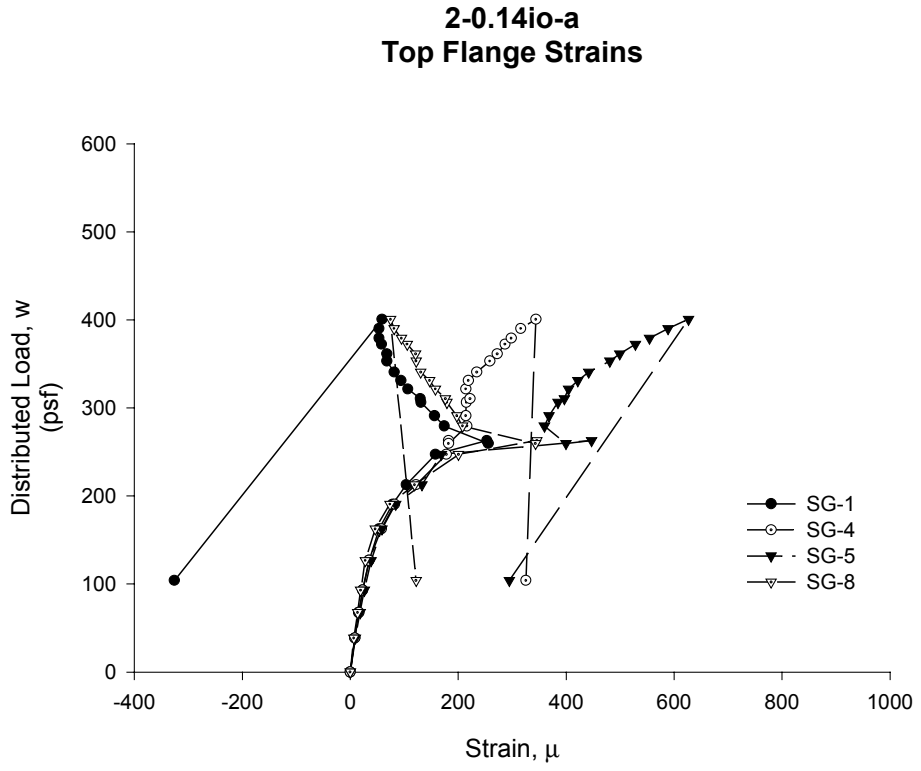

Figure B. 36 Applied Load vs. Deck Top Flange Strain for 2-0.14io-a

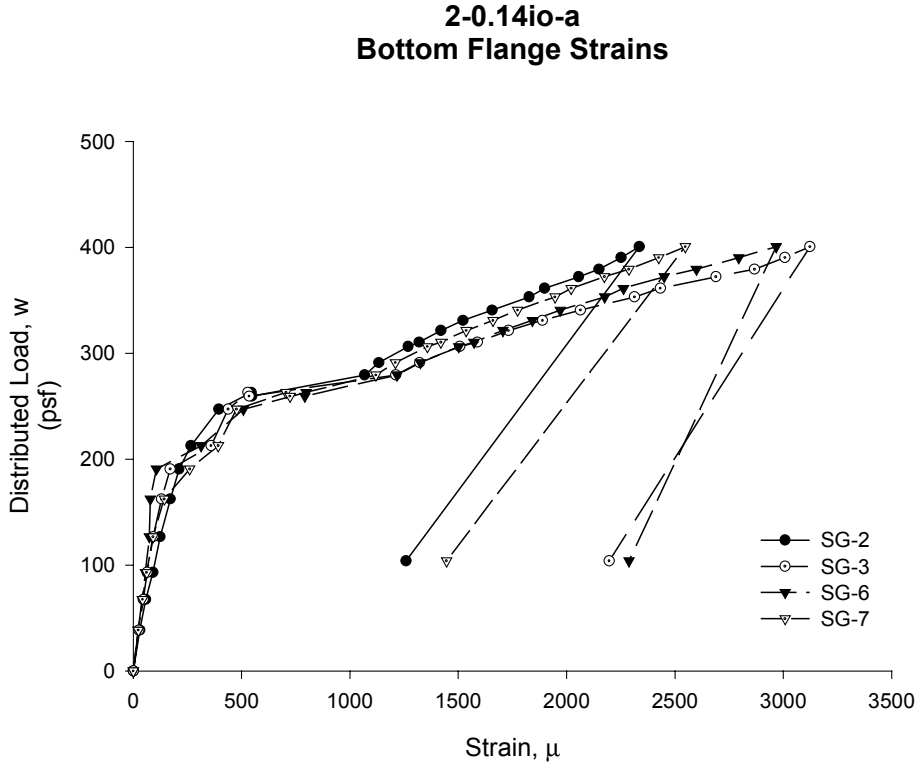

Figure B. 37 Applied Load vs. Deck Bottom Flange Strain for 2-0.14io-a

Test Designation: 2-0.14io-b

Test Date: September 12, 2000

Materials and Dimensions

General:

width:	6 feet (2 panels)
span length:	9 ft. 4 in.
deck anchorage type:	arc spot weld, 3/4 in. dia
average anchorage spacing:	1.0 ft.

Deck:

thickness:	0.0350 in. (20 gage)
depth:	2 in.
area:	0.534 in^2
yield stress:	52.5 ksi
ultimate strength:	60.7 ksi

embossment dimensions:

N_b: 1.443 in.	W_b: 0.506 in.	s: 1.000 in.
N_t: 1.155 in.	W_t: 0.360 in.	p_h: 0.140 in.

Concrete:

type:	normal weight
test strength:	4,200 psi
total depth:	4.5 in.
cover depth:	2.5 in.

RESULTS:

midspan strain due to fresh concrete:	607×10^{-6} in./in. (bot. flange)
	491×10^{-6} in./in. (top flange)
maximum load:	359 psf
deflection at maximum load:	1.876 in.
end slip at max load:	0.045 in. (left)
	0.158 in. (right)
end slip at termination of test:	0.054 in. (left)
	1.115 in. (right)

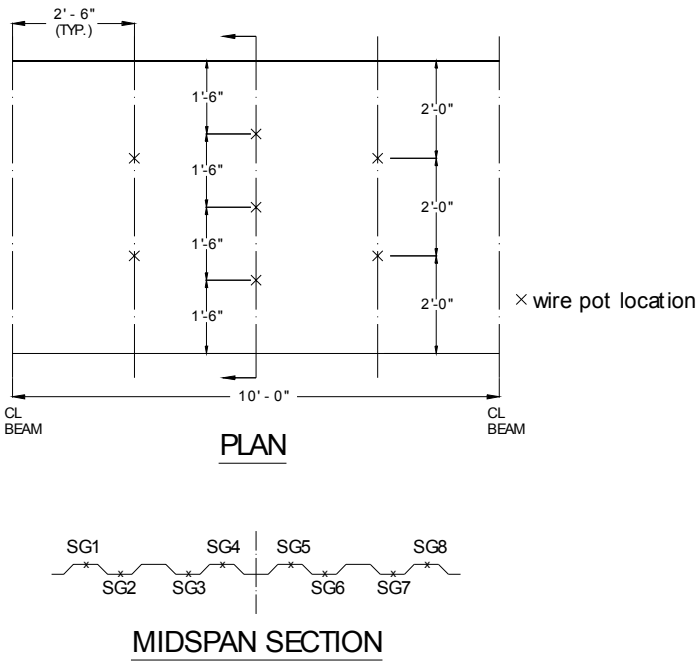

Figure B. 38 Strain Gage and Wire Pot Locations for 2-0.14io-b

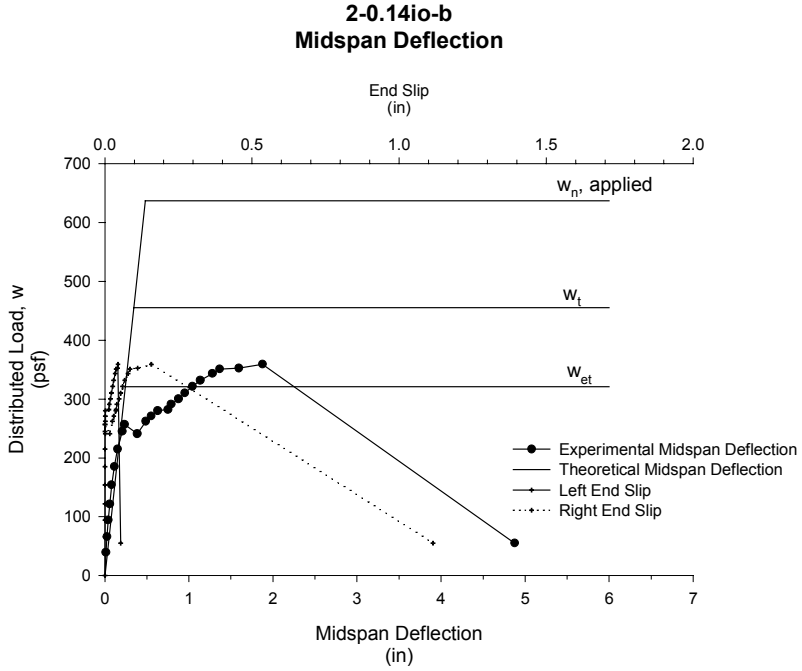

w_n = Theoretical applied distributed load that results in M_n using the calculated material properties

w_t = Theoretical applied distributed load that results in M_t (Flexural Capactity using ASCE App. D Method)

w_{et} = Theoretical applied distributed load that results in M_{et} (First Yield Moment)

Figure B. 39 Applied Load vs. Midspan Deflection and End Slip for 2-0.14io-b

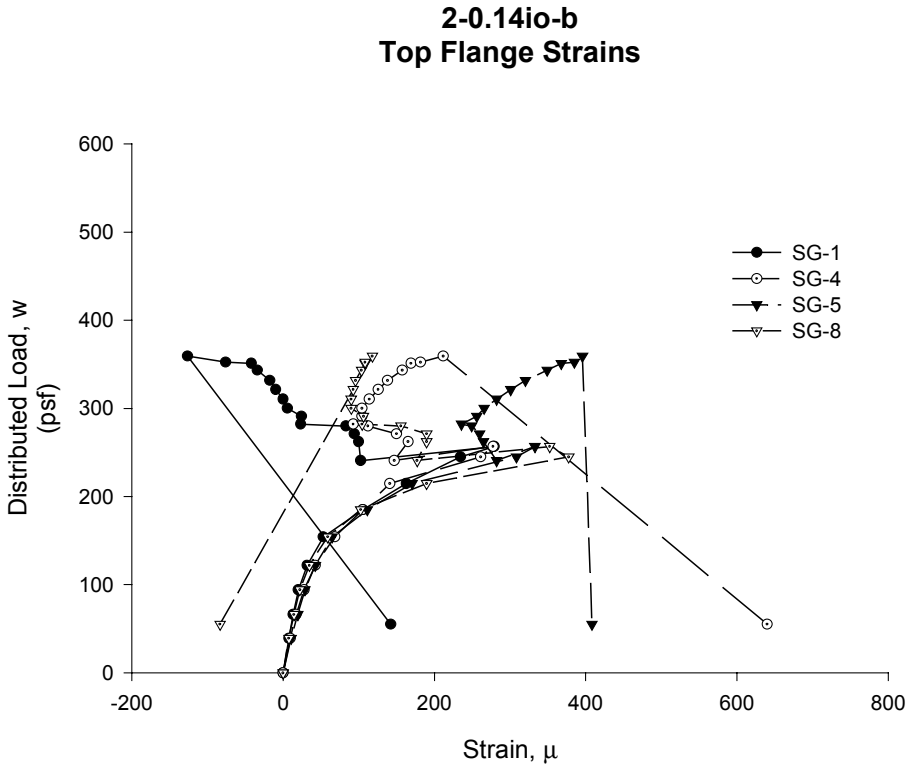

Figure B. 40 Applied Load vs. Deck Top Flange Strain for 2-0.14io-b

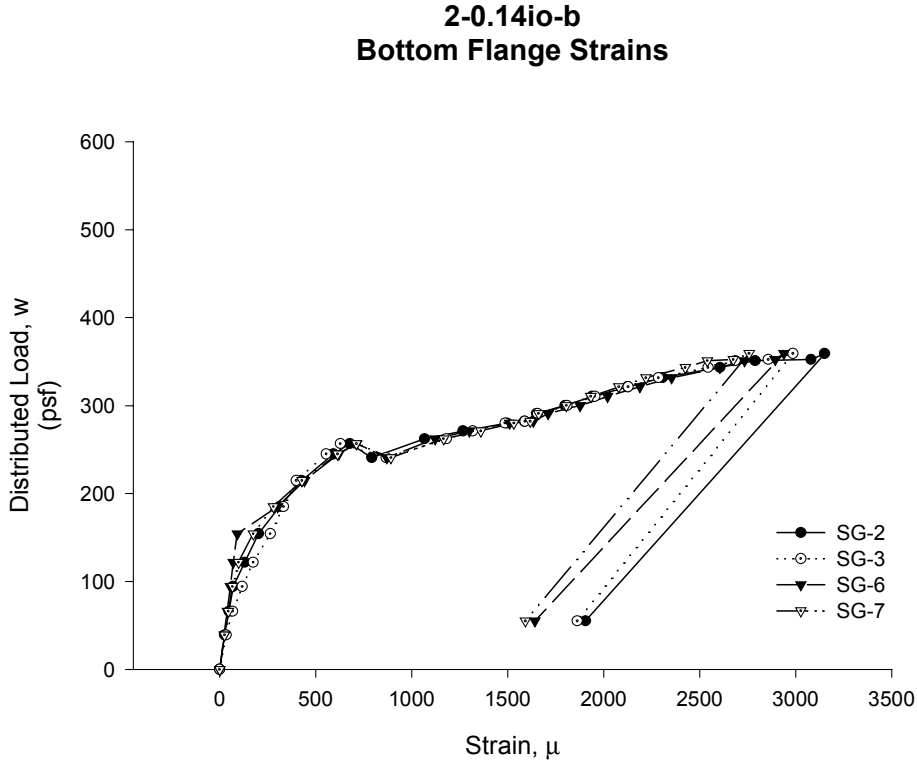

Figure B. 41 Applied Load vs. Deck Bottom Flange Strain for 2-0.14io-b

Test Designation: 3-exist-a
Test Date: March 1, 2001

Materials and Dimensions

General:

width:	6 feet (2 panels)
span length:	11 ft. 4 in.
deck anchorage type:	arc spot weld, 3/4 in. dia
average anchorage spacing:	1.0 ft.

Deck:

thickness:	0.0350 in. (20 gage)
depth:	3 in.
area:	0.581 in^2
yield stress:	52.7 ksi
ultimate strength:	62.1 ksi

embossment dimensions:

vertical:	horizontal:		
N_b: 1.77 in.	N_b: 2.31 in.	W_b: 0.563 in.	s: 3.40 in.
N_t: 1.47 in.	N_t: 2.01 in.	W_t: 0350 in.	p_h: 0.10 in.

Concrete:

type:	normal weight
test strength:	3,500 psi
total depth:	5.5 in.
cover depth:	2.5 in.

RESULTS:

midspan strain due to fresh concrete:	$625x10^{-6}$ in./in. (bot. flange)
	$666x10^{-6}$ in./in. (top flange)
maximum load:	328 psf
deflection at maximum load:	0.404 in.
end slip at max load:	0.000 in. (left)
	0.000 in. (right)
end slip at termination of test:	0.000 in. (left)
	0.018 in. (right)

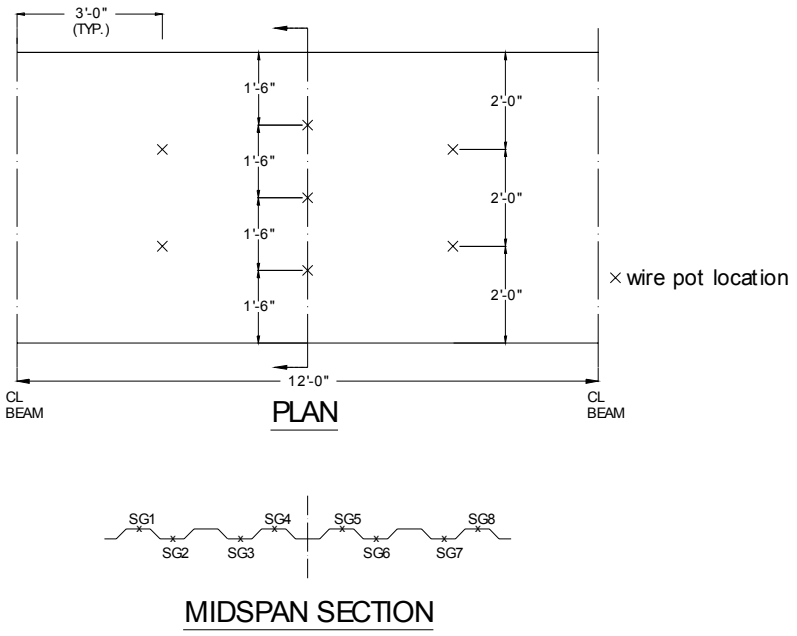

Figure B. 42 Strain Gage and Wire Pot Locations for 3-exist-a

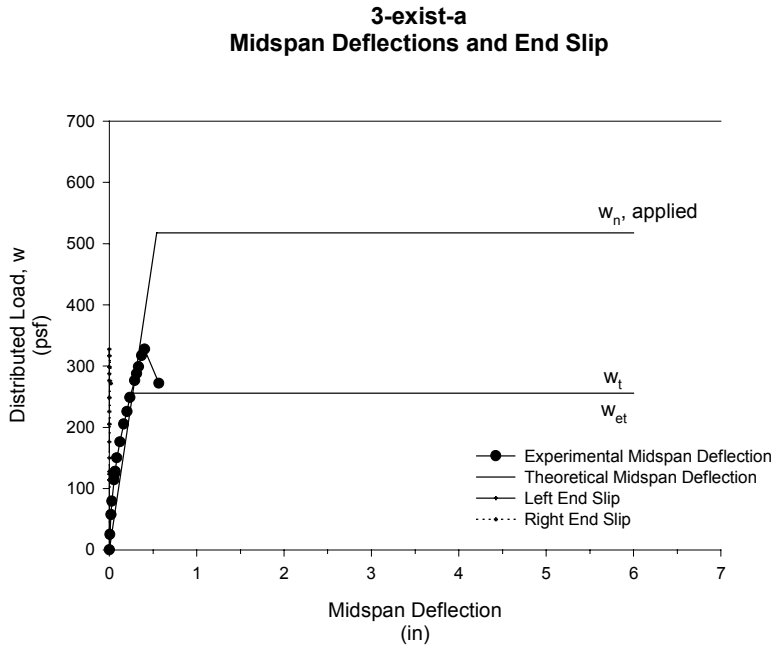

w_n = Theoretical applied distributed load that results in M_n using the calculated material properties

w_t = Theoretical applied distributed load that results in M_t (Flexural Capacity using ASCE App. D Method)

w_{et} = Theoretical applied distributed load that results in M_{et} (First Yield Moment)

Figure B. 43 Applied Load vs. Midspan Deflection and End Slip 3-exist-a

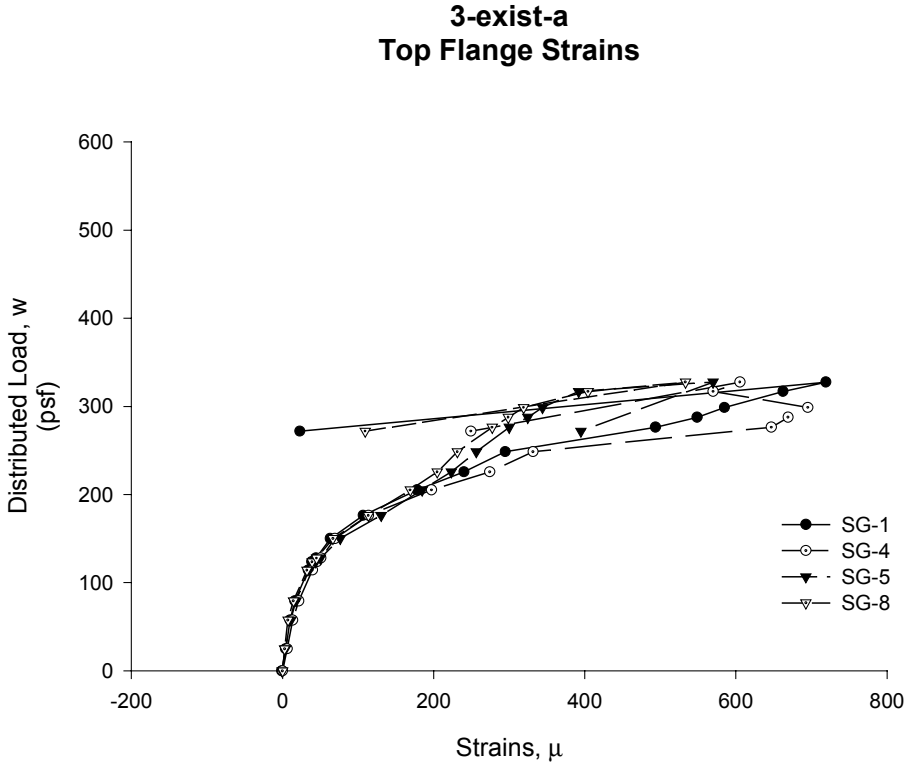

Figure B. 44 Applied Load vs. Deck Top Flange Strain for 3-exist-a

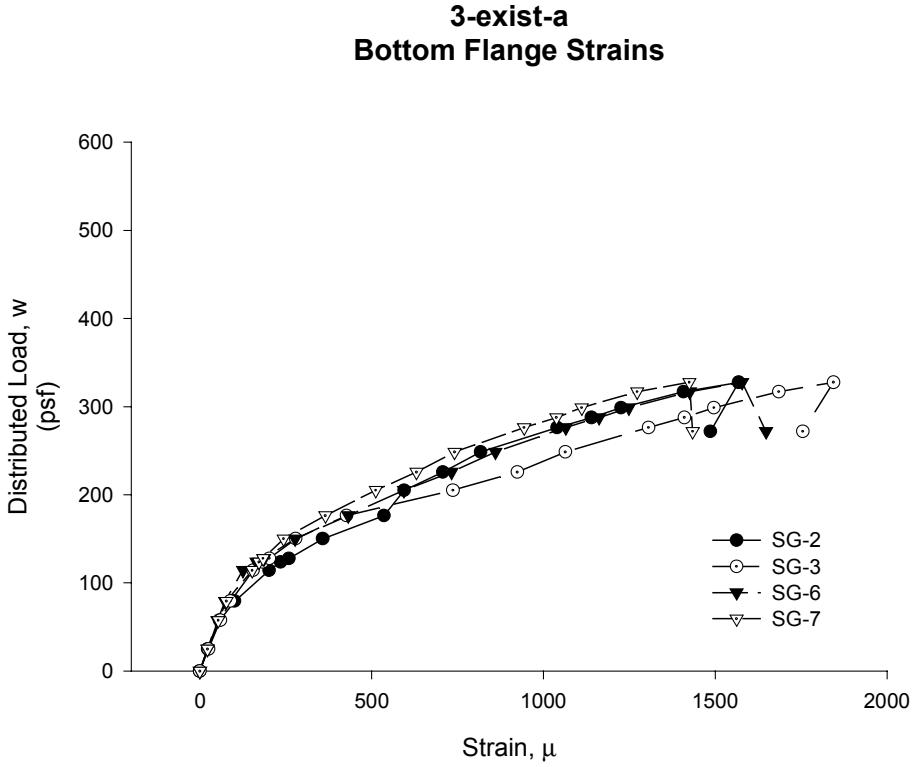

Figure B. 45 Applied Load vs. Deck Bottom Flange Strain for 3-exist-a

Test Designation: 3-exist-b
Test Date: March 1, 2001

Materials and Dimensions

General:

width:	6 feet (2 panels)
span length:	11 ft. 4 in.
deck anchorage type:	arc spot weld, 3/4 in. dia
average anchorage spacing:	1.0 ft.

Deck:

thickness:	0.0350 in. (20 gage)
depth:	3 in.
area:	0.581 in^2
yield stress:	52.7 ksi
ultimate strength:	62.1 ksi

embossment dimensions:

vertical:	horizontal:		
N_b: 1.77 in.	N_b: 2.31 in.	W_b: 0.563 in.	s: 3.40 in.
N_t: 1.47 in.	N_t: 2.01 in.	W_t: 0350 in.	p_h: 0.10 in.

Concrete:

type:	normal weight
test strength:	3,500 psi
total depth:	5.5 in.
cover depth:	2.5 in.

RESULTS:

midspan strain due to fresh concrete:	672x10^{-6} in./in. (bot. flange)
	675x10^{-6} in./in. (top flange)
maximum load:	346 psf
deflection at maximum load:	0.534 in.
end slip at max load:	0.000 in. (left)
	0.000 in. (right)
end slip at termination of test:	0.000 in. (left)
	0.000 in. (right)

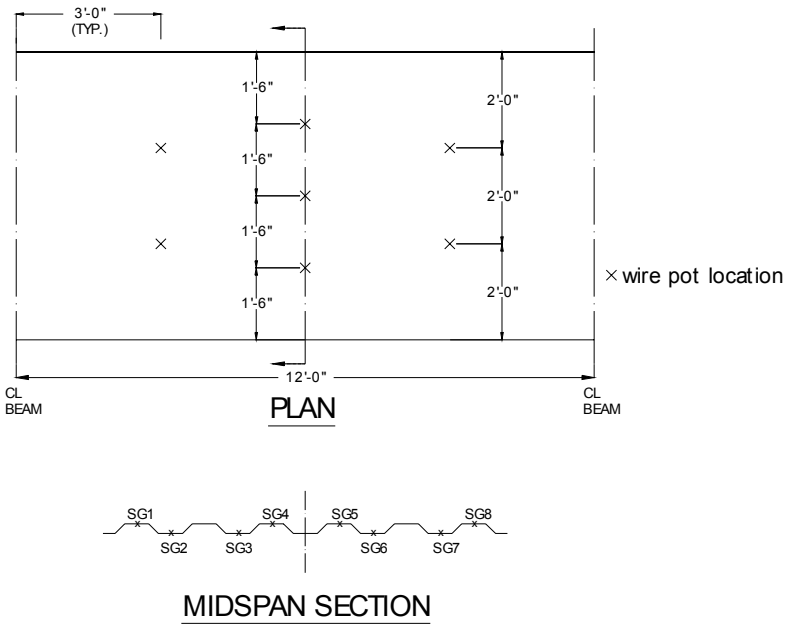

Figure B. 46 Strain Gage and Wire Pot Locations for 3-exist-b

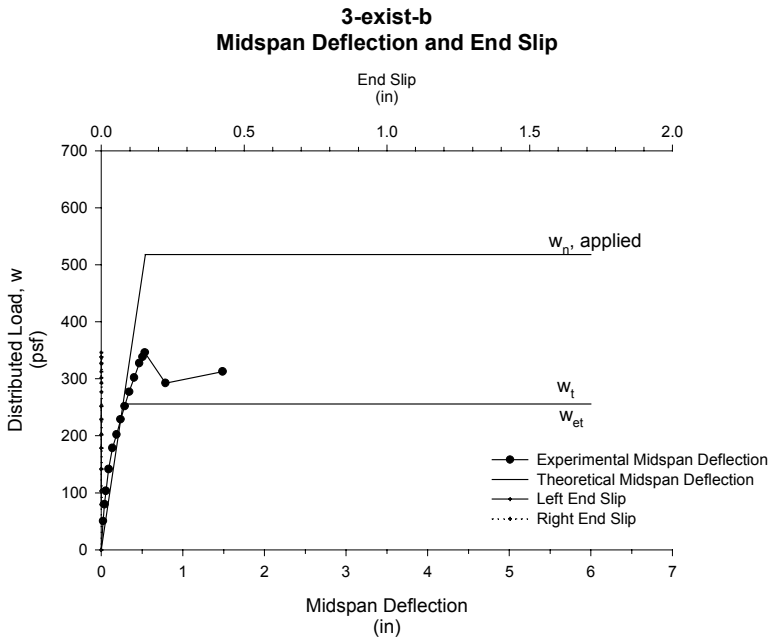

w_n = Theoretical applied distributed load that results in M_n using the calculated material properties

w_t = Theoretical applied distributed load that results in M_t (Flexural Capacity using ASCE App. D Method)

w_{et} = Theoretical applied distributed load that results in M_{et} (First Yield Moment)

Figure B. 47 Applied Load vs. Midspan Deflection and End Slip for 3-exist-b

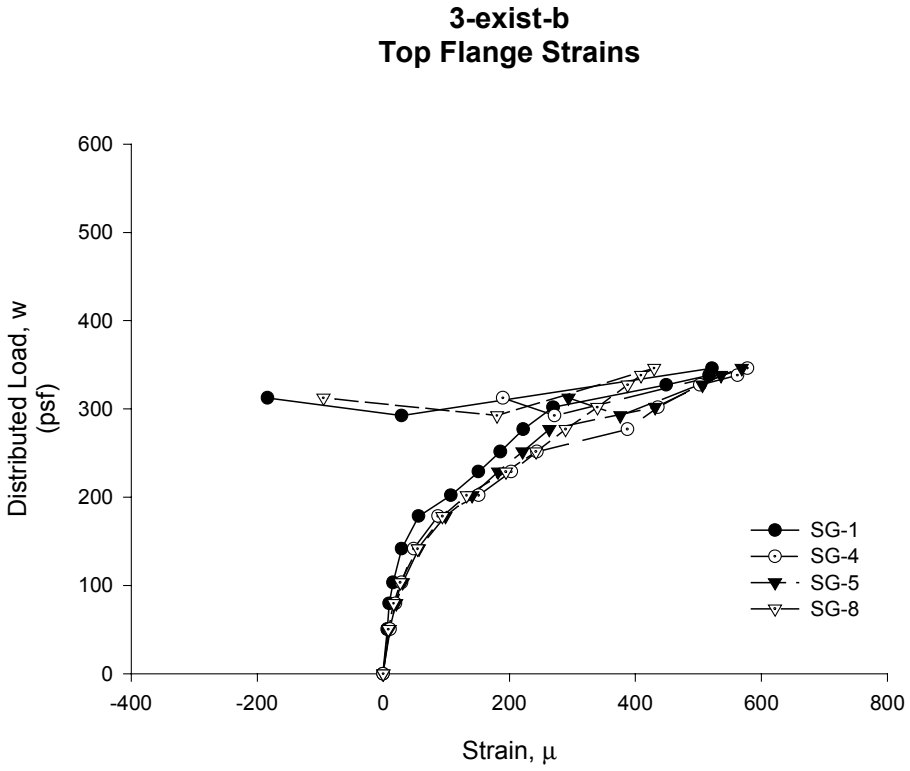

Figure B. 48 Applied Load vs. Deck Top Flange Strain for 3-exist-b

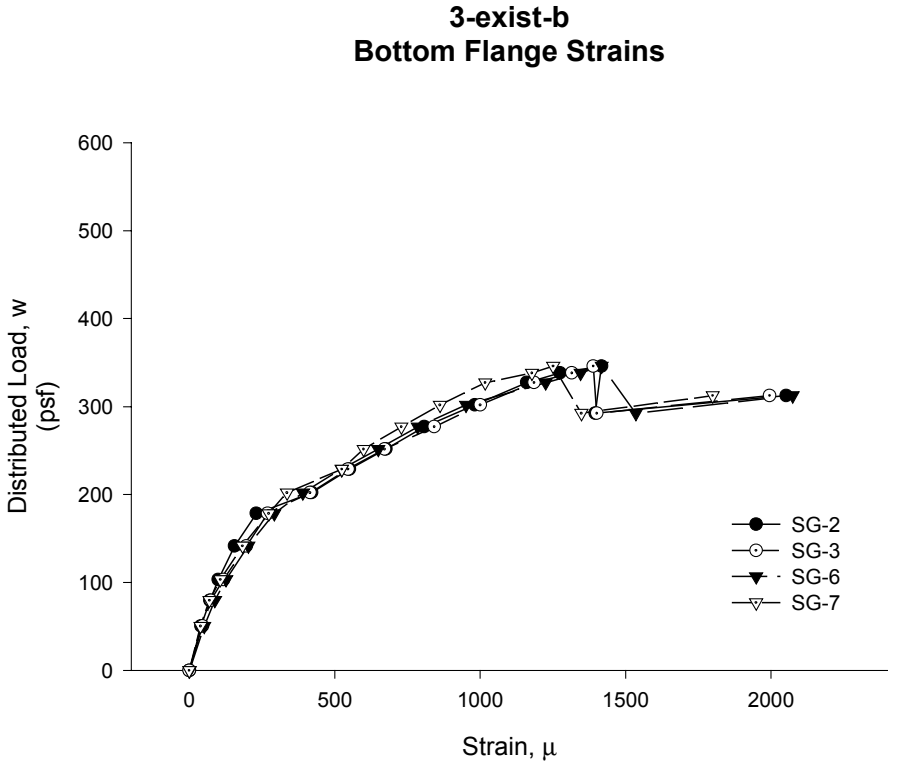

Figure B. 49 Applied Load vs. Deck Bottom Flange Strain for 3-exist-b

Test Designation: 3-0.10i-a
Test Date: January 19, 2001

Materials and Dimensions

General:

width:	6 feet (2 panels)
span length:	11 ft. 4 in.
deck anchorage type:	arc spot weld, 3/4 in. dia
average anchorage spacing:	1.0 ft.

Deck:

thickness:	0.0350 in. (20 gage)	
depth:	3 in.	
area:	0.581 in^2	
yield stress:	52.7 ksi	
ultimate strength:	62.1 ksi	
embossment dimensions:		
N_b: 2.598 in.	W_b: 0.506 in.	s: 1.000 in.
N_t: 2.309 in.	W_t: 0360 in.	p_h: 0.100 in.

Concrete:

type:	normal weight
test strength:	4,500 psi
total depth:	5.5 in.
cover depth:	2.5 in.

RESULTS:

midspan strain due to fresh concrete:	$611x10^{-6}$ in./in. (bot. flange)
	$564x10^{-6}$ in./in. (top flange)
maximum load:	422 psf
deflection at maximum load:	3.125 in.
end slip at max load:	0.082 in. (left)
	0.196 in. (right)
end slip at termination of test:	0.084 in. (left)
	0.654 in. (right)

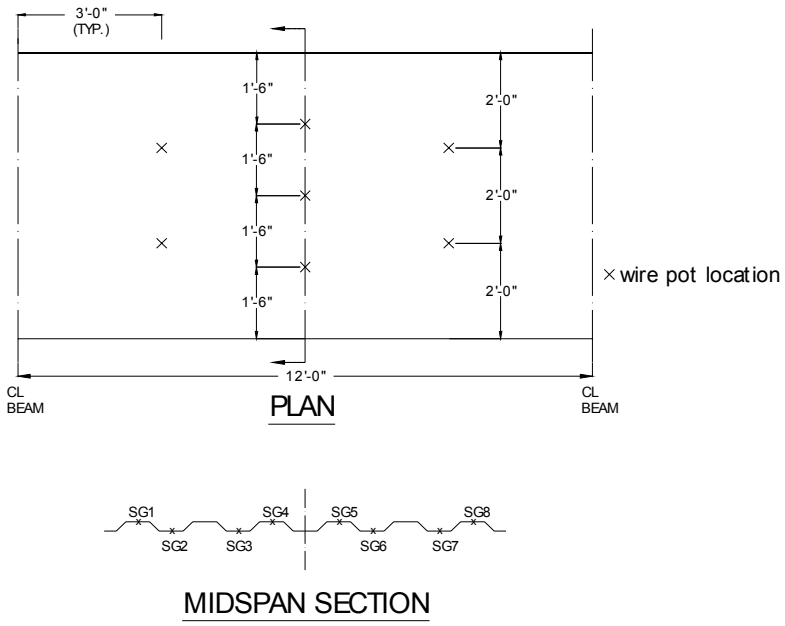

Figure B. 50 Strain Gage and Wire Pot Locations for 3-0.10i-a

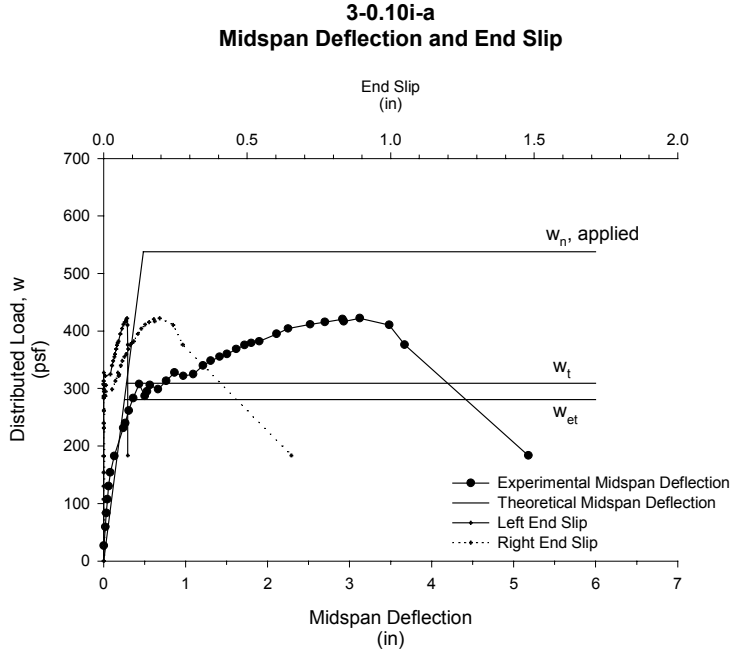

w_n = Theoretical applied distributed load that results in M_n using the calculated material properties

w_t = Theoretical applied distributed load that results in M_t (Flexural Capacity using ASCE App. D Method)

w_{et} = Thoertical applied distibuted load that results in M_{et} (First Yield Moment)

Figure B. 51 Applied Load vs. Midspan Deflection and End Slip for 3-0.10i-a

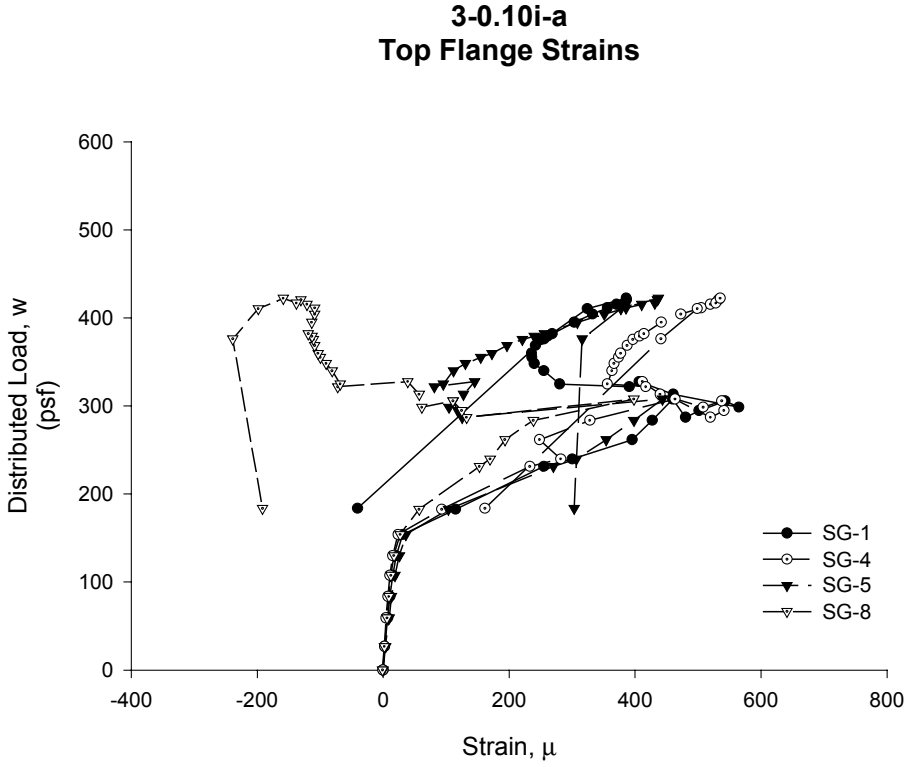

Figure B. 52 Applied Load vs. Deck Top Flange Strain for 3-0.10i-a

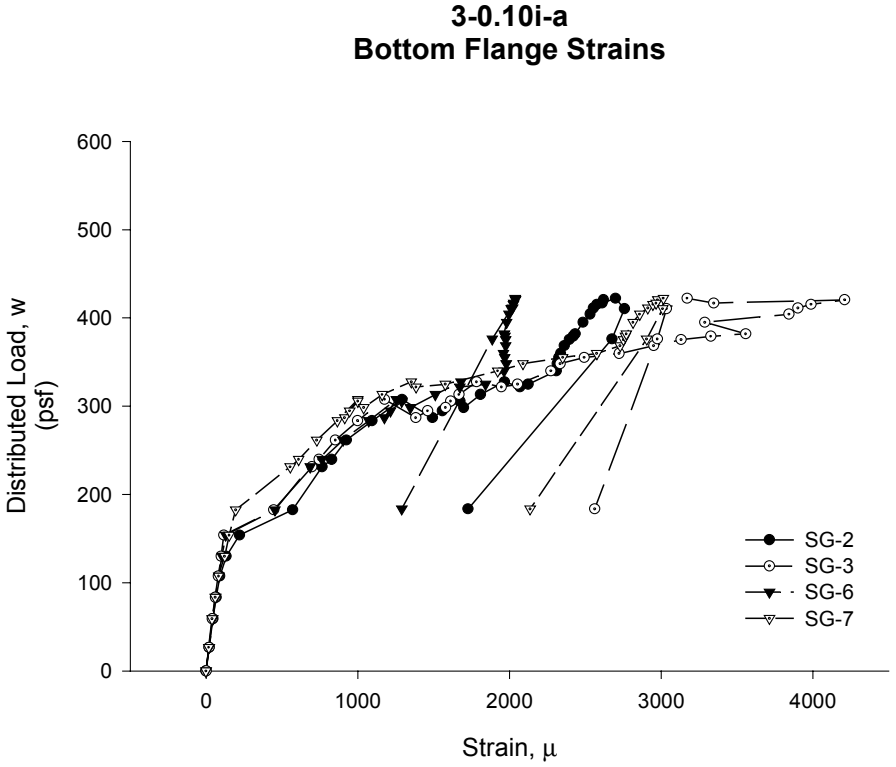

Figure B. 53 Applied Load vs. Deck Bottom Flange Strain for 3-0.10i-a

Test Designation: 3-0.10i-b
Test Date: January 19, 2001

Materials and Dimensions

General:

width:	6 feet (2 panels)
span length:	11 ft. 4 in.
deck anchorage type:	arc spot weld, 3/4 in. dia
average anchorage spacing:	1.0 ft.

Deck:

thickness:	0.0350 in. (20 gage)	
depth:	3 in.	
area:	0.581 in^2	
yield stress:	52.7 ksi	
ultimate strength:	62.1 ksi	
embossment dimensions:		
N_b: 2.598 in.	W_b: 0.506 in.	s: 1.000 in.
N_t: 2.309 in.	W_t: 0360 in.	p_h: 0.100 in.

Concrete:

type:	normal weight
test strength:	4,5\00 psi
total depth:	5.5 in.
cover depth:	2.5 in.

RESULTS:

midspan strain due to fresh concrete:	$583x10^{-6}$ in./in. (bot. flange)
	$520x10^{-6}$ in./in. (top flange)
maximum load:	424 psf
deflection at maximum load:	2.771 in.
end slip at max load:	0.071 in. (left)
	0.196 in. (right)
end slip at termination of test:	0.071 in. (left)
	0.881 in. (right)

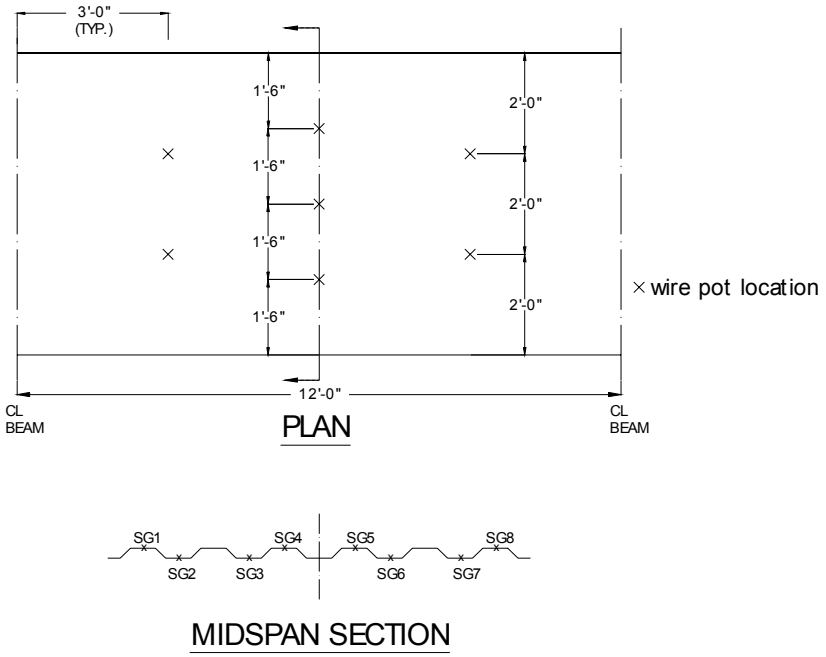

Figure B. 54 Strain Gage and Wire Pot Locations for 3-0.10i-b

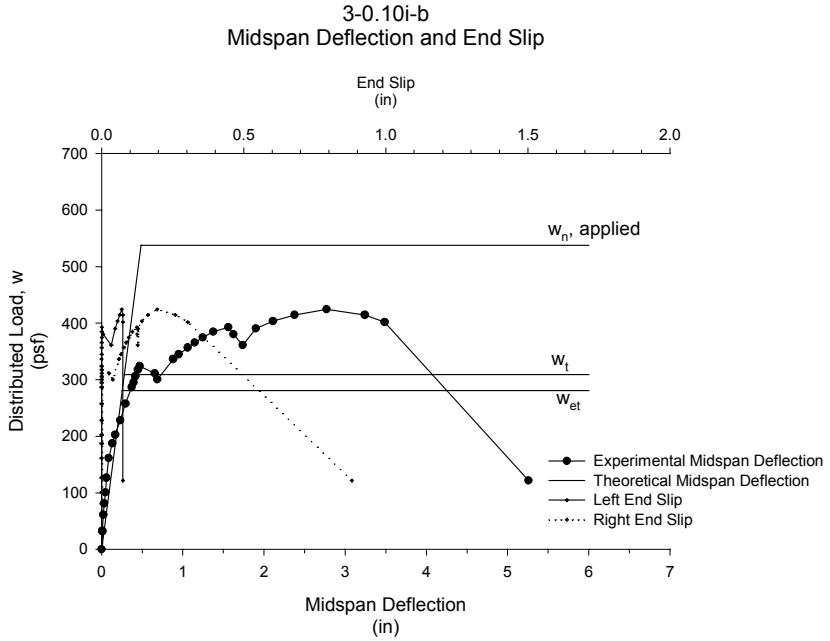

w_n = Theoretical applied distributed load that results in M_n using the calculated material properties

w_t = Theoretical applied distributed load that results in M_t (Flexural Capacity using ASCE App. D Method)

w_{et} = Theoretical applied distributed load that results in M_{et} (First Yield Moment)

Figure B. 55 Applied Load vs. Midspan Deflection and End Slip for 3-0.10i-b

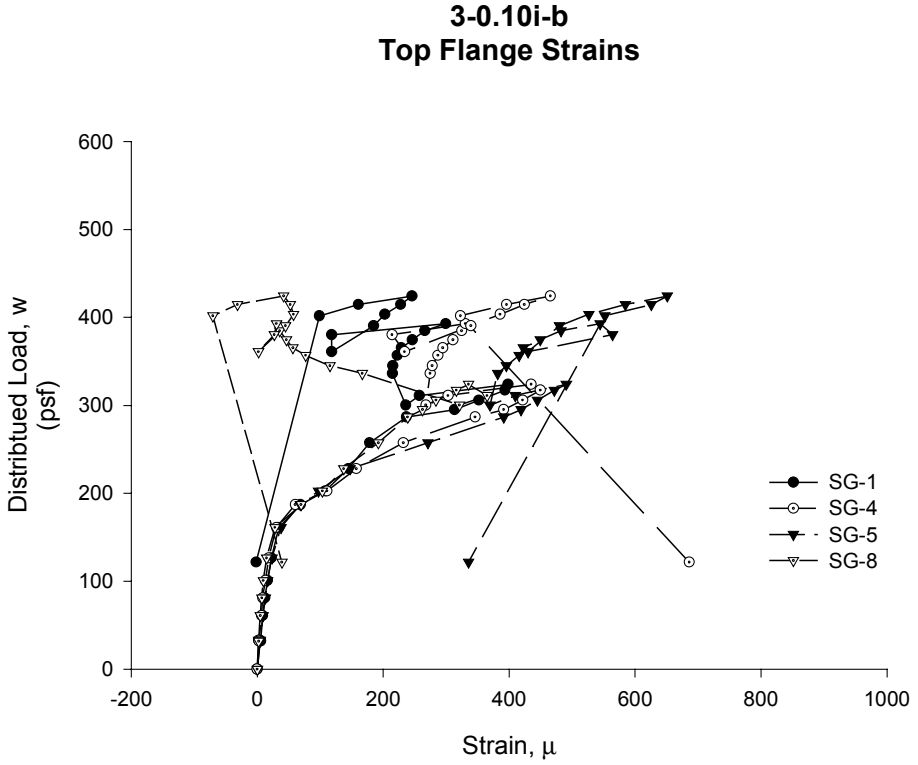

Figure B. 56 Applied Load vs. Deck Top Flange Strain for 3-0.10i-b

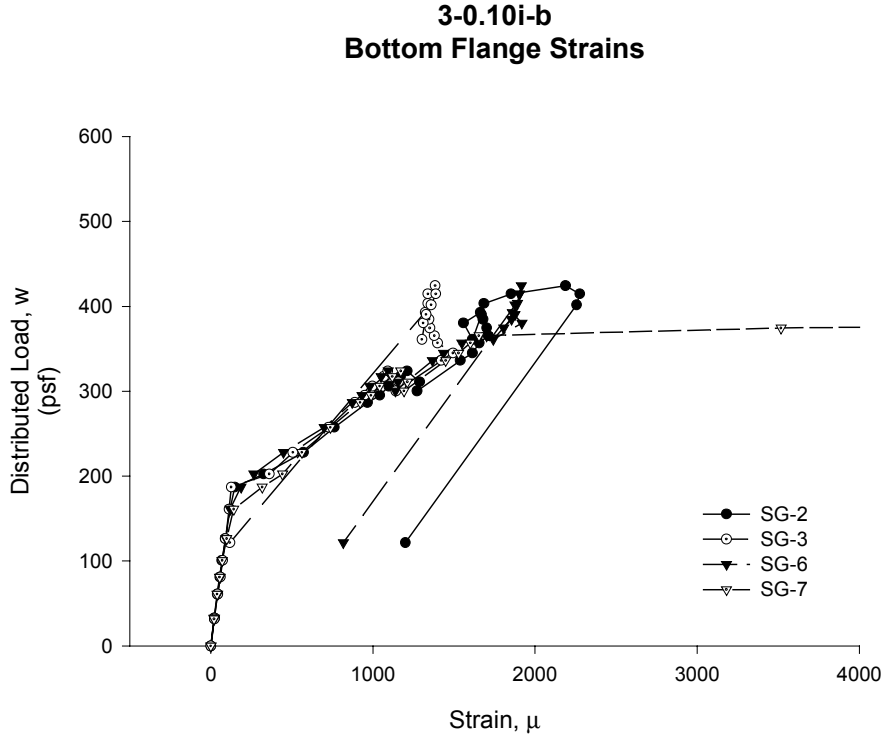

Figure B. 57 Applied Load vs. Deck Bottom Flange Strain for 3-0.10i-b

Test Designation: 3-0.125i-a
Test Date: February 20, 2001

Materials and Dimensions

General:

width:	6 feet (2 panels)
span length:	11 ft. 4 in.
deck anchorage type:	arc spot weld, 3/4 in. dia
average anchorage spacing:	1.0 ft.

Deck:

thickness:	0.0350 in. (20 gage)	
depth:	3 in.	
area:	0.581 in^2	
yield stress:	52.7 ksi	
ultimate strength:	62.1 ksi	
embossment dimensions:		
N_b: 2.598 in.	W_b: 0.506 in.	s: 1.000 in.
N_t: 2.309 in.	W_t: 0360 in.	p_h: 0.125 in.

Concrete:

type:	normal weight
test strength:	3,400 psi
total depth:	5.5 in.
cover depth:	2.5 in.

RESULTS:

midspan strain due to fresh concrete:	$664x10^{-6}$ in./in. (bot. flange)
	$521x10^{-6}$ in./in. (top flange)
maximum load:	469 psf
deflection at maximum load:	2.402 in.
end slip at max load:	0.146 in. (left)
	0.022 in. (right)
end slip at termination of test:	0.832 in. (left)
	0.023 in. (right)

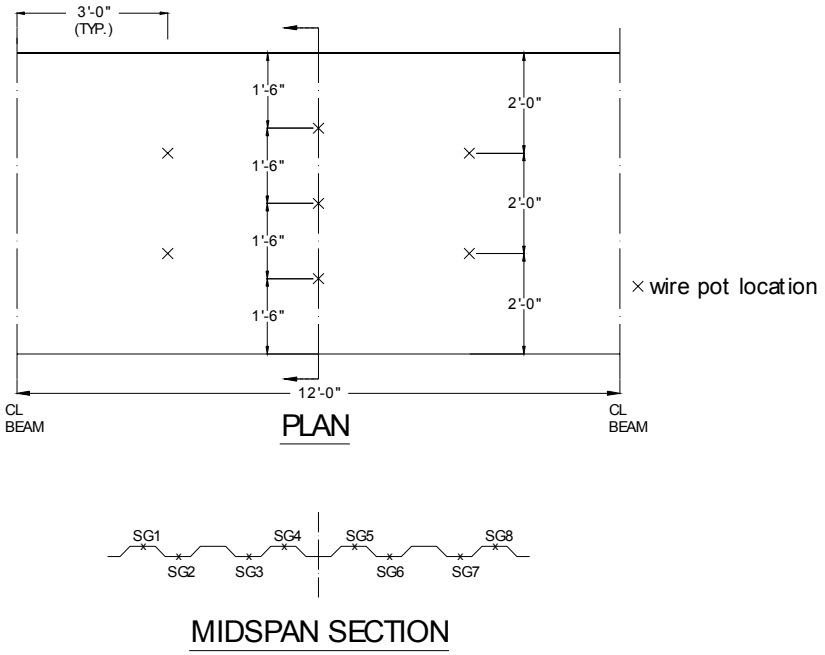

Figure B. 58 Strain Gage and Wire Pot Locations for 3-0.125i-a

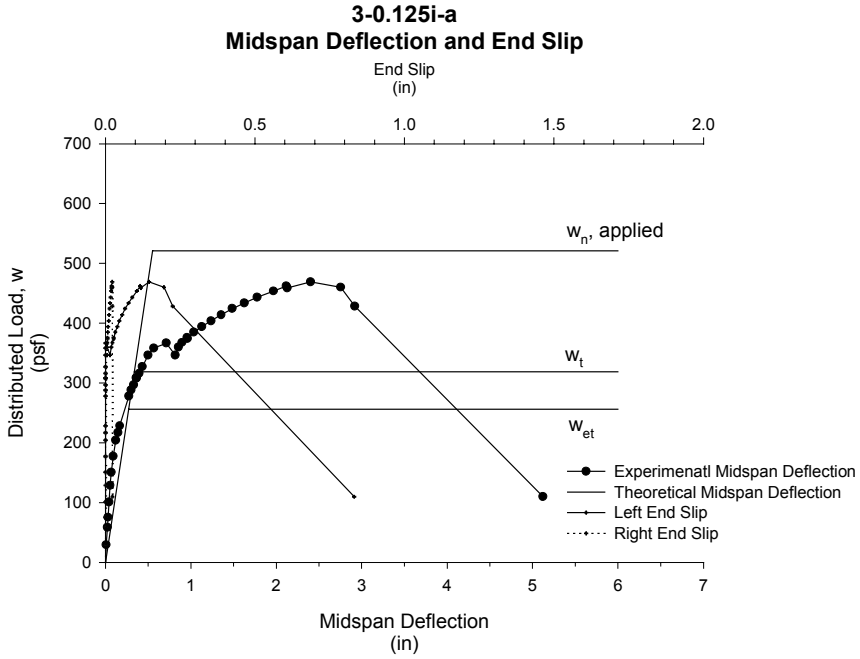

w_n = Theoretical applied distributed load that results in M_n using the calculated material properties

w_t = Theoretical applied distributed load that results in M_t (Flexural Capacity using ASCE App. D. Method)

w_{et} = Theoretical applied distibuted load that results in M_{et} (First Yield Moment)

Figure B. 59 Applied Load vs. Midspan Deflection and End Slip for 3-0.125i-a

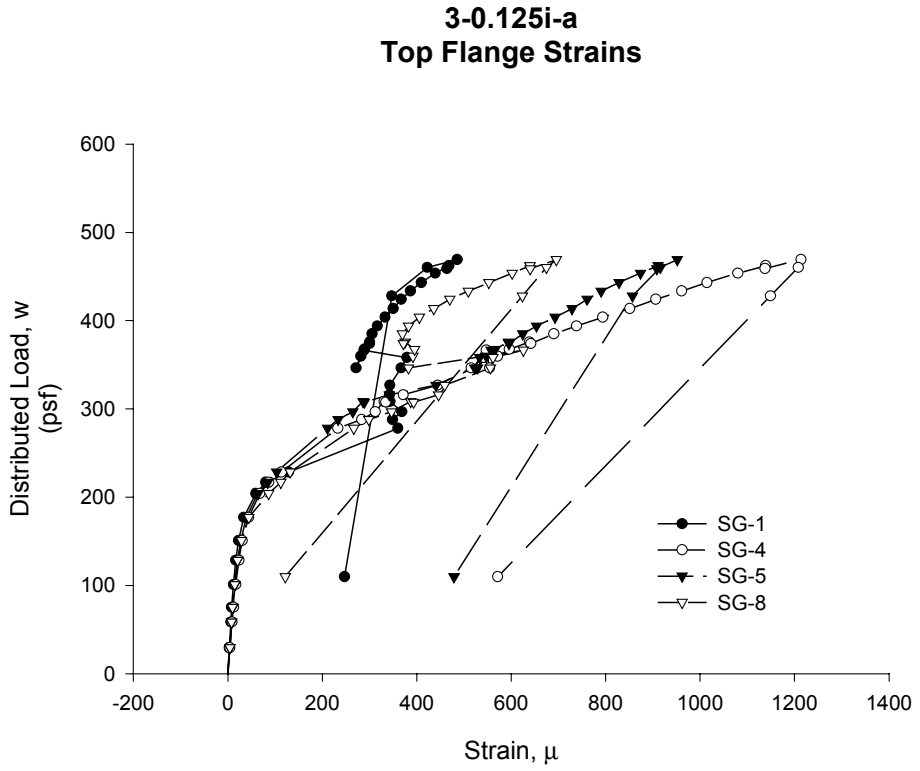

Figure B. 60 Applied Load vs. Deck Top Flange Strain for 3-0.125i-a

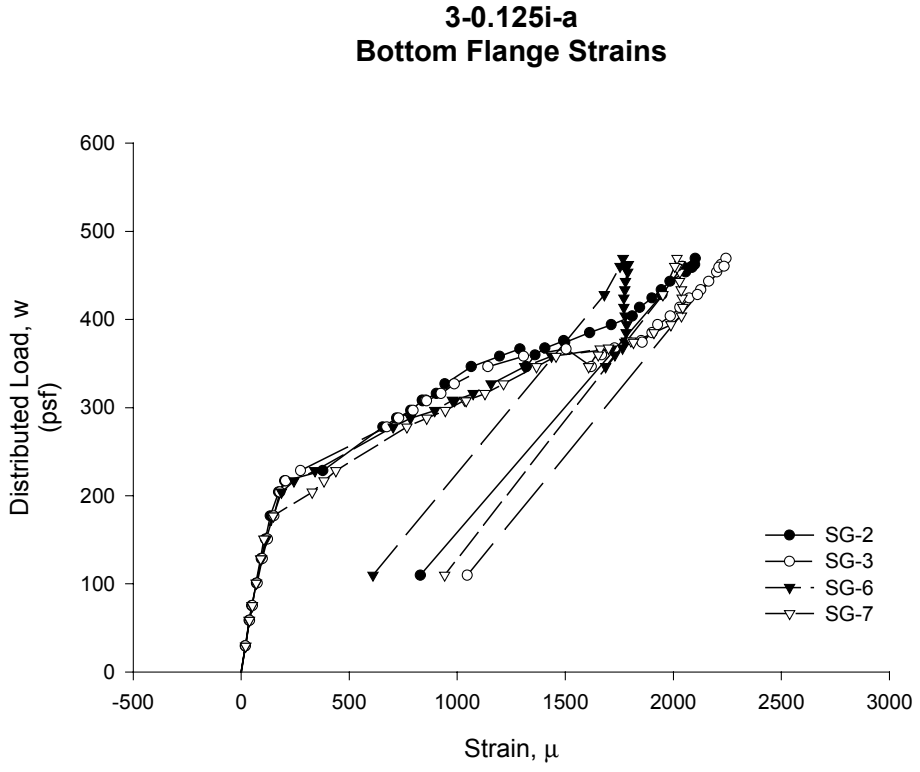

Figure B. 61 Applied Load vs. Deck Bottom Flange Strain for 3-0.125i-a

Test Designation: 3-0.125i-b
Test Date: February 20, 2001

Materials and Dimensions

General:

width:	6 feet (2 panels)
span length:	11 ft. 4 in.
deck anchorage type:	arc spot weld, 3/4 in. dia
average anchorage spacing:	1.0 ft.

Deck:

thickness:	0.0350 in. (20 gage)	
depth:	3 in.	
area:	0.581 in^2	
yield stress:	52.7 ksi	
ultimate strength:	62.1 ksi	
embossment dimensions:		
N_b: 2.598 in.	W_b: 0.506 in.	s: 1.000 in.
N_t: 2.309 in.	W_t: 0360 in.	p_h: 0.125 in.

Concrete:

type:	normal weight
test strength:	3,400 psi
total depth:	5.5 in.
cover depth:	2.5 in.

RESULTS:

midspan strain due to fresh concrete:	611×10^{-6} in./in. (bot. flange)
	569×10^{-6} in./in. (top flange)
maximum load:	456 psf
deflection at maximum load:	3.639 in.
end slip at max load:	0.129 in. (left)
	0.050 in. (right)
end slip at termination of test:	0.664 in. (left)
	0.054 in. (right)

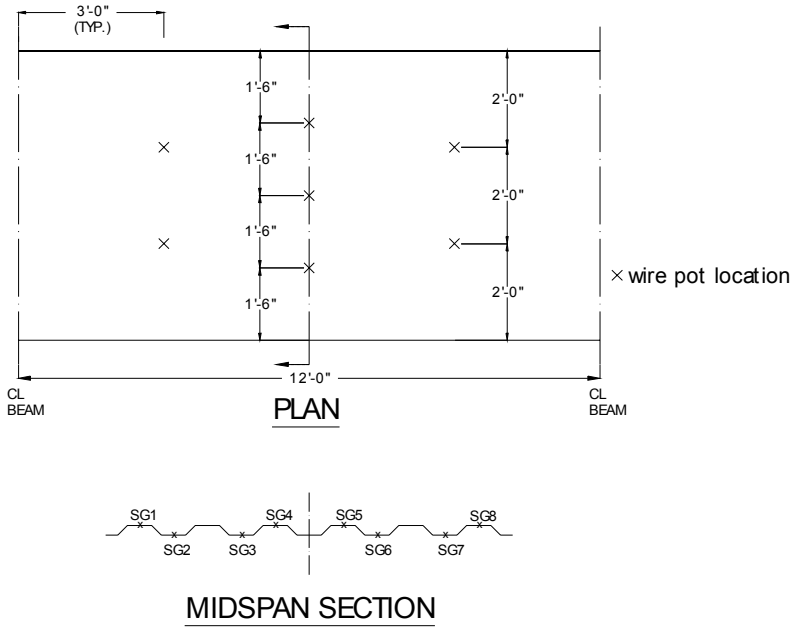

Figure B. 62 Strain Gage and Wire Pot Locations for 3-0.125i-b

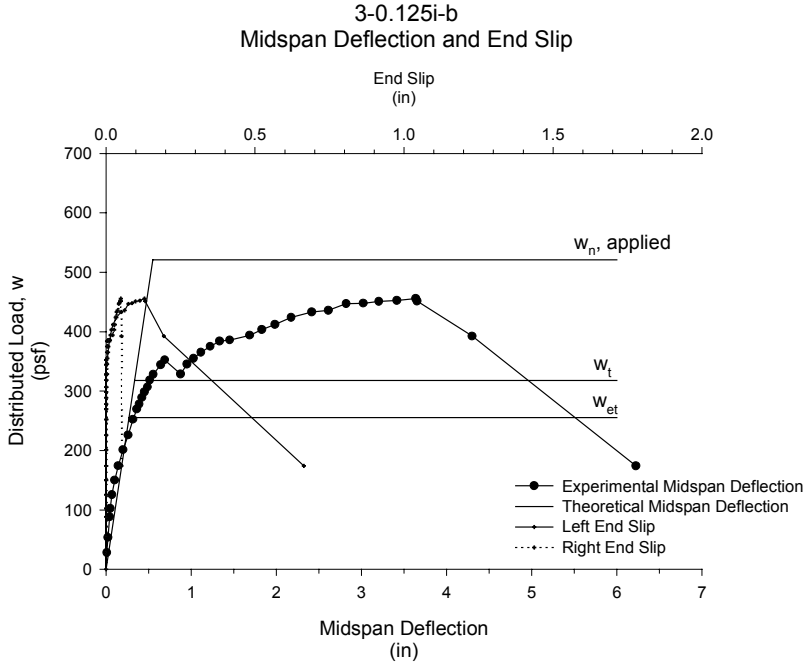

w_n = Theoretical applied distributed load that results in M_t using the calculated material properties

w_t = Theoretical applied distibuted load that results in M_t (Flexural Capacity using ASCE App. D Method)

w_{et} = Theoretical applied distributed load that results in M_{et} (First Yield Moment)

Figure B. 63 Applied Load vs. Midspan Deflection and End Slip for 3-0.125i-b

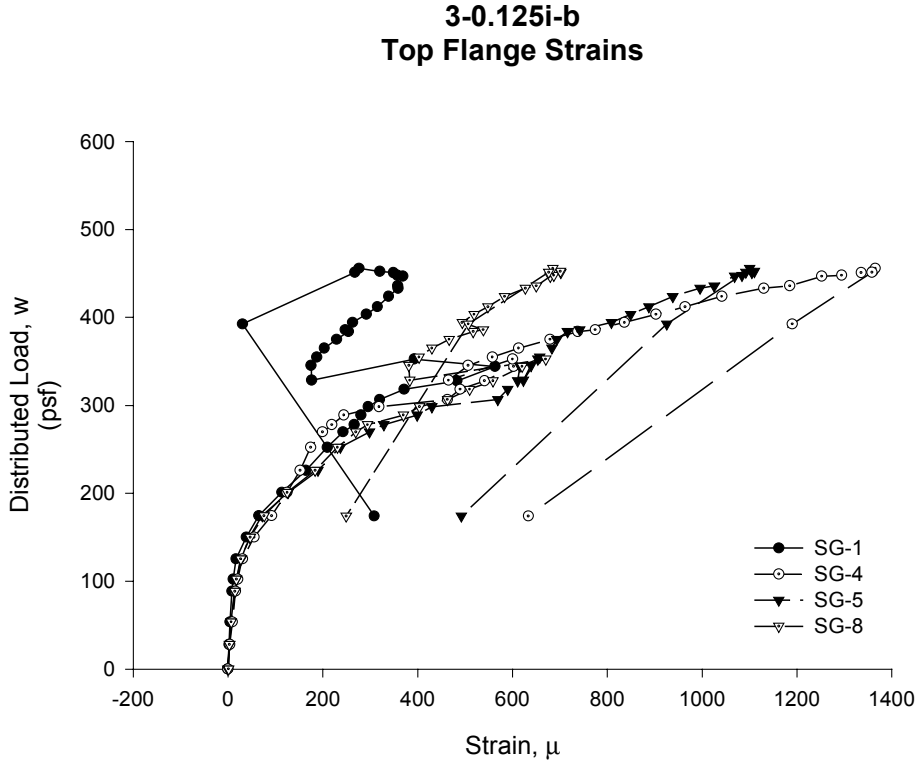

Figure B. 64 Applied Load vs. Deck Top Flange Strain for 3-0.125i-b

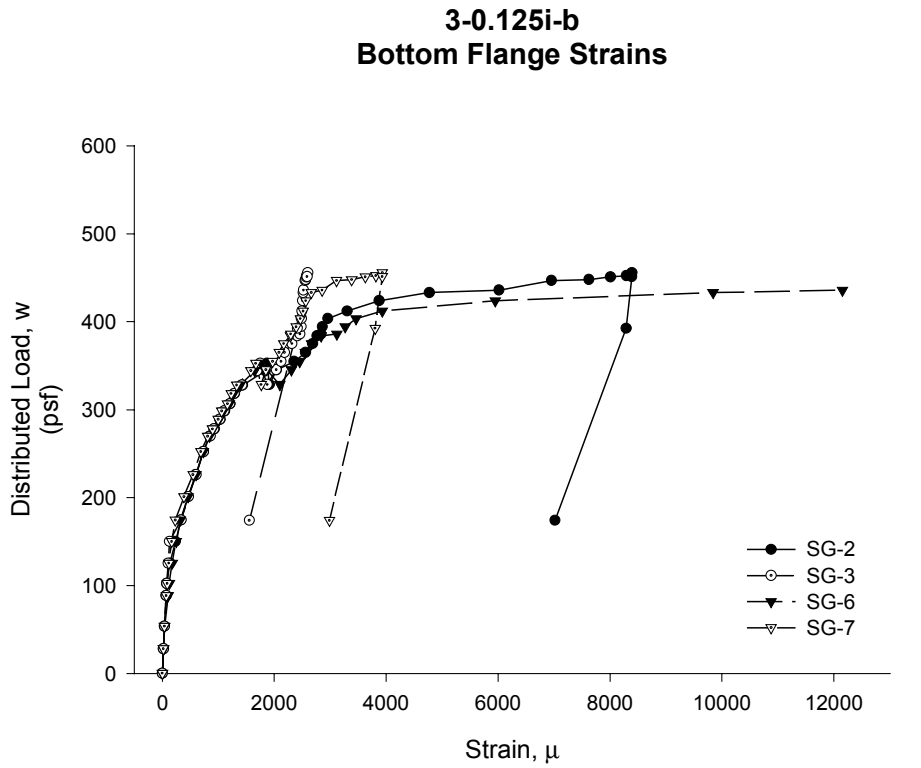

Figure B. 65 Applied Load vs. Deck Bottom Flange Strain for 3-0.125i-b

Test Designation: 3-0.125io-a
Test Date: February 28, 2001

Materials and Dimensions

General:

width:	6 feet (2 panels)
span length:	11 ft. 4 in.
deck anchorage type:	arc spot weld, 3/4 in. dia
average anchorage spacing:	1.0 ft.

Deck:

thickness:	0.0350 in. (20 gage)	
depth:	3 in.	
area:	0.581 in^2	
yield stress:	52.7 ksi	
ultimate strength:	62.1 ksi	
embossment dimensions:		
N_b: 2.598 in.	W_b: 0.506 in.	s: 1.000 in.
N_t: 2.309 in.	W_t: 0360 in.	p_h: 0.125 in.

Concrete:

type:	normal weight
test strength:	3,600psi
total depth:	5.5 in.
cover depth:	2.5 in.

RESULTS:

midspan strain due to fresh concrete:	$672x10^{-6}$ in./in. (bot. flange)
	$509x10^{-6}$ in./in. (top flange)
maximum load:	440 psf
deflection at maximum load:	2.842 in.
end slip at max load:	0.183 in. (left)
	0.017 in. (right)
end slip at termination of test:	0.796 in. (left)
	0.017 in. (right)

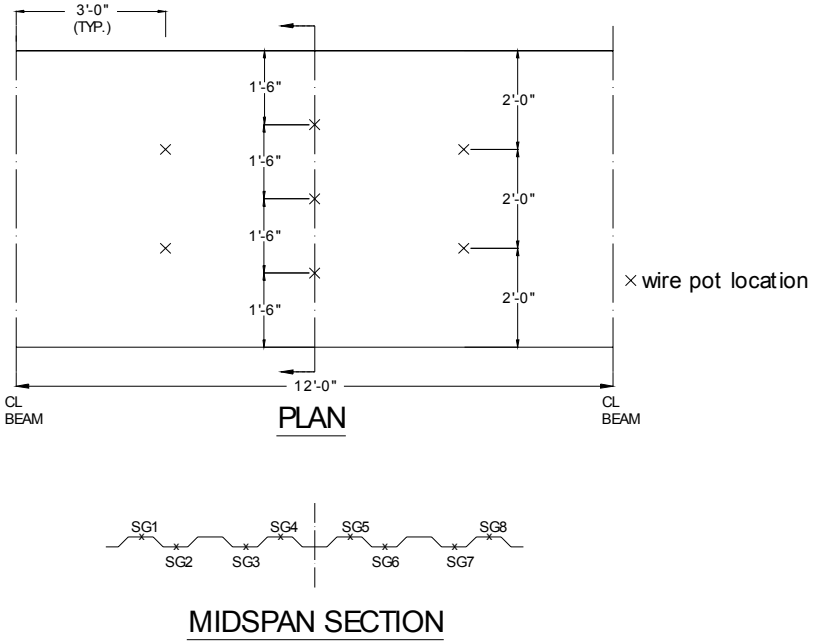

Figure B. 66 Strain Gage and Wire Pot Locations for 3-0.125io-a

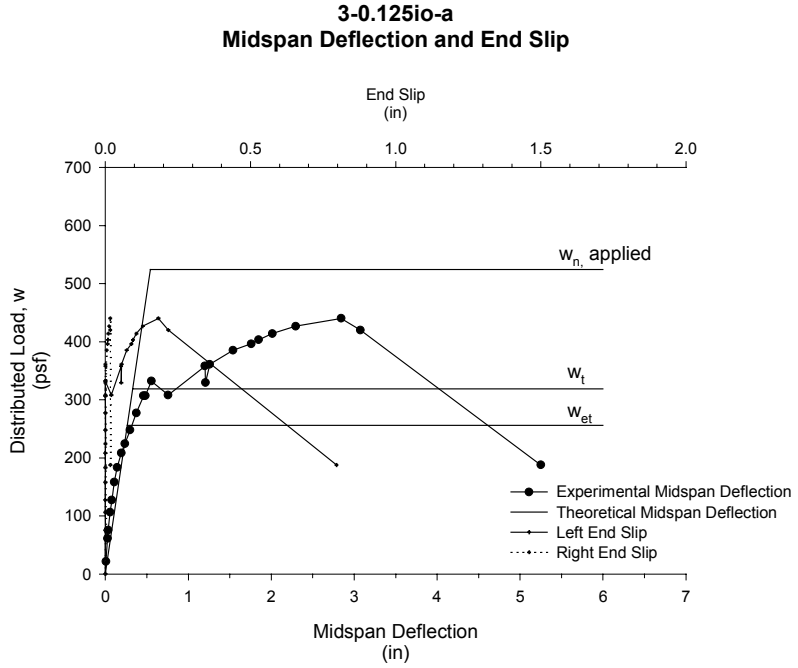

w_n = Theoretical applied distributed load that results in M_n using the calculated material properties

w_t = Theoretical applied distributed load that results in M_t (Flexural Capacity using ASCE App. D Method)

w_{et} = Theoretical applied distributed load that results in M_{et} (First Yield Moment)

Figure B. 67 Applied Load vs. Midspan Deflection and End Slip for 3-0.125io-a

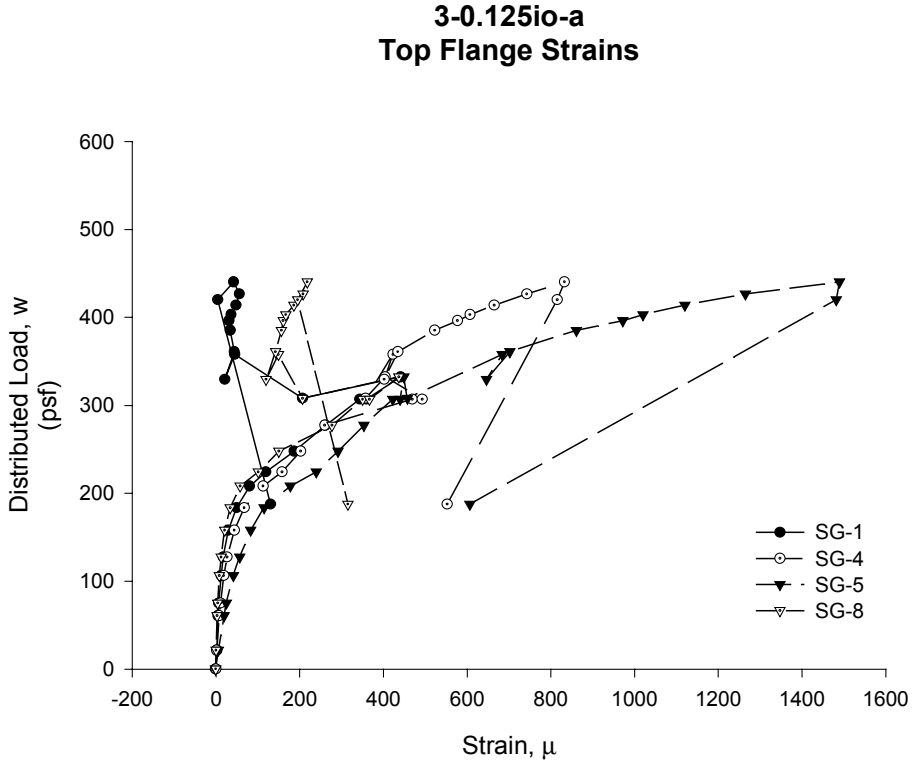

Figure B. 68 Applied Load vs. Deck Top Flange Strain for 3-0.125io-a

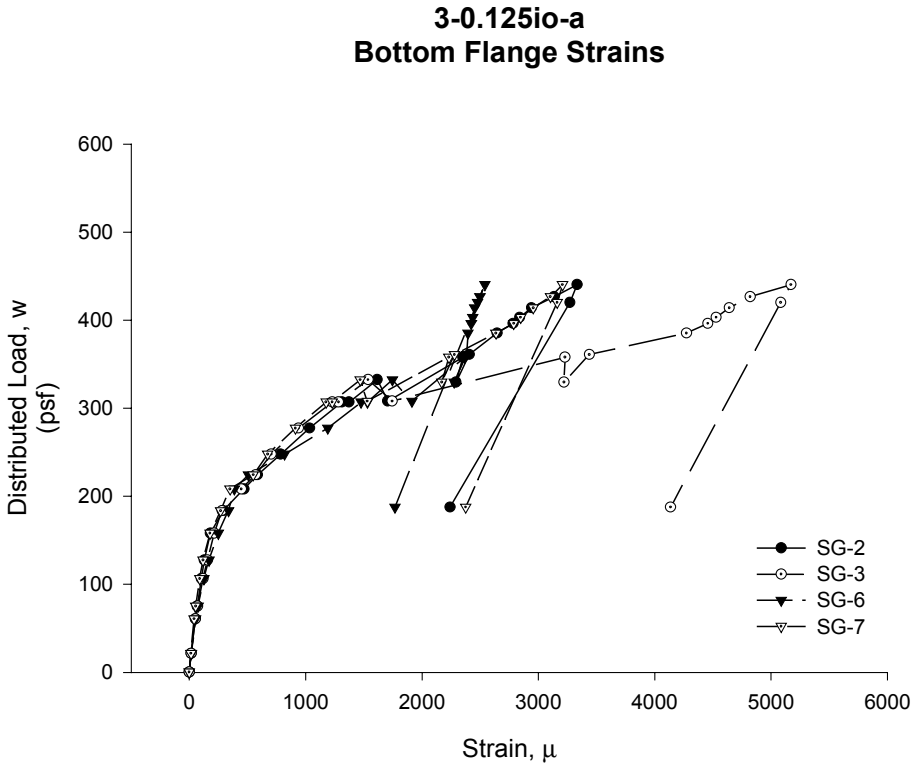

Figure B. 69 Applied Load vs. Deck Bottom Flange Strain for 3-0.125io-a

Test Designation: 3-0.125io-b
Test Date: February 28, 2001

Materials and Dimensions

General:

width:	6 feet (2 panels)
span length:	11 ft. 4 in.
deck anchorage type:	arc spot weld, 3/4 in. dia
average anchorage spacing:	1.0 ft.

Deck:

thickness:	0.0350 in. (20 gage)	
depth:	3 in.	
area:	0.581 in^2	
yield stress:	52.7 ksi	
ultimate strength:	62.1 ksi	
embossment dimensions:		
N_b: 2.598 in.	W_b: 0.506 in.	s: 1.000 in.
N_t: 2.309 in.	W_t: 0360 in.	p_h: 0.125 in.

Concrete:

type:	normal weight
test strength:	3,600 psi
total depth:	5.5 in.
cover depth:	2.5 in.

RESULTS:

midspan strain due to fresh concrete:	$597x10^{-6}$ in./in. (bot. flange)
	$596x10^{-6}$ in./in. (top flange)
maximum load:	410 psf
deflection at maximum load:	2.623 in.
end slip at max load:	0.200 in. (left)
	0.012 in. (right)
end slip at termination of test:	0.850 in. (left)
	0.012 in. (right)

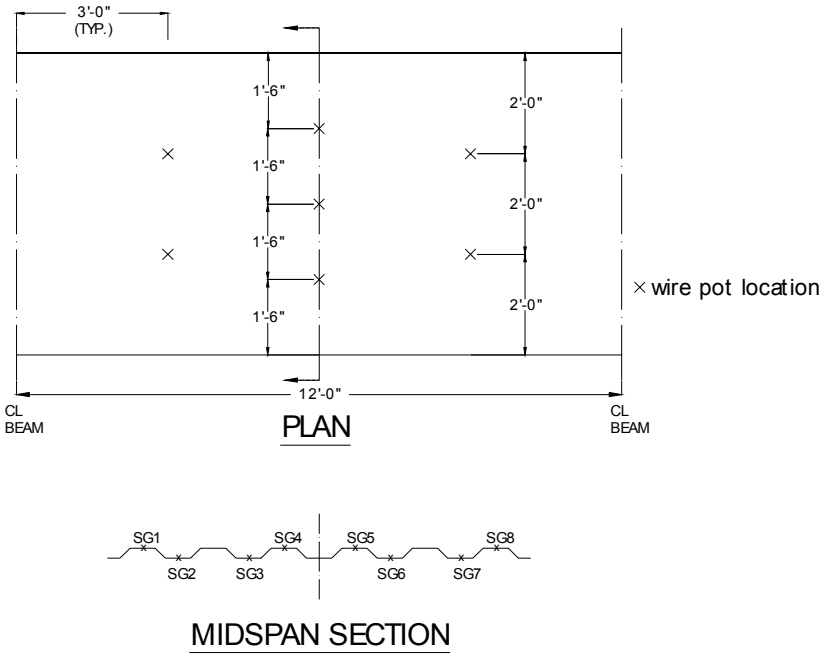

Figure B. 70 Strain Gage and Wire Pot Locations for 3-0.125io-b

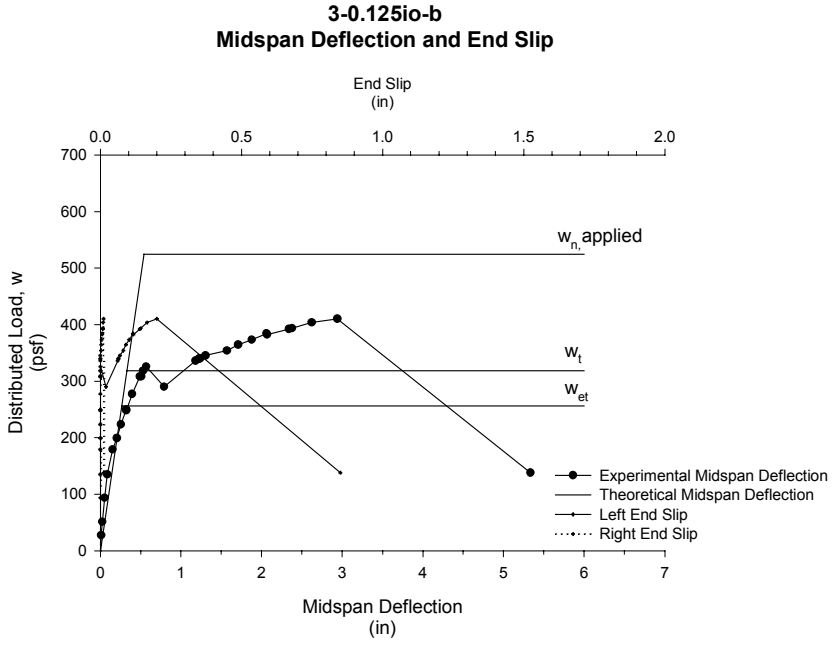

w_n = Theoretical applied distributed load that results in M_n using the calculated material properties

w_t = Theoretical applied distributed load that results in M_t (Flexural Capacity using ASCE App. D Method)

w_{et} = Theoretical applied distributed load that results in M_{et} (First Yield Moment)

Figure B. 71 Applied Load vs. Midspan Deflection and End Slip for 3-0.125io-b

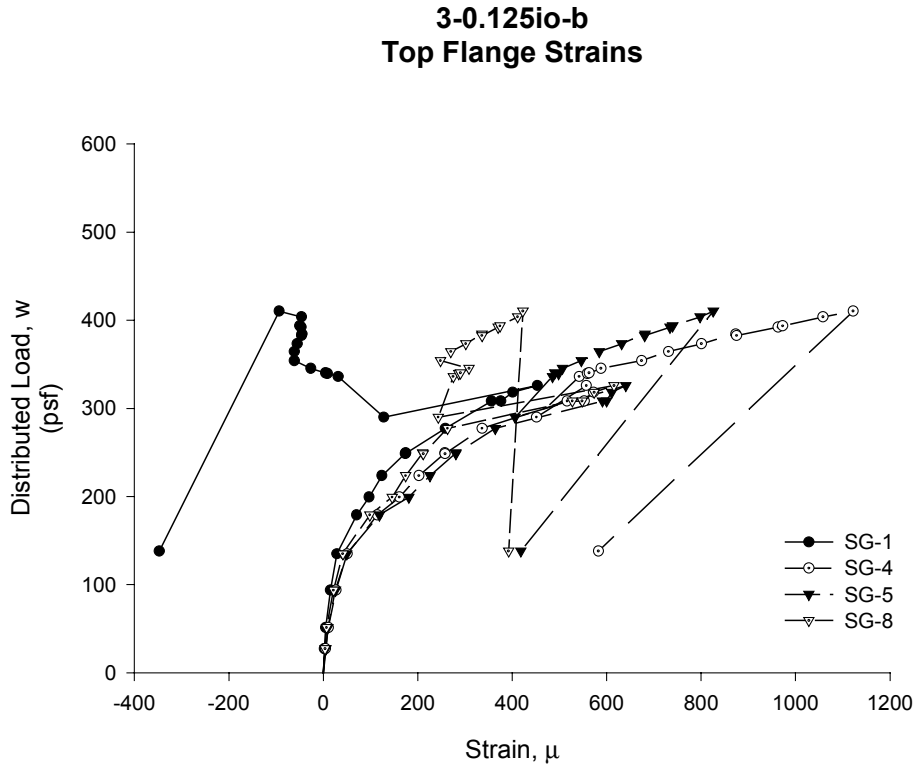

Figure B. 72 Applied Load vs. Deck Top Flange Strain for 3-0.125io-b

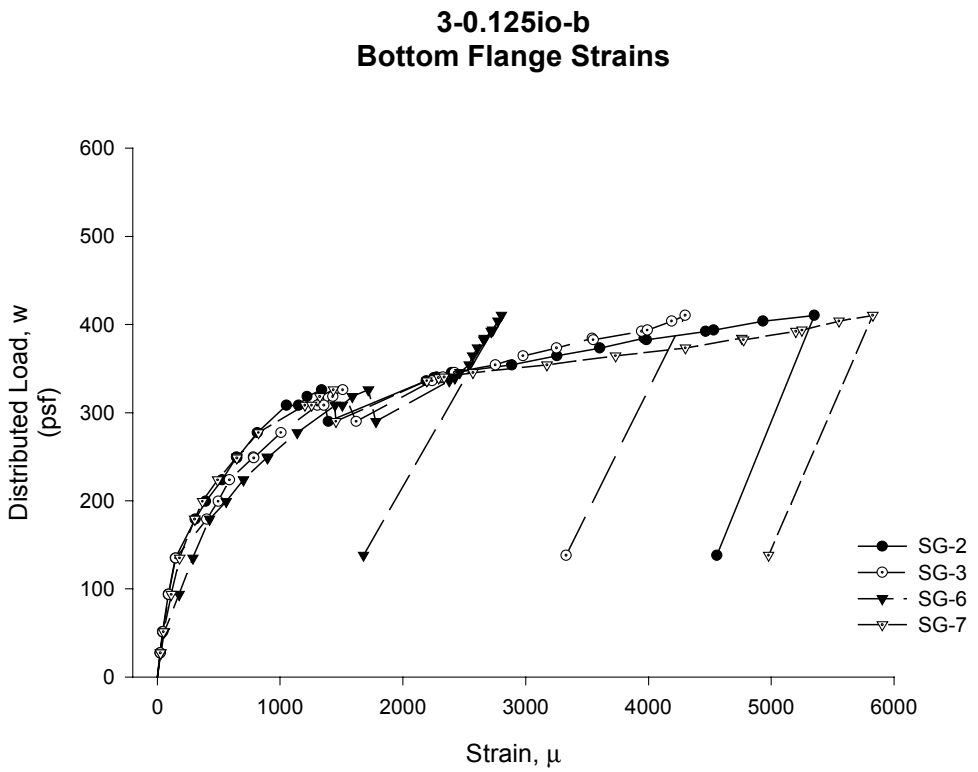

Figure B. 73 Applied Load vs. Deck Bottom Flange Strain for 3-0.125io-b

Test Designation: 3-0.14io-a
Test Date: December 14, 2000

Materials and Dimensions

General:

width:	6 feet (2 panels)
span length:	11 ft. 4 in.
deck anchorage type:	arc spot weld, 3/4 in. dia
average anchorage spacing:	1.0 ft.

Deck:

thickness:	0.0350 in. (20 gage)	
depth:	3 in.	
area:	0.581 in^2	
yield stress:	52.7 ksi	
ultimate strength:	62.1 ksi	
embossment dimensions:		
N_b: 2.598 in.	W_b: 0.506 in.	s: 1.000 in.
N_t: 2.309 in.	W_t: 0360 in.	p_h: 0.140 in.

Concrete:

type:	normal weight
test strength:	3,400 psi
total depth:	5.5 in.
cover depth:	2.5 in.

RESULTS:

midspan strain due to fresh concrete:	$549x10^{-6}$ in./in. (bot. flange)
	$439x10^{-6}$ in./in. (top flange)
maximum load:	501 psf
deflection at maximum load:	3.375 in.
end slip at max load:	0.014 in. (left)
	0.233 in. (right)
end slip at termination of test:	0.014 in. (left)
	0.886 in. (right)

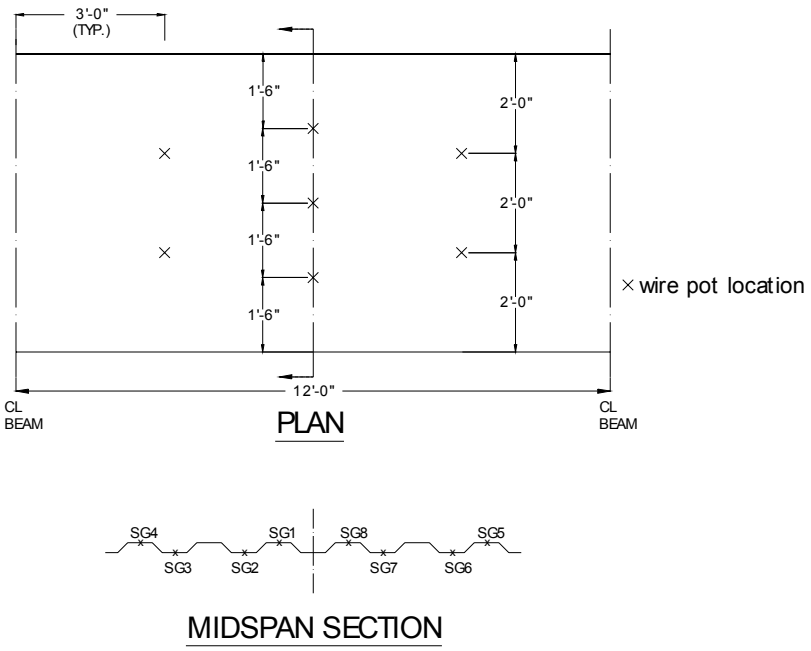

Figure B. 74 Strain Gage and Wire Pot Locations for 3-0.14io-a

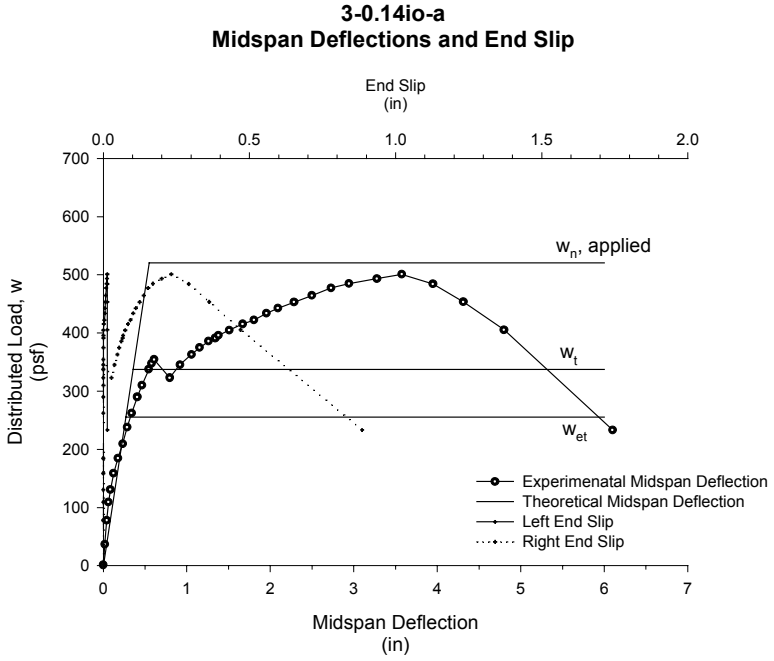

w_n = Theoretical applied distributed load that results in M_n using the calculated material properties

w_t = Theoretical applied distributed load that results in M_t (Flexural Capacity using ASCE App. D Method)

w_{et} = Theoretical applied distributed load that results in M_{et} (First Yield Moment)

Figure B. 75 Applied Load vs. Midspan Deflection and End Slip for 3-0.14io-a

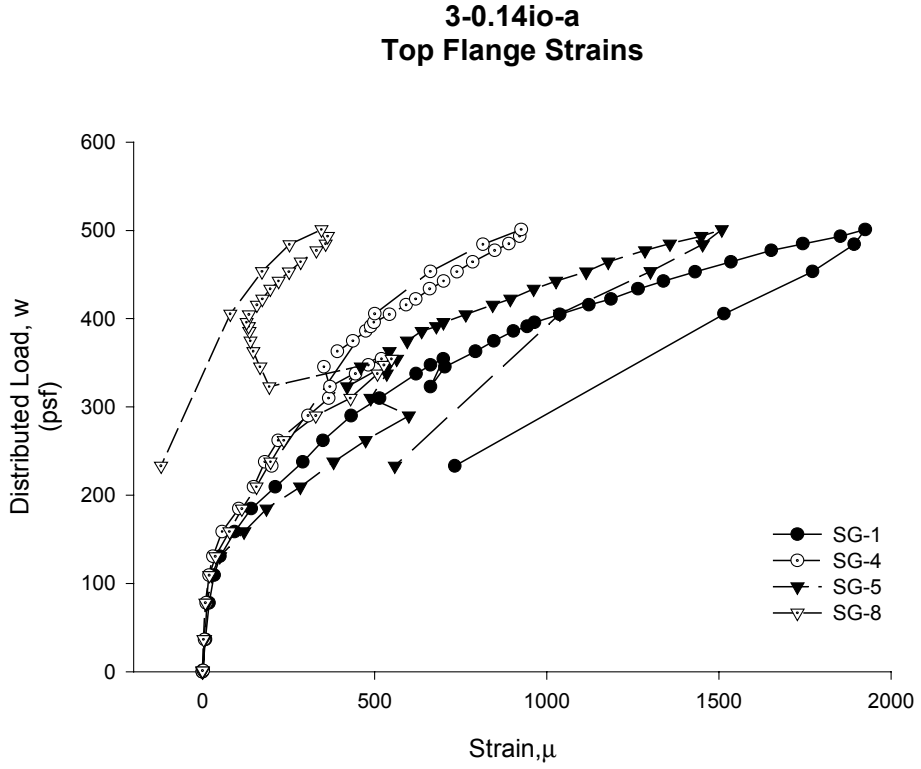

Figure B. 76 Applied Load vs. Deck Top Flange Strain for 3-0.14io-a

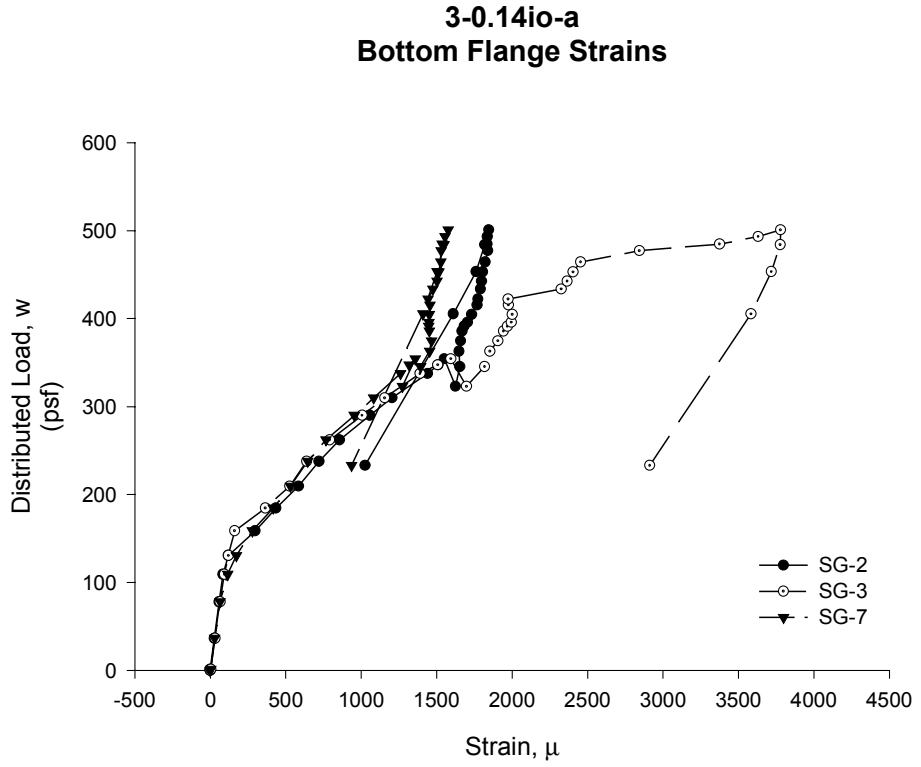

Figure B. 77 Applied Load vs. Deck Bottom Flange Strain for 3-0.14io-a

Test Designation: 3-0.14io-b
Test Date: December 14, 2000

Materials and Dimensions

General:

width:	6 feet (2 panels)
span length:	11 ft. 4 in.
deck anchorage type:	arc spot weld, 3/4 in. dia
average anchorage spacing:	1.0 ft.

Deck:

thickness:	0.0350 in. (20 gage)	
depth:	3 in.	
area:	0.581 in^2	
yield stress:	52.7 ksi	
ultimate strength:	62.1 ksi	
embossment dimensions:		
N_b: 2.598 in.	W_b: 0.506 in.	s: 1.000 in.
N_t: 2.309 in.	W_t: 0.360 in.	p_h: 0.140 in.

Concrete:

type:	normal weight
test strength:	3,400 psi
total depth:	5.5 in.
cover depth:	2.5 in.

RESULTS:

midspan strain due to fresh concrete:	630×10^{-6} in./in. (bot. flange)
	503×10^{-6} in./in. (top flange)
maximum load:	463 psf
deflection at maximum load:	3.184 in.
end slip at max load:	0.133 in. (left)
	0.025 in. (right)
end slip at termination of test:	0.268 in. (left)
	0.027 in. (right)

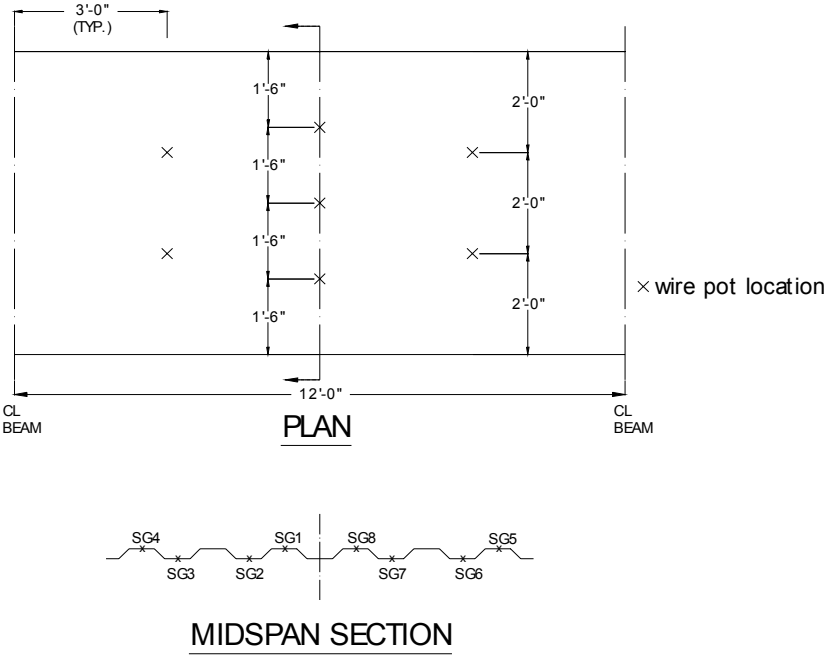

Figure B. 78 Strain Gage and Wire Pot Locations for 3-0.14io-b

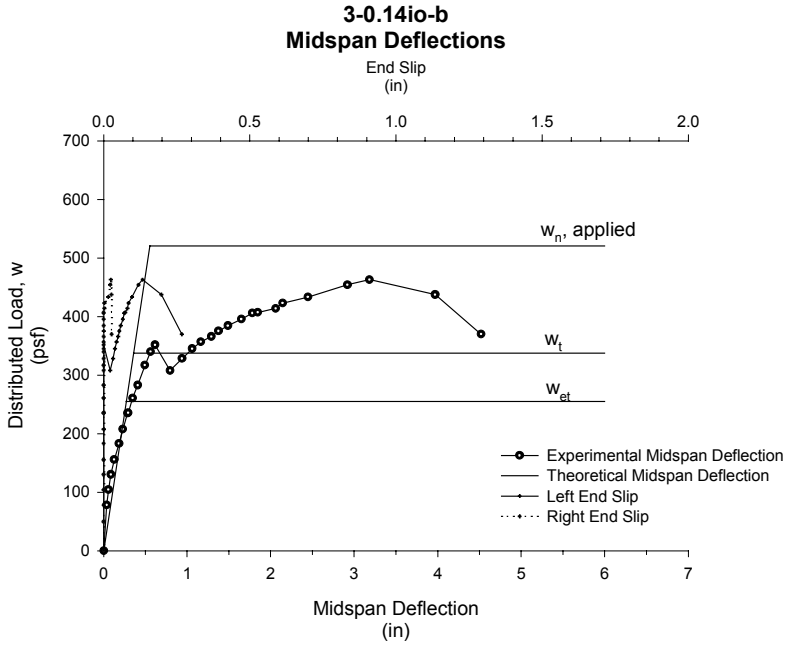

w_n = Theoretical applied distributed load that results in M_n using the calculated material properties

w_t = Theoretical applied distributed load that results in M_t (Flexural Capacity using ASCE App. D. Method)

w_{et} = Theoretical applied distributed load that results in M_{et} (First Yield Moment)

Figure B. 79 Applied Load vs. Midspan Deflection and End Slip for 3-0.14io-b

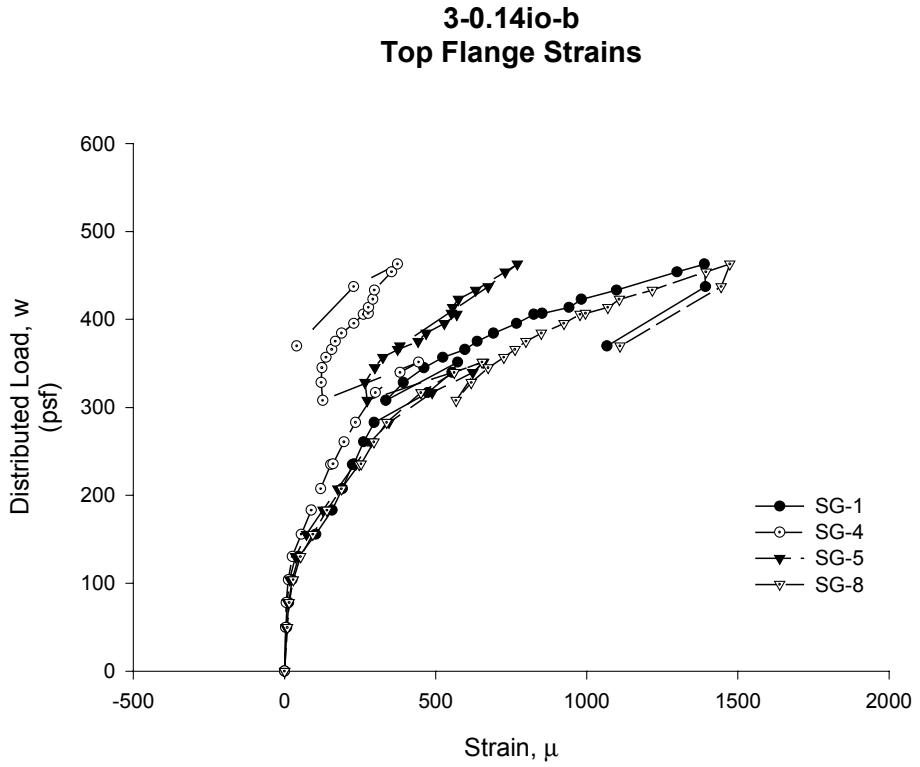

Figure B. 80 Applied Load vs. Deck Top Flange Strain for 3-0.14io-b

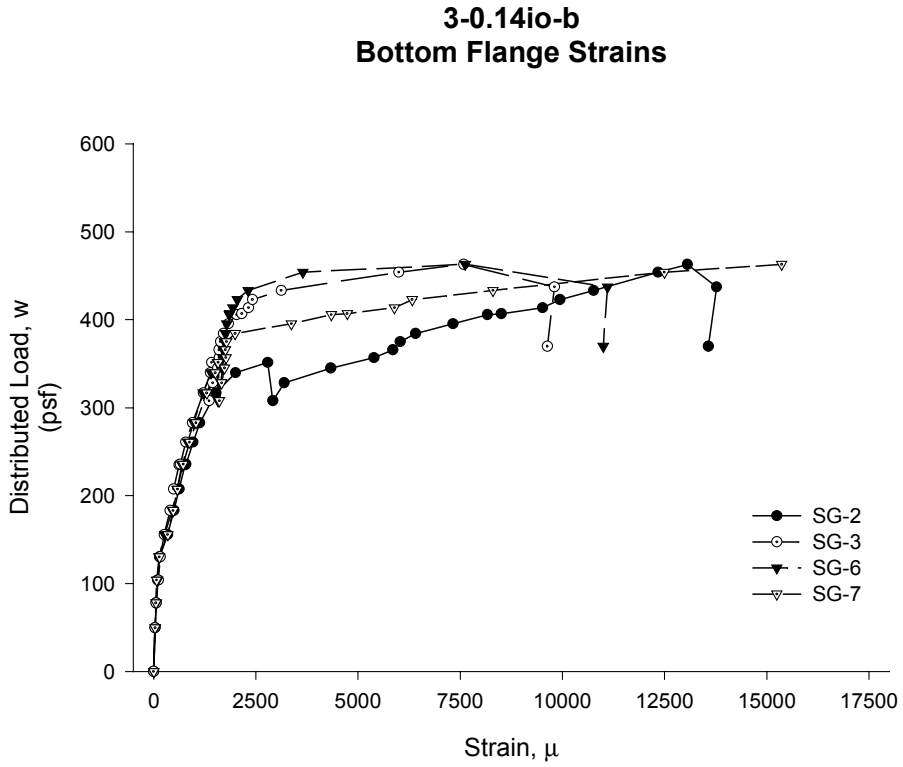

Figure B. 81 Applied Load vs. Deck Bottom Flange Strain for 3-0.14io-b

APPENDIX C: EXPERIMENTAL AND ITERATIVE METHOD LOAD VERSUS DEFLECTION GRAPHS

This appendix includes graphs comparing experimental results with the results from the strength prediction methods.

Where:

w_n = Theroretical applied distributed load that results in Mn using the calculated material properties (assuming full-composite interaction)

w_t = Theoretical applied distributed load that results in M_t (Flexural Capacity using ASCE Appendix D Method)

w_{et} = Theoretical applied distributed load that results in M_{et} (First Yield Moment)

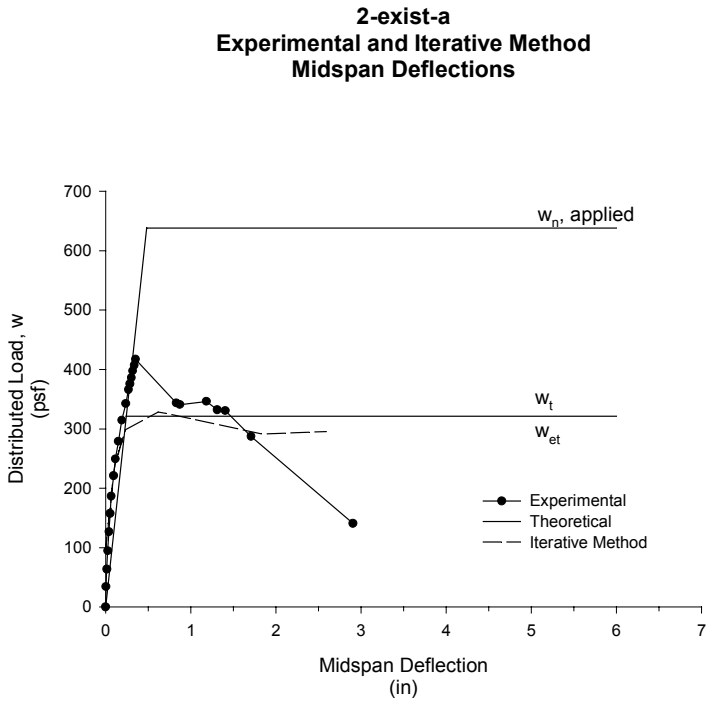

Figure C. 1 Experimental and Iterative Method Applied Load vs. Midspan Deflection for 2-exist-a

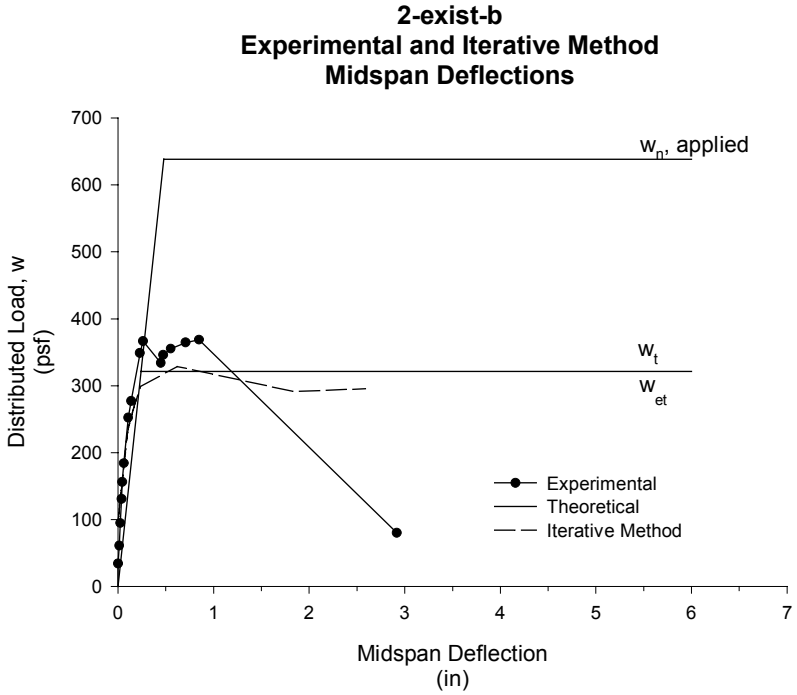

Figure C. 2 Experimental and Iterative Method Applied Load vs. Midspan Deflection for 2-exist-b

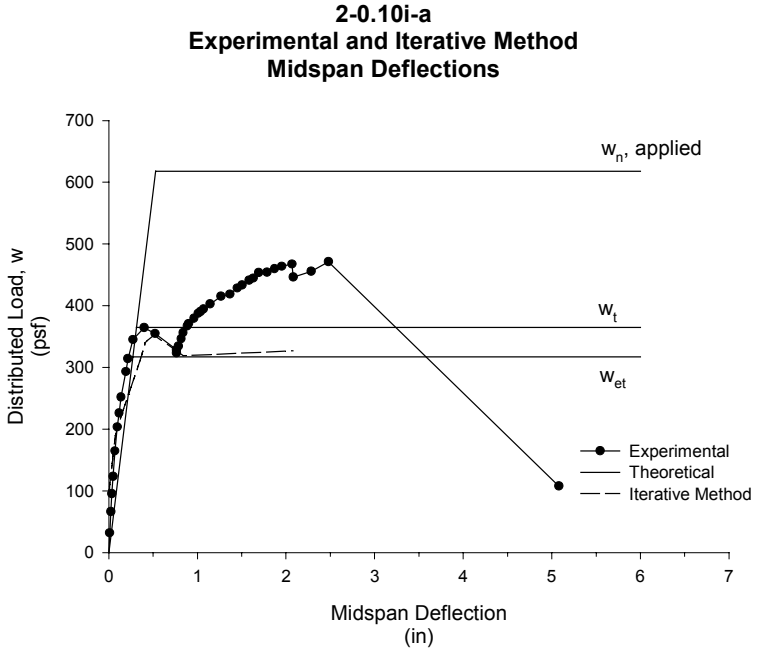

Figure C. 3 Experimental and Iterative Method Applied Load vs. Midspan Deflection for 2-0.10i-a

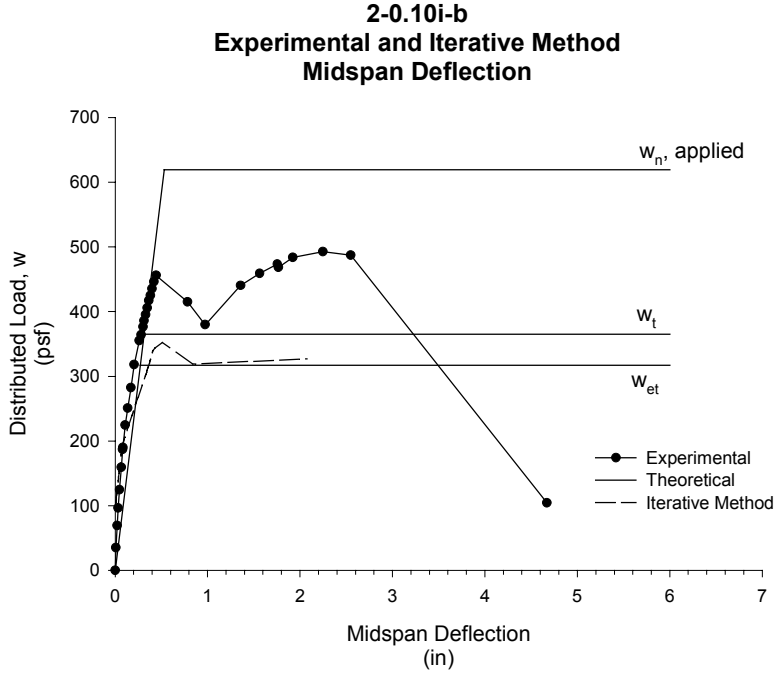

Figure C. 4 Experimental and Iterative Method Applied Load vs. Midspan Deflection for 2-0.10i-b

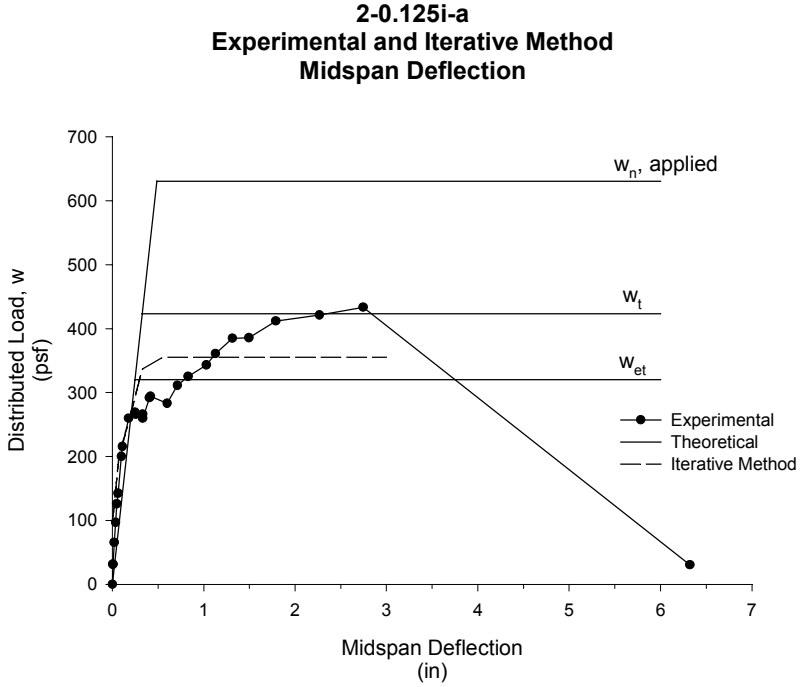

Figure C. 5 Experimental and Iterative Method Applied Load vs. Midspan Deflection for 2-0.125i-a

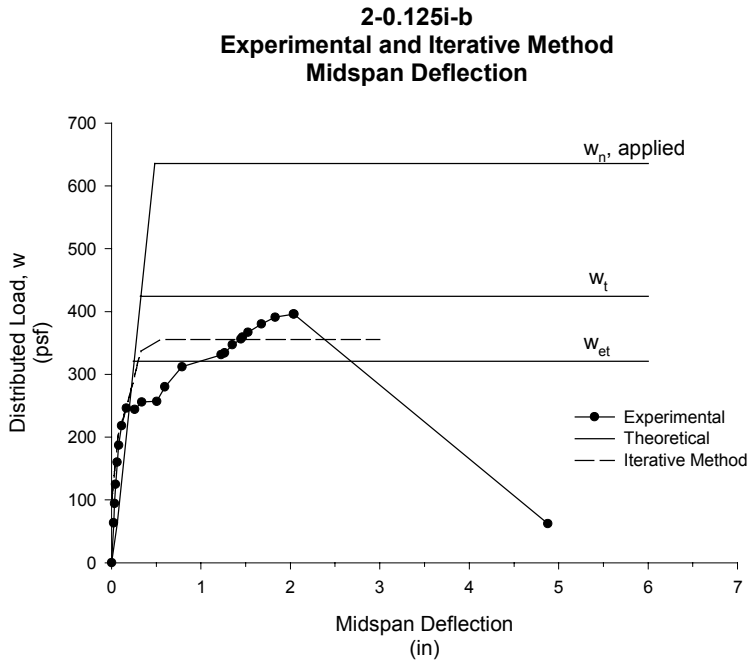

Figure C. 6 Experimental and Iterative Method Applied Load vs. Midspan Deflection for 2-0.125i-b

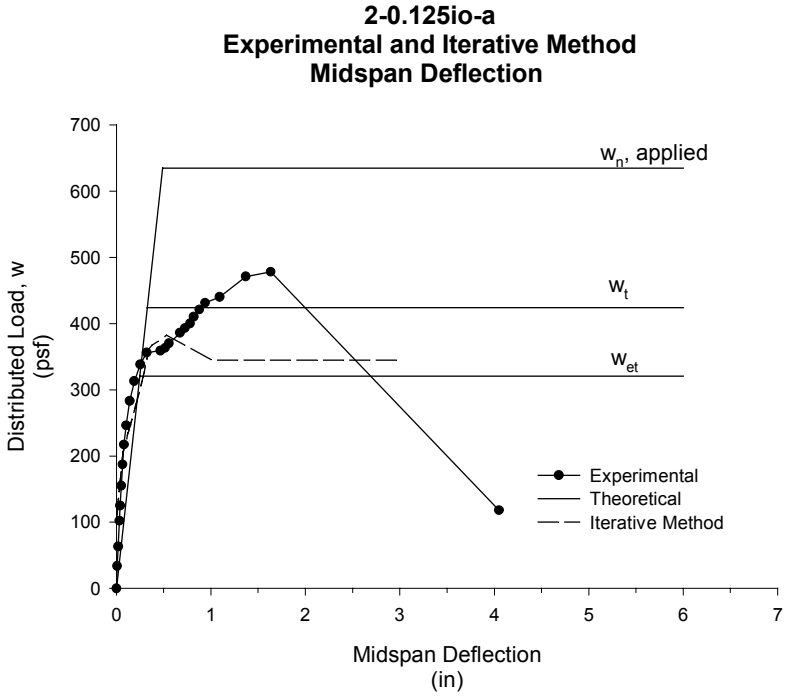

Figure C. 7 Experimental and Iterative Method Applied Load vs. Midspan Deflection for 2-0.125io-a

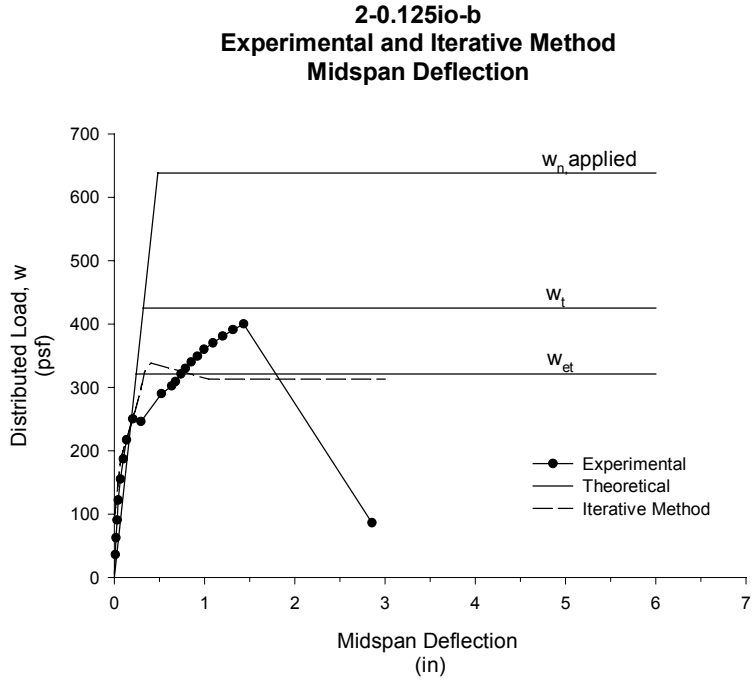

Figure C. 8 Experimental and Iterative Method Applied Load vs. Midspan Deflection for 2-0.125io-b

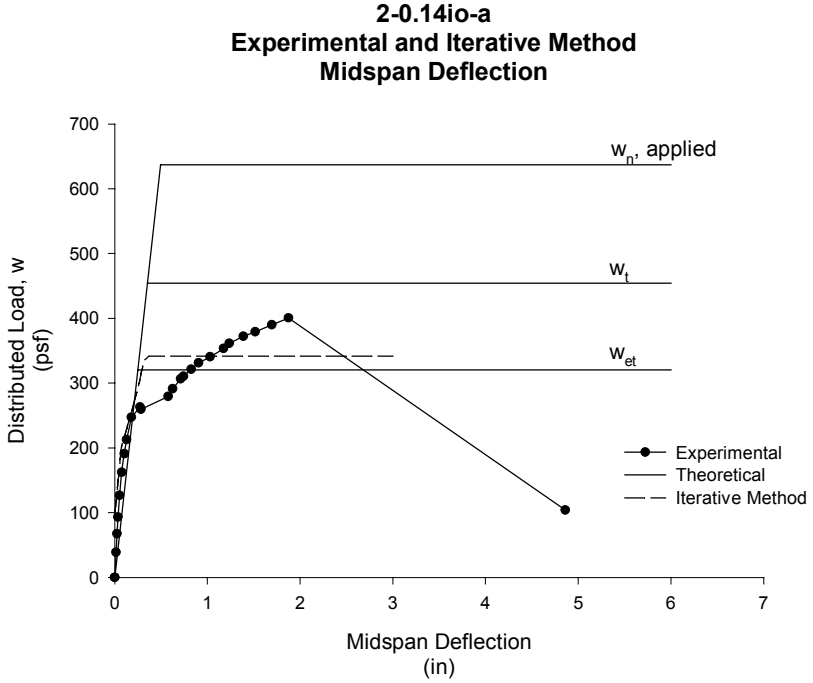

Figure C. 9 Experimental and Iterative Method Applied Load vs. Midspan Deflection for 2-0.14io-a

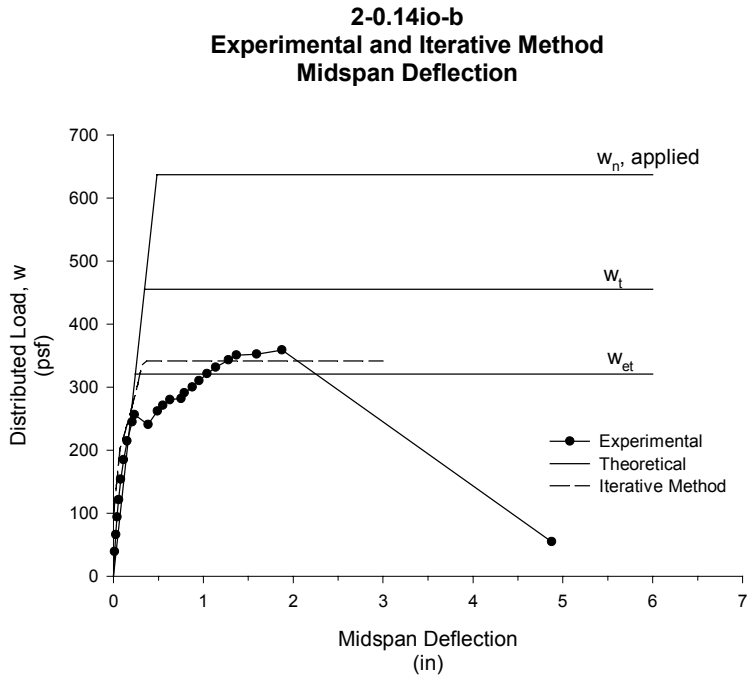

Figure C. 10 Experimental and Iterative Method Applied Load vs. Midspan Deflection for 2-0.14io-b

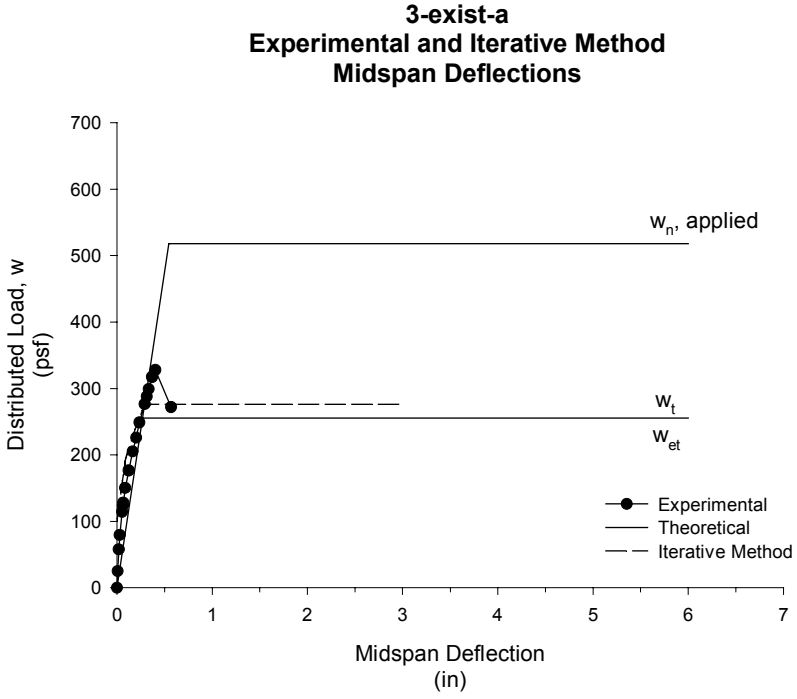

Figure C. 11 Experimental and Iterative Method Applied Load vs. Midspan Deflection for 3-exist-a

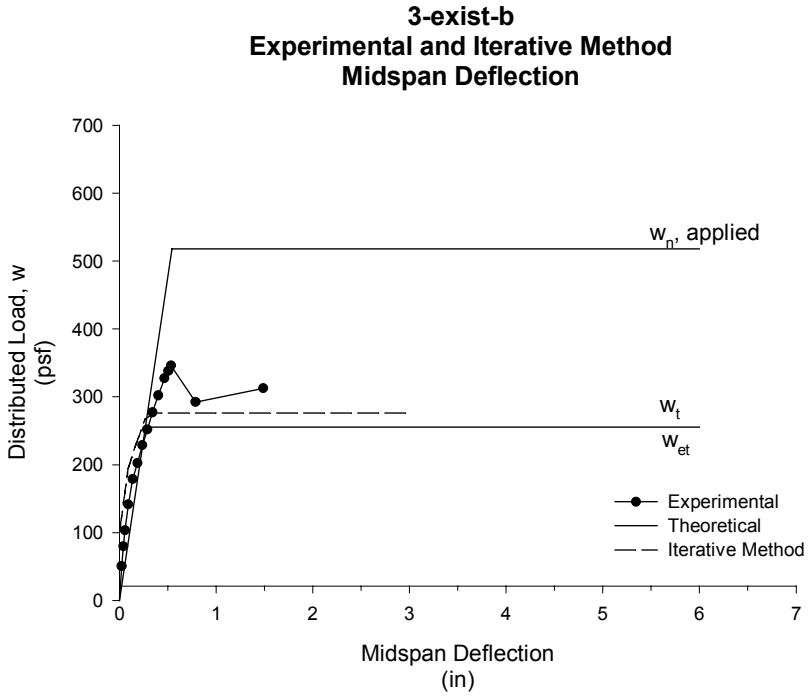

Figure C. 12 Experimental and Iterative Method Applied Load vs. Midspan Deflection for 3-exist-b

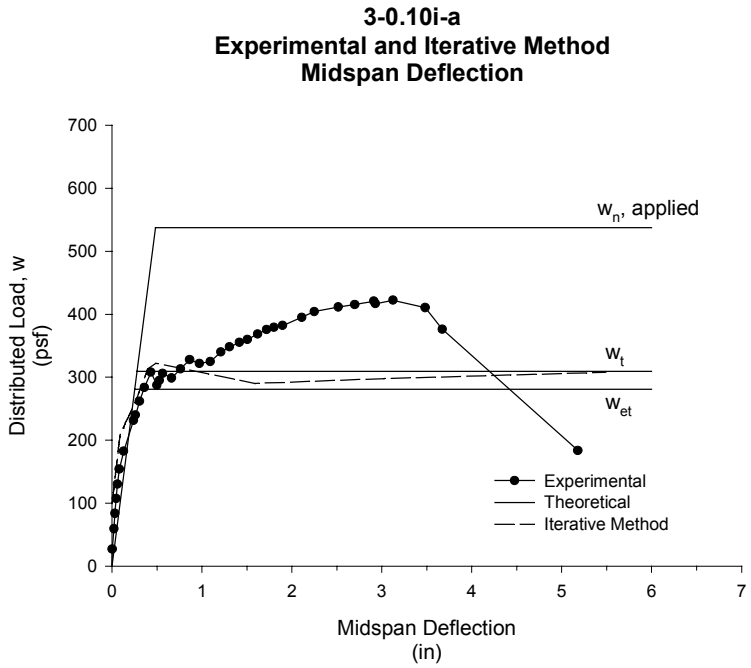

Figure C. 13 Experimental and Iterative Method Applied Load vs. Midspan Deflection for 3-0.10i-a

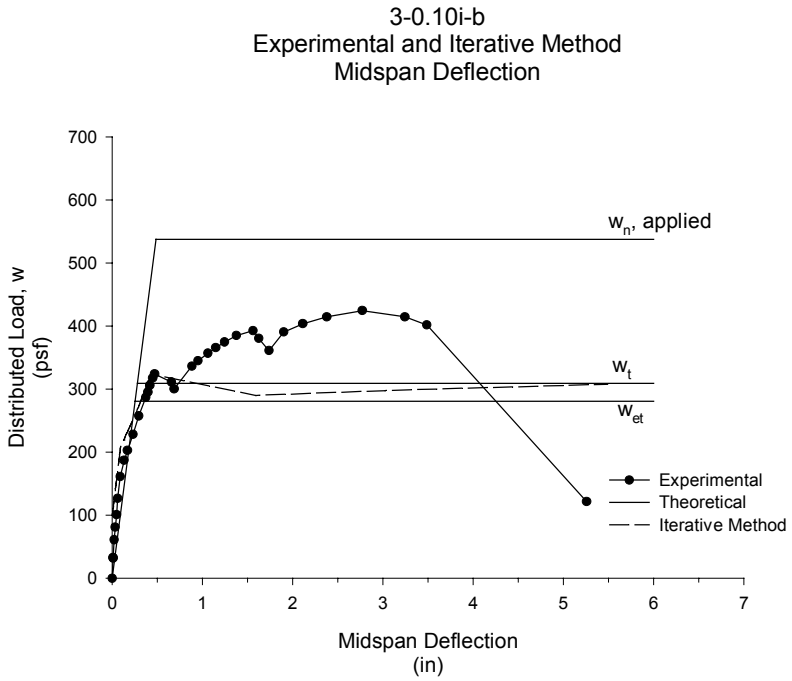

Figure C. 14 Experimental and Iterative Method Applied Load vs. Midspan Deflection for 3-0.10i-b

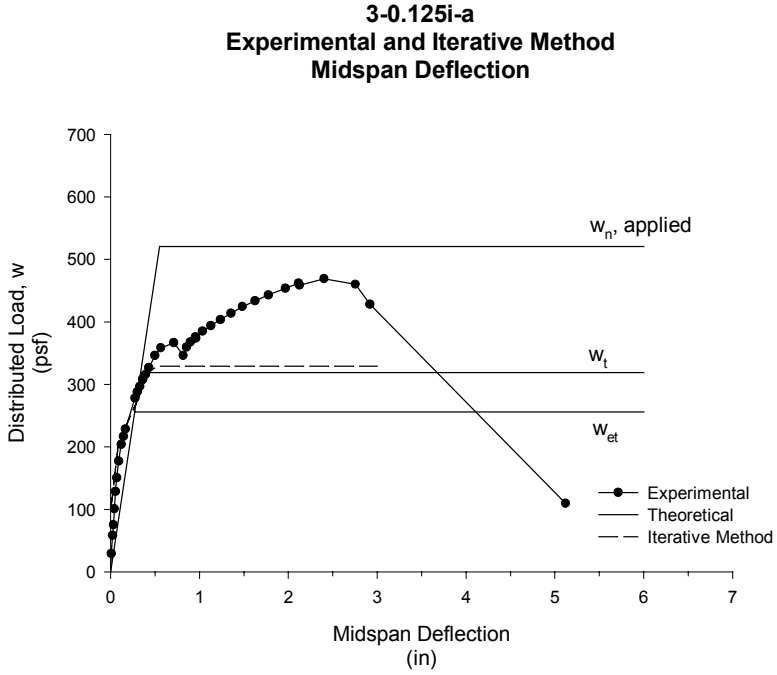

Figure C. 15 Experimental and Iterative Method Applied Load vs. Midspan Deflection for 3-0.125i-a

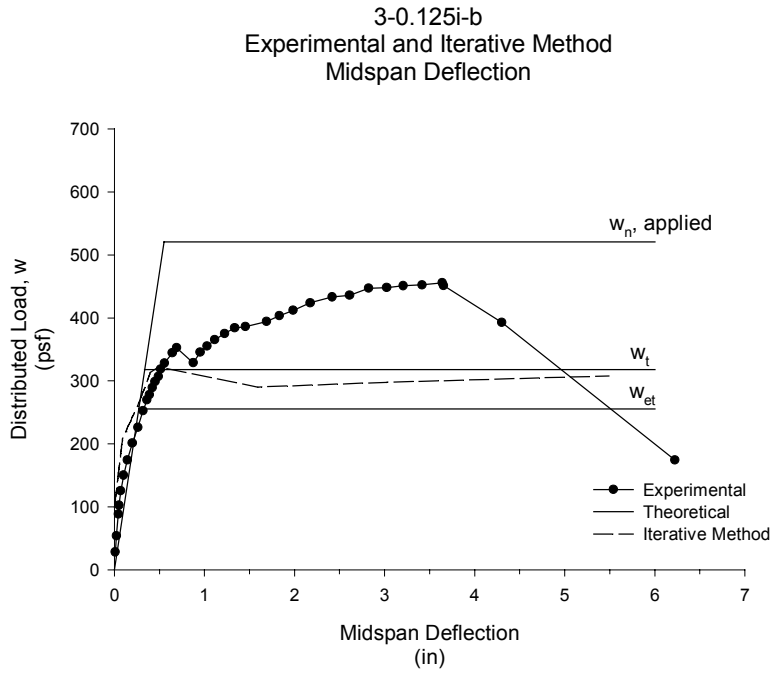

Figure C. 16 Experimental and Iterative Method Applied Load vs. Midspan Deflection for 3-0.125i-b

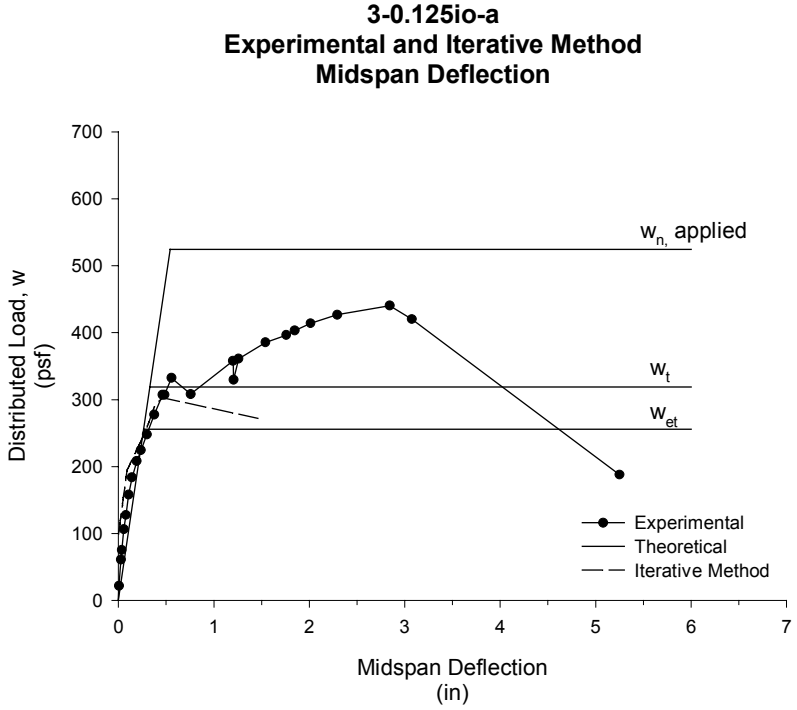

Figure C. 17 Experimental and Iterative Method Applied Load vs. Midspan Deflection for 3-0.125io-a

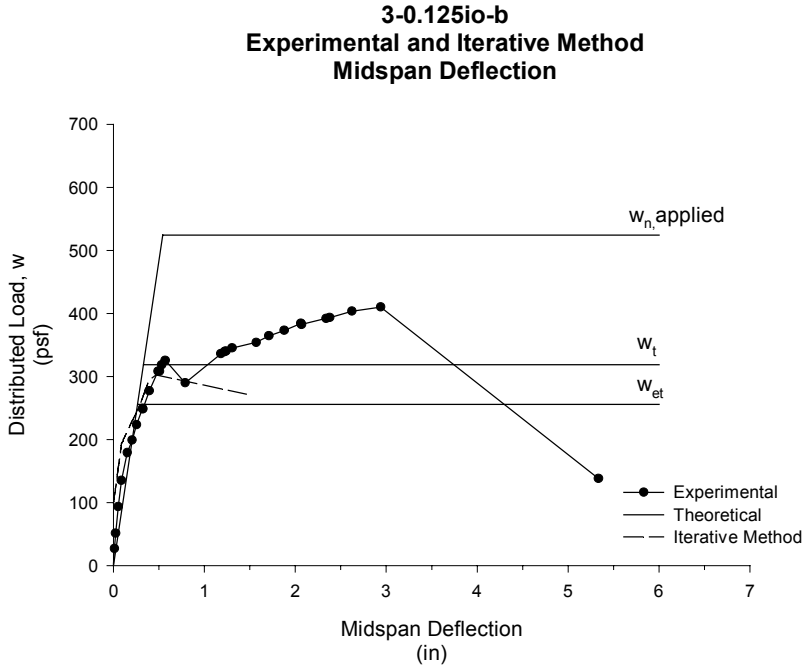

Figure C. 18 Experimental and Iterative Method Applied Load vs. Midspan Deflection for 3-0.125io-b

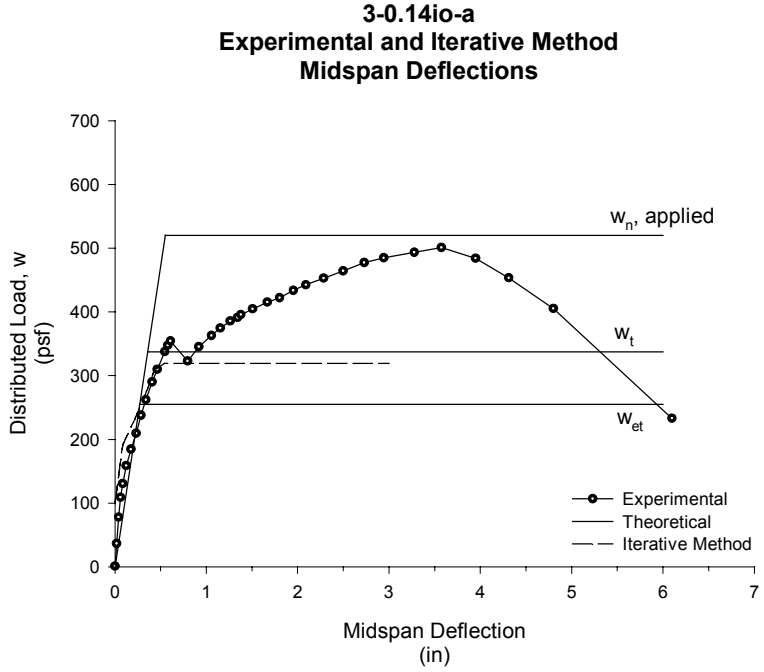

Figure C. 19 Experimental and Iterative Method Applied Load vs. Midspan Deflection for 3-0.14io-a

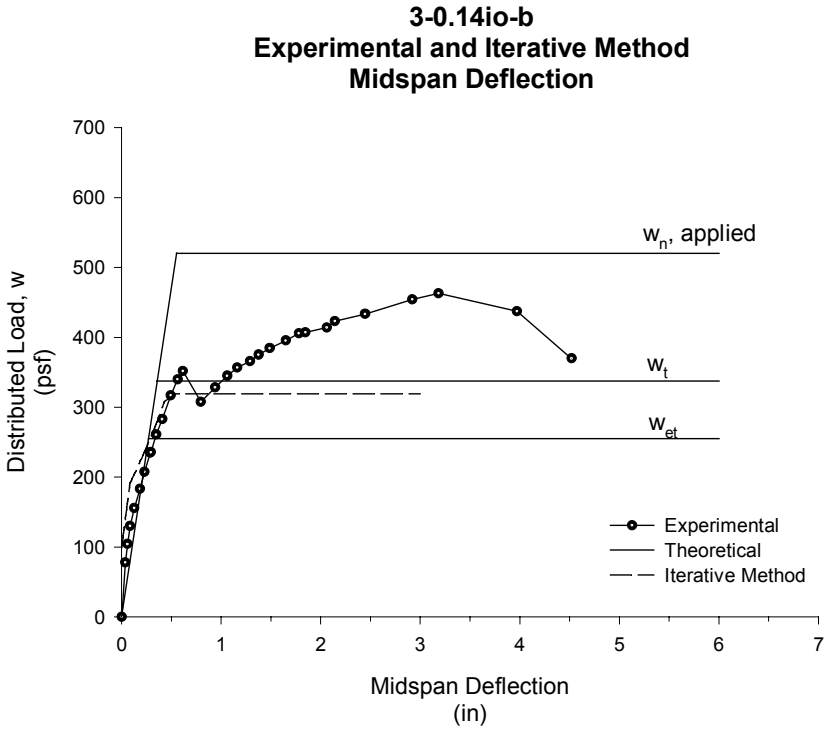

Figure C. 20 Experimental and Iterative Method Applied Load vs. Midspan Deflection for 3-0.14io-b

VITA

Grace Shen was born in Radford, Virginia May 26, 1973 to Stewart and Shawmei Shen to accompany her sister, Alice. Grace spent several of her younger years in Rochester, New York before moving to Virginia Beach, Virginia in the second grade. She graduated from Kempsville High school and then went on to get a BS in Civil Engineering at the University of Virginia. After college, Grace worked for three years with Johnson, Mirmiran, and Thompson doing design of transportation structures. She then spent a year overseas in China doing language and cultural studies before returning to get her MS degree in Civil Engineering at Virginia Tech. She hopes to one day return to China.